FUNDAMENTAL UNDERSTANDING OF SOOT INDUCED WEAR MECHANISM OF DIESEL ENGINE

By

MIHIR PATEL

Presented to the Faculty of Graduate School of
University of Texas at Arlington in Partial Fulfillment
of the Requirement for the Degree of

DOCTOR OF PHILOSOPHY

THE UNIVERSITY OF TEXAS AT ARLINGTON
DECEMBER 2011

DEDICATION

To “Krishna”

ACKNOWLEDGEMENTS

Apart from the efforts of mine, the success of this project depends largely on the encouragement and guidelines of many others. I take this opportunity to express my gratitude to the people who have been instrumental in the successful completion of this project.

First, My sincere thanks to the almighty to give this blissful life and millions of moments to cherish throughout my life, especially in last five years of my doctoral program.

I greatly appreciate my advisor Dr. Pranesh Aswath for being an exceptional mentor. His splendid knowledge of subject matter, his conscientious way of guidance makes him most impressive mentor of the department. Impressed by his versatility and fundamental knowledge in various subjects, I consider him as most suitable mentor to brainstorm various problems at hand. His extensive experience and in-depth knowledge in various fields was extremely useful during my Ph.D. research work, especially when research required interdisciplinary knowledge of subjects to scrutinize the given problem, which contributed to completely novel perspective to my doctoral research.

In the same respect, I consider myself fortunate to have outstanding committee members. Dr. Ronald Elsenbaumer, Dr. Yahwao Hao, Dr. Micheal Jin and Dr. Dejong Kim. Your constructive comments on my Ph.D. proposal have given me clear direction for my endeavor.

I am indebted to my many of my colleagues to support me at UT Arlington. Many thanks to Xin Chen, Ramoun Mourhatch, BoHoon Kim, Anuradha Somaiyaji for providing his valuable suggestions on various additives chemistries and teaching various friction and wear bench tests. I am very grateful to Hande Demirkiran, Hansika Parekh, Arunya Suresh, Bei Bei Wang, Tonye Jr. Adeogba, Shruthi Gandhi, Megen Velten, Jayapradhi Rajenderan, Olumide Oruwajoye, Pradip Sairam, Sujay Bagi for being extremely supportive during my doctoral programs. A special thank to Eray Erkan, for being extremely supportive. It was pleasure working with him for all the ASM

activities. My sincere words of appreciation to Jei Ha, for her help in various HRTEM experiments. These are the people who deserve special acknowledgement.

Dr. Ewa bardasz have supported my research at one of the most crucial juncture. I indebted her for providing a valuable dynamometer engine oils and engine components. Without her support, my research wouldn't have seen a day of light. I appreciate her support, her mentoring and her trust on my ability.

Several external sources have been crucial in providing timely impetus to this project: Dr. Yongfeng Hu and Dr. Lucia Zuin, Tom Reiger, of Canadian Light Source Center. I also acknowledge Dr. Narayan Appathurai from synchrotron Radiation Center, Madison WI, for his help to conduct X-PEEM experiments and valuable suggestion on x-ray absorption techniques. I would like to acknowledge Dr. John Rosenbaum from Chevron Oronite, for his input in particle analysis of soot. A special thank to Dr. Paolo from University of Trento, Italy for synchrotron radiation experiments. They have all contributed considerably to this project.

My sincere words of appreciation to Dr. Jiechao Jiang and David Yen, through whose efforts it was possible to obtain TEM images for my samples. Jennifer Standlee and Libia Cuauhtli were extremely helpful in guiding me through the inescapable administrative hoops of a research project.

An honorable mention goes to my families and friends for their understandings and supports in completing this project. Without helps of the particular that mentioned below, I wouldn't have achieved my dream. My parents, Kantilal Patel and Bharatiben Patel have been my lifelong inspiration, the pillars of my strength and the bedrock of my achievements. They taught me humility and how to value the lives. My Parents-In-Law Dhansukh Patel and Manjuben Patel have also been very supportive during this process. Their unwavering confidence in me, and never ceased to provide comfort and motivation have supported immensely. My brother Sanket Patel, Sister in law Divya Patel, My Brother In Law Chintal, my two nieces Kruti and Sanskruti have always been a backbone through out my life. All my relatives and my cousins were all sources of encouragement during this journey and therefore deserve special recognition as well.

Lastly, These acknowledgment and my life are incomplete without one person, my wife Urvi, who is rock solid with me through out. Words fail me to express my appreciation for her support and persistent confidence in me. During the queers of life, I have always found most comfortable and joyous with her. Her support, care, trusts, laugh and above all her love is the reason for the completion of my doctoral program. She has been my support system during this journey. She has given me wonderful son “Ayan” and a reason to smile forever. Much of what I have learned over the last year came as the result of being a father to wonderful and delightful son. In his own ways, he inspired me and, subconsciously contributed a tremendous amount joy in last one year.

Finally, I would like to thank everybody who was important to the successful realization of my dissertation as well as expressing my apology that I could not mention personally one by one.

October 12, 2011

ABSTRACT

FUNDAMENTAL UNDERSTANDING OF S

OOT INDUCED WEAR MECHANISM

OF DIESEL ENGINE

MIHIR PATEL, Ph.D.

The University of Texas at Arlington. 2011

Supervising Professor: Dr. Pranesh B. Aswath

Emission of Oxides of nitrogen and particulates matters from diesel engines have been reduced by implementing exhaust gas recirculation (EGR) protocols but at the expense of increased wear of engine components. This problem is aggravated by Environment Protection Agency (EPA) regulation such as API CJ 4 and SAPS where chemical limits have been places on the amount of phosphorous, sulfur and sulfated ash in lubrication oil. Several studies have examined the role played by diesel soot on enhanced wear but none have provided comprehensive mechanism. This would allow the possibility to comprehend fundamental understanding of soot induced wear mechanism of diesel engine.

This work begins with a study of the structure, composition and morphology of diesel soot extracted from the drain interval crankcase oil of the commercially operated diesel engine to comprehend the interaction between lubrication additives chemistries and diesel soot. The

interaction was comprehended by characterizing diesel soot using Transmission Electron Microscopy (TEM), Synchrotron X-ray Diffraction, Raman Spectroscopy (SR-XRD), X-ray Absorption Near Edge Spectroscopy (XANES) and High-resolution Transmission Electron Microscopy (HRTEM). The tribological assessment of the lubricant formulation blended with diesel soot was conducted using four ball wear tester and SRV friction tester.

Laboratory simulation was carried out understand the interaction between lubricants additives chemistries and carbon black (soot surrogate). Carbon black was blended with lubricants and treated in various conditions to forced the interaction and thereby comprehend the conditions that are responsible to induced the interaction between carbon black (soot surrogate) and lubricants additives chemistries. XANES, TEM and Raman spectroscopy were used to study the structure, composition and morphology of extracted carbon black and compared with diesel soot. Four ball wear tested and SRV friction test were employed for tribological evaluation. SEM was used to understand the morphology of wear track.

Diesel soots were also extracted from the dynamometer diesel engine tests such as Mack T 8A, Mack T 11, Mack T 12, Cummins ISM, Cummins ISM, GM RFWT. Diesel soots extracted from the drain interval crankcase oil of the dynamometer tests have experienced controlled engine operation. Studies were conducted to correlate the effect of operational parameters such as load, speed, temperature and oil chemistries of the dynamometer engine test and structure and composition of diesel soot. Engine components such as piston ring, header, roller follower pin were also investigated to understand the effect of diesel soot on tribofilm formation and its structure. XANES, HRTEM, SR-XRD, Raman spectroscopy, SEM were used to examine the soot and tribofilm.

TABLE OF CONTENTS

LIST OF ILLUSTRATIONS

Figure Page

LIST OF TABLES

CHAPTER 1

INTRODUCTION

Diesel engines have always been preferred choice of transportation due to its improved fuel economy and torque as compared to gasoline engines. [1] Their extensive application for transportation is restricted due to the emission of pollutants such as nitrogen of oxides (NOx) and particulate matters (PMs). These pollutants produce due to higher combustion temperature typical of diesel engines. Diesel engines use compression ignition instead of spark plugs to ignite the fuel. The high temperature during compression ignition causes oxygen and nitrogen from the intake air to combine as NOx. NOx reacts with hydrocarbons (HC) and sunlight to form ground-level ozone (smog); NOx also combines with other atmospheric constituents to form fine particulate matter. Ozone and particulate matter are associated with many adverse health and welfare effects, including respiratory illness, acid rain and visibility problems (haze). [1-3]

Emission of such pollutants from diesel engine has always been greater concern to protect the environment. In recent years engine manufacturer have been required to reduce the level of nitrogen oxides (NOx) in diesel engine exhaust to meet Tier 3 emission standards API CJ 4 required by the Environment Protection Agency (EPA) where maximum limit has been put on the emission of NOx to 0.2 gram/BHP hr and PMs to 0.01 gram/BHP hr by 2010. [4] This requirement is accomplished by changes in engine designs that include retarded timing, raised piston rings, selective catalytic reduction and the use of Exhaust Gas Recirculation (EGR). [5]

EGR controls the NOx emission by recirculating exhaust gases back into combustion chamber to be burned second time, thereby reducing emission associated with health risks. In doing this, many of the contaminants from the exhaust gases end up in the engine lubrication oil. Diesel engine oil now exposed to a higher lever of contaminants such as soot, which degrades lubricating oil properties physically and chemically and thereby damage the engine parts. [2,6-8] Modern Cummins M-11 engine, have reported to contain upto ~9% soot in used oils. [9,10] This

enormous amount of soot degrades oil physically by increasing viscosity [11,12] and hence pumpability of oil to the to surfaces in the relative motion and also chemically by increasing total acid number. [1] Moreover, diesel engine equipped with EGR protocol promote higher wear of engine components such as valve train, piston rings and cylinder linings during engine test with increasing levels of EGR. [13-15] This problem is further aggravated by the EPA regulation known as SAPS where chemical limits have been imposed on the amount of phosphors (0.1wt%), sulfur (0.12wt%), sulfated ash (1wt%). [4] Since phosphorous and sulfur are major contributors in formation of anti-wear film in engine and their restriction would aggravate the wear of engine components in the diesel engine equipped with EGR protocols and put increasingly higher stresses on the lubrication oil to comply with stringent EPA mandates as well as to provide protection of engine components in harsh diesel engine environment.

1.1 Current Understanding and Research

Significant researches have been done to understand the formation of diesel soot inside the engine using simulations and other characterization methods. Various characterization techniques have been employed to understand structure and composition of “exhaust soot" obtained from exhaust tail pipe. These techniques include but not limited to X-ray Diffraction, Raman Spectroscopy, Electron Energy Loss Spectroscopy (EELS), Scanning Transmission X-ray Microscope (STXM), Near Edge X-ray Absorption Fine Structure.[16-22]

Significant efforts have been made to understand the role of crankcase soot, available inside the oil sump, to promote higher wear of diesel engine equipped with EGR. Many researchers have attempted and proposed various mechanisms. These mechanisms include (a) Abrasion of anti-wear film by soot [2,14,15,23] (b) Competition between soot and anti-wear additives to adsorbed on metal surface [24] (c) Accumulation of soot at inlet and cessation of oil supply to metal contact [25,26] (d) Adsorption of active anti wear product of lubrication oil by soot [27-30] (e) Inducing transition of metal surface from anti-wear Fe_2O_3 film to pro wear FeO film. [31] (f) EGR re-circulate SOx which promote corrosive wear. [32] These mechanisms provide phenomenological explanations of role played by soot to increase wear of diesel engine

components but a comprehensive understanding is yet to be understood to help lubricating oil formulator and engine manufacturer to optimize their product.

1.2 Objective of Research

Great deal of research has been conducted in the past to understand the soot induced wear mechanism and have provided greater insight in the subject. But several phenomena have been unanswered or have contrasting explanations about the role played by soot to promote wear. However these mechanisms have general consent on conclusion that presence of soot degrades the lubrication oil properties either physically or chemically. Since diesel engines operate under harsh conditions where presence of higher temperature and reactive decomposition products of lubricating oil increase the possibility of interaction between lubricating oil and soot. This interaction might modify soot surface and/or bulk chemically and/or structurally. Hence attempts need to be made to understand such modification, if any. Researcher have also suggested types of wear that diesel soot produce during engine operation such as abrasive wear, polishing wear, corrosive wear. There is no significant correlation that has been established between soot interaction with lubricating chemistry and types of wear.

As per author's knowledge no significant efforts have been made to characterize crankcase soot and its correlation with interaction of soot and lubrication additives. Experiments carried out by Hosunam et.al suggested the interaction of zinc dialkyldithiophosphate decomposition product and diesel soot. [33] Moreover, In fully formulated lubricating oil, the proportion of additives range from ~5-9% where anti wear additives such as ZDDP is added up to 800-1000ppm. Hence any interaction that potentially changes chemical composition of diesel soot must be very small. Understanding of this interaction would certainly help to understand changes in soot structure and chemical make up at nano scale, if any. This information can be linked with types of wear that soot produces during engine operation. This understanding, in totality, can provide better insight of wear mechanism of diesel soot.

Moreover, Previous research has hypothesized that the higher hardness of soot compare to rubbing engine components might responsible to promote wear of engine parts. But as per

author's knowledge, comprehensive fundamental understanding of the source of higher hardness is yet to be done. Moreover, soot being carbonaceous material with turbostratic structure having crystalline as well as amorphous domain. Influence of these domains on the tribological behavior has not been well understood.

Previous researches have attempted to comprehend the phenomena using various laboratory bench tests as well as controlled dynamometer tests. But no significant correlations have been made between bench test, controlled engine test, chemistries of engine oil and composition of soot.

Therefore, the main goal of this research is

"To develop fundamental understanding of soot induced wear mechanism of diesel engine by comprehensive understanding of interaction of diesel engine soot with lubricating additive chemistry and tribological evaluation of this interaction in laboratory bench test, realistic field operation diesel engine and controlled diesel engine dynamometer engine test."

Fundamental comprehension of diesel soot wear mechanism was started by characterization of the diesel soot chemically, morphologically & structurally and correlating these results with diesel soot wear behavior. The soot was extracted from drain interval used oil from commercially operated diesel engine hence represent realistic field conditions that soot experience during engine operation. X-ray Absorption Near Edge Spectroscopy (XANES) was employed as higher spatial resolution surface analysis technique for chemical characterization of diesel soot. Transmission Electron Microscope (TEM) was utilized to characterize soot structurally and morphologically. In addition synchrotron radiation x-ray diffraction and Raman spectroscopy were used to study structure and composition of drain interval soot. Four-ball wear tester was employed to evaluate wear performance of diesel soot. These results are explained in the first part of the report.

Hypothesis was proposed by speculating two phenomenological models to explain the wear behavior of diesel soot based on preliminary results of high spatial resolution spectroscopy

and microscopy in tandem and their correlation with wear results acquired from four ball bench tests.

Proposed hypothesis was consolidated by conducting laboratory experiments and actual controlled dynamometer diesel engine tests. In the laboratory scale experiments, simulation of the various conditions that diesel soot experience inside the engine was done by treating carbon black in similar condition diesel soot experiences. These treated carbon black was tested using to four ball wear tester to evaluate wear performance and then compared with wear performance of diesel soot. These treatments will determine the most responsible treatments that promote higher engine wear. Detail examination of wear surface will provide information on type of wear. Frictional behavior of controlled soot and treated carbon black was also be studied using SRV bench tests. SRV bench test is close approximation of reciprocating motion of engine components and boundary regime of lubricating surface in contact.

In second part, to consolidate the proposed mechanism, diesel soot is being acquired from various controlled dynamometer diesel engine tests. In these tests, various parameters such as loading, rpm, duration, and lubricating oil formulation are being controlled to evaluate performance of diesel engine oil in presence of diesel soot. Diesel soot in such controlled environment can provide plethora of information for comprehensive understanding of diesel soot wear behavior.

To consolidate the proposed hypothesis several experiments and characterization tools were employed such as XANES, HRTEM and Raman spectroscopy. HRTEM was employed to determine possibility of nano size particles of decomposition products of oil, which are smaller than soot particles. Raman spectroscopy was employed to study the changes in crystalline domain of soot due to dynamic environment and test parameters of engine. This report provides elucidation useful to employ XANES to characterize soot at nano scale to acquire valuable information that can be utilized to understand the proposed phenomenon.

It was expected that hypothesis will be accurately consolidated by methodical use of proposed experiments and characterization tools and by thorough scrutiny of results based on

prior fundamental knowledge on the subjects. This comprehensive report is served to explain the methodical approach, thought process and fundamental knowledge that was applied to conduct the research and achieve the objective.

1.3 Structure of the research

1.3.1 Design of Experiments to develop hypothesis

Chapter 1, Introduction: This chapter introduces the motivation and objectives behind this whole research. It also provides the readers with brief concepts about sot induced wear mechanisms and the necessity of studying wear mechanism

Chapter 2, Background: This chapter provides a detailed background on soot formation, affect of soot on the lubrication oil performance, various mechanism and modus operandi used by previous researchers. In addition, the tribological testing methods and the characterization tools and principles are reviewed.

Chapter 3 studied the morphology, Structure and Chemistry of Extracted Diesel Soot: Part I: Transmission Electron Microscopy, Raman Spectroscopy, X-ray Photoelectron Spectroscopy and Synchrotron X-Ray Diffraction Study

Chapter 4 studied the morphology, Structure and Chemistry of Extracted Diesel Soot: Part II: using X-ray Absorption Near Edge Spectroscopy (XANES) and High-resolution Transmission Electron Microscopy (HR-TEM).

Chapter 5 discussed the treatment of carbon black to simulate the composition and structure of diesel soot and its tribological evaluation Part I : Wear Assessment

Chapter 6 discussed the treatment of carbon black to simulate the composition and structure of diesel soot and its tribological evaluation Part I : Friction Assessment

Chapter 7 studied the morphology, structure and chemistry of extracted diesel soot from Mack T-12 dynamometer engine test and its correlation with tribofilm formation of piston ring

Chapter 8 studied the effect of operational parameters of diesel engine dynamometer tests on the diesel soot chemistry and tribofilm formation.

Chapter 9 discussed the comparison of NEXAFS study of diesel soot obtained from crankcase oil of field and dynamometer diesel engine

Chapter 10 summarizes the research outcomes and future direction of this research.

CHAPTER 2

BACKGROUND

2.1 Heavy Duty Diesel engine oil developments and trends

Diesel engines have always been preferred mode of ground transportation as compared to gasoline engine due to its higher thermal efficiency. This efficiency is advantageous in the midst of ever increasing fuel price. Fuel consumption reduction [4,34,35] from diesel engines compared to gasoline fueled engines is estimated to result in as much as 30–35% reduction in green- house gases. A major obstacle to the extensive application of diesel engines, especially for automotive applications, is their high level of nitrogen oxides (NOX) and particulate emissions, both of which have possible negative effects on the environment and health. For instance, NOX contributes to ground-level ozone (smog) and acid rain with the consequent detrimental effects on human health. Major efforts are being directed at development of technologies that can reduce diesel engine NOX and particulate emissions. [1].

The concern over the environment is main driving force to develop the American Petroleum Institute (API) commercial “C” diesel engine oil classification. Progressive implementation of mandates such as API CF-4, API CI-4 was used to restrict the emission of NOx and PMs. [4,35] In 2007 EPA adopted new category for diesel engine oil called API CJ-4 for both NO_X and particulate emissions with the aim of reducing emissions to 0.2 gram per brake horsepower hour (g/bhp-hr) for NO_X and 0.01 g/bhp-hr for particulate emissions by 2010 for on-road diesel engines. To further control emissions, the EPA also set lower limits on diesel fuel sulfur levels that are used for on-highway (15 ppm sulfur in 2006) and off-highway (500 ppm sulfur in 2007, 15 ppm Sulfur in 2010) applications. Consumer demand for longer lasting oils and the concern over increased engine and oil sump temperatures due to current and future engine designs to meet these emissions standards have further driven the development of new engine oil service categories.[4]

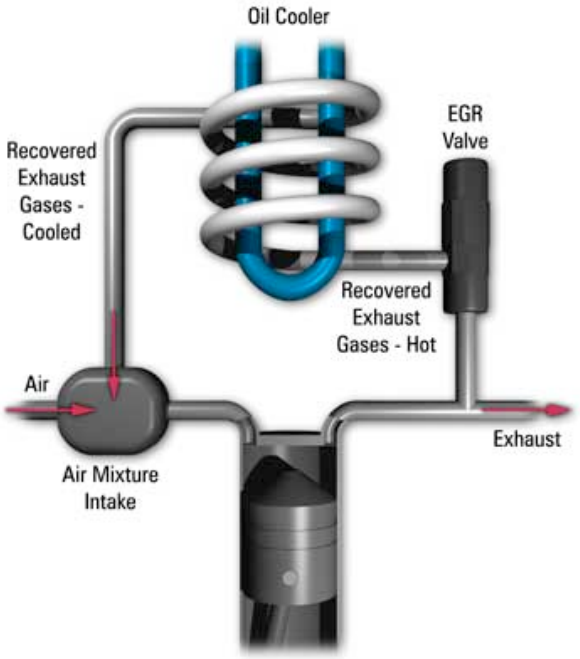

Figure 2.1 Schematic of Exhaust Gas Recirculation

Exhaust Gas Recirculation is an effective means of reducing NOX [4,36]. Higher temperature of combustion chamber of diesel engine is primary cause for formation of NOx. Recirculation of oxidized gases of exhaust reduces temperature of exhaust gas and hence formation of NOx. [1] In doing this, many of the exhaust contaminants end up in the engine lubricating oil. Diesel engine oils are now exposed to a higher level of contamination that can degrade the oil and damage engine parts. There is concern that exhaust gas recirculation can have a detrimental effect on engine durability and its effects on the oil. Oils exposed to the EGR environment show an increase in soot content, total acid number (TAN) and viscosity, while the engine and oil are both exposed to corrosive/acidic gases and solid particle buildup. Engine durability may be compromised by EGR due to acceleration of oil contamination and degradation by engine exhaust products [10-12] . The accelerated rate of lubricant oil degradation will lead to relatively short oil drain intervals. This condition goes against the current desire for an extended oil drain interval in diesel engines.

Higher level of EGR as an attempt to restrict the emission of pollution generates more

soot and experience higher peak cylinder temperature, which cause the engine to run hotter. [5] This requires improved oil technology for oxidation resistance, piston deposits, oxidative thickening, oil consumption, high-temperature stability, soot handling properties, foaming and viscosity loss due to shearing. Until 2006, amount of lubrication additives chemistries were sufficient to provide protection against the harsh environment. [5] But To ensure protection of the after treatment devices, chemical limits were set for the first time ever for heavy-duty diesel engine oils. The chemical limits for API CJ-4 target the engine oil's sulfated ash, phosphorus and sulfur content, commonly referred to as SAPS. These chemical limits include the following:[4]

- 1.00 percent maximum sulfated ash (per ASTM D874)
- 0.12 percent maximum phosphorus (per ASTM D4951)
- 0.40 percent maximum sulfur (per ASTM D4951 or ASTM D2622)

This requires paradigm shift in the engine oil technology to provide protection against the detrimental effect of contaminants (soot) due to EGR as the same time comply with EPA regulation. Thus, it is important to understand the soot induced wear mechanism of diesel engine to help lubrication additives formulators to optimize their products.

2.2 Prior state of research

Previous studies have attempted to understand the soot induced wear mechanism and have suggested various phenomenological models. Although these models have contrasting explanation among themselves but have provided the better understanding of the subject matter.

Rounds [27-30] performed tests on a four-ball wear testing machine with soot contaminated oil samples. The oil samples were obtained from a number of sources by normal oil drain process. Tests were performed on a four-ball wear testing machine using the collected samples to evaluate the oil properties in presence of soot. According to Rounds, soot did not act as an abrasive, but soot preferentially adsorbed the anti-wear additive. This was the plausible reason he provided for the wear taking place in a diesel engine. He concluded that ZDP was the

most effective anti-wear additive in the presence of diesel soot. He also performed hardness tests on soot and alumina, which is a known abrasive. Rounds disagreed with the concept that soot removed the surface coating by abrasive phenomenon, since the hardness of soot is lower than the hardness of alumina. He also suggested that engine load and EGR have a large effect on the soot pro-wear characteristics. Many authors have disputed the adsorption theory proposed by Rounds.

Ryason et al. [37] performed wear tests on a ball-on flat- disk tribometer using carbon black and steel balls made of AISI 52100 steel. Wear tests were performed on carbon black, alumina and silica. Investigations were carried out on the wear scars from the tests using scanning electron microscope (SEM) and electron probe microanalysis. The SEM pictures showed that the scars on the surfaces of the balls worn in the presence of oils containing carbon black, alumina and silica were similar, and differ from that of the ball worn in the presence of oil alone. Ryason concluded that the wear that occurred was polishing in nature. He also suggested that although the wear was abrasive in nature, the cutting of the material did not take place. The soot particles ploughed through the surface, forming a groove with a smooth curved cross-section, depressed at the center and raised at the edges.

Nagai et al. [15] performed tests on valve train and studied the wear in the presence of soot. They concluded that the wear of cam noses and rocker arm tips was found to increase significantly with the increase in EGR rate. The drain oil analysis at the end of each EGR test run indicated evidence of elements such as zinc and phosphorous. This contradicted the adsorption theory proposed by Rounds initially. Tests were also performed on four-ball wear testing machine and it was concluded that, soot strips off the anti-wear film formed on the lubricated metal surface and the subsequent metallic contact accelerated the wear process. They also concluded that soot might change to a very hard particle under the high-pressure conditions and might be abrasive to the metal.

Berbeizer et al. [24] investigated the role of carbon black on mild lubricated wear. The test setup they used involved a plane-on- plane tribometer to simulate lubricated mild wear

between ring, cylinder and particles in suspension. They conducted a systematic study of carbon black parameters on mild wear by evaluating special test blends in which different types of commercial carbon black were used as model compounds. They concluded that bore polishing is influenced more by the size, nature, and concentration of carbon black rather than by the products of oil degradation. They suggested that decreasing the amount of carbon black reaching the piston or suspension in the lubricant could reduce bore polishing. Bore polishing can also be reduced by reducing the elementary carbon black particles, or by completely changing the microstructure of graphitized carbon. These modifications were only feasible if the combustion parameters such as temperature, gas oil additives or the lubricant additives were changed. They also suggested that abrasive wear is not the sole factor contributing to increased wear, but two other important phenomena also play a role in increasing wear: a decrease of the surface coverage rate by ZDP molecules due to physical adsorption of carbon black on the surface, and a subsequent modification of the physical and mechanical properties of the reaction film by the introduction of carbon in their composition.

Kim et al. [25] conducted experiments using a statistically designed oil test matrix to investigate both oil viscosity and diesel engine oil additive components. They investigated the effects of oil formulations on diesel engine valve train wear. They concluded that laboratory wear tests could properly differentiate the anti-wear performance provided by different engine oils. They concluded that an anti-wear additive film must form on the metal surface to reduce wear. The anti-wear properties of the diesel engine oil could be improved by increasing the ZDP concentration. It was also suggested that improved specifications were needed, as the existing diesel engine oil specifications were not adequate to protect every engine.

Ratoi and Spikes [38] investigated the main factors that determine the impact of soot on friction and ZDDP film formation in formulated oils. Carbon black was used as a soot analogue for their studies. They concluded that dispersed carbon black rapidly removed ZDDP reaction films by abrasion, which could be prevented by using appropriate dispersant additives. Chinas-Castillo and Spikes [39] studied the behavior of diluted soot containing oils in lubricated contacts. Carbon

black colloid, lampblack colloid, and used engine oil were used for their study. Ultra-thin film interferometry and image analysis techniques showed that soot colloid particles are entrained in the lubricated contact inlets where they can influence the friction and wear characteristics of the base stock. The study showed that the entrainment of soot particles occur at slow speeds, affecting the film characteristics of clean engine oils and the process is more pronounced at high temperatures.

Needelman and Madhavan [40] studied the effect of lubricating oil components, and nature of contamination on engine wear. They proposed the chain-reaction of wear and conducted a survey of engine oil contamination and the necessary improvements that had to be accomplished to reduce this contamination. They concluded that contamination of the lube oil causes wear of engine components and also suggested that, a special relationship is present between the size of the contaminant particles and the thickness of dynamic oil films. The contaminant particles larger than the oil film cause wear of engine components by making simultaneous contact with both the surfaces.

Cadman and Johnson [2] studied the effect of EGR on engine wear using analytical ferrography technique. The collected oil samples from the engine were analyzed for metal wear debris using analytical ferrography technique. A 15% EGR showed a significant increase in the concentration of the wear particles. Equilibrium particulate concentrations with 15% EGR were 10 times higher than normal baseline levels. They also believed that soot acts as an abrasive to remove the anti-wear surface coating provided by the additives in the lubricant.

Corso and Adamo [31,41] suggested that soot contaminants interact with the adsorption/chemisorption mechanism of ZDP on metal surfaces inducing a transition from anti-wear Fe3O4 to pro-wear FeO. This transition apparently occurs due to the presence of soot in the lubricant limiting the access of oxygen to the metal surfaces.

Akiyama et al. [32] studied the phenomena of abnormal cylinder wear in EGR equipped diesel engines. They concluded that the cylinder wear of a diesel engine, which is equipped with EGR, increases at low temperatures and suggested that the abnormal wear may be due to

corrosion of cast iron. Corrosion of cast iron is due to formation of sulfuric acid formed when condensed water reacts with the combustion SO*x* (oxides of sulfur). However, this may not be the primary reason for engine wear as the sulfur content in diesel engines has been reduced to 0.05 wt.%.

Gautam et al. [14,40] investigated the effects of soot contaminated engine oil on three-body wear. Phosphorous level, dispersant level and sulfonate substrate level were the three oil additives they tested and concluded that there is an interaction between oil additives and soot in reducing the oil's anti-wear properties. They also concluded that wear increases with higher soot concentration and decreases with higher phosphorous concentration. They also performed tests on the ball-on-flat-disk setup with soot and alumina and compared their wear ratios. It was concluded that abrasion could be the major mechanism involved in the diesel engine wear.

Gautam et al. [40] also investigated the effects of base stock, dispersant level, and ZDP level on three-body wear. The study considered soot at two levels and hence could not determine the non-linear effect of soot on three-body wear. Results indicated that the oil's anti-wear properties were reduced as a result of soot. The statistical analysis led to the conclusion that base stock and dispersant levels were significant on oil's wear performance, while the effect of ZDP was negligible within the range of concentrations tested. Ball-on-flat-disk tests showed that the wear scar diameter as a result of soot was similar to that due to alumina indicating that the wear due to soot is abrasive in nature. EDAX (energy dispersive X-ray analysis) tests performed on soot samples showed that there was no adsorption of anti-wear agents by soot.

2.3 Formation of soot

Diesel soot is the finer particle produced during the high temperature pyrolysis or combustion of diesel fuel. Advances in the understanding of soot formation in diesel combustion systems during the recent have accepted that soot formation steps can be summarized as (1) formation of molecular precursors of soot, (2) nucleation or inception of particles from heavy polycyclic aromatic hydrocarbon molecules, (3) mass growth of particles by addition of gas phase molecules, (4) coagulation via reactive particle-particle collisions, (5) carbonization of particulate

material, and, finally, (6) oxidation of polycyclic aromatic hydrocarbons and soot particles. [42-45]

It is obvious that the formation of soot, i.e., the conversion of a hydrocarbon fuel molecule containing few carbon atoms into carbonaceous agglomerate containing some millions of carbon atoms, is an extremely complicated process. It is a kind of gaseous-solid phase transition where the solid phase exhibits no unique chemical and physical structure. Therefore, soot formation encompasses chemically and physically different processes, e.g., the formation and growth of large aromatic hydrocarbons and their transition to particles, the coagulation of primary particles to larger aggregates, and the growth of solid particles by picking up growth components from the gas phase.

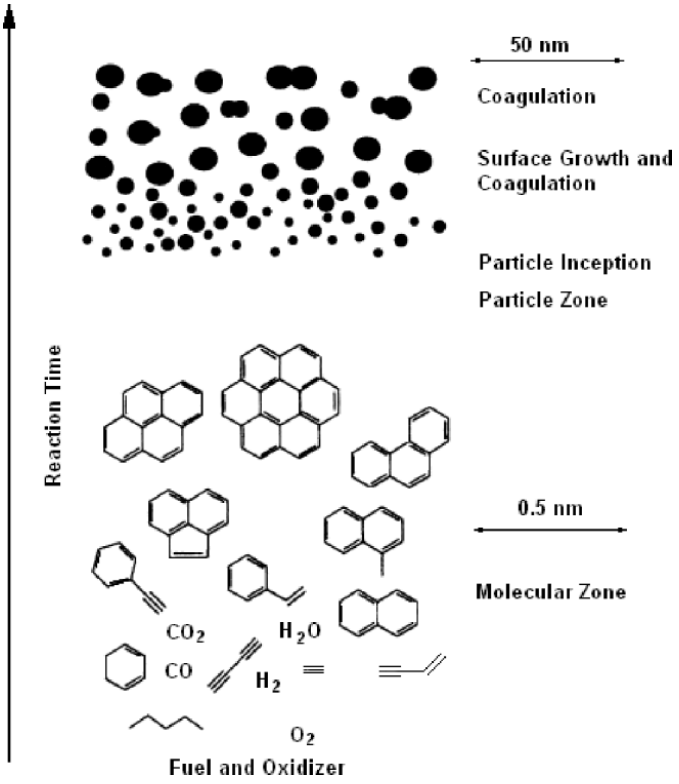

Figure 2.2 schematic reaction path leading to soot formation

Fig. 2.2 depicts a schematic reaction path leading to soot formation. According to the depiction given in Fig. 2.2, the hydrocarbon fuel is degraded during oxidation into small hydrocarbon radicals. The latter adds hydrocarbon radicals for growth and the growing

unsaturated (radicalic) hydrocarbons form aromatic rings when they contain a sufficiently large number of carbon atoms. The formation of larger aromatic rings occurs mainly via the addition of acetylene. All these processes occur within molecular length scales. The growth in the third dimension is supposed to happen by coagulation of larger aromatic structures forming primary soot particles. These primary particles quickly coagulate, simultaneously picking up molecules from the gas phase for surface growth. Surface growth contributes a major part in determining the final soot concentration in sooting flames, while coagulation – switching the length scales to particle dimensions determines the final size of the soot particles.[44-46]

The irregular aggregate structure of soot particles is also attributed to coagulation. Although many important details of polycyclic aromatic hydrocarbon molecules (PAHs) and soot formation remain poorly understood, there is considerable agreement on the general features of the processes involved, which are summarized above.

Soot is found to be in the form of necklace-like agglomerates, which are around 100 nm in size. These agglomerates are composed of collections of smaller, basic particle units that are spherical or nearly spherical. Soot clusters may contain as many as 4000 spherules. The size of the spherules varies in diameter from 10–80 nm, but mostly lies between 15–50 nm. The surface of the spherules has adhering hydrocarbon material or SOF and inorganic material (mostly sulfates). The spherules are called “primary soot particles” and the cluster like or chain-like soot aggregates are defined as “secondary particles”, which are composed of several tens to hundreds of primary spherical particles.

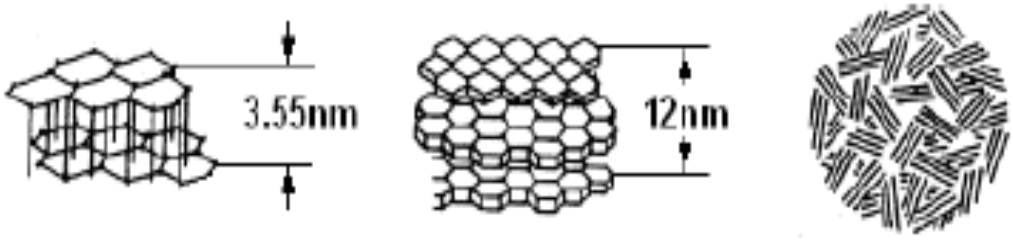

Platelets Crystallite Particles

Figure 2.3 Substructure of soot particles

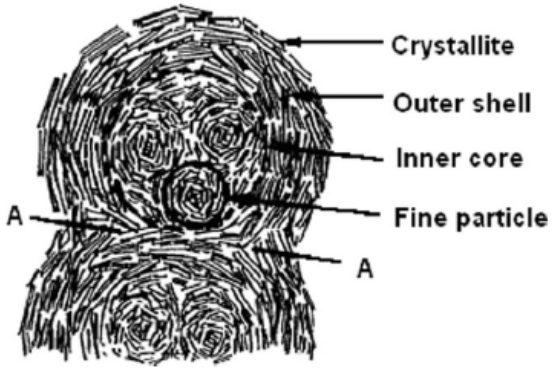

Figure 2.4 Schematic of primary particle of soot

A primary particle contains 105–106 carbon atoms. In general, diesel soot showing particles consisting of clusters of spherules. Viewing the spherules by transmission electron microscopy (TEM) reveals laminations with surface steps, which are produced by numerous, concentric crystallites. In diesel soot, carbon atoms of a primary soot particle are packed into hexagonal face-centered arrays, commonly referred to as platelets. Platelets are arranged in layers to form crystallites and there are typically two to five platelets per crystallite. The mean layer spacing is 3.55 nm, only slightly larger than that of graphite. The thickness of crystallites is about 12 nm and there are of the order of 103 crystallites per primary soot particle. The crystallites are arranged in turbostratic fashion, with their planes more or less parallel to the particle surface. Dislocations of five- and seven-member rings produce surface wrinkling. The platelet model mentioned above applies to the outer shell. However, the inner core contains fine particles with a spherical nucleus surrounded by carbon networks with a bending structure. This indicates that the outer shell, composed of graphitic crystallites, is of a rigid structure, while the inner core is chemically and structurally less stable due to the thermodynamic instability of its structure. [44-46]

2.4 Tribological wear tester

To understand the tribological behavior of test formulations two tribo bench testers have used. The four ball wear tester and SRV (Schwingun / Reibung / Verschleiss) tester to comprehend the behavior of test formulations in different test configuration. A four-ball wear

tester is used for making preliminary evaluation of the anti wear properties of lubrication oil in sliding contact by means for four balls. A SRV is used to evaluate the lubricating oil's coefficient of friction when subjected to high frequency linear oscillation motion. The wear and friction results in totality can give better insight about the tribological behavior of the formulations.

2.4.1 Four Ball Wear test conditions and procedure

Three ½ inch diameter steel balls are clamped together and covered with the formulation to be evaluated. A fourth ½ inch diameter steel ball referred as top ball is pressed with force of 20 kgs into the cavity formed by the three clamped balls for three point contact. The temperature of the test lubricates is regulates at 75° C and then top ball is rotated at 1200 rpm for 60 min.

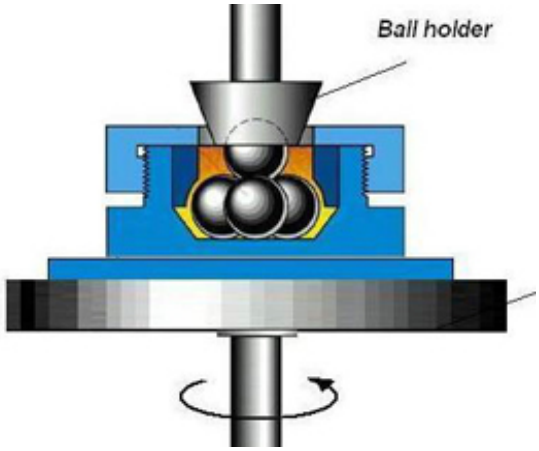

Figure 2.5 Schematic of Four Ball Test Configuration

Testing formulations are compared using average size of the scar diameter worn on the three lower clamped balls. To measure the wear scar diameter three clamped balls were removed from their clamped position. Wear scar were wiped. Two measurements were made on each lower clamped ball at 90 degree to each other. If wear scar were elliptical, then first measurement was made in direction of striations and other was made across the striations. An average of 6 wear scars readings is reported as scar diameters.

2.4.2 SRV friction test conditions and procedure

A SRV test were performed on using oscillating cylinder at constant frequency of 50 hz and stroke amplitude of 11 mm under the constant load of 220 N against the test disk that had been submerged with testing lubricating oil formulation. A testing disk was attached to platform which was held at constant temperature of 75° C. Both reciprocating cylinder and clamped disk were made from 52100 steel. The test configuration yields hertzian line contact geometry. The test was run for 60 mins, once test was finished, the friction force is measured by peizo electric devices in the test disk assembly and recorded as function of time.

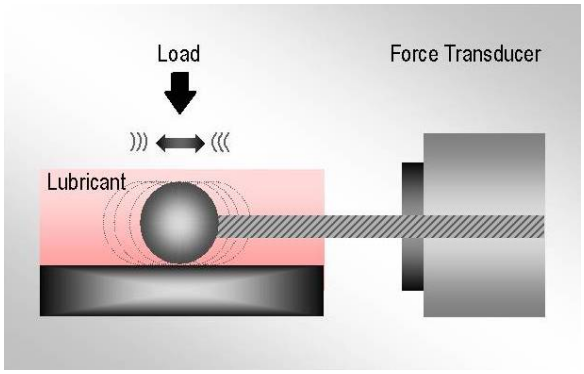

Figure 2.6 Schematic of SRV Friction Test

2.5 Diesel Soot Extraction

Used diesel engine oil was acquired from Freightliner diesel engine oil changing facility. The used engine oil was collected from the sump during the drain interval from a single diesel engine and was diluted using hexane as solvent in 50 wt.% dilution. The mixture was centrifuged at 12000 rpm for 2 hours. The supernatant was discarded and remaining residue of soot was washed with hexanes, which was followed by centrifuging at 12000 rpm for 2 hours. This process was repeated until oil is removed completely. To avoid the possibility of any trapped oil molecules a Soxhlet extraction method was used where extraction was carried out for 48 hours using hexanes as solvent. The extracted soot was dried and ground for further analysis.

2.6 Transmission Electron Microscopy

A JEOL 1200 EX STEM 120 kV, having a 0.34 nm point resolution, equipped with an EDAX Energy Dispersive X-ray spectrometer (EDS), was employed to study structure, morphology and composition of soot. Selected Area Diffraction Pattern (SADP) was used to probe structural information. SADP of diesel soot was compared with carbon black to determine possible structural change. EDS was used to acquire compositional information. Extracted soot was spread onto copper grid to load inside the TEM chamber for further characterization. High resolution transmission electron microscopy of the diesel soot was also conducted using a Hitachi H-9500 microscope operating at an accelerating voltage of 300 kV with a lattice resolution of 0.18 nm.

2.7 Surface Area Analysis

Surface area of the soot and carbon black were analyzed by the BET nitrogen physisorption method using a Micrometrics Instrument Corporation instrument.

2.8 X-ray Photoelectron Spectroscopy

A Perkin-Elmer Phi 560 X-ray Photo-electron Spectroscopy was employed to probe compositional characterization of soot. XPS has also been employed to validate the results of EDX TEM. Al Kα X-ray (hv = 1486.6 eV) was used for excitation radiation operated at 14 kV and 300 watts. The vacuum was maintained below 6 x 10^{-7} torr during spectrum acquisition. A wide survey scan spectra was first acquired, followed by high resolution scans of P 1s, S 1s, Ca 1s and Zn 1s.

2.9 X-ray Absorption Near Edge Spectroscopy (XANES)

X-ray absorption near edge spectroscopy (XANES) is a non-destructive technique to chemically characterize the surface at nanometer scale. [47,48] It employs high-energy soft x-ray photon from synchrotron radiation. In XANES, an X-ray beam is directed to a probe, and the X-ray energy is scanned. If an X-ray photon has sufficient energy to excite a core level electron of an atom in the probe, a photoelectron is created and will leap into unoccupied states. The X-ray photon is absorbed and cannot be detected anymore. However, transmitted beam intensity and

incident beam intensity can be monitored with detectors during energy scan. The logarithm of the intensity ratio of the XANES spectrum contains the some characteristic absorption edges and shifts. This absorption edge can be used as fingerprint to identify the chemical make up of surface. This x-ray absorption technique has capability to probe local environment surrounding atom and its oxidation state. The identification of compounds on the surface can be done by comparison of spectra of diesel soot with various model compounds one can identify the structure of chemical species in soot. More information on XANES can be found else where.

2.9.1 Data Acquisition of XANES

X-ray absorption spectra were obtained for carbon, boron, phosphorous, sulfur, zinc, iron, oxygen and calcium. XANES experiments were carried out at Canadian Light Source, Saskatoon, Canada having 2.9GeV storage ring as well as at Synchrotron Radiation Center, Madison, WI having 800 MeV and 1 GeV storage ring. Three beam lines were used at Canadian Light Source to obtain K and L shell absorption edge. Phosphorous, sulfur and calcium K absorption edge is recorded using Soft X-ray Micro-characterization Beam line (SXRMB) covering region of 1700-10000 eV with photon resolution of 0.2eV and beam spot size of 300μm x 300μm. Phosphorus & sulfur L-edge spectra were obtained using Variable Line Grating-Plane Grating Monochromator (VGM-PGM) beam line covering region of 5-250eV with photon resolution of 0.2eV. The PGM beam spot size is 500μm x 500μm. Zinc L edge spectra were obtained using Spherical Grating Monochromator (SGM) beam line that covers the energy range between 250-2000eV with photon resolution of 0.2eV in 1000μm x 100μm spot size. XANES spectra were acquired in Total Electron Yield (TEY) mode and Fluorescent Yield (FLY) mode. Double Crystal Monochromator (DCM) beamline have been employed at Synchrotron Radiation Center to probe phosphorous and sulfur K edge. DCM beam line covers 1500- 4000 eV with spot size 2mmx 2mm. Calcium L edge were obtained at the Synchrotron Radiation Center (Wisconsin, Madison) using HERMON beam line covering 64-1400 eV with 0.2 eV resolution.

2.10 High-resolution Transmission Electron Microscopy

High-resolution transmission electron microscopy of the diesel soot was conducted using a Hitachi H-9500 microscope at an accelerating voltage of 300 kV with a lattice resolution of 0.18 nm. High-resolution lattice images of crystalline nanoparticles were acquired. Selected area diffraction patterns were acquired from selected regions coupled with energy dispersive spectra using x-rays to determine the chemical makeup of different regions within the soot particles.

2.11 Synchrotron radiation X-ray Diffraction

X-ray diffraction (XRD) patterns were collected both on a traditional laboratory diffractometer (Rigaku PMG, XRD lab at University of Trento) and at the MCX beamline at the Italian synchrotron radiation (SR) facility (ELETTRA at Trieste). The bending magnet beamline MCX has an energy range of 8 – 23 keV with an energy resolution ($\Delta E/E$) of 2×10^{-4} and a photon flux of 10^{11} photons/second.

The high brilliance and high angular resolution of synchrotron radiation (SR) allows identification and characterization of the minor components present on the soot. SR also allows photon energy tuning, therefore it is possible to perform measurements below and above the Zn absorption edge to better characterize the decomposition products, if any. SR X-ray diffraction of soot and carbon black were conducted at 9.4 keV and 10 keV, which lie below and above the Zn K-absorption edge.

2.12 Raman Spectroscopy

The Raman spectrometer used for the study was a Thermo scientific DXR spectrometer using diode pumped solid-state type laser as a source of illumination. The collection system was used in backscattered configuration. The samples were analyzed without any sample preparation by visualizing the sample using 10x microscope objective lens. To record the Raman spectra a solid-state laser was used with a frequency of 532 nm with maximum power output of 10 mW. It was necessary to use low laser power to avoid excessive sample heating. For this study a laser power of 1 mW was used. The laser spot diameter was 2 μm with 25μm slit size, for the fully focused laser beam. The spectral resolution was 5 cm^{-1} at 532 nm with wavelength range from 50

cm^{-1} to 3500 cm^{-1}.

A dense layer of soot with a thickness of one millimeter was pressed with steel spatula onto a glass slide. This creates a macroscopically smooth surface. The sample holder is placed under a microscope and focused using white light. This white beam is then replaced with laser beam to acquire the spectra. Curve fitting for the determination of spectral parameters was performed with software program OriginLab. Curve fitting was executed by combination of various line shape. Best fit of the curve was accomplished without fixing or limiting the range of any spectral parameters during iteration.

2.13 Diesel engine dynamometer tests

2.13.1 Mack T 8 A

The Mack T-8A procedure, which simulates field-service, heavy-duty operation, stop-and-go operation, and high-soot loading, evaluates the soot-handling capability of engine crankcase oil with regard to viscosity. The tests utilize a Mack E7-350 mechanically governed diesel engine with turbocharger, four cycle EGR equipped diesel engine. Tests are conducted on a flush-and-run format - with a warm-up, a 2-h flush for each test, and then a constant speed and fuel rate input for the duration of the test. Typically, the engine is rebuilt before a reference (calibration) test. The T- 8A test is 150 hours in duration, specified in the CF-4 category. [49]

2.13.2 Mack T 11

The Mack T-11 procedure evaluates the soot handling performance, as measured by viscosity increase, of lubricating oils operating in diesel engines equipped with cooled exhaust gas recirculation. The Mack T-11 test involves the use of a Mack E-TECH V-MAC III diesel engine with Exhaust Gas Recirculation (EGR). Two 30-min oil flushes are followed by a 252-h test at constant speed and load conditions. The V-MAC III consists of an electronically controlled fuel injection with six electronic unit pumps, using 2002 model year cylinder heads. It is an open chamber, in-line, six-cylinder, four-stroke, turbocharged, charge air-cooled, and compression ignition engine. The bore and stroke are 124 by 165 mm (4 7/8 X 6 1/2 in.), and the displacement is 12 L (728 in3). This test was developed to evaluate the viscosity increase and soot

concentration (loading) performance of engine oils in turbocharged and intercooled four-cycle diesel engines equipped with EGR. [49]

2.13.3 Mack T 12

The Mack T-12 is a procedure that evaluates an oil's ability to minimize wear of the cylinder liner, piston rings and bearing wear following in engines with exhaust gas recirculation (EGR).

The Mack T-12 is part of the API CJ-4 performance category of engine oil procedures, and it simulates heavy-duty, on-highway truck operations after 2007.The Mack T12 test uses a Mack E-TECH V-MAC III diesel engine with Exhaust Gas Recirculation (EGR). A warm-up and a 1-h break-in are followed by a two phase test consisting of 100 h at 1800 r/min and 200 h at 1200 r/min, both at constant speed and load conditions. This test method was developed to evaluate the wear performance of engine oils in turbocharged and inter-cooled four-cycle diesel engines equipped with EGR and running on ultra-low sulfur diesel fuel. [49]

2.13.4 Cummins ISB

The Cummins ISB procedure is used to evaluate a crankcase lubricant's ability to reduce camshaft lobe and valve train wear. This procedure simulates repetitive cyclic operation found in the field with engines configured to meet 2007 emissions regulations. The Cummins ISB test method is a 350-hour test developed to evaluate the durability and reliability of the camshaft and tappet interface when run with different lubricating oils. The test method utilizes a modern medium-duty diesel engine equipped with exhaust gas recirculation. The test method uses a 2004 EPA emission compliant Cummins 5.9L ISB diesel engine. Test duration is 350 hours in two stages. During the 100 hours stage A, the engine is operated with retarded fuel injection timing to generate excess soot. During the 250 hours stage B, the engine is operated at cyclic conditions to induce valve train wear.

Prior to each test, the engine is cleaned and assembled with new overhead valve train components. All aspects of the assembly are specified. A forced oil drain, an oil sample, and an oil addition are performed at the end of each 25-hour period for the first 100 hours of the test. Oil

samples are taken every 50 hours. Oil additions are not made during the last 250 hours of the test cycle. Oil performance is determined by assessing crosshead wear, tappet weight loss, and cam profile wear at 3.25% soot. [49]

2.13.5 Cummins ISM

The Cummins ISM procedure is used to evaluate a lubricant's effectiveness at reducing soot-related wear of overhead components, sludge, and oil filter plugging. High-load, heavy-duty field conditions with high soot and exhaust gas recirculation (EGR) flow rates using a 2007 emission-compliant engine are simulated. The Cummins ISM test method assesses the performance of engine oils, to control engine wear and deposits under heavy-duty operating conditions selected to accelerate soot generation, valve train wear, and deposit formation in a turbocharged, after cooled four- stroke-cycle diesel engine equipped with exhaust gas recirculation hardware. This test method uses a 2002 Cummins ISM diesel engine. Test duration is 200 hours in four 50-h stages. During stages 1 and 3, the engine is operated with retarded fuel injection timing and is over fueled to generate excess soot. During stages 2 and 4, the engine is operated at conditions to induce valve train wear. [49]

2.13.6 Roller Follower Wear Test (RFWT)

The roller follower wear procedure simulates commercial and military applications. It determines the effects of lubricating oils on camshaft roller follower axle wear. The test engine is a General Motors 6.5-liter, indirect-injected diesel. The engine is rated at 160 horsepower at 3,400 rpm and is run at 1,000 rpm with near maximum load for 50 hours without an oil change.

Make-up oil is added at 25 hours. Oil gallery and coolant-out temperatures are controlled to 120°C. New roller followers are installed at the beginning of each test. At test end, the roller follower axles are removed and their wear is measured using a linear profilometer. Samples are taken at 25 and 50 hours. The used lubricant is analyzed for Viscosity at 40°C, Viscosity at 100°C, Total base number (TBN),Wear and additive metals as specified. [49]

CHAPTER 3

MORPHOLOGY, STRUCTURE AND CHEMISTRY OF EXTRACTED DIESEL SOOT: PART I: TRANSMISSION ELECTRON MICROSCOPY, RAMAN SPECTROSCOPY, X-RAY PHOTOELECTRON SPECTROSCOPY AND SYNCHROTRON X-RAY DIFFRACTION STUDY

3.1 Introduction

Exhaust Gas Recirculation (EGR) is one of the most effective post combustion protocols that heavy-duty diesel engine manufacturers have adopted as an effort to reduce emission of NOx and to comply with stringent emission norms API CJ 4 imposed by EPA. [1,4] One of the undesirable effects of EGR is the accumulation of soot and transfer of highly reactive acidic materials to crankcase oil resulting in increased wear of power train components, piston cylinder and piston rings. [15,50] This puts increasingly greater stress on the functionality of lubrication oil to handle soot accumulation and adverse effect of corrosive products transferred from EGR. This problem is further aggravated by the EPA regulation known as SAPS where chemical limits have been imposed on the amount of phosphorous (0.1wt%), sulfur (0.12wt%), sulfated ash (1wt%). [4] Since phosphorous and sulfur are major contributors in formation of anti-wear film in engine, their restriction would aggravate the wear of engine components in the diesel engine equipped with EGR protocols. This requires lubricating additives manufacturers to optimize their products to sustain the stringent and conflicting demands of chemical limits of main anti-wear elements while maintaining longer drain interval at the same time comply with EPA pollution norms.

Many studies have contributed significantly to understand this problem and various mechanisms have been proposed to explain the soot induced wear of diesel engine components equipped with EGR. [1,11-14,23-25,31,32,39-41,51-59]. Although these mechanisms have contrasting explanation of the role played by soot to induce wear they have also established that the presence of soot degrades the lubrication oil properties physically and/or chemically.

Diesel engines operate under harsh conditions where presence of higher temperature and reactive decomposition products of lubricating oil increase the possibility of interaction between lubricating oil and soot. These interactions with reactive compounds might be responsible for adsorption of decomposition product on the soot structure. In addition, there also exists the possibility of modification in crystalline structure of diesel soot. Studies have suggested that three body wear condition are present when soot particles are trapped between two surfaces in relative motion. [10,15,27-30,37,38,50,60-62] Hence, it is possible that during three body wear, trapped diesel soot between two rubbing components experience extremely high local temperature and pressure that might induce modification in crystalline and/or amorphous domains of carbonaceous soot. It has also been shown that the higher hardness of soot particle compared to diesel engine component is another factor responsible for increased wear. [53] This higher surface hardness of the soot particles can possibly be due to changes in the turbostratic structure.

Previous studies have demonstrated similarity in structure and morphology of various commercial carbon blacks and soot obtain from various sources such as coal, exhaust tail pipe, burner etc. [53] Hence, In addition, the mechanism of synthesis of soot particle and carbon black particle also differs significantly. Soot is formed by high temperature pyrolysis of diesel fuel and its morphological parameters depend upon various combustion chamber parameters. On the other hand, carbon black has been manufactured by thermal oxidative decomposition of hydrocarbons and its morphological characteristics are controlled by choice of feedstock and process conditions. [63] This might induce some morphological differences between soot and carbon black. Hence BET nitrogen physisorption method has used to measure surface area of soot and carbon black. In the present study, a suitable carbon black was used for the comparison.

Structure and morphology of “Exhaust Soot” obtained from tail pipe has been well documented. [22,53,63] but there is limited knowledge about soot recovered from crankcase oil. Hence, the objective of this study was to determine the structural, morphological and

compositional characterization of crankcase soot and to examine the modification, if any. Energy dispersive x-ray spectroscopy (EDX) using TEM, bright field TEM together with selected area diffraction, x-ray photoelectron spectroscopy (XPS) and synchrotron x-ray diffraction and Raman spectroscopy were used to characterize the extracted soot.

This study is split into two parts. This study details the structural, morphological and chemical characterization of diesel soot while the companion study uses XANES spectroscopy to examine the local coordination of different chemical species in crankcase soot together with lattice imaging using high resolution transmission electron microscopy

3.2 Results and Discussion

3.2.1 Transmission Electron Microscopy analysis of Diesel Soot

Transmission electron microscopy was employed to probe the structural, morphological and chemical characterization of extracted soot. Figure 3.1(a) is a bright field transmission electron micrograph of the carbon black that shows very little agglomeration and primary particles that range in size from 20-50 nm. TEM images of carbon black also show the presence of a few agglomerates in the size range of 200-500 nm and a few larger primary particles as well in the size range of 150-200 nm. These agglomerates are composed of collection of smaller basic particle units that are spherical or nearly spherical as shown in Figure 3.1(a). Figure 3.1(c) is the bright field TEM image of diesel soot which shows significant agglomeration of the primary particles, the agglomerates range in size from few hundred nanometers to some that are as large as 1 μm in size. However, the primary particles of diesel soot vary in diameter from 20-30 nm while primary particles of carbon black vary from 20- 50 nm.

Significant research has been done to understand the internal structure and morphology of carbon black.[18,22,64] The primary particle is comprised of crystalline and amorphous domains. The crystalline domain is packed into hexagonal closed packed array, similar to graphite but in a turbostratic fashion. This graphite like crystalline domain typically consists of 3 – 4 graphene layers called platelets. Typically 4 to 5 Platelets are arranged in form of layer to make crystallites. Crystallite with interlayer distance of about 3.5 Å, which is regarded as highly,

disordered graphitic structure or turbostratic structure. Earlier studies have suggested the structural and morphological similarity between carbon black and soot obtained from various sources but with significant variation in particle size and agglomeration. [20]

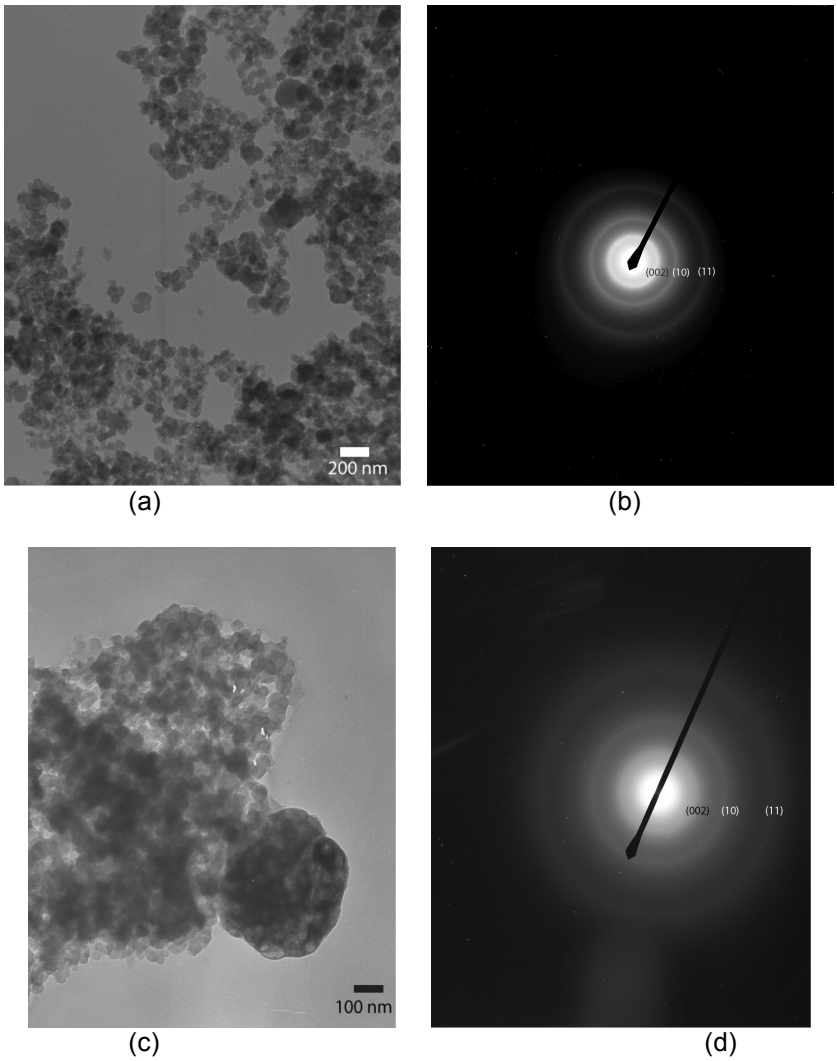

Figure 3.1 (a) Bright field transmission electron micrograph of carbon black. (b) Selected area diffraction pattern of carbon black (c) Bright field transmission electron micrograph of diesel soot (d) Selected area diffraction pattern of diesel soot

In addition, carbon black is predominantly carbonaceous (>90%) and presence of other elements such as oxygen, hydrogen does not contribute to diffraction phenomena. Owing to these facts, carbon black has been used as reference material for comparison of structural changes in diesel soot.

Selected area diffraction in the TEM was used to probe the structure of carbon black and diesel soot. The SAD for carbon black is shown in Figure 3.1(b) and that for diesel soot is shown in Figure 3.1(d). Diffraction pattern of carbon black have three intense rings arising from (200) basal planes, (10) prism and (11) pyramidal planes. The diffraction patterns primarily arise from crystalline portion of the turbostratic structure. The d-spacing of the planes that give rise to the rings were calculated from the electron diffraction patterns and is shown in Table 3.1. In addition shown in the table are the ratios of the d-spacing. Close agreement in radii and radii ratio suggests that SAD of diesel soot is primarily originating from crystalline domains of carbonaceous material of primary particles and is very similar to carbon black.

Table 3.1 d-Spacing measurement for electron diffraction patterns for carbon black and diesel soot

	1^{st} Ring d spacing (R1)	2^{nd} Ring d spacing (R2)	3^{rd} Ring d spacing (R3)	R2/R3	R1/R3
Carbon Black	0.361 nm (002)	0.209 nm (10)	0.121 nm (11)	1.71	2.93
Diesel Soot	0.367 nm (002)	0.221 nm (10)	0.127 nm (11)	1.70	2.91

A detailed examination of the structure of soot was undertaken using high-resolution transmission electron microscopy. Figure 3.2 is a bright field HR-TEM image of diesel soot that clearly illustrates the turbostratic structure. Individual particles of the turbostratic structure range in size from 10-30 nm in diameter. The individual graphene layers are stacked atop each other in a circular fashion. Regions marked as T correspond to the turbostratic structure while regions marked A correspond to amorphous carbon. This structure is very similar to earlier studies conducted on carbon black. [18,20] This result suggests insignificant changes in the turbostractic structure of diesel soot due to interaction between lubrication additives

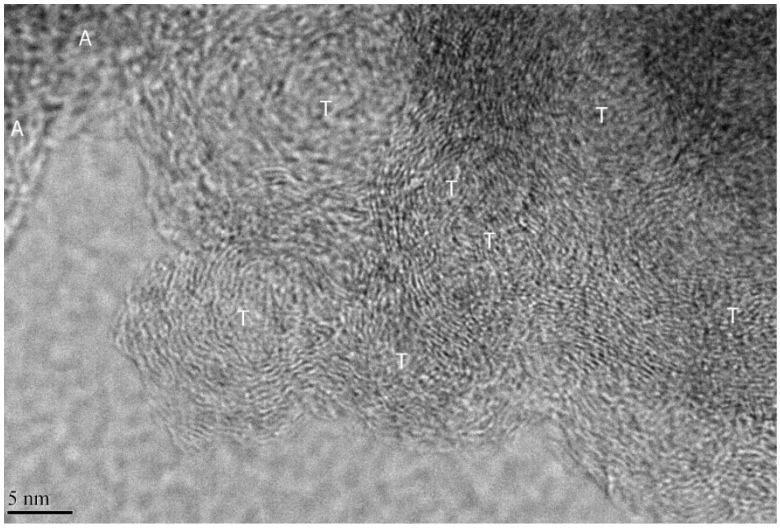

Figure 3.2 High-resolution bright field transmission electron micrograph of diesel soot showing turbostratic and amorphous regions

Diesel soot is produced during the high temperature pyrolysis or combustion of hydrocarbon and is composed of primarily carbon and other elements such as hydrogen and oxygen are present in very small amounts. [53] One of the objectives of the present study was to understand the possibility of interaction between lubrication oil additives chemistries and diesel soot. Moreover, diesel soot experiences harsh diesel engine environment and reactive decomposition products of lubricating oil might change its chemical make up. Hence, Energy dispersive X-ray spectroscopy was used as a preliminary characterization tool to determine the chemical composition of diesel soot. EDS spectra were acquired from multiple regions of the soot including agglomerates as well as regions that contain dispersed turbostratic structure.

Figure 3.3(a) is from one of the agglomerated regions that show the presence of C from the turbostratic structure as well as presence of Ca, P, S, Zn and O. On the other hand spectra from a dispersed soot region shown in 3(b) shows primarily the presence of C with a little bit of O. Figure 3.3(c) shows another EDS spectra from a small agglomerate that shows the presence of Ca, S, O and C but no P and Zn. The Cu peak in all three spectra originates from the copper grid used to mount the soot particles in the TEM stage.

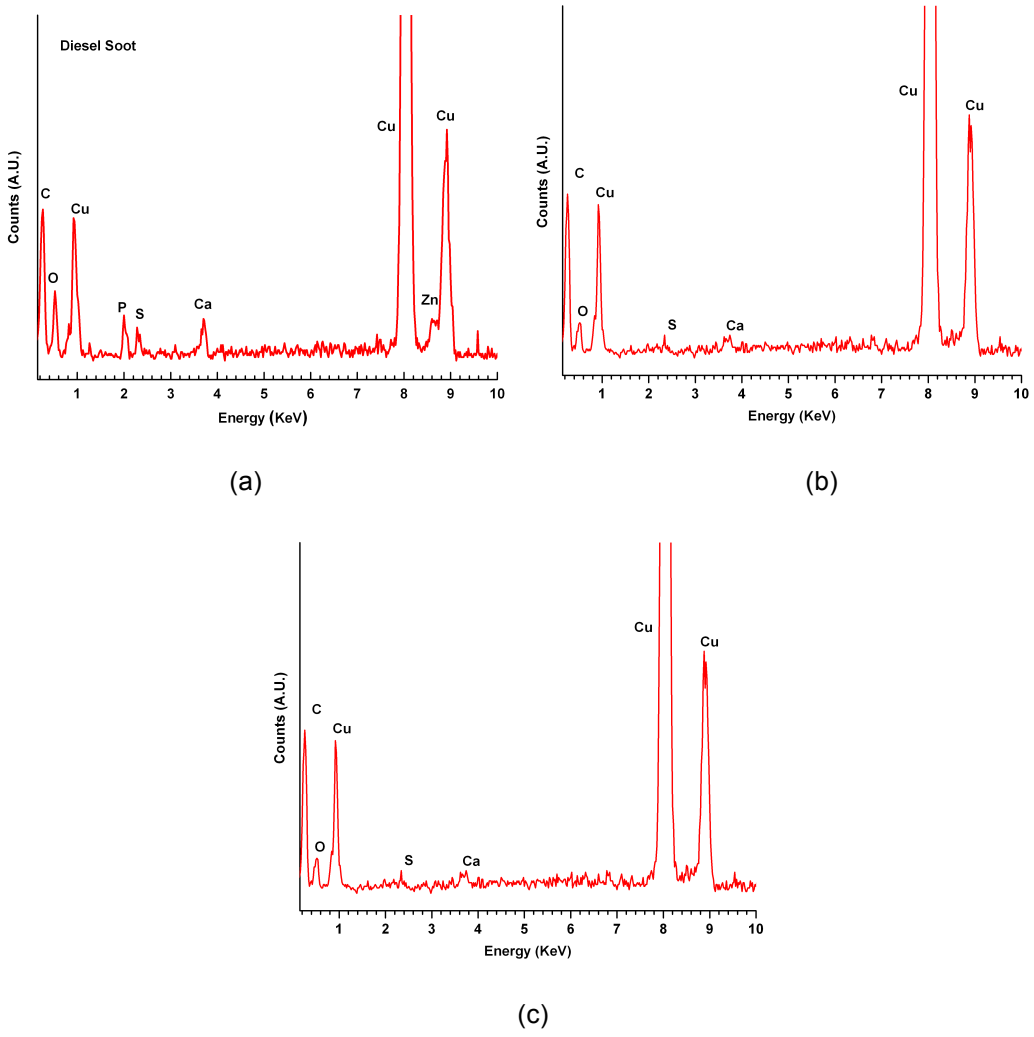

Figure 3.3 (a) EDS spectra of diesel soot showing the presence of Ca, P, S, Zn, O and C in diesel soot (b) EDS spectra of diesel soot showing the presence of C and O in diesel soot (c) EDS spectra of diesel soot showing the presence of Ca, S, O and C in diesel soot

It is well known fact that phosphorus, sulfur, zinc and calcium are main constituents of lubricating additive chemistry. It is worth noticing that, EDS could record the presence of phosphorus, sulfur, zinc and calcium only when electron beam was focused on bigger agglomerates while complete absence of such elements on smaller agglomerates was noticed. It was also observed that intensities of peak of phosphorous, sulfur, zinc & calcium differ on different agglomerates. In addition, some agglomerates shows presence of calcium and sulfur while phosphorus was absent in them. The multiple hexane wash and centrifuging of the oil

coupled with Sohexlet extraction minimizes the presence of trapped engine oil in the agglomerates suggesting the presence of these elements originates from decomposition products of engine oil and/or wear debris from engine components.

Furthermore, the SAD from an region that contains agglomerates of soot particles, exhibits ring pattern originating from the smaller individual crystalline carbonaceous domains. In addition, phosphorous, sulfur, zinc and calcium that were detected by EDS are unlikely to be present on the soot structure particles in their elemental forms and more likely to be present as compounds and/or amorphous glassy structures. Amorphous compounds cannot be detected by SAD and we believe that a number of these crystalline compounds are very small and not always seen in traditional TEM. On the other hand, the $CaSO_4$ particles are quite large (>1 μm) and are not shown here.

Surface area of the particles was measured using the BET nitrogen adsorption method indicated that carbon black has a surface area of 112.87 m^2/gram and diesel soot has a surface area of 22.33 m^2/gram. The difference in primary particle size for soot and carbon black are not very different, hence the large difference in surface area can be explained by the higher level of agglomeration in diesel soot in comparison to carbon black.

3.2.2 X-ray Photoelectron Spectroscopy Analysis of Diesel Soot

TEM – EDX results revealed the presence of P, S, Zn and Ca from the additive package incorporated into the diesel soot is most likely present as compounds and/or amorphous structures. In order to get better insight into these chemistries, x-ray photoemission spectroscopy was employed to examine the extracted soot. Figure 3.4 (a) – 4 (b) show high-resolution zinc and calcium spectra acquired using x-ray photoemission spectroscopy respectively. Both spectra indicate a low signal to noise ratio indicative of the small amount of these elements present in soot. De-convoluted spectra of zinc suggest the presence of a peak at a binding energy 1023.05 eV which is binding energy of zinc 1s electron of zinc sulfate. De-convoluted spectra of calcium indicates the presence of a peak at 348.7 eV and 351.8 eV which represents the binding energy of calcium 1s electron of calcium sulfate and calcium oxide respectively.

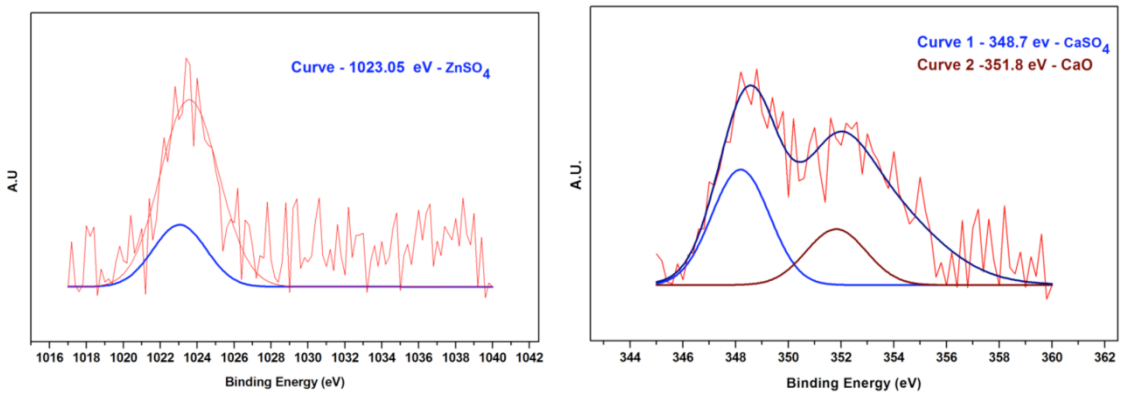

(a) (b)

Figure 3.4 (a) X-ray Photoelectron Spectroscopy high resolution spectra for zinc (b) X-ray Photoelectron Spectroscopy high resolution spectra for calcium

Previous studies have shown that $CaSO_4$ is due to the incorporation of over-based calcium sulfonates detergent additive in the tribofilms. [63] Hence, it is likely that the $CaSO_4$ may have come off as wear debris from the tribofilm and is embedded into soot agglomerate. The other possibility for the presence of calcium sulfate and calcium oxides may arise from the decomposed over based detergent, calcium sulfonates in the oil.

3.2.3 Raman Spectroscopy Analysis of Diesel Soot

Raman spectroscopy is a promising characterization tool to investigate the short-range highly disordered graphitic structure. Earlier studies have shown that different types of soot could be distinguished based on the degree of graphitization. In addition, integrated intensity ratio of D and G peak is inversely proportional to microcrystalline planer size La that corresponds to the in-plane dimension of the single microcrystalline domain in graphite [65-67]. Valuable information can be obtained by analyzing different spectral features such as intensity, peak position, line shape and bandwidth between 800 – 2000 cm^{-1}.

Fig. 3.5 shows the typical Raman spectra observed for diesel soot, carbon black and graphite acquired with a laser with λ = 532 nm in the range 800-2000 cm^{-1}. The spectra exhibit two broad and strongly overlapping peak at intensity maxima ~1350 cm^{-1} and at ~1590 cm^{-1}. Previous studies revealed that the intensity maxima at ~1590 cm^{-1} (known as G band) is analogues to ideal graphitic vibration mode. Furthermore, increased degree of disorder in the

graphite structure gives rise to the peak maxima at ~1350 cm^{-1} corresponds to disordered graphite. This peak is known as D1 peak (Defect bands).

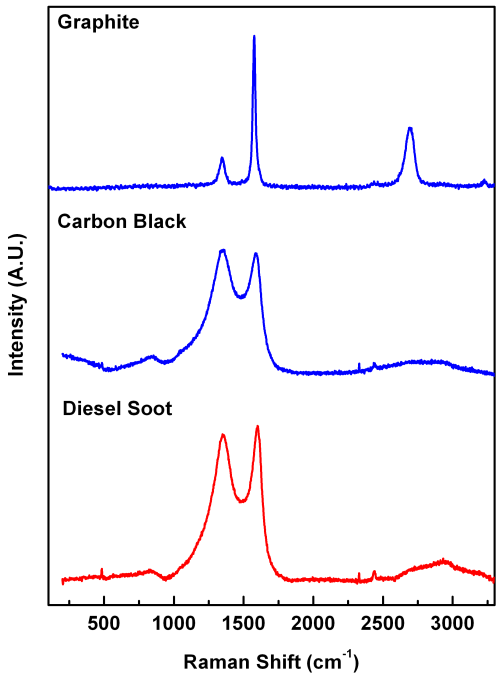

Figure 3.5 Raman spectra of graphite, carbon black and diesel soot

The high signal intensity between the two peak maxima can be attributed to another band at ~1500 cm^{-1}, designated as D3 (A) band which originates from the amorphous carbon fraction of soot (organic molecules, fragments or functional groups) and / or amorphous sp2 bonded forms of carbon. Cuesta et al. [19,68-71] and Dippel et al. [19] assumed Lorentzian line shape for this band, whereas Jawhari et al.[21] proposed Gaussian line shape due to a statistical distribution of amorphous carbon on interstitial places in the disturbed graphitic lattice of soot. Raman spectra recorded with λ = 532 nm also exhibit second order spectra in the range of about 2300 cm^{-1} to 3300 cm^{-1}. For the given studies only first order spectra have been considered for further analysis.

3.2.3.1 Spectra analysis by curve fitting

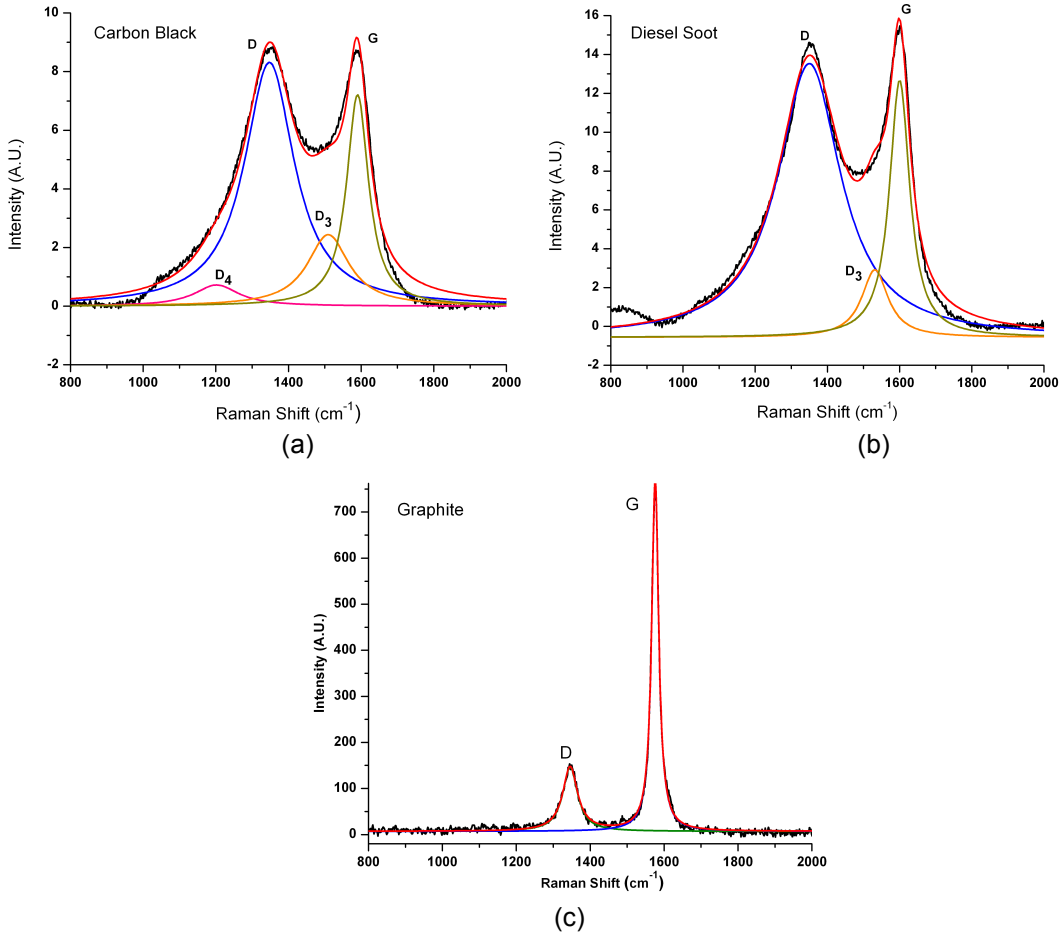

Figure 3.6 (a) Deconvoluted Raman spectra of carbon black using Lorentzian curve fit for the D1, D3, D4 and G peaks (b) Deconvoluted Raman spectra of diesel soot using Lorentzian curve fit for the D1, D3 and G peaks. (c) Deconvoluted Raman spectra of graphite using Lorentzian curve fit for D1 and G peaks

For the analysis and determination of spectral parameters by curve fittings various line shapes were evaluated. Raman spectra of diesel soot and carbon exhibit a broad band at about ~1500 cm^{-1}. The band at 1500 cm^{-1} is associated with amorphous sp^2 bonded carbon. It is also worth taking into consideration that sp^3 bonded carbon have vibrational features frequency below 1500 cm^{-1}. This observation suggests the higher probability of sp^2 bonded amorphous carbons. The best fit was invariably achieved by either one or two combination of line shape for G, D1 and D3 peaks. One can use the Lorentz line shape for all three G, D1 and D3 peaks or one can use the Lorentzian line shape for G and D1 peak and Gaussian like shape for D3 peak.

In this study we have used the Lorentzian peak fit for all three peaks of soot and carbon black as it offers the best fit. This fitting of the spectrum is in good agreement with recent studies by Sadezky et. Al [70]. The polycrystalline graphite exhibits two sharp peaks at ~ 1345 cm^{-1} and 1575cm^{-1} that correspond to the D1 and G peak respectively. The peak at ~ 1500 cm^{-1} is not observed in graphite. The graphite with just the D1 and G peak was fitted with two Lorentzian curve fits. The curve fitted spectra of diesel soot, carbon black and graphite are show in Figure 3.6(a-c) respectively. For the carbon black a fourth peak was introduced in the fitting (D4), which takes into account for the disordered graphitic lattice due to polyenes and/or ionic impurities.

Further analysis of the spectra can be obtained by analyzing full width half maximum (FWHM) of the peaks, peak intensity and peak position. Table 3.2 details the curve fitted data and ratio of G/D peak intensity. The curve fitted spectral data reveals that for all samples FWHM of G peak is narrower than that of other two bands. This validates the fact that G peak corresponds to crystalline phase of carbon. Comparing the FWHM of graphite with diesel soot and carbon black, it evident that graphite has greater portion of crystalline phase.

In addition, Table 3.2 breaks down the contribution from the different disordered forms of carbon including D1 the disordered graphitic lattice with contributions from graphene layer edges that are wrapped around, D3(A) the amorphous carbon and D4(I) arising from disordered graphitic layers from ionic impurities and polyenes.

Overall the ratio of G/(D1+D3+D4) for carbon black and diesel soot are very similar suggesting a similar ratio of idealized graphite lattice and disordered carbon, however, a careful examination of the ratio's G/D1, G/D3 and G/D4 indicate some significant differences. The smaller G/D1 ratio for diesel soot indicates a larger proportion of graphene layer edges have reacted in soot resulting in a higher level of disorder. Other studies in functionalizing of graphene have shown that edges of the graphene layer may be functionalized more easily resulting in smaller G/D1 ratios [71]. This might be preferential location for reactive decomposition species for absorbtion. But more scientific investigation is required to validate the speculation. On the other hand G/D3 ratio for diesel soot is much smaller than the G/D3 ratio for carbon black indicating a

smaller proportion of amorphous carbon in diesel soot compared to carbon black. Lastly, the absence of D4(I) peak in diesel soot indicates the absence of polyenes and/or other ionic impurities.

Table 3.2 Raman spectroscopic data for carbon black, diesel soot and graphite

		Peak Position	Intensity	G/D1	G/D3	G/D4	G/(D1+ D3+D4)
Carbon Black	G	1590.21	828.562	--	--	--	0.29
Carbon Black	D1	1347.44	2171.804	0.38	--	--	
Carbon Black	D3 (A)	1509.39	534.336	--	1.55	--	
Carbon Black	D4 (I)	1201.96	169.469	--	--	4.89	
Diesel Soot	G	1600.03	1402.114	--	--	--	0.27
Diesel Soot	D1	1349.96	4683.579	0.30	--	--	
Diesel Soot	D3 (A)	1531.49	483.818	--	2.90	--	
Diesel Soot	D4(I)	--	--	--	--	--	
Graphite	G	1575.80	27212.51	--	--	--	2.55
Graphite	D1	1345.64	10644.08	2.55	--	--	

G = Ideal Graphitic Lattice
D1 = Disordered graphitic lattice (graphene layer edges)
D3 (A) = Amorphous carbon
D4 (I) = Disordered graphitic lattice, polyenes, ionic impurities

Although Raman spectra distinguish the contribution from crystalline and amorphous domains no additional spectral features were observed to confirm contribution from interaction between lubrication additives chemistries and diesel soot.

3.2.4 Synchrotron Radiation XRD analysis of Diesel soot

Synchrotron radiation X-ray diffraction was employed to acquire insight of interaction between lubrication additives chemistries and diesel soot and to validate results acquired from TEM EDX and XPS. Diesel-soot and carbon black X-ray diffraction patterns were collected on a

traditional laboratory diffractometer (Rigaku IIID/max, XRD-lab at University of Trento, Trento, Italy) as well as at the MCX beamline (ELETTRA, the Italian synchrotron radiation facility at Trieste, Italy). Traditional laboratory diffractometer was used for initial assessment of composition of the soot which suggests the presence of calcium sulfate compounds. In addition, the earlier EDS analysis indicates the presence of Zn and P.

In order to determine the presence of Zn, synchrotron radiation x-ray diffraction was employed. A measurements were performed using different monochromatic wavelengths (energy) and patterns are shown in d* (reciprocal space) scale in Figure 3.7(a) and 7(b). Peaks at 0.43 and 0.5 correspond to the (111) and (200) planes originate from the aluminum sample holder used in synchrotron radiation (SR) XRD measurements. SR XRD measurements were made below (9.4 keV) and above (10 keV) the absorption edge of Zn (Zn K-edge is located at 9.6 keV). Any amorphous Zn phases, if present, would appear as increased background intensity in the spectra acquired with the SR beam with energy above the Zn K absorption edge.

The diffraction spectra show considerable diffuse scattering signal that originates from turbostratic soot structure and from other incoherent scattering and fluorescence, which form the “background” signal. There also exist several Bragg peaks superposed on the diffused scattering background. These results indicate that various crystalline phases present along with soot structure of soot.

In order to distinguish the contribution from carbonaceous background of soot and contribution from crystalline phase, similar experiments were conduction on carbon black, as shown in Figure 3.7(b). Electron diffraction study and the Raman analysis in the earlier sections indicate significant similarities between the carbon black and diesel soot and to a first approximation, it was assumed that the bulk of the background signal was coming from turbostratic structure of carbon black. In order to identify the nature of the crystalline peaks that appear to be superimposed on the large background peaks in diesel soot, the spectra from carbon black was subtracted from the spectra for diesel soot to yield a spectra for the crystalline

phases as shown in Figure 3.7(c). The spectra is superimposed for energy corresponds to above and below absorption of Zn K edge.

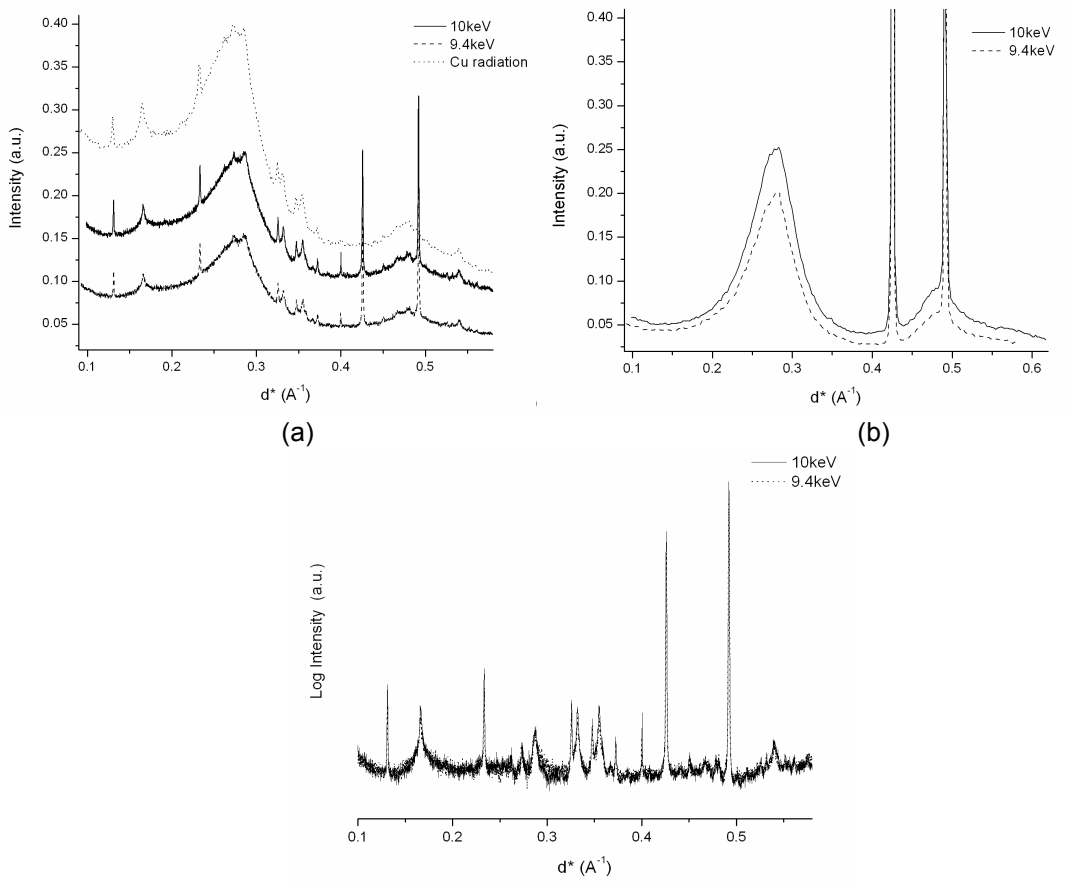

Figure 3.7 (a) Conventional and synchrotron radiation x-ray diffraction spectra of diesel soot. Synchrotron x-ray spectra were acquired at 9.4 and 10 keV. (b) Synchrotron radiation x-ray diffraction spectra of carbon black with spectra acquired at 9.4 and 10 keV (c) X-ray diffraction spectra of diesel soot after the spectra for carbon black was subtracted from it. Spectra correspond to acquisition energies of 9.4 and 10 keV. Spectra are plotted in terms of lattice spacing as they were acquired at different energies

3.2.4.1 Fluorescence signal in the SR XRD measurements

From synchrotron measurements we can notice that diffuse scattering contribution (amorphous phase and fluorescence) is quite different between carbon black and diesel-soot. There are two possible explanations: (i) presence of a crystalline phase containing zinc and (ii) presence of an amorphous phase containing zinc. Measurements of carbon black were used as a blank to subtract the "background" signal, as shown in Figure 3.7(c). The superimposed spectra

above and below the Zn K absorption edge indicate no remarkable difference between the superimposed patterns that suggests absence of any zinc crystalline phases in the soot sample. Although, the spectra after background subtraction using carbon black appear identical but considerable difference has been observed between the background signal from diesel soot and carbon black while changing energy from 9.4 to 10 keV. This strong effect in soot spectra above and below the absorption threshold of Zn K edge suggests the presence of zinc in amorphous form rather than any crystalline state.

3.2.4.2 Phase Identification – Search-Match

In order to identify the crystalline phases present in diesel soot ICDD PDF4+ database of High Score Search-Match software (Panalytical) was used. The spectra collected at 9.4 keV (SR XRD) with lowest diffuse scattering / fluorescence and lower signal to noise ration was used for the phase identification.

The search-match procedure was performed several times, using different constraints from the known chemical composition of metallic elements, namely, Ca, Zn (also Fe in some cases). Non-metallic elements considered were: H, C, O, S, P. Various speculated compounds such as CaO, $Ca(OH)_2$, $CaCO_3$, $CaSO_4$, $Zn_3(PO_4)_2$, $ZnSO_4$, ZnS were tried for search-match procedure.

Detailed analysis suggests that the most probable phases are different calcium sulfates in their hydrated phase. Good matches were found with gypsum ($CaSO_4.2H_2O$) and bassanite ($CaSO_4.0.5H_2O$), respectively the dihydrate and hemihydrate phases. Figure 3.8 is the SR x-ray diffraction spectrum from diesel soot that has been matched with known crystalline phases. From the observed pattern (after background removal), it is quite apparent that there is no CaO, $ZnSO_4$ or ZnS. Moreover, no Zn-containing phase shows unique matches (i.e., peaks attributed to a given phase only). On the contrary, two calcium sulfate hydrate phases gypsum (G) have bassanite (B) have unique matches, accounting for nearly all observed peaks. An additional (third) phase might be present, but it would be little justified: as an example, attempts to match other possible phases such as calcium hydrogen phosphate hydrate ($Ca_8H_2(PO_4)_6 \cdot 5H_2O$) and

calcium hydrogen phosphite ($CaH_2O_5P_2$) were met with little success. It is also possible to add as a third phase as a Zn compound (zinc phosphate hydrate, $Zn_3(PO_4)_2.H_2O$), but no good match were found. All in all, we suggest the crystalline fraction to be made of gypsum and bassanite. The origin of these phases is likely from the detergent used in engine oil.

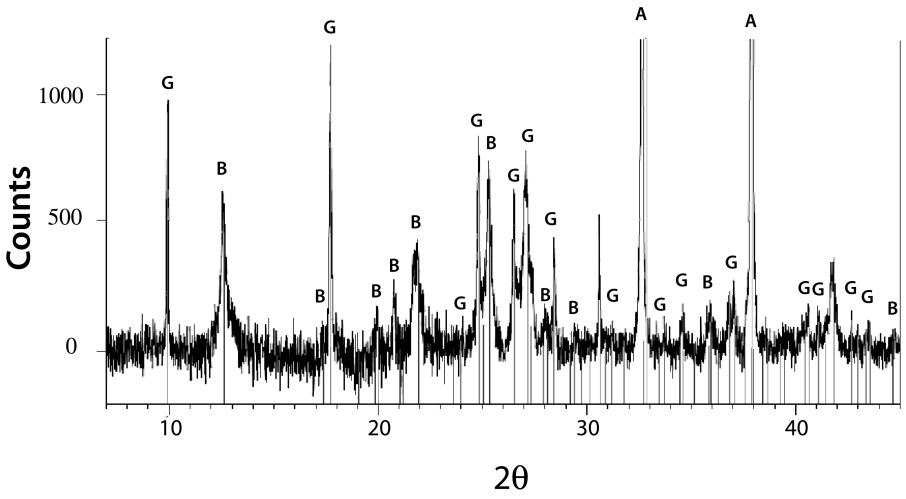

Figure 3.8 X-ray diffraction spectra of crystalline constituents of diesel soot that have been indexed. G corresponds to gypsum ($CaSO_4.2H_2O$), B corresponds to bassanite ($CaSO_4.0.5\ H_2O$) and A corresponds to the Al sample holder

It is well known that over-based calcium sulfonates detergents are the primary detergents used in diesel engine oils, these detergents are made up of nanocrystalline $CaCO_3$ particles surrounded by micelle like calcium sulfonate ligands that keep $CaCO_3$ dispersed. The over-based detergents serve to neutralize acidic byproducts of combustion and help keep insoluble polar byproducts suspended in oil. The primary source of Ca in oil is the detergent while the source of sulfur is likely from a combination of the detergent as well as anti-wear additives such as ZDDP and to smaller extent from the fuel source as well.

3.2.4.3 Quantitative phase analysis

If we assume the soot to be made of an amorphous matrix, with additional "background" signal from incoherent scattering and fluorescence, and two crystalline phases only (gypsum and bassanite), and considering also the contribution from the Al sample holder, the powder pattern of the soot measured using SR XRD can be used for a quantitative estimate of the crystalline

phases. Since there is an "unknown" contribution form amorphous and other scattering terms, and also the sample holders cannot be quantified, the result of a Quantitative Phase Analysis (QPA) is just semi-quantitative, i.e., can be used to investigate the relative ratio between the two sulfate phases.

QPA was made using TOPAS, with standard structural data for gypsum and bassanite. The "background" signal was removed before the refinement. Al was added to account for the sample holder. With these data all diffraction peaks seem to be reasonably matched, apart from one line, at about 20.8°, which is apparently too strong for being matched by the given phases. So a free pseudo-Voigt peak function was added at that angle. Results from the semi-quantitative analysis indicates that the ratio of gypsum/bassanite = 0.5.

3.3 Discussion

In the present study structural, morphological and chemical characterization were conducted on extracted crankcase soot while the local coordination of the different elements in soot using XANES is detailed in the companion study [72] The chemical characterization of crankcase soot using energy dispersive x-ray spectroscopy revealed the presence of phosphorous, sulfur, zinc and calcium on the larger agglomerates and complete absence of these elements on the individual primary particle of soot. Kawamura et. al used freeze fractal replica (FFR) method using TEM to investigate the state of soot in used diesel engine oil. He suggested that small soot particle in range of 0.02 μm do not affect the anti wear properties due to effectiveness of dispersant in engine oil on smaller particles. While particles greater than 0.03 μm might play dominant role in increase wear. [73] In similar studies, Narita et al. suggest soot with particle diameter equivalent to oil film thickness between the cam nose and tappet shows possibilities of promoting wear.[74] Moreover, statistically designed experiments by Bardasz et al, studies the effect of dispersant level, dispersant type, oxidation level and detergent metal type on average roller follower shaft wear and viscosity growth and suggested that thickening oil is due to amount of soot and agglomerates rather than oxidative thickening. [61] These studies suggest that bigger agglomerates of soot induced higher wear but mechanism is poorly understood. In the

present study, EDX results reveal the presence of phosphorus, sulfur, zinc and calcium on the agglomerates and their absence on the primary soot particle provide insight about this mechanism.

X-ray photoelectron spectroscopy results and synchrotron x-ray diffraction results substantiate EDX results as well as provide better insight about the various compounds present on the soot structure. XPS spectra have lower signal to noise ratio indicate the smaller concentration of the compounds on the soot structure. On the other hand, synchrotron x-ray diffraction uses high brilliance and intense photon flux to probe the samples. These results reveal the presence of crystalline calcium sulfate phase in its hydrated (gypsum) and hemishydrated (bassanite) form. In addition, synchrotron x-ray diffraction results also indicate the presence of zinc compound in the amorphous phase. These results also reveal the usefulness of 3rd generation synchrotron technique over traditional laboratory instrument to detect smaller concentrations of various compound present on soot. The particle size of the calcium sulfates detected by SR x-ray diffraction are much larger than the soot agglomerates and are typically 1-2 μm in size.

Furthermore, presence of crystalline calcium sulfate and amorphous zinc compounds on the soot structure could also originate from decomposed reactive lubrication additives chemistries interacting with soot agglomerates. If these compounds originate from decomposed reactive lubrication additives chemistries then it suggests interaction between reactive decomposition lubrication chemistries and diesel soot occurs during engine operation and/or in the oil sump. This phenomenon partially validates mechanism proposed by Round et al where preferential adsorption of decomposed ZDDP was responsible for reductions in effectiveness of anti wear additives. [11,12] But further investigation is needed to probe the specific chemistries of zinc compounds and forms the basis of the companion study. Previous studies also suggested the physical adsorption of the decomposition chemistries on soot surfaces as a possible mechanism [27-30]. However, multiple washing, dilution, centrifuging followed by soxhlet extraction discard

such possibilities of physical adsorption being the cause for the presence of these chemical species on diesel soot.

On the other hand, if the compounds originate from tribofilm then it indicates interaction between tribofilm and soot. The mechanism, formation and structure of tribofilm have been well documented. Depending on the loading conditions, additives chemistries and other tribological conditions, tribofilm structure varies. [27-30] In general, ZDDP serve as protective anti wear additives by forming protection tribofilm under severe tribochemical reactions. These tribofilm primarily made up of short chain or long chain amorphous zinc poly phosphate depending on the severity of loading conditions and tests. [75-82] The presence of zinc based compounds in amorphous state in soot would suggest interaction between tribofilm and soot. In addition, previous studies have shown influence of over-based detergent chemistries on the structure of tribofilm. [75-82] They have shown that presence of over-based detergent chemistries form tribofilm made up of calcium sulfate and calcium phosphate. This might explain presence of crystalline phase of calcium sulfate as bassanite and gypsum on the soot structure. Hence, it can be postulated that three body wear which has been a model proposed in several [62,67,83,84] may be an important mechanism for the incorporation of amorphous phases of Zn and crystalline sulfates of calcium into the soot. The hardness of the amorphous Zn polyphosphates have been suggested to be as high as 20-30 GPa by Mosey et. al. [10,23,53,61] in their molecular dynamic simulation studies and in experimental characterization of tribofilms it has been shown that hardness as high as 20 GPa have been measured by Aswath and co-workers [85]. The hardness of the steel substrate is typically in the range of 7-8 GPa and it is conceivable that presence of hard amorphous polyphosphates of Zn may contribute to third body wear. On the other hand both, bassanite and gypsum have a hardness of 2 on the Moh's scale, just above talc and not likely the source of any abrasive wear in diesel engines.

Structural characterization of crankcase soot using selected area diffraction in a TEM suggest insignificant changes in the turbostratic structure of soot in comparison to carbon black. Raman spectroscopy used to probe short-range disorder structure of soot and carbon black

indicates that the ratio of G/(D1+D3+D4) peaks for carbon black and diesel soot are very similar suggesting a similar ratio of idealized graphite lattice and disordered carbon, however, a careful examination of the ratio's G/D1, G/D3 and G/D4 indicate some significant differences. Although Raman spectra distinguish the contribution from crystalline and amorphous domains but no additional spectral features were observed to confirm contribution from interaction between lubrication additives chemistries and diesel soot using Raman spectroscopy.

3.4 Conclusions

Diesel soot was extracted from used engine oil by dilution with hexanes followed by centrifuging and sohexlet process. The morphology, structure, morphology and chemistry of diesel soot was characterized and compared to carbon black using transmission electron microscopy, Raman spectroscopy and synchrotron x-ray diffraction. Results indicate that the primary structure of diesel soot is similar to carbon black with a turbostratic structure. Differences between diesel soot and carbon black are primarily in the incorporation of tribological by products and decomposition products of the engine oil additive package in diesel soot. Crystalline phases present in addition to turbostratic carbon in diesel soot are hydrates of calcium sulfate which include gypsum and bassanite in a ratio of 1:2. Amorphous phases present in diesel soot include the phosphates and sulfates/sulfides of zinc.

CHAPTER 4

MORPHOLOGY, STRUCTURE AND CHEMISTRY OF EXTRACTED DIESEL SOOT: PART II: X-RAY ABSORPTION NEAR EDGE STRUCTURE (XANES) SPECTROSCOPY AND HIGH RESOLUTION TRANSMISSION ELECTRON MICROSCOPY

The chemical composition of diesel soot extracted from used diesel engine has been investigated using X-ray Absorption Near Edge Structure (XANES) spectroscopy and high-resolution transmission electron microscopy. Boron, phosphorous, sulfur, calcium, oxygen, iron L edge XANES spectra and phosphorous, sulfur and calcium K edge XANES spectra were recorded to characterize the chemical make-up of soot. The XANES spectra indicate the presence of phosphates of zinc and calcium and sulfates of zinc and calcium as well as the presence of sulfides of zinc. Zinc phosphate, zinc sulfide calcium sulfate and calcium phosphate are degradation products formed by thermo-oxidative and tribochemical decomposition of additives in engine oil. Presence of these decomposition products embedded in diesel soot indicates that these products interact with diesel soot resulting in a final soot product that is a blended mixture of turbostratic carbon and tribochemical products. In addition the high-resolution x-ray diffraction and synchrotron x-ray diffraction results, elucidated in the companion study, suggest that calcium sulfate is present as gypsum and bassanite co-mingled with soot in a crystalline state . The phosphates of zinc that are present are is in the amorphous state. High-resolution transmission electron microscopy coupled with energy dispersive spectroscopy and lattice imaging indicates the presence of nanoparticles of $Ca_3(PO_4)_2$ and Fe_2O_3 embedded at the surface of the turbostratic soot structure. Both $Ca_3(PO_4)_2$ and Fe_2O_3 are hard particles and appear to have been incorporated within the turbostratic soot structure during third body wear.

4.1 Introduction

The lubrication additives in modern diesel engine have to function within limits placed on their concentration in the harsh environment of diesel engine. Soot contamination of the diesel engine occurs when the engine operates under high load or when fuel injection retards the combustion process. [76,77] Post a combustion strategy such as exhaust gas recirculation (EGR) also increases soot concentration in the modern diesel engine.[10,86] Diesel engine lubrication oil additives package contains anti-wear additives, detergent and dispersants that plays significant role in controlling the deleterious effect of higher wear of engine components. However, the soot that builds up in the crankcase results in increased wear over time [58].

Zinc dialkyl dithiophosphates (ZDDP) have been used in lubrication oil as antiwear and antioxidant additives for over 70 years. However, the effectiveness of ZDDP in presence of soot and other oil additives is of critical concern, in particular when limits have been imposed on the amount of phosphorous, sulfur and sulfated ash in engine oils. Recent studies have indicated that ZDDP is antagonistic to wear in the presence of soot [23,33,54,59,87,88]. The mechanism of decomposition of ZDDP and formation of intermediate products that play significant role in forming protective antiwear film has been studied extensively. [89] Experiments carried out by Hosunam et.al indicated that there is an interaction between ZDDP decomposition products and diesel soot. [90-95] Round has also suggested the preferential adsorption of decomposition products of lubrication additives chemistry on soot surface. [33][27,28,30] Thus, it is important to understand the exact mechanism of interaction between ZDDP and diesel soot that has the potential to alter the properties of diesel soot. Moreover, calcium based detergent and dispersants also play a critical role in curbing the deleterious effect of soot by separating the soot particles and preventing them from agglomeration in addition to assisting in neutralizing acidic products transferred to crankcase through EGR process.[86]

In the companion study [86], we employed high-resolution x-ray diffraction and synchrotron x-ray diffraction for structural characterization of soot. We reported the presence of hydrated calcium sulfate (gypsum) and semi-hydrated calcium sulfate (bassanite) in crystalline

form within the soot structure and the possible presence of amorphous Zn based compounds incorporated into the soot agglomerates. In this study, X-ray Absorption Near Edge Structure (XANES) spectroscopy and high-resolution transmission electron microscopy (HRTEM) have been employed to chemically and structurally characterize diesel soot and any other constituents of the decomposition products/wear debris that are incorporated into soot. XANES is particularly useful in determining the local coordination, valence and chemical bonding of individual elements and is useful even at small concentrations; coupled with HRTEM it is possible to characterize both the crystalline amorphous phases in diesel soot.

4.2 Experimental Procedure

4.2.1 Diesel Soot Extraction

Diesel soot was extracted from used diesel engine oil that was acquired from a Freightliner oil changing facility during the drain interval from a single diesel engine. Used diesel engine oil was diluted using hexane as solvent in 50% wt. The mixture was centrifuged at 12000 rpm for 2 hours. Supernatant was discarded and remaining residue of soot was washed with hexanes, which was followed by centrifuging. This process was repeated till all remnants of oil were removed completely. To avoid the possibility of any trapped oil, a Soxhlet extraction method was further used where extraction was carried out for 48 hours using hexanes as solvent. The extract was dried and used for further analysis.

4.2.2 XANES Spectroscopy

XANES experiments were carried out at Canadian Light Source, Saskatoon, Canada using the 2.9GeV storage ring and at The Synchrotron Radiation Center, Wisconsin, Madison using the 800 MeV storage ring. Three beam lines were used at Canadian Light Source to obtain K and L shell absorption edge spectra. Phosphorous, sulfur and calcium K absorption edge was recorded using Soft X-ray Micro-characterization Beam line (SXRMB) covering region of 1700-10000 eV with photon resolution of 0.2eV and beam spot size of 4 mm x 300μm. Phosphorus & sulfur L-edge spectra were obtained using Variable Line Grating-Plane Grating Monochromator (VGM-PGM) beam line covering region of 5-250eV with photon resolution of 0.2eV. The PGM beam

spot size is 500μm x 500μm. Oxygen K-edge, Fe L-edge and zinc L edge spectra were obtained using Spherical Grating Monochromator (SGM) beam line that covers the energy range between 250-2000eV with photon resolution of 0.2eV in 100 μm x 100μm spot size. XANES spectra were acquired in Total Electron Yield (TEY) mode and Fluorescent Yield (FY) mode. Calcium L edge were obtained at the Synchrotron Radiation Center (Wisconsin, Madison) using HERMON beam line covering 64-1400 eV with 0.2 eV resolution.

In order to examine the stability of the decomposition products embedded in soot, multiple (up to 10 spectra) of the P L-edge (PGM Beamline at CLS) and O K-edge (SGM beamline at CLS) were acquired from the same location with the intent to study local damage to the decomposition products by synchrotron radiation.

4.2.3 High Resolution Transmission Electron Microscopy

High-resolution transmission electron microscopy of the diesel soot was conducted using a Hitachi H-9500 microscope at an accelerating voltage of 300 kV with a lattice resolution of 0.18 nm. High-resolution lattice images of crystalline nanoparticles and the turbostratic structure of soot were acquired. Selected area diffraction patterns were acquired from selected regions coupled with energy dispersive spectra using x-rays to determine the chemical makeup of different regions within the soot particles.

4.3 Results and Discussion

X-ray absorption near edge structure (XANES) is a non-destructive technique to chemically characterize the surface at nanometer scale. It employs high-energy soft/hard x-ray photons from a synchrotron radiation source with high flux. In XANES, a photon beam of known incident energy is directed at the sample surfaces. If the photon has sufficient energy to excite a core level electron of an atom in the sample, a photoelectron is created and it moves into unoccupied states and the photon is absorbed and cannot be detected anymore. However, the hole created in either K or L levels are filled up by electron from another shell followed by emission of a fluorescent photon which gives rise to the fluorescent yield spectra. Another approach that is used is to connect the sample to a ground and measure the neutralization current which yields the total

electron yield spectra. The total electron yield spectra are much more surfaced sensitive than the fluorescent yield spectra, which yield information from deeper down in the sample [96]. The absorption edge can be used as a fingerprint to identify the chemical make up of the material being examined. The XANES technique has capability to probe local environment surrounding atom and its oxidation state.

4.3.1 Diesel soot L absorption edge of XANES

4.3.1.1 Phosphorous L edge XANES spectra analysis

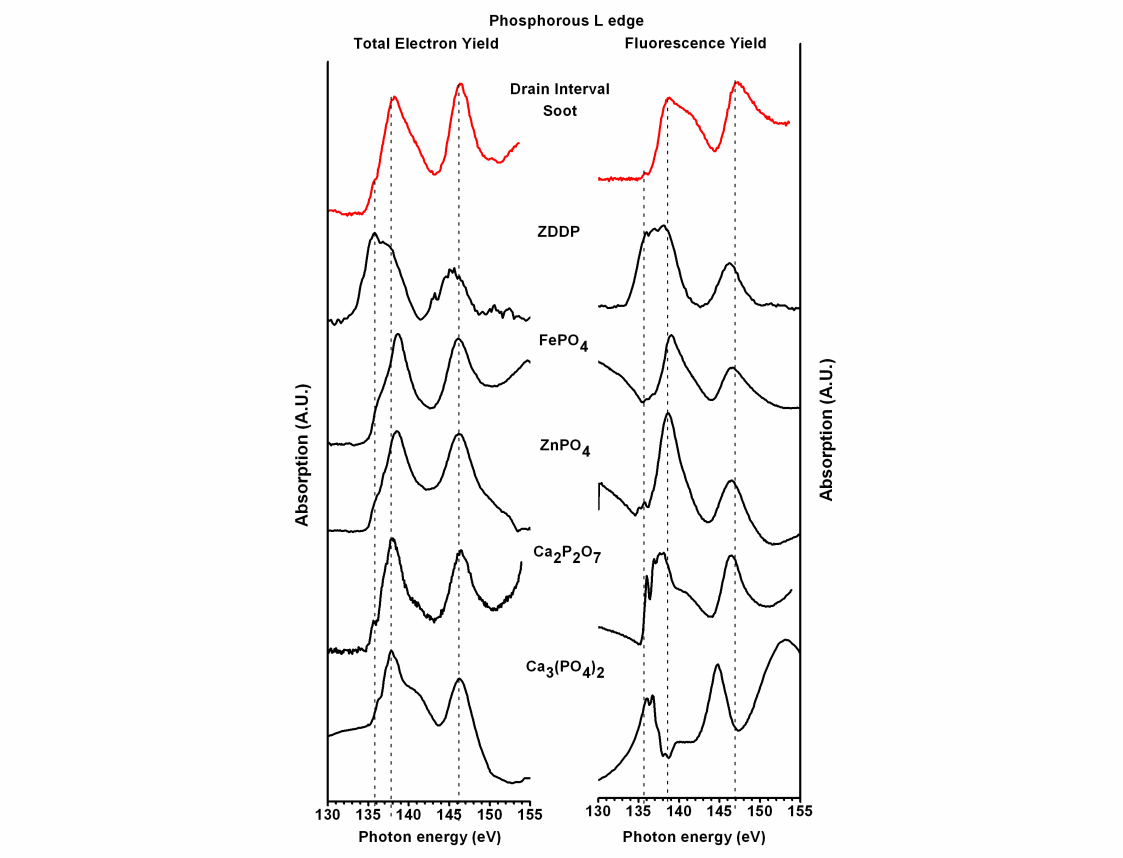

Figure 4.1 Normalized Total Electron Yield (TEY) and Fluorescent Yield (FY) phosphorous L edge spectra of diesel soot and model compounds

The P L-absorption edge has been used extensively to examine tribological surfaces [47,48,97]. The TEY spectra provide surfaces sensitive information in the top 5 nm of the surface while FY spectra provide information from the top 50 nm [47,98-101][48,100,102,103]. P L-edge XANES spectra of ZDDP, zinc phosphate $Zn_3(PO_4)_2$, tri-calcium phosphate $Ca_3(PO_4)_2$, calcium

pyrophosphate $Ca_2P_2O_7$, iron phosphate $FePO_4$ and that diesel soot in both TEY and FY mode are shown in Figure 4.1.

Nichols et. al [104] in their study of tribofilms formed with ZDDP as well as model compounds of short and long range zinc polyphosphates used the P L-edge to characterize the polyphosphate's by chain length. The primary peak marked as "c" in the $Zn_3(PO_4)_2$ may be attributed to the transition of 2p electrons of a p-like t2* molecular orbital and peak d was attributed to a d-type shape resonance [104] In their study with short and long range polyphosphates Nichols also showed that two pre-edge peaks to the left of peak c is associated with the spin orbit splitting of the phosphorous 2p level that arise from transitions of electrons from occupied $2p_{3/2}$ and $2p_{1/2}$ levels to unoccupied antibonding orbitals and may be used to fingerprint the polyphosphates of zinc. In particular, it was shown that ratio of peak height "c" to that of the first pre-edge peak "a" may be used. In TEY mode, comparison of model compounds with diesel soot suggest that characteristic phosphorous L edge peak align closely to $Zn_3(PO_4)_2$, and $Ca_3(PO_4)_2$ while presence of $FePO_4$ is not likely. In FY mode, comparison with these model compounds suggests the presence of phosphorous primarily as $Zn_3(PO_4)_2$. The presence of $FePO_4$, is not likely. Absence of iron phosphates substantiates the result obtained by TEM-EDX in the companion study [104] where iron was not present in significant amounts. In addition, the P L-edge spectra of the diesel soot does not match with that of fresh un-decomposed ZDDP, which eliminates the possibilities of any trapped oil on to the soot structure. Hence, from the L absorption edge, phosphorous is likely to be in the form of $Zn_3(PO_4)_2$ and $Ca_3(PO_4)_2$, with absence of any longer chain polyphosphates of zinc.

4.3.1.2 Sulfur L edge XANES spectra analysis

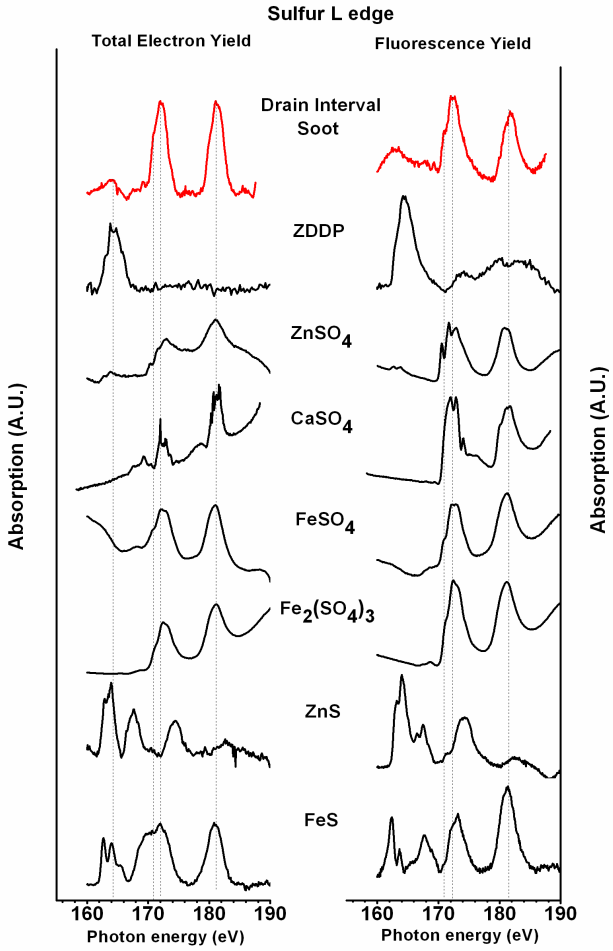

Figure 4.2 Normalized Total Electron Yield (TEY) and Fluorescent Yield (FY) sulfur L edge spectra of diesel soot and model compounds

Sulfur L-edge spectra have been used extensively in the past to study tribofilms and provide information on the local coordination of sulfur near the surface of the tribofilm [96] [66,76,105,106]. The sulfur L absorption edge spectrum of diesel soot was recorded in TEY and FY mode. This spectrum was compared using model compounds of sulfates and sulfides of zinc, calcium and iron as shown in Figure 4.2. All sulfates and sulfides have unique distinctive characteristic absorption spectra except $FeSO_4$ and $Fe_2(SO_4)_3$ that are quite similar. Model compounds of the sulfides have distinctive peaks at lower energy, which distinguishes sulfides form sulfates. Comparison with diesel soot spectrum indicates that soot absorption edge closely

align with absorption edge of $ZnSO_4$ and $CaSO_4$ with the presence of sulfides being unlikely. Both TEY and FY spectra indicates the possible presence of sulfates of calcium and zinc incorporated into the soot. Comparison with the spectra for ZDDP also indicates that there is no physically absorbed ZDDP in the soot structure. Sulfates and sulfides of iron are not likely to be present as the XANES spectra of Fe L-edge do not suggest the presence of sulfides or sulfates of Fe.

4.3.1.3 Zinc L edge XANES spectra analysis

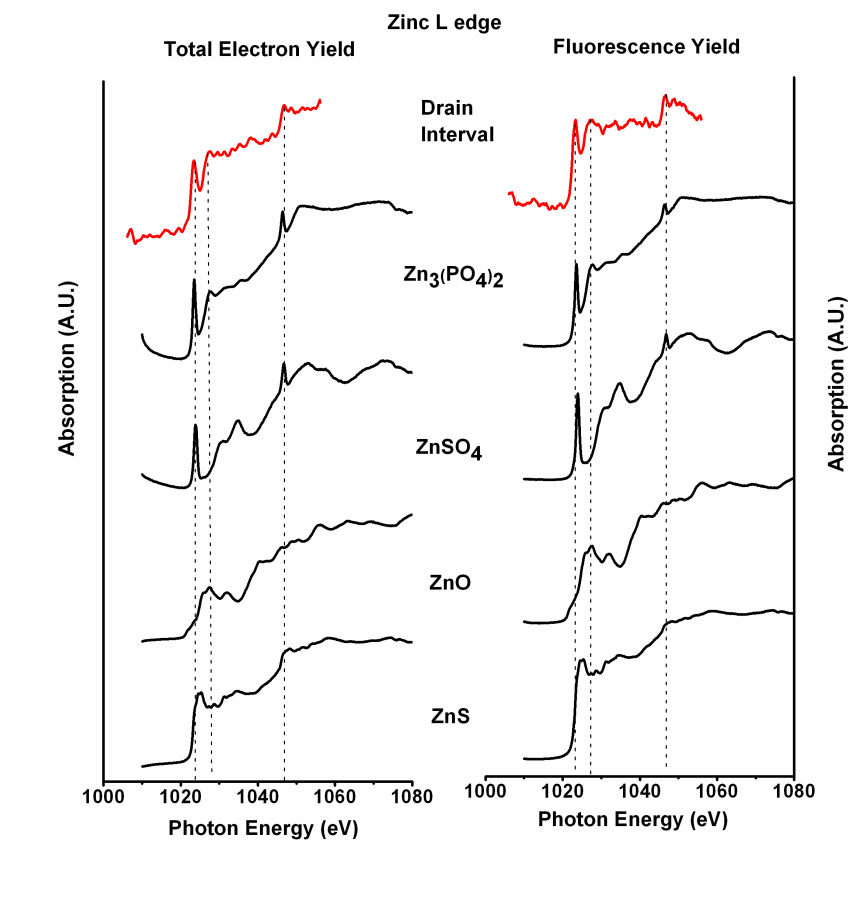

Figure 4.3 Normalized Total Electron Yield (TEY) and Fluorescent Yield (FY) zinc L edge spectra of diesel soot and model compounds

ZDDP being the primary anti-wear agent used in engine oils, the tribo-thermal oxidative decomposition of ZDDP is responsible for the formation of tribofilms on the surface with polyphosphates of Zn as well as sulfides and sulfates of Zn [107] . Zinc L-edge has been used extensively in the past to determine the local coordination of Zn in the tribofilm [107]. In this study,

the zinc L absorption edge spectrum was recorded in TEY and FY mode to examine the state of Zn in soot. EDS spectra in the companion study [65] indicates that Zn is present in soot while the x-ray diffraction study using synchrotron radiation indicates no crystalline phases are present but suggests presence of Zn possibly as amorphous phases due to the different levels of energy absorption on either side of the Zn K-absorption edge.

For the comparison, oxide, sulfate, sulfide and phosphates of zinc were used as model compounds as shown in Fig. 3. $ZnSO_4$ and $Zn_3(PO_4)_2$ has distinctive white line energy peak at 1024±1 eV, which is absent in ZnS and ZnO. ZnS and ZnO have a broader peak compared to $ZnSO_4$ and $Zn_3(PO_4)_2$. Although the white line peaks of $ZnSO_4$ and $Zn_3(PO_4)_2$ lay close to each other the post edge fine structure of $ZnSO_4$ and $Zn_3(PO_4)_2$ differentiate them. The spectra from soot is rather noisy due to the low concentration of Zn and hence it is difficult to differentiate between $ZnSO_4$ and $Zn_3(PO_4)_2$ based on the Zn L-edge. However, the synchrotron x-ray spectra [96] did not indicate the presence of any crystalline $ZnSO_4$ suggesting the likely form of Zn in amorphous $Zn_3(PO_4)_2$ or short chain phosphate of Zn.

4.3.1.4 Iron L-edge XANES spectra

Fe is present in the substrate of all the tribological regions in contact within an engine. In the companion study [96] it was shown that Fe is not a major component in diesel soot using traditional TEM and EDS, however, EDS can only provide insight into elements that are present in concentrations of over a few percent. In order to determine if very small amounts of Fe was present in the diesel soot, Fe L-edge spectra was acquired in both FY and TEY modes, and shown in Fig. 4. The model compounds of Fe show some similarities and also some distinctive differences. $FeSO_4$ has two sharp peaks at 709 and 711 eV. On the other hand $FePO_4$ and Fe_2O_3 are similar in many ways with their white line at 711 eV and a smaller pre-edge peak at 709 eV, on the other hand the pre-edge peak for FeS at 709 eV is almost the same intensity as that of the white line at 711 eV. Comparing the model compounds with the spectra from diesel soot it is evident that the spectra for Fe is weak as evidenced by the larger noise in the spectra and the most likely compounds present are Fe_2O_3 and perhaps a small amount of $FePO_4$. It is not likely

that sulfides or sulfates of Fe are present. The presence of oxides of Fe is more likely as severe abrasive wear results in the formation of Fe_2O_3 and /or Fe_3O_4 [96] in the wear debris.

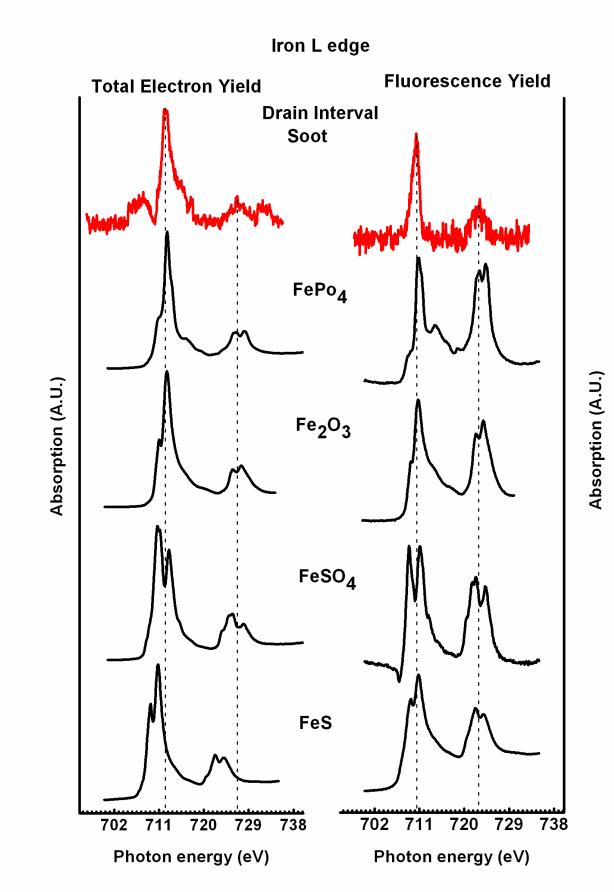

Figure 4.4 Normalized Total Electron Yield (TEY) and Fluorescent Yield (FY) iron L edge spectra of diesel soot and model compounds

4.3.1.5 Calcium L edge XANES spectra

Ca has an electronic configuration of $2p^6 3d^0$ with a high probability of transition of electrons from the 2p to the 3d shells. Earlier studies on calcium $L_{2,3}$ edge using density of states and other approaches have taken into account the 2p-3d spin-orbit interactions as well as 3d-3d coulomb and exchange interactions.[75]. Model compounds of calcium sulfate ($CaSO_4$), calcium hydroxide ($Ca(OH)_2$), calcium phosphate ($Ca_3(PO_4)_2$) and hydroxyapatite ($Ca_{10}(PO_4)_6(OH)_2$) were examined. Shown in Fig. 5 is the calcium absorption edge recorded in TEY mode to elucidate the results acquired from high-resolution x-ray diffraction, synchrotron x-ray diffraction and energy dispersive

spectroscopy illustrated in the companion study[108]. The two primary peaks in the spectra located at 350 eV and 353 eV correspond to the L_3 and L_2 absorption edges[96], The other minor peaks before the L_3 and L_2 edges correspond to various different 2p transitions. Absorption edges of $Ca(OH)_2$ and $Ca_{10}(PO_4)_6(OH)_2$ are slightly lower energy state than $CaSO_4$ and $Ca_3(PO_4)_2$. $Ca_3(PO_4)_2$ has a much more pronounced pre- edges compare to calcium sulfate. The diesel soot spectrum closely resembles the spectra from calcium sulfate and to a lesser extent that of $Ca_3(PO_4)_2$ and $Ca_{10}(PO_4)_6(OH)_2$. These results substantiate the results obtained in the companion study [108] where it was shown that crystalline Ca exists largely as bassanite and gypsum.

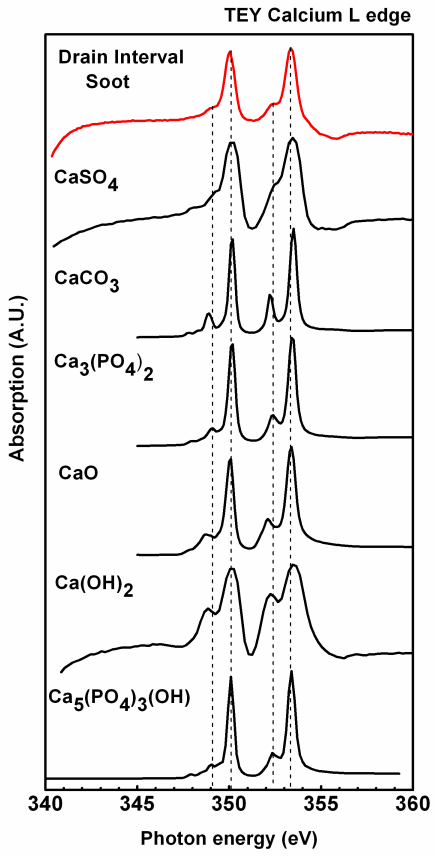

Figure 4.5 Normalized Total Electron Yield (TEY) calcium L edge spectra of diesel soot and model compounds

4.3.2 Diesel Soot K Absorption Edge

4.3.2.1 Boron K-Edge XANES Spectra Analysis

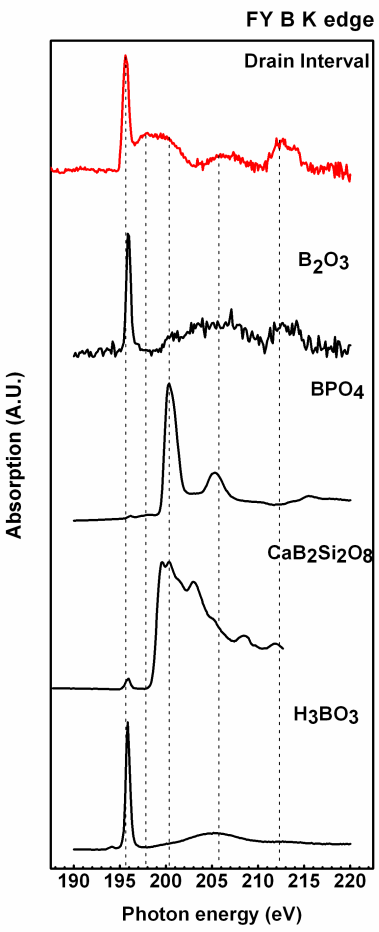

Figure 4.6 Normalized Fluorescent Yield (FY) boron K edge spectra of diesel soot and model compounds

The B K-edge absorption spectrum has been used in the past to examine the fate of boron on the surface of tribofilms [96]. In this study the FY spectra provides information on the nature of B present in the soot debris recovered from used engine oil. Fig. 6 shows the FY B K-edge spectra of diesel soot as well as several model compounds. Boron exists in two valence states +3 and +4 with the white line for the +3 valence state at a lower energy compared to the +4 valence state. B_2O_3 and H_3BO_3, both of which contain B in the +3 valence state have their primary absorption edge at 196 eV. An important distinction between B_2O_3 and boric acid (H_3BO_3) is the

presence of a post edge fine structure in B_2O_3 at approximately 212 eV that is absent in H_3BO_3. BPO_4 can exist with boron in either +3 or +4 or a mixture of the two. In the current study BPO_4 with B in the +4 valence state was used as the model compounds and it has its white line at 200.3 eV with a post edge peak at 205.8 eV. For comparison a calcium borosilicate compound Danburite ($CaB_2Si_2O_8$) with B in a +4 valence state was used as a reference and it has its white line at approximately 200 eV.

A comparison of the B K-edge spectra from the diesel soot with the model compounds indicates that B is likely present in the diesel soot in the form of B_2O_3 (B^{+3}) and to a smaller extent in the form of BPO_4 (B^{+4}). The source of the B_2O_3 is likely the borated dispersant used in the oil which is very reactive, the BPO_4 on the other hand is likely formed by reaction of the borated dispersant with decomposition products of ZDDP in the oil and formation of tribofilm. Under severe boundary lubrication conditions, the BPO4 may be removed from the tribofilm and incorporated into the soot debris. In an earlier study of tribofilms formed when borated dispersants were used it was shown that boron in the tribofilms are not present as BN and B in the tribofilm is partly present in its tetravalent state even though in the dispersant that was used in was in its trivalent state. [109,110]

4.3.2.2 Phosphorous K absorption edge

The white line for the phosphorous K-edge spectrum arises from transitions of 1s electrons to unoccupied 2p orbitals. Phosphorus K absorption edge of diesel soot was recorded in TEY and FY mode as shown in Figure 4.7. This spectrum was compared with phosphates of zinc, calcium and iron. $FePO_4$ has distinctive pre edge at 2150eV, which is absent in $Zn_3(PO_4)_2$ and $Ca_3(PO_4)_2$. Also the main peak of $FePO_4$ lies at 2154.5eV, which is higher energy state than $Zn_3(PO_4)_2$ and $Ca_3(PO_4)_2$. In addition, a careful examination of the post edge structure indicates the presence of distinctive shoulder in the case of $Ca_3(PO_4)_2$, which is absent in the case of either the $Zn_3(PO4)_2$, or $FePO_4$. The characteristics K absorption edge of soot closely aligns with $Zn_3(PO_4)_2$ in both the TEY and FY mode. Possibility of $FePO_4$ is not likely due to absence of pre edge in the soot spectrum. Phosphorous L absorption edge spectra suggest the presence of

$Zn_3(PO_4)_2$ and $Ca_3(PO_4)_2$, while the K-edge clearly confirms the presence of $Zn_3(PO_4)_2$ and absence of any $FePO_4$.

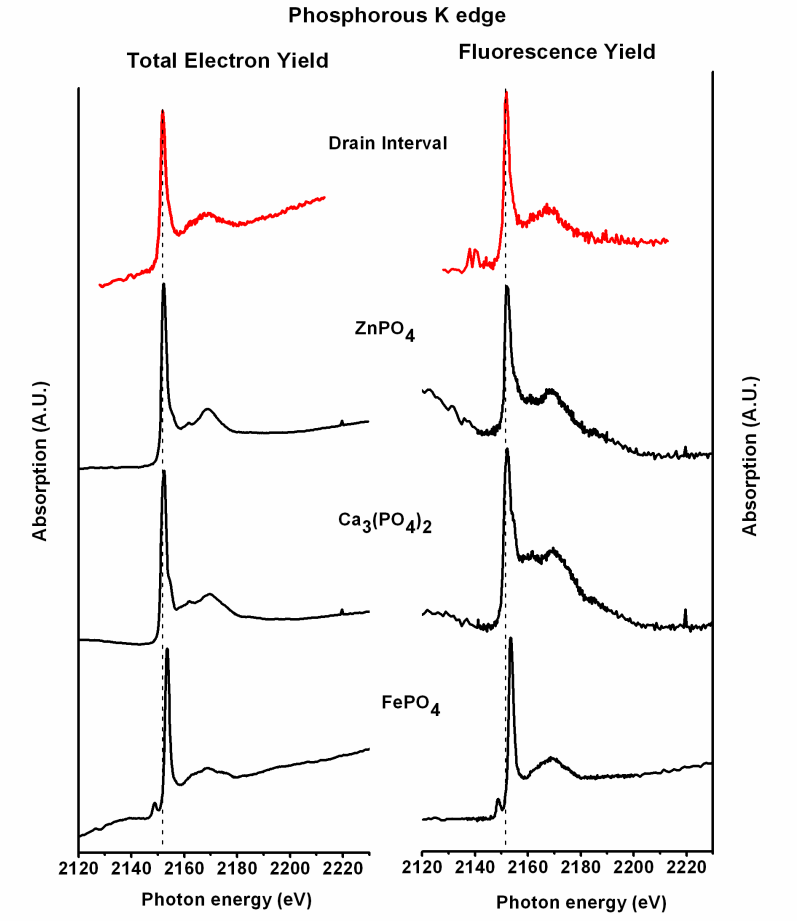

Figure 4.7 Normalized Total Electron Yield (TEY) and Fluorescent Yield (FY) phosphorous K edge spectra of diesel soot and model compounds

4.3.2.3 Sulfur K absorption edge

The XANES spectrum of sulfur K absorption edge was compared with sulfates of zinc, calcium and iron and with sulfides of zinc and iron as shown in Figure 4.8. Higher energy states of iron sulfate at 2482.3 eV differentiate it from zinc and calcium sulfate. Zinc sulfate and calcium sulfate can be differentiated by the presence of a post edge at 2484.8 eV in the case of $CaSO_4$ that is absent in the case of $ZnSO_4$. The sulfides have their white lines at lower energies than the sulfates with the zinc sulfide having an absorption edge at 2473 eV and a fairly rich post edge

structure. Iron sulfide two strong peaks at 2471 eV and 2482 eV. A careful examination of the spectra of diesel soot (both TEY and FY) indicates that in addition to the sharp absorption edge at 2481.2 eV that is common to both $ZnSO_4$ and $CaSO_4$ there is a post edge at 2484.8 eV that is only present in $CaSO_4$.

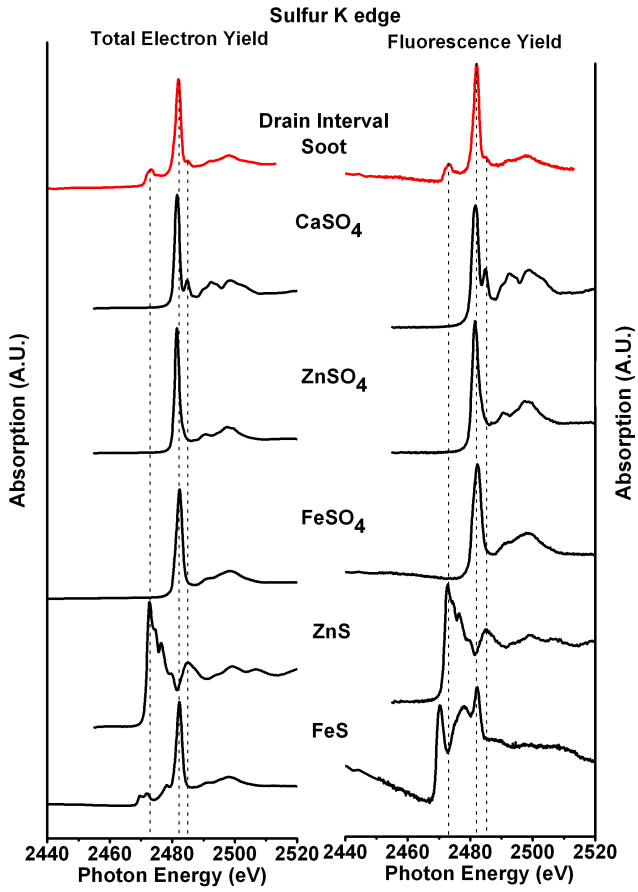

Figure 4.8 Normalized Total Electron Yield (TEY) and Fluorescent Yield (FY) sulfur K edge spectra of diesel soot and model compounds

Diesel soot also has an additional peak at 2472 eV that likely arises from zinc sulfide as a minor constituent of soot. While the L-edge spectra of sulfur clearly suggests the presence of sulfates in the diesel soot, the K-edge spectra is able to distinguish between the cationic species most likely present in the soot. In addition, the higher flux of photons in the K-edge spectra helps in identifying the presence of ZnS in soot as well. In addition, it is important to note the absence

of $FeSO_4$ in soot, which collaborates the evidence seen in Fe L-edge spectra and the EDS spectra as well.

4.3.2.4 Oxygen K absorption edge

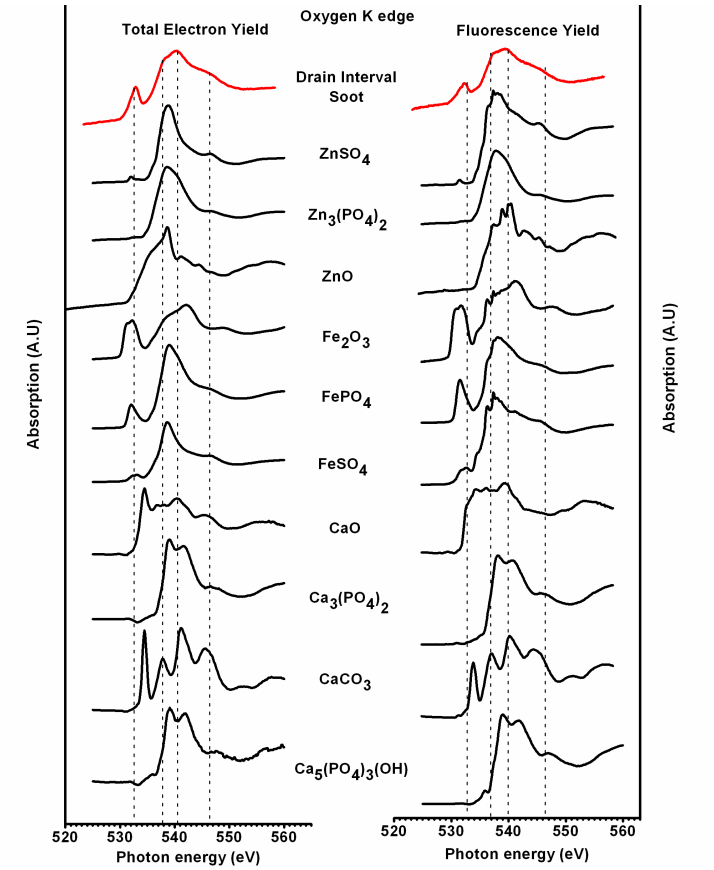

Figure 4.9 Normalized Total Electron Yield (TEY) and Fluorescent Yield (FY) oxygen K edge spectra of diesel soot and model compounds

There are multiple sources for the presence of oxygen in diesel soot and it is never very easy to isolate the source of oxygen. Nevertheless, in order to get an estimate of the source of oxygen in soot the TEY and FY spectra of oxygen K-edge of soot was compared to several model oxides, phosphates and sulfates of Fe, Zn and Ca. Shown in Fig. 9 are the spectra of soot and model compounds of oxygen in TEY and FY mode. While it is difficult to isolate a single source of oxygen, we can eliminate $FePO_4$ and $FeSO_4$ as the companion Fe, P and S spectra do not show evidence for the presence of these compounds. The presence of a diffuse pre-edge structure 533 eV indicates the possible presence of Fe_2O_3. The broad absorption edge which spans from 536-

543 eV possibly includes contribution from Fe_2O_3, $CaSO_4$ (not shown), $Zn_3(PO_4)$ and to a lesser extent from $Ca_3(PO_4)_2$. The source of $CaSO_4$ is from the overbased sulfonated detergent while the $Zn_3(PO_4)$ comes from decomposition of ZDDP as well as wear debris from the tribofilm. $Ca_3(PO_4)_2$ also likely comes from reaction products on the surface tribofilms between detergent and ZDDP.

4.3.2.5 Calcium K absorption edge

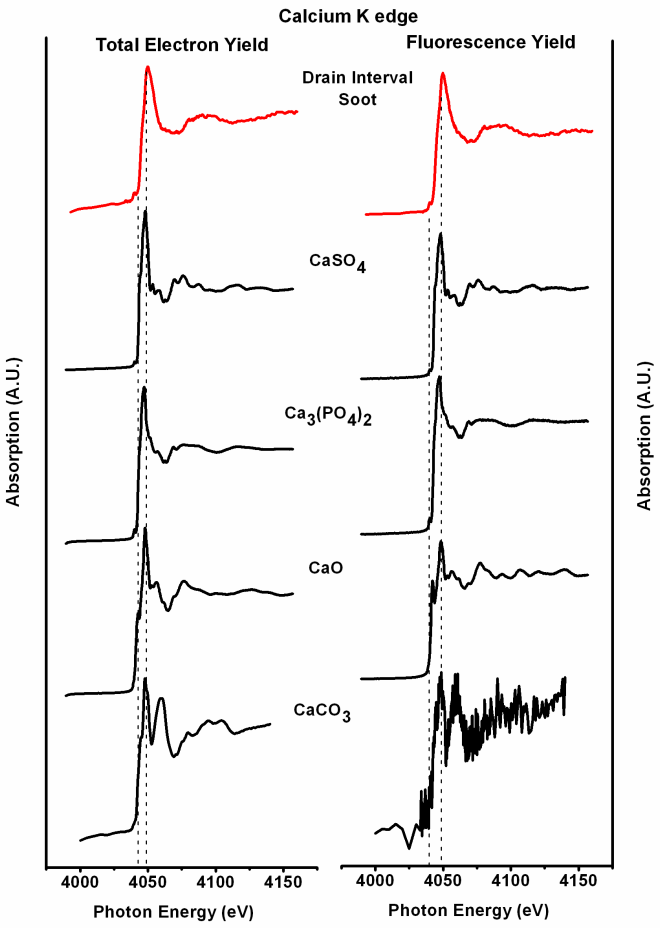

Figure 4.10 Normalized Total Electron Yield (TEY) and Fluorescent Yield (FY) calcium K edge spectra of diesel soot and model compounds

Calcium K absorption edge was recorded in TEY and FY mode for soot and model compounds, as shown in Fig. 10. $CaSO_4$, CaO and $Ca_3(PO_4)_2$ were used for comparison. The white line for $CaSO_4$, CaO and $Ca_3(PO_4)_2$ are located at 4050 eV, 4049.8 eV and 4049.4 eV

respectively, CaO has distinguishing pre edge at 4043 eV, which is absent in the other Ca compounds. $CaSO_4$ has more defined fine structure compared to $Ca_3(PO_4)_2$. Comparison of the soot spectra and model compounds spectra clearly indicates that the spectra appears to be close to both $CaSO_4$ and $Ca_3(PO_4)_2$ and the absence of CaO. The P K-edge spectra indicates that the phosphates were most likely Zn based and to a lesser extent Ca based, and the S K-edge spectra also indicated that the presence of $CaSO_4$ and lesser extent the presence of $ZnSO_4$. It is safe to come to the conclusion that Ca largely exists as $CaSO_4$ and to a smaller extent as the $Ca_3(PO_4)_2$.

4.3.3 Multiscan Spectra of Soot

In several earlier studies of diesel soot it has been suggested that either interaction between soot and antiwear chemistries and/or adsorption of decomposition products of ZDDP on to the surface of soot may be responsible for decreased wear performance. However, the stability of these adsorbed products were never examined [109] In order to examine the stability of the chemical species attached to soot particles, multiple scans at the same location of the P L-edge and O K-edge were acquired. Earlier studies of carbonaceous soot using electron energy loss spectroscopy (EELS) have indicated that the beam energy may vaporize volatiles resulting in essentially similar spectra from different soot samples [27-30,111] In studies of polymers with EELS and XAS it was shown by Rightor et. al. [112] that radiation damage could be induced using both the techniques but damage induced by XAS was smaller that that induced by EELS. However, in all prior studies multiple scans over long periods of time were not examined. It is anticipated that the high flux of photons in the synchrotron beam over multiple exposures provides sufficient radiation energy to examine the stability the phases embedded within the soot.

Fig 4.11 shows 10 scans of the P L-edge acquired over the energy range of 130-155 eV. These spectra were acquired with a step size of 0.1 eV with a residence time of 2 seconds at each step and the multiple spectra were acquired in succession from the same region. In each spectrum the exposure to the beam is approximately 500 seconds for a total of 5000 seconds of exposure time. It is clear from the 10 spectra that there is little difference between the 1^{st} and the

10^{th} spectra indicating that the P that is present as $Zn_3(PO_4)_2$ and $Ca_3(PO_4)_2$ remains stable under synchrotron radiation and there is no evidence of decomposition of phosphorous-based.

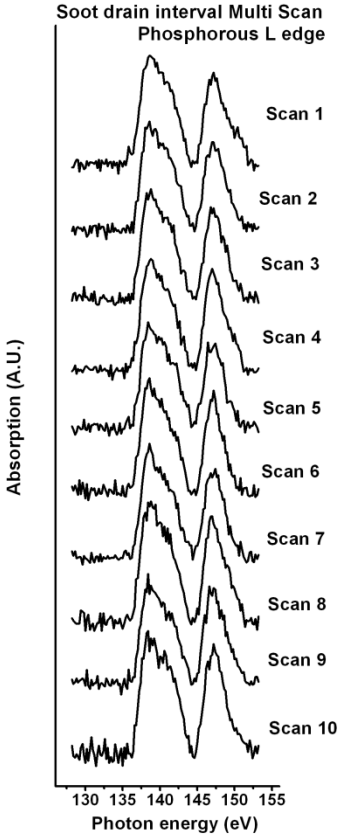

Figure 4.11 Fluorescent yield (FY) spectra of 10 successive scans of diesel soot at the P L-edge

The oxygen K-edge multi-spectra are shown in Fig. 4.12. These spectra were acquired over an energy range of 520-560 eV with a step size of 0.1 eV and a residence time of 2 seconds at each step and the multiple spectra were acquired in succession from the same region. In each spectrum the exposure to the beam is approximately 800 seconds for a total of 4000 second of exposure time. The presence of the pre-edge suggests the presence of Fe_2O_3 and the post edge structure indicates the presence of $CaSO_4$, $Zn_3(PO_4)_2$ and $Ca_3(PO_4)_2$. More importantly, both the 1^{st} and 5^{th} spectra are identical indicating the stability of the oxygen containing species within the soot structure.

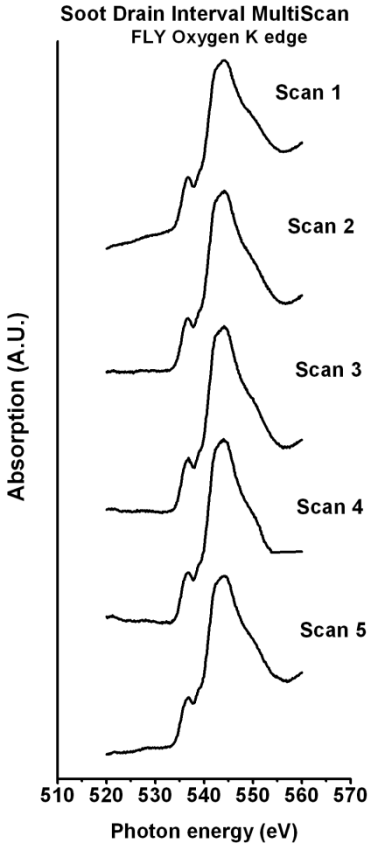

Figure 4.12 Fluorescent yield (FY) spectra of 5 successive scans of diesel soot at the O K-edge

4.3.4 High Resolution Transmission Electron Microscopy

Transmission electron microscopy has been used extensively in the past to examine wear debris [113] and provides valuable insight into the generation of wear debris which is essentially composed of tribofilms delaminated from the wear surface as well as abrasive wear particles that are generated by the tribological process. High resolution TEM has been also used to probe the structure of carbon black, which has a turbostratic structure [98,114,115] as well as diesel soot [18,63]. Several samples of diesel soot harvested from used engine oil were examined.

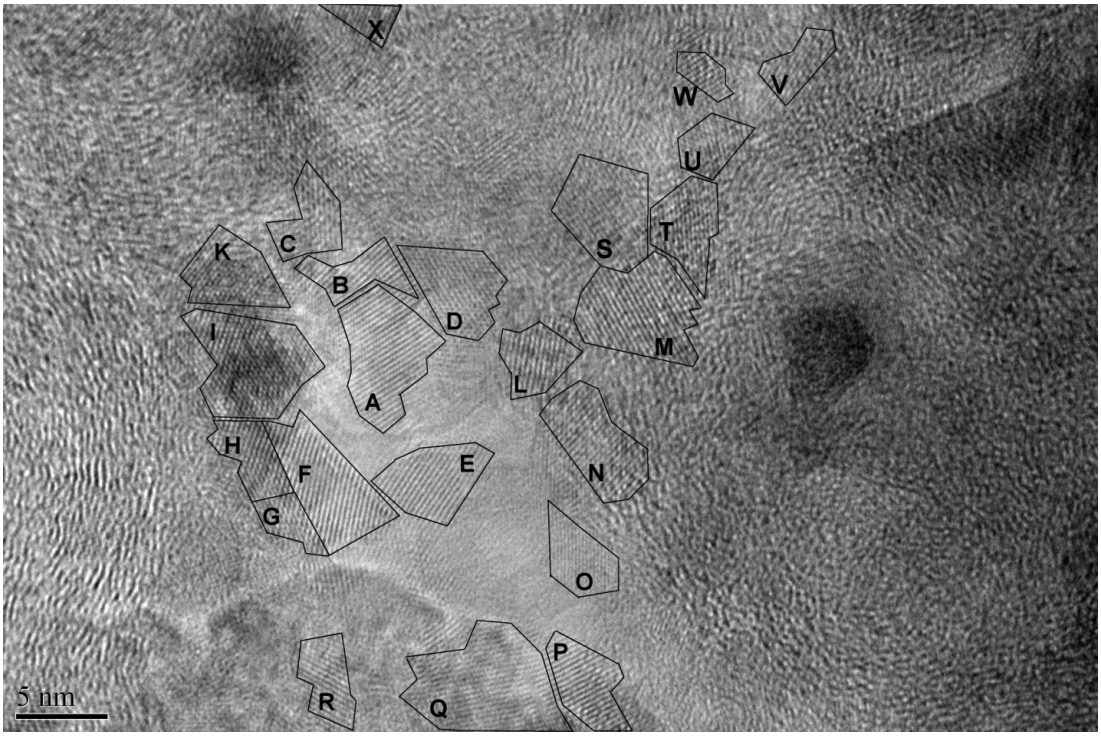

Figure 4.13 High-resolution bright field transmission electron micrograph of diesel soot showing turbostratic and amorphous regions of diesel soot and the nano crystalline particles embedded within the soot particles. ,Note the seamless interface between the nano-particles and the soot structure

Figure 4.13 is a typical high-resolution bright field transmission electron microscopic image of diesel soot that shows regions encompassing turbostratic carbon structure, which is the main, constituent of diesel soot. In addition, there are several nanocrystalline regions identified that are physically embedded within the soot and cannot be removed by washing, ultra sonication and centrifuging the soot.

Table 4.1 Inter-planar crystal spacing and indices of crystallographic plane of nano-crystalline

Nano crystalline Particles	Inter-planar crystal spacing d (Å)		The indices of crystallographic plane (hkl)
	Standard	Measured	
A	2.814	2.85	$Ca_5(PO_4)_3)OH$ (211)
B	2.69	2.69	Fe_2O_3 (104)
C	2.72	2.754	$Ca_5(PO_4)_3$ OH (300)
D	2.778	2.783	$Ca_5(PO_4)_3OH$ (112)
	2.261	2.283	$Ca_5(PO_4,CO_3)_3OH$ (130)
E	2.814	2.812	$Ca_5(PO_4)_3$ OH (211)
F	2.814	2.809	$Ca_5(PO_4)_3$ OH (211)
G	2.717 / 2.261	2.718 / 2.256	$Ca_5(PO_4,CO_3)_3OH$ (300), (130)
H	2.69 / 2.72	2.70	Fe_2O_3 (104) / $Ca_5(PO_4)_3$ OH (300)
I	2.811/2.261	2.824/2.35	$Ca_5(PO_4,CO_3)_3OH$ (211), (130)
J	2.72 / 2.69	2.711	Fe_2O_3 (104) / $Ca_5(PO_4)_3$ OH (300)
K	2.51	2.468	Fe_2O_3 (104)
L	2.72	2.729	$Ca_5(PO_4)_3OH$ (300)
M	2.814	2.8339	$Ca_5(PO_4)_3OH$ (211)
N	2.717/2.261	2.778/2.365	$Ca_5(PO_4,CO_3)_3OH$ (300)/$Ca_5(PO_4,CO_3)_3OH$(130)
O		2.02	Unknown
P	2.778 / 2.811	2.792	$Ca_5(PO_4)_3OH$ (112)/$Ca_5(PO_4,CO_3)_3OH$ (211)
Q	2.814	2.868	$Ca_5(PO_4)_3OH$ (211)
R	2.814	2.856	$Ca_5(PO_4)_3OH$ (211)
S	2.70	2.702	Fe_2O_3 (104) / $Ca_5(PO_4)_3$ OH (300)
T	2.811	2.812	$Ca_5(PO_4,CO_3)_3OH$ (211)
U	2.261	2.258	$Ca_5(PO_4,CO_3)_3OH$ (130)
V	2.69 / 2.72	2.712	Fe_2O_3 (104)/$Ca_5(PO_4)_3$ OH (300)
W	2.814	2.832	$Ca_5(PO_4)_3OH$ (211)
X	2.69	2.665	Fe_2O_3 (104)

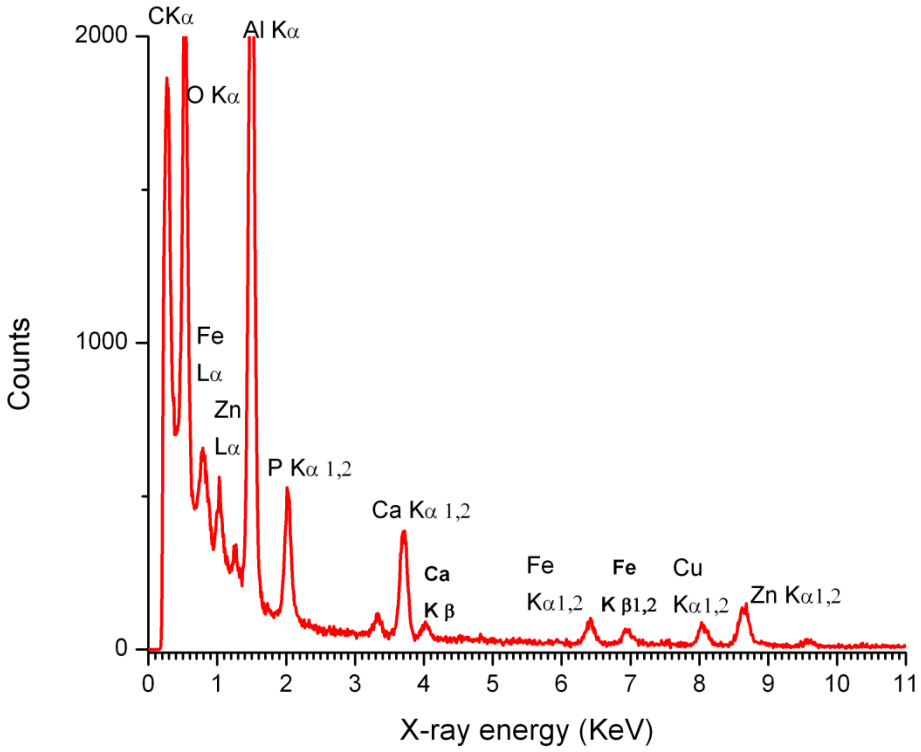

Figure 4.14 EDS spectra of diesel soot showing the presence of Ca, P, S, Zn, Fe, O and C in diesel soot from the region of interest in Figure 4.13. Cu and Al are from the sample holder. Note that the Ca and P peaks are very strong in comparison to the Zn peaks

An energy dispersive spectrum of the region that included most of the nanocrystalline particles is shown in Figure 4.14. EDS spectra suggest the presence of C, O, P, Ca, Fe and Zn in the area while no S peak was recorded. The peaks of Al and Cu originate from samples holder. The XANES results from previous sections suggest the presence of sulfate and phosphates of calcium and zinc, and presence of ferric oxide. The interplanar spacing between the crystallographic planes was determined and is shown in Table 4.1 and 4.2. Matches were made with possible compounds of Zn, Ca, and Fe including carbonates, phosphates and oxides. It is evident from the matched data that the likely candidates for the crystalline particles include Fe_2O_3, hydroxyapatite ($Ca_5(PO_4)_3OH$) and carbonate hydroxyl apatite ($Ca_5(PO_4,CO_3)_3OH$. The absence of sulfur in the EDS spectra indicates that the $CaSO_4$ that was identified in the synchrotron x-ray diffraction arises from larger particles not embedded within the turbostratic structure of diesels soot. In an earlier study of wear in the presence of diesel soot it was

suggested that polishing wear is a possible mechanism to account for enhanced wear [63] in addition in a study with ashless antiwear agents it was shown that the presence of small (<20 nm) particles of Fe_2O_3/Fe_3O_4 promotes polishing wear [116]. The hardness of Fe_2O_3 and phosphates of calcium is in the range of 5-6 in the Moh's scale which is much larger than the 2-3 for gypsum and bassanite [98] There is presence of Zn in the EDS spectra but none of the crystalline planes match those of known phosphates, carbonates and oxides of Zn indicating that Zn is present in amorphous state. XANES indicates that Zn is present as short chain Zn-phosphates that likely originated from the tribofilm and is generally present as an amorphous tribofilm at contacting surfaces.

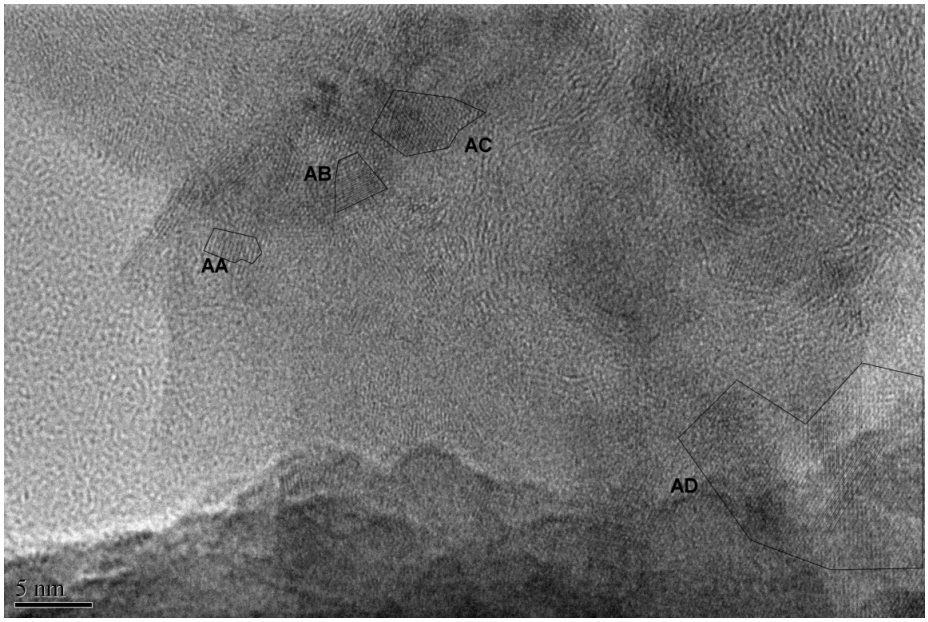

Figure 4.15 High-resolution bright field transmission electron micrograph of diesel soot showing turbostratic and amorphous regions of diesel soot and the nano crystalline particles embedded within the soot particles

Figure 4.15 is another representative HRTEM image of soot particles from a different area that also shows the presence of turbostratic carbon structure as well as the presence of crystalline embedded particles. An energy dispersive spectrum of the region that included most of the nanocrystalline particles is shown in Figure 4.16. EDS spectra of the region including the crystalline particles indicates the presence of C, O, Ca, P, S and Fe and the measurement of the

lattice spacing indicates the presence of Fe_2O_3 and $Ca_5(PO_4)_3OH$ as in the previous cases, shown in Table 4.2 Other regions (not shown) show similar outcomes.

Table 4.2 Inter-planar crystal spacing and indices of crystallographic plane of nano-crystalline particles present on diesel soot

Nano crystalline Particles	Inter-planar crystal spacing d (Å)		The indices of crystallographic plane (hkl)
	Standard	Measured	
AA	2.69 / 2.72	2.71	Fe_2O_3 (104)/ $Ca_5(PO_4)_3$ OH (300)
AB	2.69 / 2.72	2.70	Fe_2O_3 (104)/ $Ca_5(PO_4)_3$ OH (300)
AC	2.51 2.51	2.42 2.48	Fe_2O_3 (110) Fe_2O_3
AD	2.51/ 2.51	2.53/2.51/2.72	Fe_2O_3 (110) / Fe_2O_3/Fe_2O_3

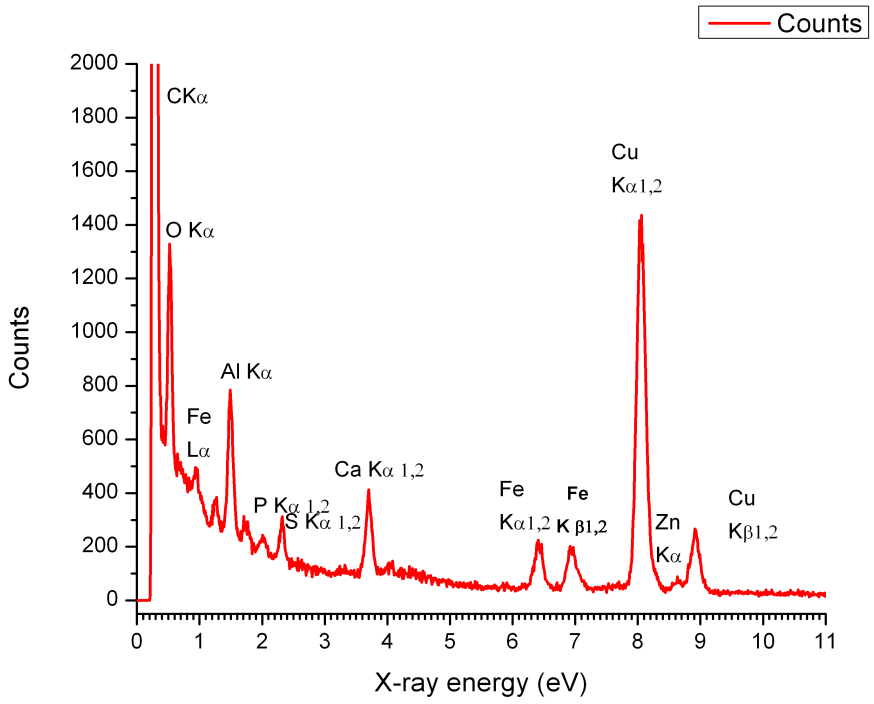

Figure 4.16 EDS spectra of diesel soot showing the presence of Ca, P, S, Zn, O and C in diesel soot from the region of interest in Figure 4.15. Cu and Al are from the sample holder. Note the strong presence of Fe peaks in these spectra

4.4 Discussion

In the companion study [117] , it is worth taking into consideration that energy dispersive x-ray spectroscopy in the TEM could detect phosphorous, sulfur, zinc and calcium only on bigger agglomerates of size few hundreds of nanometers or bigger and its absence on smaller primary soot particle which typically range in size from 20-50 nm. In addition, SAD patterns shown in the companion study [96] originates from crystalline domains of turbostratic structure of soot. Furthermore, high-resolution x-ray diffraction spectra indicate presence of calcium sulfate in hydrated form (gypsum) and semi-hydrated form (bassanite) in their crystalline form and their presence as distinctive peaks in the x-ray spectra indicates that their particle diameter is in the range of a few μm.

In this study the XANES spectra of K and L absorption edge suggest the presence of zinc phosphate, ZnS, $CaSO_4$ and to a lesser extent $Ca_3(PO_4)_2$. It has been shown in XANES spectra of tribofilms that L absorption edge in TEY mode can probe sampling depth of ~ 5-7 nm while FY probe depths of ~ 50-70nm. On the other hand K absorption edge can probe ~ 50-70 nm in TEY mode and few μm in FY mode.[96] This implies that K absorption edge XANES spectra was obtained from larger volume of diesel soot, which is supported, by TEM and EDX results. Thus, TEM, EDX and XANES results in tandem, suggest the possibilities of these compounds present on diesel soot surface and/or incorporated in the turbostratic structure of diesel soot.

Zinc phosphate, ZnS, $CaSO_4$ and $Ca_3(PO_4)_2$ are decomposition products of lubrication additives (such as ZDDP and overbased calcium sulfonate) and wear debris from tribofilms. Zinc phosphate is decomposition products formed due to break down of ZDDP in tribo-chemical reaction in boundary lubrication condition and serve as protective antiwear film.[48] Presence of zinc phosphate can be related to ZDDP degradation on metallic surfaces, which results in the formation of phosphates and sulfates of zinc.[86] Yamaguchi et al. used XANES, to study depletion of ZDDP in used engine oil where formation of $Zn_3(PO_4)_2$ coupled with depletion of ZDDP were reported in used engine oil after 200 hours. [107] Presence of $Zn_3(PO_4)_2$ on soot residue give rise to the possibility that $Zn_3(PO_4)_2$ from the wear debris might interact with soot and

get chemisorbed on the soot structure. There also exist a possibility of used oil trapped on soot residue but multiple washing with hexane eliminates that possibility. These results confirm the interaction of $Zn_3(PO_4)_2$ with soot and its absorption on soot structure. Ratoi et . al, Nagai et. al, and Mainwaring suggested that soot abrades the anti-wear films. [116] Abrasion of anti wear films can produce small wear debris of anti-wear film, typically made up of amorphous zinc phosphates with nano-crystalline oxides of Fe [15,23,38]. If this is so, then presence of zinc phosphate on soot surface should be in form of hard wear debris. Studies have also reported the possibility of ZDDP reacting with soot surface which on hydrolysis gives rise to phosphate and the presence of strong detergents retards the absorption of phosphates [65,98] .

Rounds suggested the mechanism of preferential adsorption of antiwear components from oil phase to soot surface. [116] These oil soluble decomposition products were postulated to be either physisorbed or chemisorbed on soot surface. In our study, multiple dilutions with hexane and centrifugal separation minimize the likely hood of physically absorbed species on soot surface. Thus, it is likely that chemisorptions or embedding of $Zn_3(PO_4)_2$ on soot structure is more likely than physisorption. It is likely that these particles are extracted from the tribofilm during 3-body wear.

Ratoi et. al., [27-30] also suggest the effectiveness of certain type of dispersants is crucial to avoid agglomeration. Several studies have reported that use of overbased detergents can provide substantial wear protection. [38] Thus, origin of calcium in the soot debris is from the detergent in the fully formulated oil. The overbased detergents are made up of nano-particles of $CaCO_3$ encapsulated within a calcium sulfonate micelle structure. Over time the detergent breaks down contributing Ca to the soot residue as well as to the formation of tribofilm. Examination of tribofilms formed with overbased calcium detergents showed the formation of phosphates of Ca in the tribofilms [83,118,119] which may be removed by three body wear and incorporated into the soot residue. High-resolution x-ray diffraction study in the companion study [66], suggests that calcium sulfates are present as gypsum and bassanite in the crystalline forms with particle sizes larger than 1 μm while no evidence of calcium phosphates were recorded. XANES spectra in this

study reveal the presence of calcium sulfates and to a lesser extent phosphates of Ca. Moreover, the high resolution TEM clearly indicates that the phosphates of Ca are present as nano-particles embedded on the surface of turbostratic structure of soot. The presence of these decomposition products on soot structure suggests the interaction between soot and lubrication additives chemistry from both the oil and tribofilm.

It is important to note that the nanocrystalline particles are continuous with the turbostratic soot structure and suggests the possibility of mechanical embedding with a strong interface which cannot be removed by washing, ultra sonication and centrifuging the soot. A schematic of this soot structure with embedded nanoparticles is shown in Fig. 17. It is well documented Fe_2O_3 in wear debris originates from abrasive rubbing between two surface in relative motion under boundary lubrication conditions. [96]. The origin of nano crystalline particle of $Ca_5(PO_4)_3OH$ and $(Ca_5(PO_4,CO_3)_3OH$ is likely from the interaction of the detergent with phosphorous containing species from ZDDP. It is postulated that the mechanical embedding or chemical bonding of these nanocrystalline particles on soot surface might take place due to three body wear during operation. During engine operation, trapped diesel soot particles / agglomerates between two rubbing surfaces experiences repeated extreme local temperature and high contact pressure which might be responsible for mechanical embedding or chemical bonding of identified nanocrystalline particles. As mentioned previously that these nanocrystalline particles composed of Fe_2O_3, $Ca_5(PO_4)_3OH$ and $(Ca_5(PO_4,CO_3)_3OH$ are harder on Moh's scale. [75,115]. Hence, it is possible that mechanically embedded or chemically bonded harder nanocrystalline particle might promote higher wear, abrasive in some cases [117] and catastrophic failure in extreme conditions.

It is unlikely that un-decomposed additives such as ZDDP are physically adsorbed on to the soot particles, as it does not show up in the XANES spectra. Hence it can be concluded that the primary reason for the increase in wear in the presence of diesel soot is likely from the presence of hard nano-particles embedded within the surface of the turbostratic structure of soot as shown in Figure 4.17.

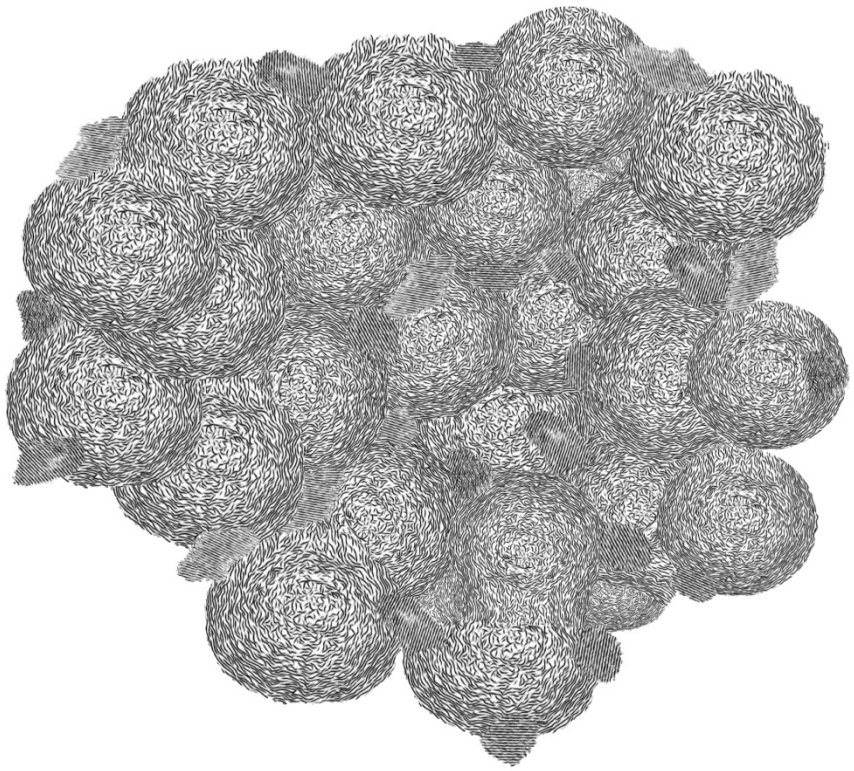

Figure 4.17 Schematic of the turbostratic structure of diesel soot with embedded nanocrystalline particles. The nanocrystalline particles can be phosphates of Ca as well as Fe_2O_3

4.5 Conclusions

X-ray absorption near edge structure (XANES) was used to examine the chemistry of diesel soot that was harvested from an exhaust gas recirculated diesel engine. XANES spectra were acquired at the P L and K edge, S L and K edge, Ca L and K edge and Zn L-edge.

(i)The L-edge spectra of P indicates the presence of P in diesel soot from decomposition products of ZDDP and not fresh ZDDP and the phosphates present are likely short chain phosphates due to the absence of any pre-edge structure distinctive of longer chain phosphates.

(ii)The sulfur L-edge spectra suggests that most of the sulfur is present in the form of sulfates and the likely candidates are $CaSO_4$ and those of $ZnSO_4$ are also possible. $FeSO_4$ is not a likely candidate as very little Fe is present from EDS analysis in the companion study.

(iii) The Zn L-edge spectra clearly indicates that ZnO is not present, the phosphates and sulfates of Zn can be differentiated based on their fine structure post edge, however, the low

concentration of Zn in the soot results in a noisy spectra and it is difficult to resolve between the phosphates and sulfates of Zn. However, the companion study [53,59] did not indicate the presence of any crystalline sulfates of Zn, hence the likely form of Zn is amorphous phosphates of Zn. It is well known that tribofilms are made up of amorphous short and long chains of zinc polyphosphates and it is not unlikely that the abrasive action of soot on the tribofilms results in the incorporation of wear debris from the tribofilms in the soot.

(iv) The Ca L-edge absorption edges of the $Ca(OH)_2$ and $Ca_{10}(PO_4)_6(OH)_2$ are at a lower energy than that of the sulfates and phosphates of Ca. Spectra from diesel soot indicates that the Ca exists primarily as $CaSO_4$.

(v) The Fe L-edge spectra indicate the presence of Fe_2O_3/Fe_3O_4 while the presence of sulfates and phosphates of Fe were not detected.

(vi) The B K-edge spectra indicate the presence of B_2O_3 and BPO_4. The B_2O_3 is possibly sourced from the borated dispersant used in the lubricant. On the other hand the BPO4 is present in the tribofilm based on reactions between the borated dispersant and ZDDP decomposition products at the tribological surfaces. Boundary lubrication conditions coupled with the presence of soot at the tribological contact region may be responsible for stripping some of the BPO4 from the tribofilm and incorporating it into the soot residue.

(vii) The O K-edge spectra are more complex and diffuse and suggest the origin of oxygen is from phosphates of Zn as well as sulfates of Ca. In addition, the presence of a distinctive pre-edge peak indicates the presence of Fe_2O_3. The Fe_2O_3 is likely incorporated into the soot residue during three body wear under boundary conditions where soot particulates trapped in the tribocontact have particles of Fe_2O_3 incorporated into them.

(viii) The P K-absorption edge provides information from a larger volume of material due to the larger interaction volume at higher energies. The phosphates of Fe and Zn are clearly distinguished by the pre-edge peak which is present in $FePO_4$ but absent in Zn and Ca phosphates. In addition, a post edge shoulder present in $Ca_3(PO_4)_2$ is absent in $Zn_3(PO_4)_2$. The K-edge spectra of soot closely match that of $Zn_3(PO_4)_2$.

(ix) The S K-edge spectra are very useful in distinguishing between sulfides and sulfates as well as between different sulfides. In addition, one can distinguish between the different sulfates. The S K-edge spectra indicate that sulfur in soot is largely present as $CaSO_4$ and to a smaller extent as $ZnS/ZnSO_4$ with almost the complete absence of $FeSO_4$.

(x) Ca K-edge spectra can clearly distinguish between CaO and CaSO4 and $Ca_3(PO_4)_2$ and the spectra indicates an absence of CaO, P K-edge spectra and S K-edge spectra indicates that P is coordinated with Zn and S with Ca and from the Ca K-edge spectra the Ca largely exists as $CaSO_4$ and to a lesser extent as $Ca_3(PO_4)_2$.

(xi) High resolution transmission electron microscopy couple with energy dispersive spectroscopy reveals the presence of crystalline nano-particles embedded on the periphery of the turbostratic structure of soot. A closer examination of the interplanar spacing with lattice imaging coupled with elemental analysis of these nano-particles indicates that the particles are constituted of phosphates of Ca as well as Fe_2O_3. These compounds have a hardness of around 5-6 on the Moh scale and can contribute to polishing wear under three body boundary lubrication conditions.

CHAPTER 5

A LABORATORY SIMULATION OF COMPOSTION AND STRUCTURE OF DIESEL SOOT BY TREATMENT OF CARBON BLACK AND ITS TRIBOLOGICAL ASSESSMENT

PART I: WEAR ASSESSMENT

5.1 Introduction

Soot induced wear of the diesel engine is a well known problem [96]. A great deal of attention has been paid to this problem since 2007 when the environmental protection agency (EPA) implemented emission norms API CJ 4 in an effort to reduce emission of pollutants from diesel engine along with the mandates to extend the life of diesel particulate filters and catalytic converters by lubrication decomposition products in tail pipe. [1,11-14,23,24,31,32,39-41,51-56,58,59,88,120] Previous studies [10,15,28-30,37,38,60-62,121,122] have provided significant insights in the comprehension of soot induced wear mechanism. Several of these studies [4,86] that have used carbon black as a soot surrogate have led to various phenomenological models to explain behavior of soot under different tribological conditions. These studies have shown that carbon black is analogous to diesel soot in terms of the turbostratic structure, but significant differences have been observed between carbon black and diesel soot in terms of their morphology, agglomeration, elemental compositions, particle sizes etc.[1,11-14,23,24,31,32,39-41,51-56,58,59,88,120] In fact, much work on ‘soot’ dispersions has been done using carbon blacks as soot surrogates. As might be expected, there is little agreement on which carbon black most closely resembles engine crankcase oil soot. An obvious difference is the formation conditions of soot in the engine and in making carbon blacks. In the engine, most of the soot that finds its way into the crankcases is formed when a burning oil droplet is quenched in the oil film on the cylinder wall, i.e. a relatively low temperature process. [10,15,28-30,37,38,60-

62,121,122]On the other hand, carbon black has been manufactured by thermal oxidative decomposition of hydrocarbons and its morphological characteristics are controlled by choice of feedstock and process conditions. [1,11-14,23,24,31,32,39-41,51-56,58,59,88,120]. Evidence for the effect of formation temperature has been given by Jao and coworkers, who found that carbon blacks conducted electricity, whereas engine crankcase oil soot did not. From the point of view of dispersant – crankcase soot interaction, the important property of soot is its surface chemistry. [10,15,28-30,37,38,60-62,121,122]

Clague et al [18] had employed various characterization tools in their study to understand the efficacy of carbon black as soot surrogate have reported various similarities and differences between carbon black and soot. Moreover, elemental composition of carbon black suggests presence of carbon, oxygen and hydrogen as major constituents along with small amount of sulfur and other elements from feedstock. Studies of the chemical make up of crankcase soot using x-ray absorption near edge structure (XANES) spectroscopy and energy dispersive spectroscopy (EDS) have shown the presence of various sulfates and phosphates of calcium and zinc on soot which originate from decomposition products of lubrication additives chemistries and wear debris of tribofilm. [10]. Our previous studies [22,53,63,123] have detailed, both the similarities and differences between carbon black and crankcase soot. We have shown the presence of hard nano size crystalline particle of calcium phosphates, carbonate hydroxylapatite and iron oxide embedded within the turbostratic structure of soot using high resolution transmission electron microscopy (HRTEM). Presence of these chemistries and hard nano crystalline particles on the turbostratic structure of soot is one of the important differences when compared to carbon black.

In the present study carbon black is subjected to different treatments in an attempt to alter its chemistry and structure to simulate carbon black. To evaluate, if the treatments have successfully simulated the chemistry and structure of diesel soot, various post characterization techniques such as transmission electron microscopy, Raman spectroscopy and XANES spectroscopy were employed. The results obtained from these experiments were then compared

with extracted diesel soot from crankcase oil. Tribological behavior of these treated carbon blacks was studied by using four ball wear tester. Scanning electron microscope and optical microscope were used to study the mode of wear.

A successful treatment to simulate diesel soot structure and chemistry would provide significant information to develop a mechanism through which diesel soot structure and chemical make up might get modified during engine operation. This study is also intended to get further insight into the mechanism for soot induced wear. Although, it is difficult to predict any specific conditions that diesel soot encounter due to extremely dynamic situation prevails during engine operation the laboratory tests developed in this study is an attempt to chemically and structurally modify carbon black to simulate wear similar to diesel soot.

5.2 Experimental Procedure

5.2.1 Bench test formulations

Three approaches were used in formulating oils for tribological evaluation (i) Mineral base stock with AW additive and dispersant with and without carbon black (ii) Fully formulated oils with and without carbon black (iii) Mineral base stock with AW additive and dispersant blended in with treated carbon black that were extracted from previous two formulations. The amount of phosphorous was decided as per API CJ 4 SAPS norms where maximum limit of phosphorous was 0.1 wt.%. The baseline chemistry was composed of mineral oil with ZDDP (0.1 wt.% P) with 5 wt.% dispersant hereafter referred to as Formulation A [provide details of dispersant]. In order to assess the oxidative stability of this formulation, it was oxidized at 120°C for 100 hours in an air environment yielding Formulation B.

Carbon black was treated by blending it in two lubricants formulations; (a) Mineral oil + 0.1 wt. % P from ZDDP + 5 wt. % Dispersant. (b) Fully formulated commercial diesel engine oil. Earlier studies [reference] using diesel engine dynamometer tests suggests amount of soot in crankcase is as much as 7 - 12wt %. It is extremely difficult to conduct treatment on carbon black blended with 7 to 12 wt.% due to the very high viscosity of the oil. The amount of carbon black was decided based on the test that was conducted to understand the soot laden viscosity

increase in Mack T 7 engine using API CH 4 and API CJ 4 oil. These tests have shown the considerable increase in the viscosity after the threshold of 3% soot loading. [51] Hence, the oils were treated with 3 wt. % carbon black in order to minimize the contribution from viscosity increase in the wear outcome and focus on primarily on the role played by carbon black on wear. In order to keep the carbon black dispersed in the oil 5 wt. % of dispersant was added to the base oil formulations.

In order to assess the role of carbon black on wear, baseline formulation A was blended with 3 wt. % carbon black yielding formulation C. In order to understand the effect of accelerated oxidation due to blow by, baseline formulation A was blended with 0.1 wt. % iron nepthanate as synthetic blow-by and is referred to as formulation D. Moreover, In order to compare the deterioration of anti wear properties of formulations with treated and untreated carbon black, 3 wt. % diesel soot was blended with base line formulation A. Hereafter, this formulation is referred as formulation F. This diesel soot was extracted from the used crankcase diesel engine oil acquired from a commercially operated single diesel engine.

To simulate the chemistry and structure of diesel soot, formulation C that has [Mineral Oil + 0.1 wt. % P from ZDDP + 5 wt. % Dispersant + 3 wt.% Carbon black] was treated in different conditions. These conditions are detailed in the following section. To understand the effect of oxidation on formulation blended with carbon black, formulation C was oxidized in air at 120° C for 100 hours. Hereafter, this formulation is referred as formulation E. Formulation C was also subjected to accelerated oxidation using synthetic blow-by wherein formulation C was blended with 0.1 wt. % iron napthanate and oxidized in air at 120° C for 100 hours. This formulation is referred as formulation G.

In order to simulate rubbing and high contact pressure formulation C was milled for 24 hours using inert zirconia ball in planetary ball milling machine.. This formulation is referred as formulation In order to study the cumulative effect of oxidation and high contact loads and temperature formulation C was oxidized in air at 120° C for 100 hours followed by 24 hours milling using inert zirconia ball. Hereafter, this formulation is referred as formulation I.

Previous studies have characterized the chemical make up of diesel soot and have suggested the presence of amorphous zinc phosphate as well as crystalline calcium sulfate in hydrated (gypsum) and hemihydrated (bassanite). [18] It is well known fact that amorphous zinc phosphate can originate from ZDDP anti-wear additives while calcium sulfate can originate from overbased detergents. [73,96] Thus, these two formulations were chosen to distinguish the effect of a clean chemistry with just dispersant and a fully formulated oil which has a complete additive package including a calcium based detergent.

Table 5.1 Mineral base stock with AW additive and dispersant with and without carbon black

No.	Test Formulations	Treatment
A	Mineral Oil + 0.1 wt.%P ZDDP + 5% Dispersant	--
B	Mineral Oil + 0.1 wt.%P ZDDP + 5% Dispersant	Oxidizing
C	Mineral Oil + 0.1 wt.%P ZDDP + 5% Dispersant + 3% Carbon Black	No Treatment
D	Mineral Oil + 0.1 wt.%P ZDDP + 5% Dispersant + 0.1 wt.% Iron Nepthanate	Oxidizing
E	Mineral Oil + 0.1 wt.%P ZDDP + 5% Dispersant + 3% Carbon Black	Oxidizing
F	Mineral Oil + 0.1 wt.%P ZDDP + 5% Dispersant + 3% Diesel Soot	--
G	Mineral Oil + 0.1 wt.%P ZDDP + 5% Dispersant + 0.1 wt.% Iron Nepthanate +3% Carbon Black	Oxidizing
H	Mineral Oil + 0.1 wt.%P ZDDP + 5% Dispersant+ 3% Carbon Black	Milled
I	Mineral Oil + 0.1 wt.%P ZDDP + 5% Dispersant + 3% Carbon Black	Milling + Oxidizing

Table 5.2 Fully formulated oils with and without carbon black

No.	Test Formulations	Treatment
J	Fully Formulated Commercial Oil (0.1 wt.%P)	--
K	Fully Formulated Oil + 3% Carbon Black	Oxidizing
L	Fully Formulated Oil + 3% Carbon Black	Milling
M	Fully Formulated Oil + 3% Carbon Black	Milling + Oxidizing

Anti-wear properties of fully formulated oil were evaluated by using fully formulated oil referred to as formulation J. The fully formulated oil was commercially available API CJ 4 oil with 0.1 wt % P. The fully formulated oil is blended with 3 wt.% carbon black and then treated in a fashion similar conditions to those described for formulation C. To evaluate the effect of oxidation of fully formulated oil on carbon black, formulation that has fully formulated oil and 3 wt% carbon black was subjected to oxidation in air for 120° C for 100 hours. This formulation is referred as formulation K. Moreover, fully formulated oil blended with 3 wt % carbon black was also milled for 24 hours using zirconia balls. This formulation is referred as formulation L. Fully formulated oil with 3 wt% carbon black was also subjected to oxidation in air for 120° C for 100 hours followed by 24 hours milling using inert zirconia ball. Hereafter, this formulation is referred as formulation M.

Table 5.3 Mineral base stock with AW additive and dispersant blended in with treated carbon black

No.	Test Formulations
N	Baseline + 3% Carbon Black Extracted from treatment L
O	Baseline + 3% Carbon Black extracted from treatment M
P	Baseline + 3% Carbon Black extracted from treatment H
Q	Baseline + 3% Carbon Black extracted from treatment I

In addition, experiments were also conducted wherein an oil with ZDDP (0.1 wt.% P)+ 3 wt. % carbon black and 5 wt.% dispersant and fully formulated oil with 3 wt. % carbon black were subjected to different treatments in order to change the characteristics of the carbon black. The carbon black from these treatments were then extracted and added to fresh oil that has ZDDP (0.1 wt.% P) and 5 wt. % dispersant at a treat rate of 3 wt. %. These formulations were evaluated tribologically to examine the role of soot pre-treatment on wear with fresh oil, this eliminates the possibility that the change in wear outcomes may arise due to oil degradation that may occur in the carbon black treatment and we can focus on the role played by the treated carbon black on wear with a fresh oil.

5.2.2 Treatment of Carbon Black

5.2.2.1 Milling of carbon black

Kawamura et al used freeze fractal replica (FFR) method using TEM to investigate the state of soot in used diesel engine oil. He suggested that small soot particle in range of 0.02 μm do not affect the anti wear properties due to effectiveness of dispersant on smaller particles. While particle greater than 0.03 μm might play a dominant role in increase wear. [73] Earlier studies by Jao et al have hypothesized on the abrasive nature of diesel soot that is responsible for the soot induced wear of diesel engine components. [86] Jap et al have suggested that the higher hardness of soot particle compared to rubbing components might be responsible for abrasive wear pattern observed on the diesel engine components. [73,96] Moreover, Jao et al used electron energy loss spectroscopy to study hardness of soot obtained from various heavy duty and light duty diesel engines. They used plasmon energies of different carbon materials with different sp^2 and sp^3 ratio to correlate valence electron density to density of materials and thereby hardness of materials.[86] Li et al have demonstrated that transformation of graphite into amorphous carbon and hence obvious different sp^2-sp^3 ratio using high energy ball milling. [74] Hence, it can be speculated that when carbonaceous materials such as graphite, carbon black, diesel soot particles and/or agglomerates get trapped between two rubbing components in relative motion, they experience extremely high pressure and temperature at the local point of

contact. Previous studies have suggested that higher pressure and temperature influences the crystalline domain of turbostratic structure and hence results in variation in sp^2 to sp^3 ratio. [9]. On the other hand, our companion studies have shown the presence of mechanically embedded hard abrasive iron oxide, calcium phosphate and carbonate hydroxylapatite on the soot structure. [53]

Our companion studies have demonstrated the presence of amorphous zinc phosphate on soot.[9] But the mechanism by which these chemistries get incorporated on soot structure is not yet completely understood.

A planetary ball mill was used with inert zirconia balls (0.25”-0.5” diameter) to impart rubbing and impact loads on to carbon black particles in the appropriate oil environment. Planetary ball milling rotates the milling container with certain speed, which impart centrifugal force to material inside the container. Depending on the rotation speed, material trapped between two milling balls experience high energy impact as well as friction during rotation.. Rotation speed of planetary ball mill was 300 rpm with ball to carbon lack ratio of 10:1. The blend was milled for 24 hours without interruption. Once milling is executed, zirconia balls were removed from the blend and the oil with the dispersed carbon black is used for further tribological assessment [formulation H and formulation L]

5.2.2.2 Oxidation treatment

It is well known fact that diesel engine operates with higher temperature and pressure and the oil in the sump is at elevated temperature. [124] This higher temperature may induce interaction between soot and reactive decomposition compounds of lubrication additives chemistries. Thermal decomposition of lubrication additives have been studied extensively [69] to understand the mechanism of tribofilm formation. In this study we aim to create conditions that force the interaction between decomposition products of lubrication additives and soot. In order to achieve this, oil with ZDDP (0.1 wt.% P) together with 5 wt.% dispersant and 3 wt.% carbon black was placed in a test tube and subjected to an oxidizing environment. The test tubes were placed in a large aluminum block with holes drilled to fit the test tubes, the intent being to have a large heat sink so that there are minimum changes in temperature of oil. The aluminum block is placed

in a furnace held at a constant temperature of 120°C. The test tubes were supplied with constant flow of dry via silicone tubes, which were immersed in the oil to ensure constant mixing and oxidation of blend. Test tubes were also vented to discharge the gases produced during oxidation. The blend was oxidized at 120° C for 100 hours. The blend is then used as test formulation for tribological evaluation.

5.2.2.3 Milling and Oxidizing Treatment

To simulate the cumulative effect of above two treatments together formulations (ZDDP (0.1 wt. %P) + 5 wt. % Dispersant in base oil) were blended with carbon black and ball milled for 24 hours followed by thermal oxidation for 120° C for 100 hours as detailed in the previous section. The treated blends were used for further tribological assessments.

5.2.2.4 Accelerated Oxidizing using Synthetic Blowby

Accelerated oxidation produces more decomposition products and hence increases the interaction with soot. To execute this treatment 0.1 wt.% iron napthanate (synthetic blow by) was added to formulation (ZDDP (0.1 wt.% P) + 5 wt.% detergent + 3 wt.% carbon black) and oxidized at 120° C for 100 hours as detailed earlier. The treated blends were used for further tribological assessment.

5.2.3 Bench test conditions and procedure

To understand the tribological behavior of treated carbon black a four ball wear tester was used to understand the wear behavior of the different treated carbon black conditions. Three ½ inch diameter steel balls are clamped together and covered with the formulation to be evaluated. A fourth ½ inch diameter steel ball referred as top ball is pressed with force of 20 kgs into the cavity formed by the three clamped balls for three point contact. The temperature of the test lubricates is regulates at 75° C and then top ball is rotated at 1200 rpm for 60 min. 52100 steel balls with a hardness of HRC 60-66 were used for the four ball test. Testing formulations are compared using average diameter of the scar diameter worn on the three lower clamped balls. Two measurements were made on each lower clamped ball at 90 degree to each other. If wear

scar were elliptical, then first measurement was made in direction of striations and other was made across the striations. An average of 6 wear scars readings is reported as scar diameters.

5.3 Results and Discussion

5.3.1 Tribological Evaluation

5.3.1.1 Mineral Base Stock Formulations

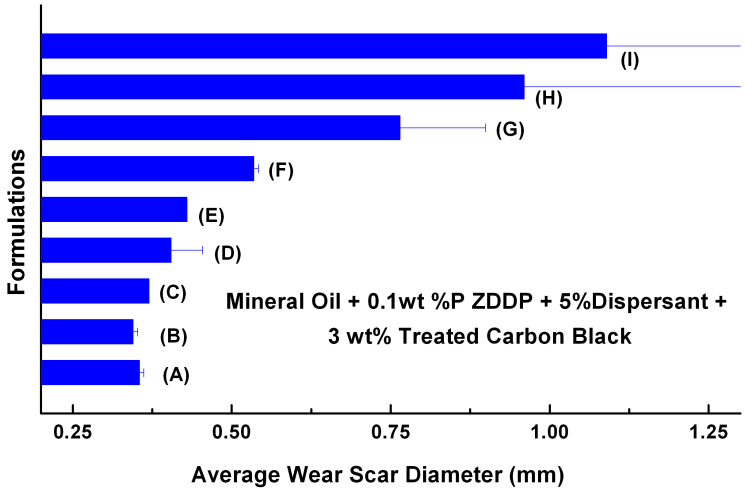

Figure 5.1 Average wear scar diameter wear scar diameter from test with formulation A-I

Baseline tests were conducted with mineral base stock with ZDDP (0.1 wt.% P) and 5 wt. % dispersant. Test formulations were also prepared by physically blending carbon black to test formulations and kept untreated to compare the results from treated test formulations. Figure 5.1 shows the average wear scar diameters measured on the stationary balls for formulations (A)-(I). Formulations A-I were prepared by adding anti wear additive ZDDP (0.1 wt. % P) to base oil together with 5 wt.% dispersant together with 3 wt.% of the appropriate carbon black (as required) . Figure 5.2 shows the corresponding optical microscope images of the average four ball wear scar formed by testing formulations detailed in Table 5.1.

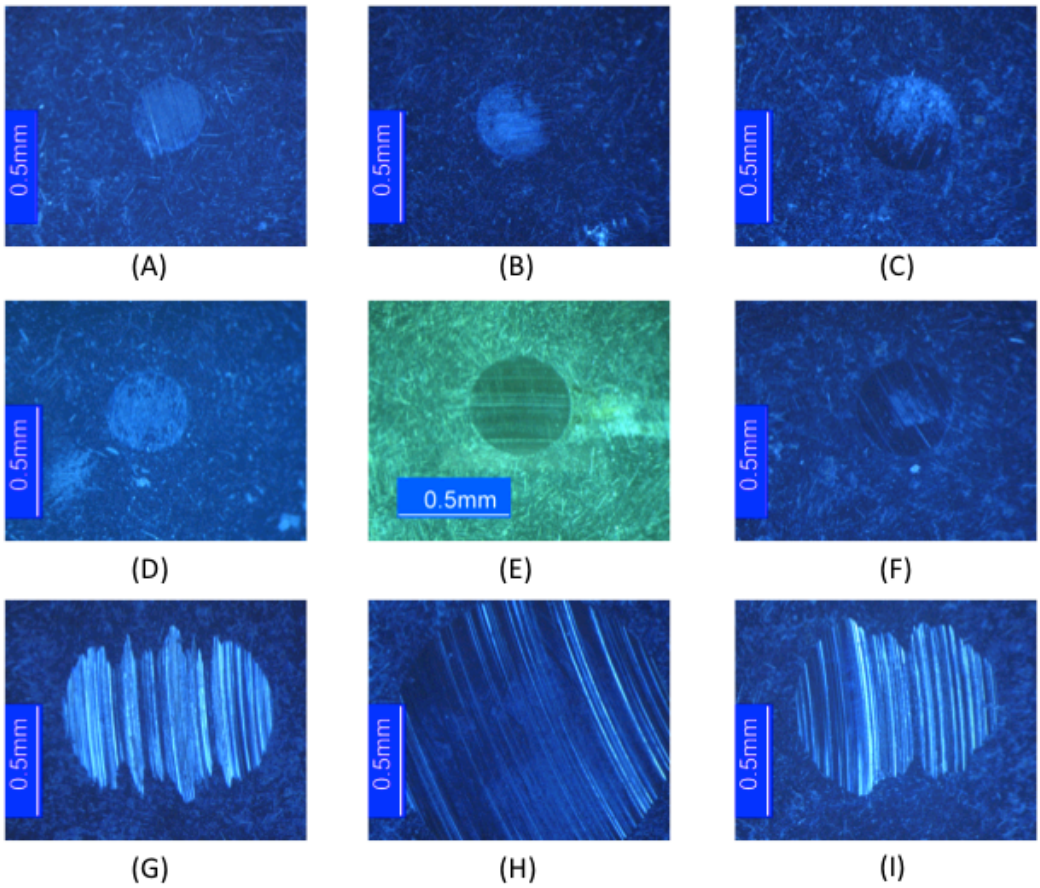

Figure 5.2 Optical micrographs of ball wear tracks from test formulation A- I

The test formulations A, B and D do not contain any carbon black. The test formulation A that has [Mineral Oil + 0.1 wt. % P ZDDP + 5% dispersant] has an average wear scar diameter 0.34 mm. The WSD does not change on oxidizing this formulation for 120°C for 100 hours. Moreover, addition of synthetic blow to formulation A (formulation D) -by increases WSD marginally to 0.36 mm. Optical microscope images of these formulation, as show in Figure 5.2, are relatively featureless indicates the presence of protective tribofilm. Figure 5.3 is scanning electron microscope image of the wear scar formed on the stationary four ball by test formulation A that had [Mineral Oil + 0.1 wt. % P ZDDP + 5% dispersant] which shows the presence of a patchy protective tribofilm on the wear surface, there is little evidence of abrasive wear in this case.

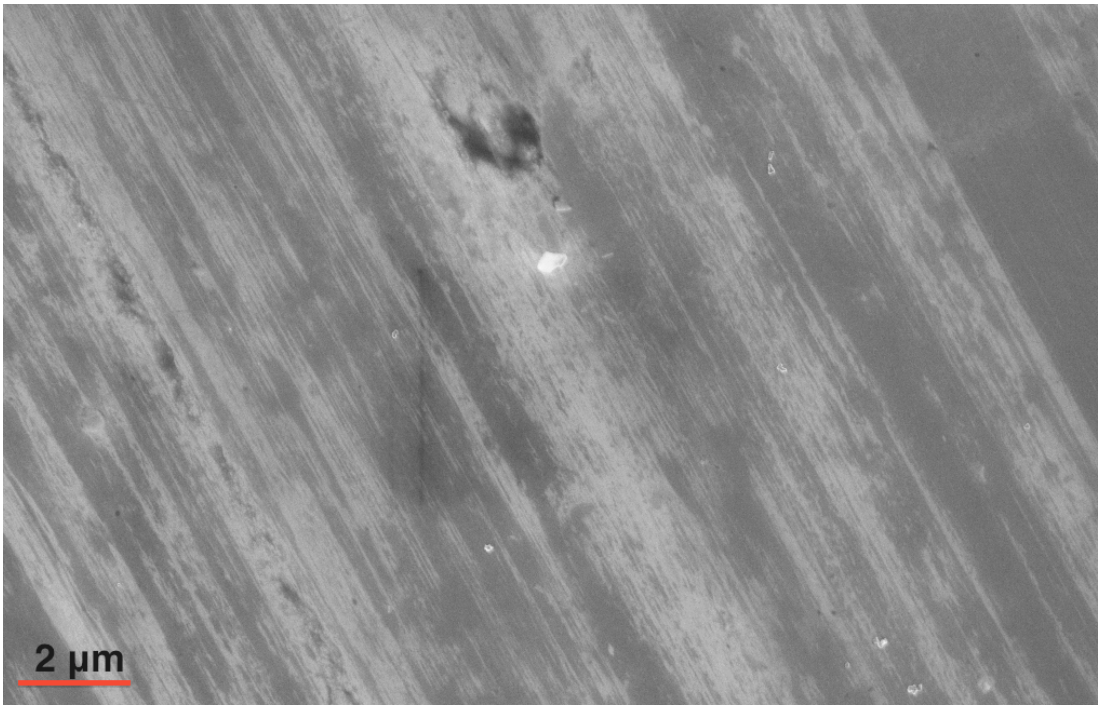

Figure 5.3 Scanning electron microscope image of the wear scar formed on the stationary four ball by test formulation A that had {Mineral Oil + 0.1 wt % P ZDDP + 5% dispersant}

Very small increase in diameter of the wear scar was observed when 3 wt.% carbon black is physically blend with formulation A (formulation C) as shown Figure 5.1. This WSD formed by formulation C is lower than wear scar formed by formulation D that was blended with synthetic blow-by but without carbon black. This indicates that the anti wear properties of formulations deteriorate in presence of synthetic blow in an oxidizing environment in absence of carbon black when compared to the formulation where carbon black was physically blended in with the test lubricant.

Extracted diesel soot was added to the lubricant A yielding formulation F. The WSD measured indicates that the diesel soot results in the deterioration of the anti wear properties of test lubricants much more compared with formulations with synthetic blow (D) or formulations that contained a blend of carbon black with the lubricant (C). The optical microscope image indicates the presence of a abrasive wear tracks in direction of rotation. Figure 5.4 is SEM images of the wear scar formed on the stationary four ball by test formulation blended with 3 wt.% diesel soot,

i.e. formulation F. This SEM image has areas that are smooth with patches of tribofilm as well as areas with severe abrasion indicating the deleterious efforts of the presence of diesel soot in the formulation.

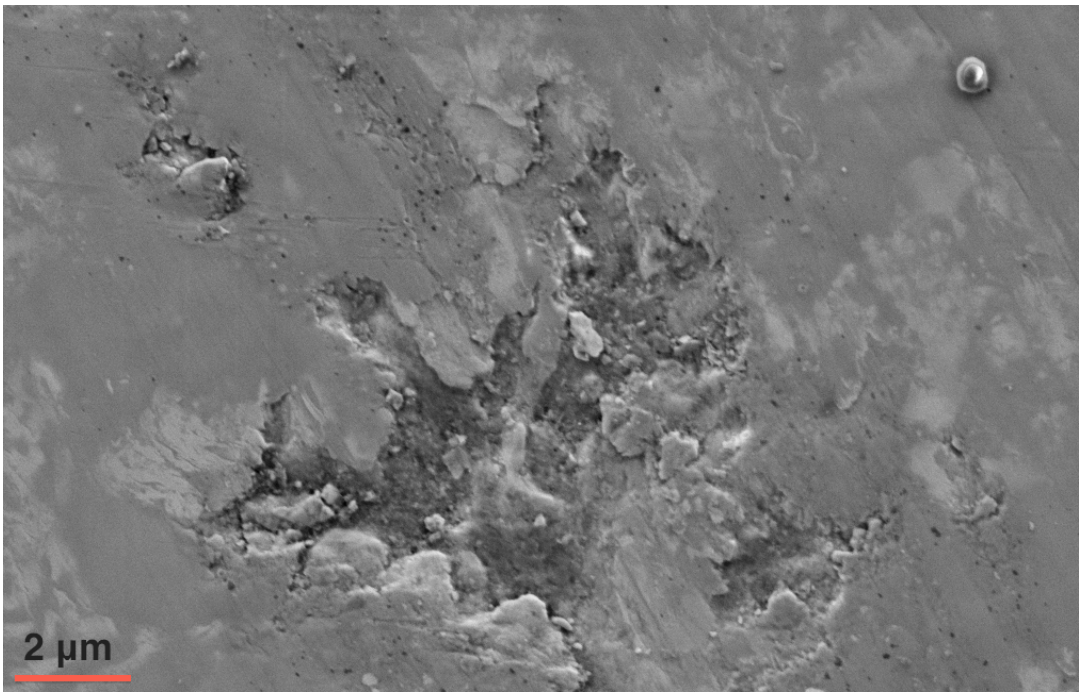

Figure 5.4 Scanning electron microscope image of the wear scar formed on the stationary four ball by test formulations blended with 3wt% diesel soot}

Results (F)-(I) in Figure 5.1, are obtained with test formulations F-I. These test formulations were blended with carbon black and then treated in various condition detailed in Table 5.1 WSD of these test formulations are higher than previous test formulations with and without the carbon black. These results indicate the role played by the different treatments in deteriorating the anti wear property of test lubricants. It is worth noticing that formulation G was blended with carbon black while formulation D was blended without carbon black, both of them contain iron napthenate. Furthermore, formulations G and D are oxidized at 120° C for 100 hours. Interestingly, average WSD of formulations G is twice the formulation D. Also, milling of the test lubricants with carbon black (formulation H) deteriorates the anti wear properties more than just the oxidizing treatment (compare E and H) oxidized treatment, which is indicated by increase in WSD from 0.76mm to 1.00 mm. Moreover, the cumulative effect of milling and oxidizing of test

lubricant with carbon black (formulation I) has highest WSD of 1.2 mm. An optical microscope image of worn clamped balls indicate the severe abrasive in direction of rotation.

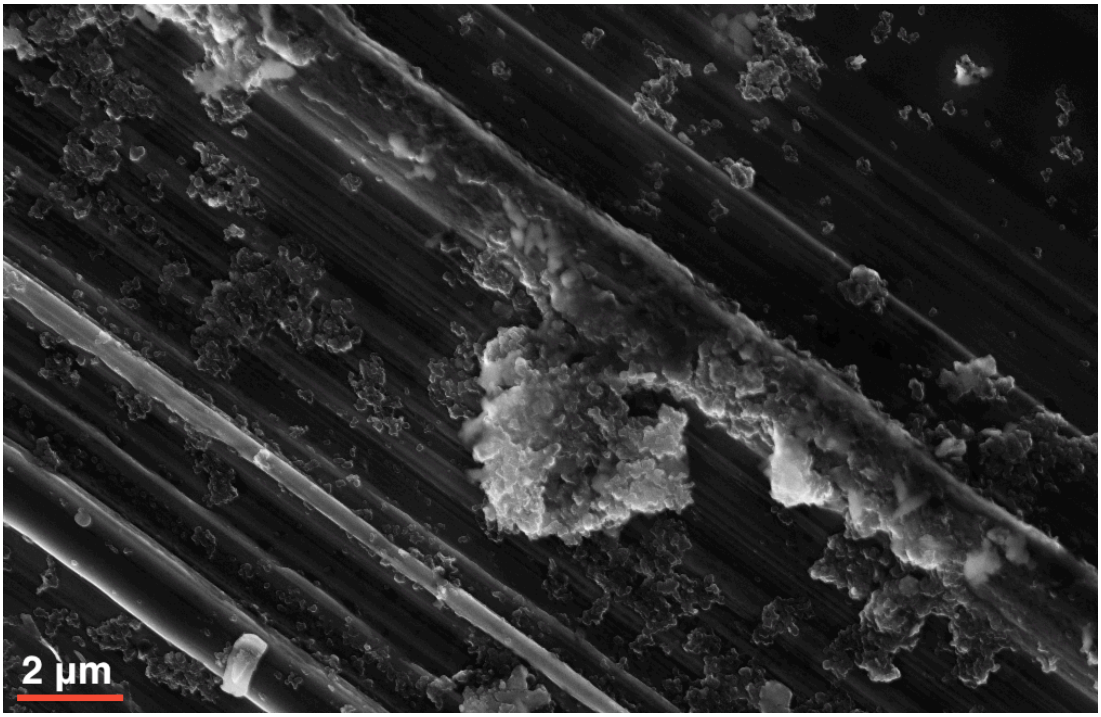

Figure 5.5 Scanning electron microscope image of the wear scar formed on the stationary four ball by test formulation that has {Mineral Oil + 0.1 wt % P ZDDP + 5% dispersant + 3wt% Carbon Black} which was treated in milling condition

Figure 5.5 is SEM image of the wear scar formed on the stationary four ball by test formulation H which was treated in milling condition. SEM image indicate the scratches running in the direction of rotation that indicate the abrasive wear is the predominant wear mode. Abrasive wear tracks have deeper grooves; perhaps due to three body wear mechanism. In addition, some patchy features can be seen that are remnants of tribofilm in the grooves.

Similar wear abrasive tracks have also been observed on the wear scar on stationary ball formed by the test formulation I, which was treated in milling and oxidizing condition. The primary difference between the two is the deeper and more severe wear scars in the treatment that was oxidized and milled.

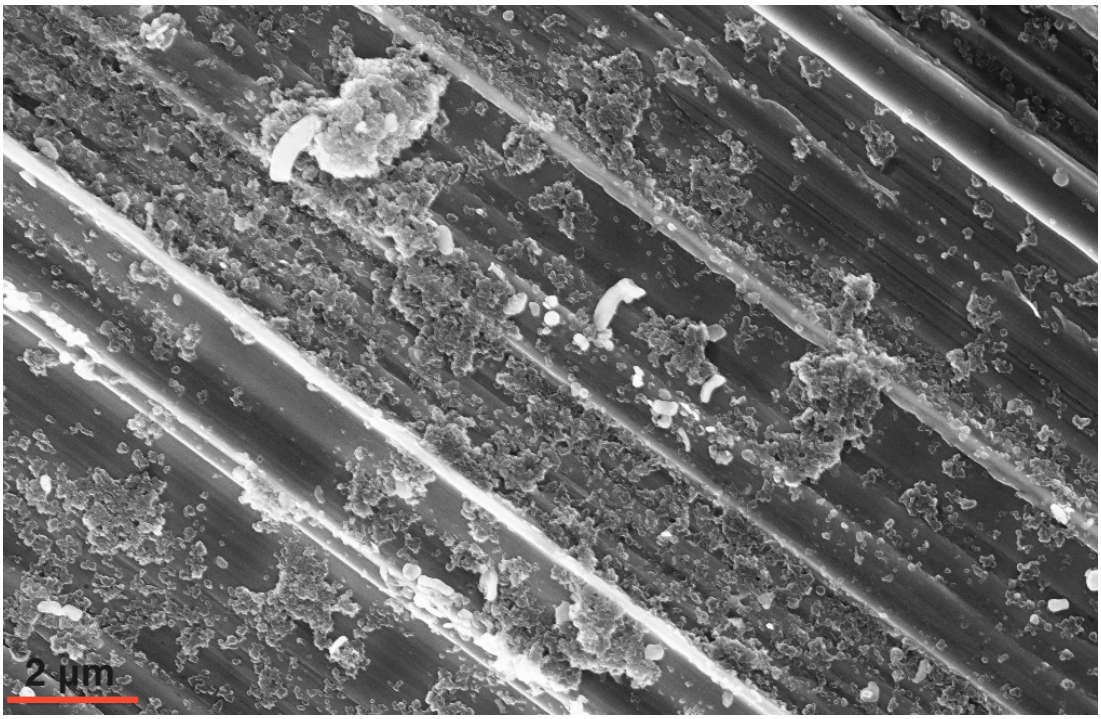

Figure 5.6 Scanning electron microscope image of the wear scar formed on the stationary four ball by test formulation that has {Mineral Oil + 0.1 wt % P ZDDP + 5% dispersant + 3wt% Carbon Black} which was treated in milling and oxidizing condition

5.3.1.2 Wear test formulations with blend of fully formulated commercial oil

Several test blends prepared by physically blending carbon black in fully formulated commercial oil followed by various treatments are detailed in Table 5.2 as formulation J - M. Figure 5.7 shows the average wear scar diameters measured on the four ball specimens for corresponding formulations. Figure 5.8 shows the corresponding optical microscope images of the typical four ball wear scar formed by testing formulations J - M.

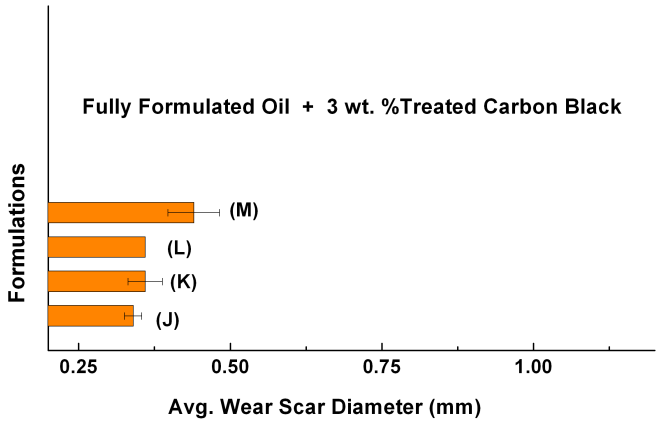

Figure 5.7 Average wear scar diameter wear scar diameter from test with formulation J – M

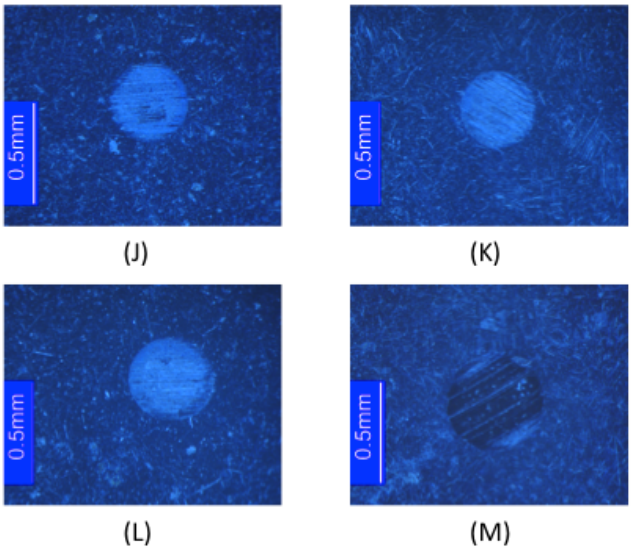

Figure 5.8 Optical micrographs of ball wear tracks from test formulation J-M

As shown in Figure 5.7, J is the base line wear test where test formulation was tested without carbon black and has a WSD of is 0.33mm. The optical microscope image shows featureless wear scar indicative of the presence of a tribofilm that is protective. On the other hand, treated carbon black formulations K - M were evaluated to examine the role of both untreated and treated carbon black on the anti wear properties of these formulations, as shown in Figure 5.7. The deterioration of wear properties is analogous to those seen in the base oil study however, in the case of fully formulated oils the effect is mitigated.

5.3.1.3 Wear test formulations with blend of treated carbon black and ZDDP

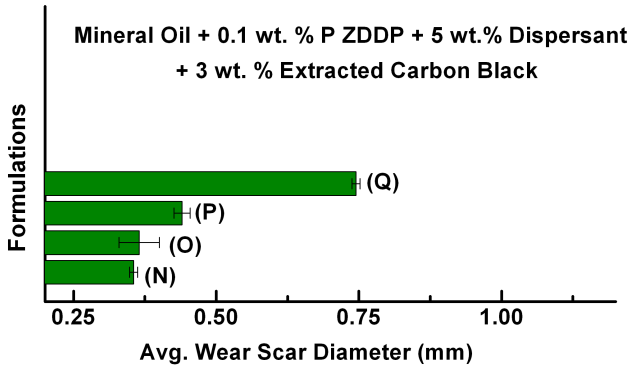

Figure 5.9 Average wear scar diameter wear scar diameter from test with formulation N-Q

In order to get an estimate of the role of treated carbon black on wear behavior, the carbon black from the milled and milled and oxidized conditions in base oil (i.e. formulation H, I) was extracted. The extracted carbon black was added back into formulation A and compared with formulation D. Figure 5.9, shows the average wear scar diameters for test formulations N-Q. Figure 5.10 shows the corresponding optical microscope images of the typical four ball wear scar formed by test formulations N-Q as shown in table 5.3. Formulation N and O are made by blending carbon black extracted from formulation L and M respectively with formulation A. L and M are fully formulated oils which had 3 wt.% carbon black that was milled and milled and oxidized respectively. The relatively small wear scar diameter for N and O formulations indicate that fully formulated oils result in smaller deterioration of wear properties when blended with treated carbon black. On the other hand, formulations P and Q were blended by mixing treated carbon black extracted from formulations H and I respectively. The wear scar diameters of formulations P and Q are lower than formulation H and I. However, the wear scar diameter formed by formulation P and Q is higher than formulations that are without carbon black. Moreover, the wear scar diameters formed by formulation P is similar to wear scar diameter formed by formulation that has diesel soot, i.e formulation F.

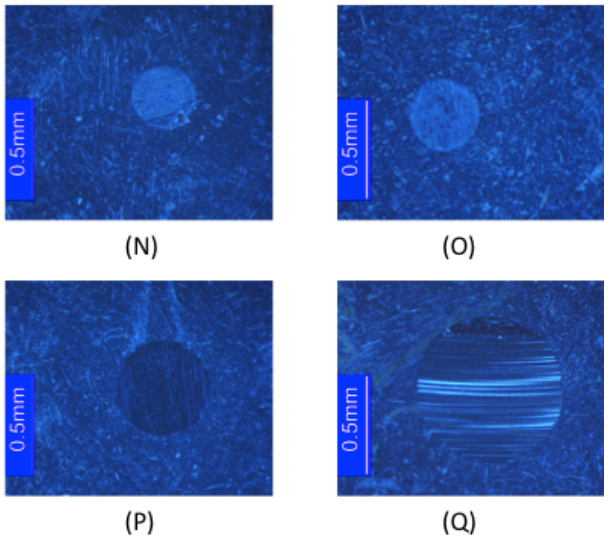

Figure 5.10 Optical micrographs of ball wear tracks from test formulation N-Q

Higher wear scar in the bench tests, after the extraction of treated carbon black, indicate the effect of oxidation and milling on the lubrication anti wear properties. Various treatments on carbon black might modify the structure and/or chemical make up of carbon black. To evaluate this modification, if any, further experiments were conducted using transmission electron microscopy, x-ray absorption spectroscopy (XANES).

5.3.2 Structural Characterization of Treated Carbon Black

Transmission electron microscopy was employed to probe the structural, morphological and chemical characterization of extracted carbon black and diesel soot. Figure 5.11 (a) is a bright field transmission electron micrograph of the fresh carbon black that shows agglomeration of carbon black partcile and primary particles that range in size from 75-125 nm. TEM images of carbon black demonstrate a few agglomerates in the size range of 200-500 nm and a few larger particles as well in the size range of 150-200 nm. These agglomerates are composed of collection of smaller basic particle units that are spherical or nearly spherical as shown in Figure 5.11 (a).

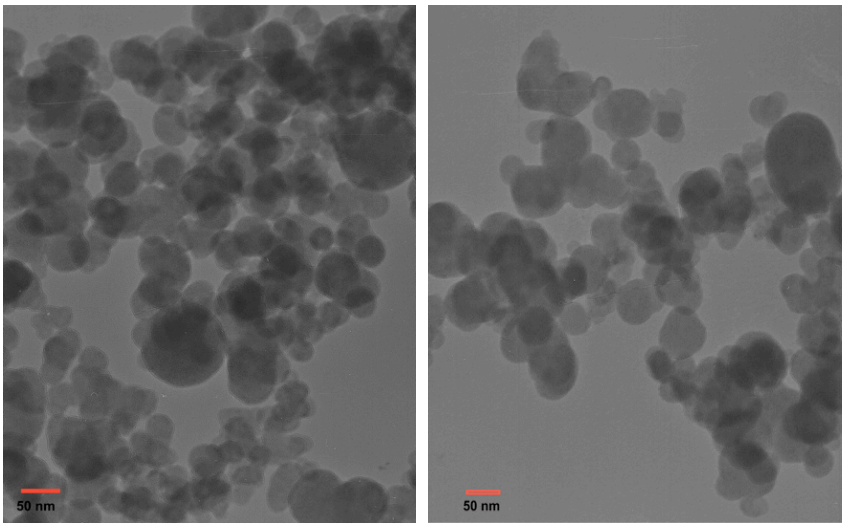

(a) (b)

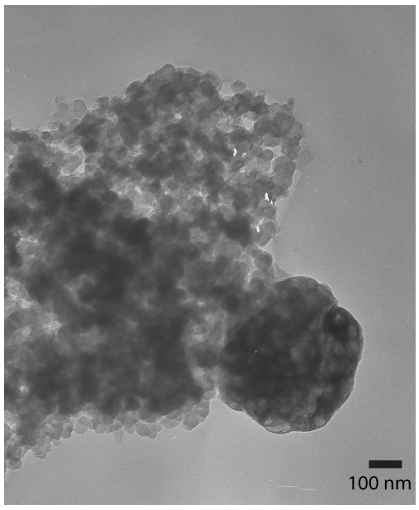

(c)

Figure 5.11 (a) Bright field TEM image of carbon black, (b) Bright field TEM image of milled carbon black, (c) Bright field TEM image of milled diesel soot

Figure 5.11 (b) is the bright field TEM image of milled carbon black, which shows significantly less agglomeration of the primary particles. TEM images of extracted carbon black from milled condition exhibit the breaking of agglomerates. However, the primary particles of extracted carbon black from milled condition remains similar to fresh unmilled carbon black. Figure 5.11 (c) is the bright field TEM image of diesel soot which shows significant agglomeration of the primary particles, the agglomerates range in size from few hundred nanometers to some

that are as large as 1 μm in size. However, the primary particles of diesel soot vary in diameter from 20-30 nm while primary particles of carbon black vary from 20- 50 nm.

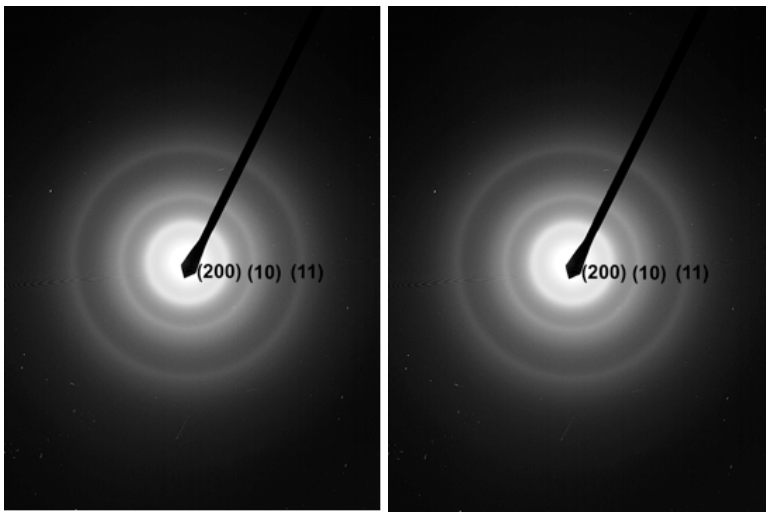

(a) (b)

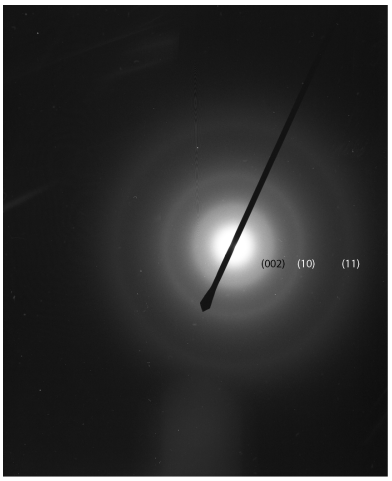

(c)

Figure 5.12 (a) Selected Area Diffraction image of carbon black, (b) Selected Area Diffraction image of milled carbon black, (c) Selected Area Diffraction image of milled diesel soot

Selected area diffraction in the TEM was used to probe the structure of fresh carbon black, extracted carbon black from milled condition and diesel soot. Figure 5.12 (a), (b) and (c) are the selected area diffraction patter (SADP) for unmilled carbon black, extracted carbon black from milled condition and diesel soot respectively. Diffraction pattern of unmilled carbon black has

three intense ring arising from (200) basal planes, (10) prism and (11) pyramidal planes. Similar ring patterns have been demonstrated by SAD of extracted carbon black from milled condition and diesel soot. The diffraction patterns primarily arise from crystalline portion of the turbostratic structure. The d-spacing of the planes that give rise to the rings were calculated from the electron diffraction patterns and is shown in Table 5.4. In addition shown in the table are the ratios of the d-spacing. Close agreement in radii and radii ratio between unmilled carbon black, extracted carbon black from milled condition and diesel soot suggests that SAD of diesel soot is primarily originates from crystalline domain of carbonaceous material situated at outer periphery of primary particles and is very similar to carbon black.

Close agreement in radii and radii ration between three samples also imply no structural differences between unmilled carbon black, extracted carbon black from milled condition and diesel soot. Structural characterization using SAD represent average structural information of micron size sample area, owing to the fact that aperture used to focus the diffraction beam in SAD is in the micron size scale. If milling of carbon black induces extremely small changes in the crystalline region of carbon black, then SAD is unlikely to provide complete structural information.

5.3.3 Raman Spectroscopy of Treated Carbon Black

Raman spectroscopy is a promising characterization tool to investigate the short-range highly disordered graphitic structure. Some of the previous studies found that different types of soot could be distinguished based on degree of graphitization. [73,96]

Fig. 13 shows the typical Raman spectra observed for diesel soot, carbon black and graphite acquired with a laser with 532 nm in the range 800-2000 cm^{-1}. Similar experimental conditions were used to acquire the Raman spectra on the extracted carbon blacks from formulations G, H, I, L and M as mentioned in table 5.5. The spectra exhibit two broad and strongly overlapping peak at intensity maxima ~1350 cm^{-1} and at ~1590 cm^{-1}. Previous studies revealed that the intensity maxima at ~1590 cm^{-1} (known as G band) is analogues to ideal graphitic vibration mode. Furthermore, increased degree of disorder in the graphite structure gives rise to the peak maxima at ~1350 cm^{-1} corresponds to disordered graphite. This peak is

known as D1 peak (Defect bands). In addition, integrated intensity ratio of D and G peaks is inversely proportional to microcrystalline planer size La that corresponds to the in-plane dimension of the single microcrystalline domain in graphite [73,96].

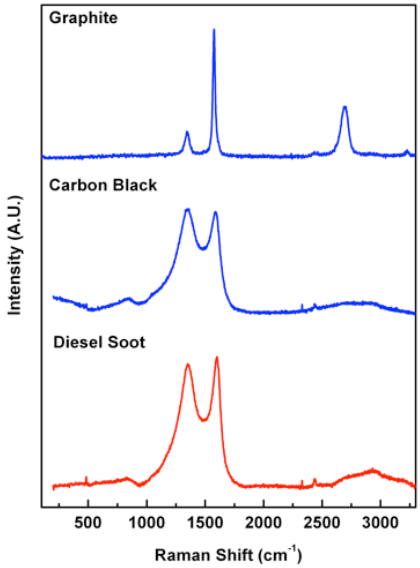

Figure 5.13 Raman spectra of graphite, carbon black and diesel soot

The high signal intensity between the two peak maxima can be attributed to another band at ~1500 cm^{-1}, designated as D3 (A) band which originates from the amorphous carbon part of soot (organic molecules, fragments or functional groups) and/or amorphous sp^2 bonded forms of carbon. Cuesta et al. [5] and Dippel et al. [125,126] assumed Lorentzian line shape for this band, whereas Jawhari et al. [21,22,68-70,123] proposed Gaussian line shape due to a statistical distribution of amorphous carbon on interstitial places in the disturbed graphitic lattice of soot. Raman spectra recorded with = 532 nm also exhibit second order spectra in the range of about 2300 cm-1 to 3300 cm-1. For the given studies only first order spectra have been considered for further analysis.

5.3.3.1 Spectra analysis by curve fitting

For the analysis and determination of spectral parameters by curve fitting various line shapes were evaluated. Raman spectra of extracted carbon blacks and diesel soot exhibit a broad band at about ~1500 cm-1.

Table 5.5 Raman spectroscopic data for treated carbon black, diesel soot and graphite

		Peak Position	Intensity	G/D1	G/D3	G/D4	G/(D1+D3 +D4)
Carbon Black	G	1590.21	828.56	--	--	--	
Carbon Black	D1	1347.44	2171.80	0.38	--	--	
Carbon Black	D3 (A)	1509.39	534.34	--	1.55	--	
Carbon Black	D4 (I)	1201.96	169.47	--	--	4.89	0.29
Diesel Soot	G	1600.03	1402.11	--	--	--	
Diesel Soot	D1	1349.96	4683.58	0.30	--	--	
Diesel Soot	D3 (A)	1531.49	483.82	--	2.90	--	
Diesel Soot	D4(I)	--	--	--	--	--	0.27
Graphite	G	1575.80	27212.51	--	--	--	
Graphite	D1	1345.64	10644.08	2.55	--	--	2.55
CB BO Mill	G	1601.76	654.43	--	--	--	
CB BO Mill	D1	1354.55	2670.64	0.25	--	--	
CB BO Mill	D3	1537.69	390.12	--	1.68	--	
CB BO Mill	D4	--	--	--	--	--	0.21
CB BO bake	G	1602.15	582.61	--	--	--	--
CB BO bake	D1	1353.95	2293.54	0.25	--	--	--
CB BO bake	D3	1535.40	373.02	--	1.56	--	
CB BO bake	D4	--	--	--	--	--	0.22
CB BO Mill Bake	G	1601.48	706.32	--	--	--	--
CB BO Mill Bake	D1	1355.10	2801.67	0.25	--	--	--
CB BO Mill Bake	D3	1535.82	349.13	--	2.02	--	
CB BO Mill Bake	D4	--	--	--	--	--	0.22

Table 5.5 - continued

CB FFO Bake	G	1599.16	748.64	--	--	--	--
CB FFO Bake	D1	1351.71	2709.14	0.28	--	--	--
CB FFO Bake	D3	1528.72	441.73	--	1.69	--	
CB FFO Bake	D4	--	--	--	--	--	0.24
CB FFO Mill	G	1598.85	698.25	--	--	--	--
CB FFO Mill	D1	1350.56	2287.80	0.31	--	--	--
CB FFO Mill	D3	1523.64	392.31	--	1.78	--	
CB FFO Mill	D4	--	--	--	--	--	0.26

The band at 1500 cm-1 is associated with amorphous sp^2 bonded carbon. It is also worth taking into consideration that sp^3 bonded carbon have vibrational features frequency below 1500 cm^{-1}. This observation suggests the higher probability of sp^2 bonded amorphous carbons. The best fit was invariably achieved by either one or two combination of line shape for G, D1 and D3 peaks. One can use the Lorentz line shape for all three G, D1 and D3 peaks or one can use the Lorentzian line shape for G and D1 peak and Gaussian like shape for D3 peak.

In this study we have used the Lorentzian peak fit for all three peaks of soot and carbon black as it offers the best fit. This fitting of the spectrum is in good agreement with recent studies by Sadezky et. Al [21,22,68-70,123]. The polycrystalline graphite exhibits two sharp peaks at ~ 1345 cm^{-1} and 1575cm^{-1} that correspond to the D1 and G peak respectively. The peak at ~ 1500 cm^{-1} is not observed in graphite. The graphite with just the D1 and G peak was fitted with two Lorentzian curve fits. The curve fitted spectra of different soot, carbon black and graphite are show in Figure 5.14 (a), (b), (c).

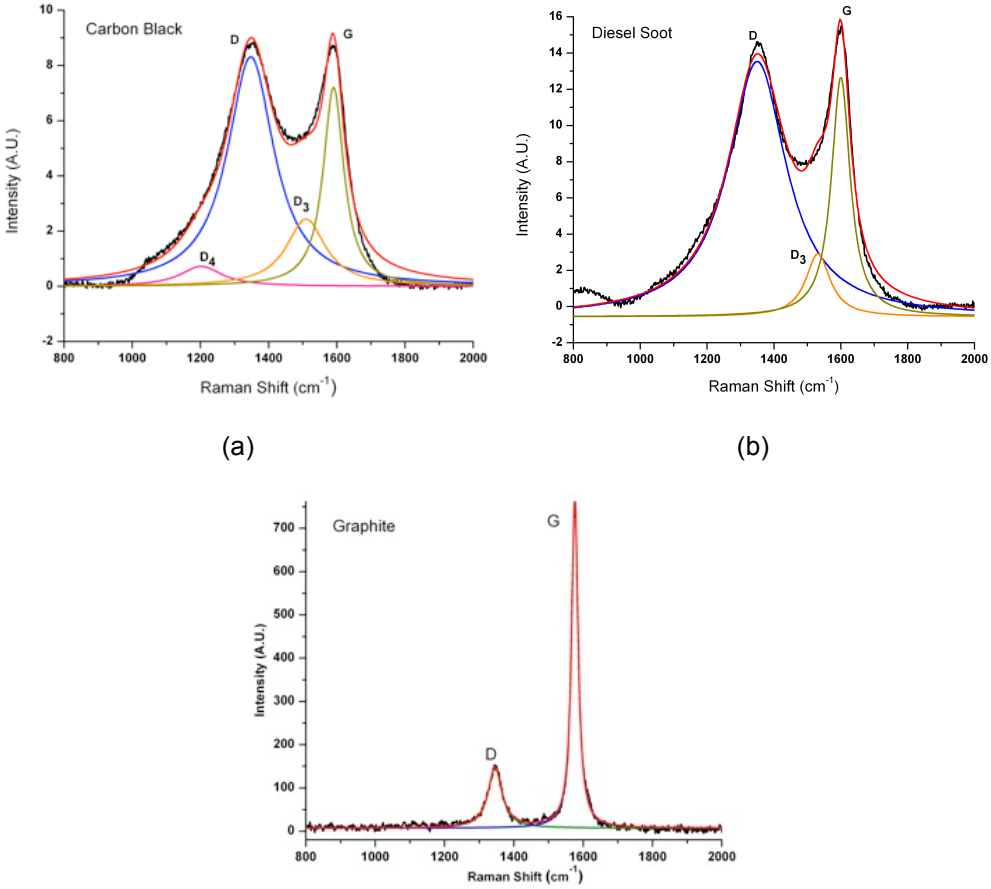

Figure 5.14 (a) Deconvoluted Raman spectra of carbon black using Lorentzian curve fit for the D1, D3, D4 and G peaks (b) Deconvoluted Raman spectra of diesel soot using Lorentzian curve fit for the D1, D3 and G peaks. (c) Deconvoluted Raman spectra of graphite using Lorentzian curve fit for D1 and G peaks

For the carbon black a fourth peak was introduced in the fitting (D4), which takes into account the disordered graphitic lattice due to polyenes and/or ionic impurities. Figure 5.15 (a) - (e) are curve fired spectra of extracted carbon black from formulation G, H, I, L and M respectively.

Further analysis of the spectra can be obtained by analyzing full width half maximum (FWHM) of the peaks, peak intensity and peak position. Table 5.5 details the curve fitted data and ratio of G/D peak intensity. The curve fitted spectral data reveals that for all samples FWHM of G peak is narrower than that of other two bands. Comparing the FWHM of graphite with diesel soot,

fresh carbon black and extracted carbon black, it evident that graphite has greater portion of crystalline phase. In addition, Table 5.5 breaks down the contribution from the different disordered forms of carbon including D1 the disordered graphitic lattice with contributions from graphene layer edges that are wrapped around, D3(A) the amorphous carbon and D4(I) arising from disordered graphitic layers from ionic impurities and polyenes. Overall the ratio of G/(D1+D3+D4) for carbon black and diesel soot are very similar suggesting a similar ratio of idealized graphite lattice and disordered carbon. Analogues results have been notices for extracted carbon blacks from various treatments. However, a careful examination of the ratio's G/D1, G/D3 and G/D4 indicate some significant differences. The smaller G/D1 ratio for diesel soot indicates a larger proportion of graphene layer edges have reacted in soot resulting in a higher level of disorder. The G/D1 ratio of all extracted carbon black samples are smaller than diesel soot which, suggests higher disorder in the treated carbon black than diesel soot. This is due to the greater proportion of graphene layer edge that have reacted during treatments. Moreover, the G/D1 ratio of the carbon black extracted from the formulation G, H and I are identical. Formulation G, H and I is blended by mixing 3 wt. % carbon black to [Mineral base stock + 0.1 wt.% P from ZDDP + 5% Dispersant] in oxidized, milled and milled & oxidized treatment respectively. However, G/D1 ratio of carbon black that extracted from formulation K and L have slightly higher but close to the G/D1 ratio of diesel soot. Other studies in functionalizing of graphene have shown that edges of the graphene layer may be functionalized more easily resulting in smaller G/D1 ratios [19]. This might be preferential location for reactive decomposition species for absorption.

On the other hand G/D3 ratio for diesel soot is much larger than the G/D3 ratio for all treated carbon black samples which, indicates a smaller proportion of amorphous carbon present in the diesel soot compared to the treated carbon black samples. However, G/D3 ratio of the extracted carbon blacks lies between the fresh carbon black and diesel soot. A comparison of the G/D3 among the extracted carbon black suggests that carbon black that extracted from the milling conditions have higher level of amorphous carbon than the carbon black that extracted

from oxidizing conditions. Moreover, carbon black that extracted from milling and oxidizing treatment demonstrates highest amount of amorphous carbon among the other extracted carbon blacks. Li et al have demonstrated that transformation of graphite into amorphous carbon using high energy ball milling and hence obvious different sp^2-sp^3 ratio between graphite and amorphous carbon. This observation is similar to what is seen in the carbon black that is extracted from the milling conditions. [21]

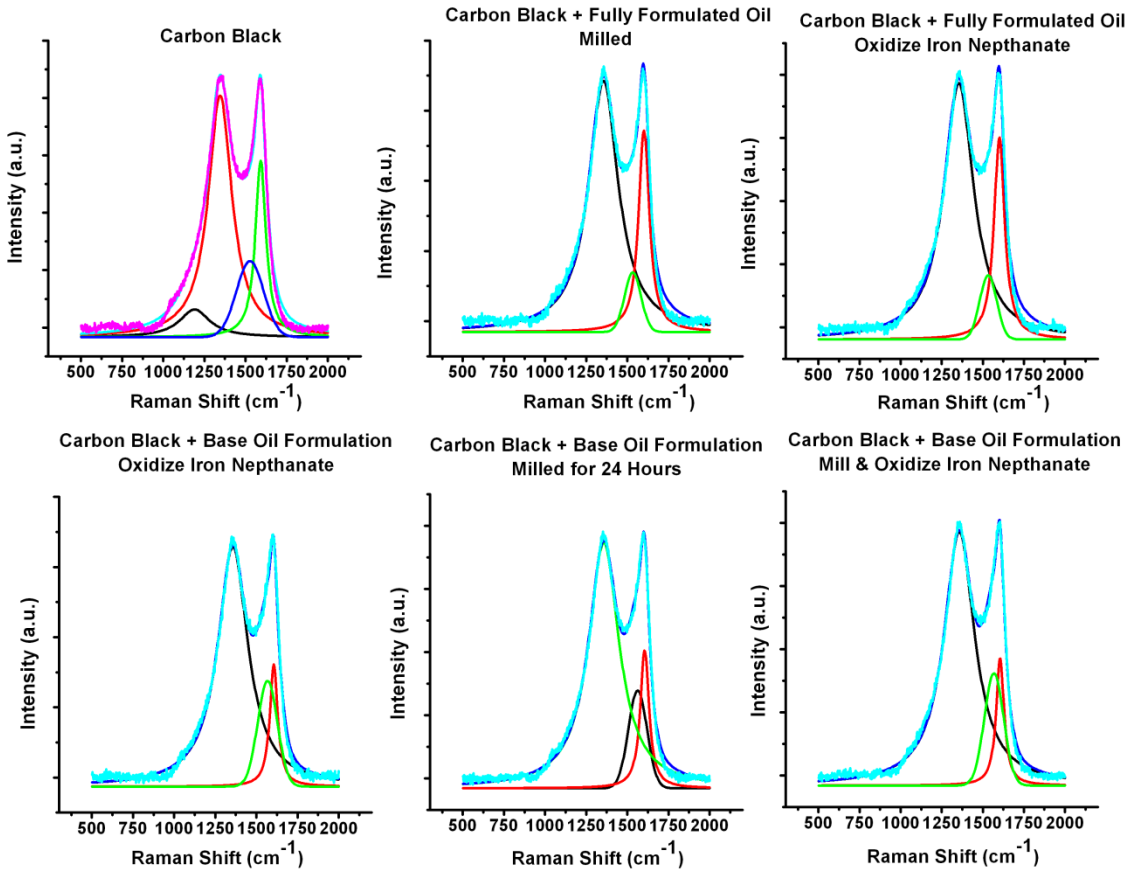

Figure 5.15 (a) Deconvoluted Raman spectra of treated carbon black using Lorentzian curve fit for the D1, D3, D4 and G peaks

Lastly, the D4(I) peak is present in fresh and untreated carbon black while absence of D4(I) peak in the diesel soot as well as in all extracted carbon black indicates the absence of polyenes and/or other ionic impurities. This also indicates the success of treatments to replicate the D4 peak of diesel soot.

These results illustrate the usefulness of Raman spectroscopy to probe the short-range disorder structure. Although raman spectra distinguish the contribution from crystalline and amorphous domains but no additional spectral features were observed to confirm contribution from interaction between lubrication additives chemistries and diesel soot. Analogues results were also recorded on the extracted carbon blacks from the various treatments.

5.3.4 Chemical Characterization of Treated Carbon Black

This investigation is further extended by conducting chemical characterization on the extracted carbon black samples using X-ray Absorption Near Edge spectroscopy. K absorption edge of phosphorous, sulfur and calcium were acquired using SXRMB beam line at The Canadian Light Source.

5.3.4.1 Phosphorous K absorption edge

The spectra of phosphorus K absorption edge of treated carbon black were recorded in TEY and FLY mode as shown in Figure 5.16. The white line for the phosphorous K-edge spectra arises from transitions of 1s electrons to unoccupied 2p orbitals. These spectra were compared with phosphates of zinc, calcium and iron. This spectrum was compared with phosphates of zinc, calcium and iron. FePO4 has distinctive pre edge at 2150eV, which is absent in $Zn_3(PO_4)_2$ and $Ca_3(PO_4)_2$. Also the main peak of $FePO_4$ lies at 2154.5eV, which is higher energy state than $Zn_3(PO_4)_2$ and $Ca_3(PO_4)_2$. In addition a careful examination of the post edge structure indicates the presence of distinctive shoulder in the case of $Ca_3(PO_4)_2$ which is absent in the case of either the $Zn_3(PO_4)_2$ or $FePO_4$. The characteristics K absorption edge of all the extracted carbon blacks closely align with $Zn_3(PO_4)_2$ in both the TEY and FLY mode. Possibility of $FePO_4$ is not likely due to absence of pre edge in soot spectrum.

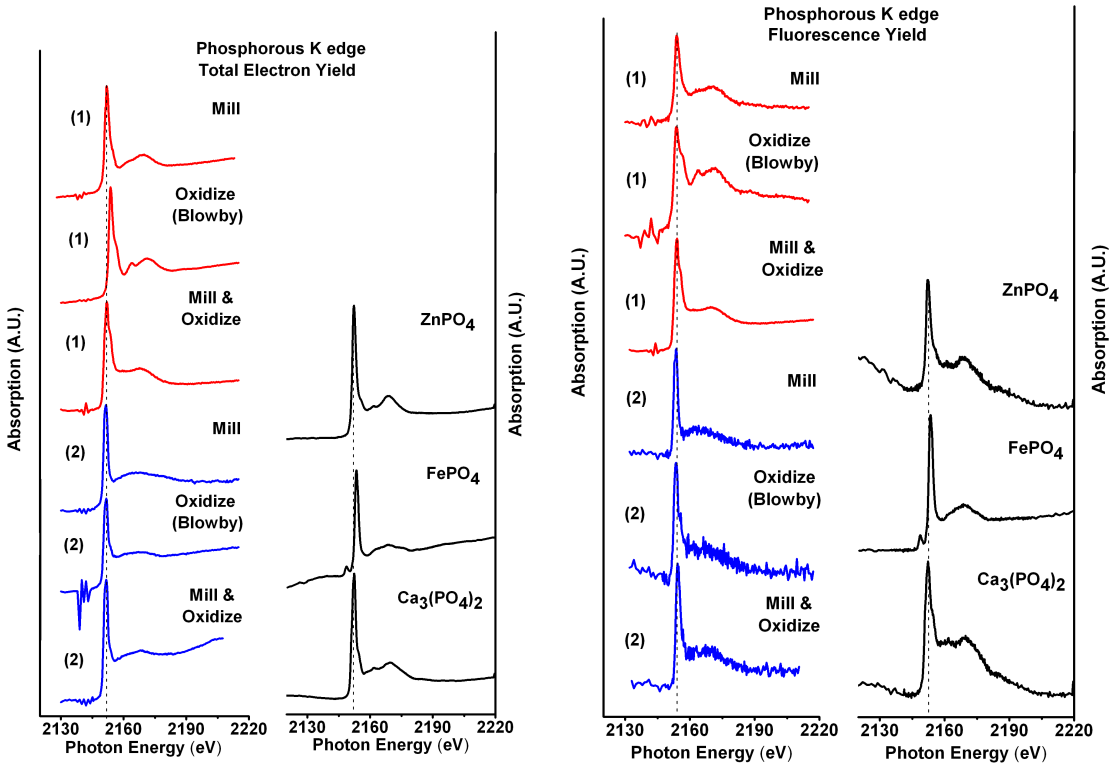

Figure 5.16 Normalized Total Electron Yield (TEY) and Fluorescent Yield (FY) phosphorous K edge spectra of diesel soot and model compounds

Spectra (1), (2) and (3) are treated carbon blacks that extracted from the formulation of [Mineral Oil + 0.1 wt. % P ZDDP + 5% dispersant + 3wt% Carbon Black]. Extracted carbon blacks from this formulation can only have presence of $Zn_3(PO_4)_2$.as there is no source of Ca in the treatment. On the other hand, carbon black extracts from fully formulated oil can have zinc phosphate as well as calcium phosphate.

5.3.4.2 Sulfur K absorption edge

The spectrum of sulfur K absorption edge was compared with sulfates of zinc, calcium and iron and with sulfides of zinc and iron as shown in Figure 5.17. Higher energy states of iron sulfate at 2482.3 eV differentiate it from zinc and calcium sulfate. Zinc sulfate and calcium sulfate can be differentiated by the presence of a post edge at 2484.8 eV in the case of $CaSO_4$, which is absent in the case of $ZnSO_4$. The sulfides have their white lines at lower energies than the

sulfates with the zinc sulfide having an absorption edge at 2473 eV and a fairly rich post edge structure. FeS has two strong peaks at 2471 eV and 2482 eV.

A careful examination of the spectra of extracted carbon black (both TEY and FY) indicates that in addition to the sharp absorption edge at 2481.2 eV that is common to both $ZnSO_4$ and $CaSO_4$ there is a post edge at 2484.8 eV that is only present in $CaSO_4$ that is absent in all the extracted carbon blacks. In addition, all carbon blacks also have an additional peak at 2472 eV that likely arises from ZnS. The peak at 2472 eV is dominant in all extracted carbon black except carbon black extracted from [Mineral Oil + 0.1 wt. % P ZDDP + 5% dispersant + 0.1 wt. % Iron Nepthanate (blowby) + 3wt. % Carbon Black].

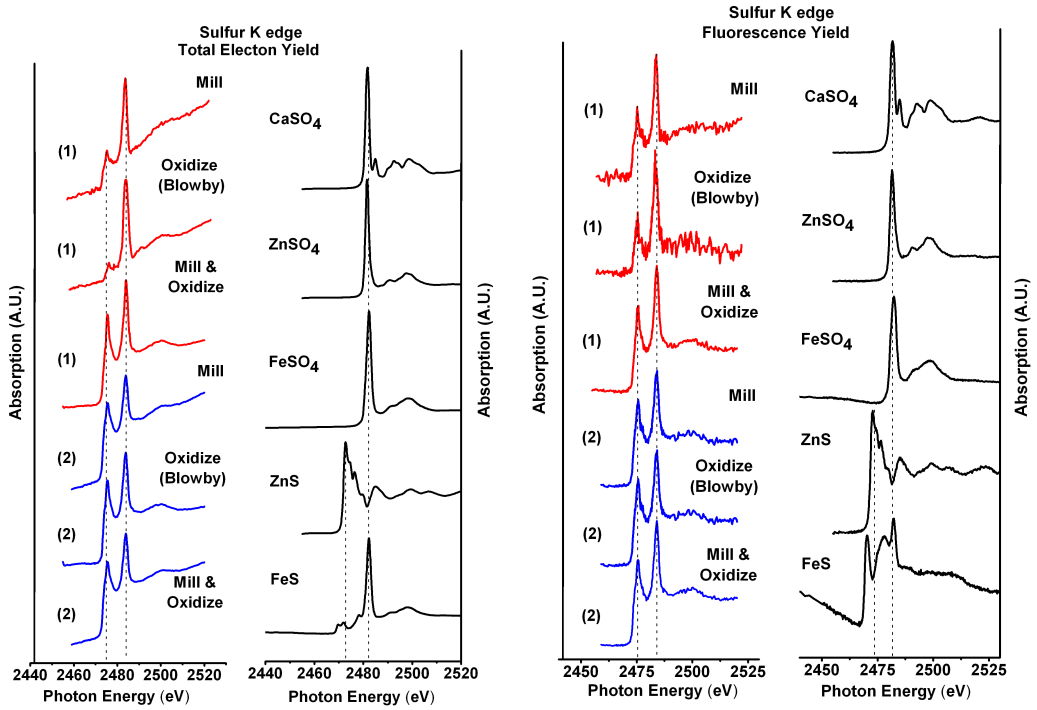

Figure 5.17 Normalized Total Electron Yield (TEY) and Fluorescent Yield (FY) sulfur K edge spectra of diesel soot and model compounds

A semi-quantitative approach was used to determine the types of sulfur present on the diesel soot as well as extracted carbon blacks. The spectra were deconvoluted using least square method using linear background subtraction. The relative height of the sulfate peak at 2484 eV and sulfide peak at 2473 eV were compared. The height ratio of sulfide to sulfate peak were

calculated and reported in table 5.6. Previous studies have reported that presence of sulfate on the tribofilm increase wear while presence of sulfide is more protective. As shown in Table 5.6, sulfide to sulfate peak height ratio of diesel soot is 0.167. A careful examination of each of the treated carbon blacks indicates that carbon black extracted from formulation G where oxidation was accelerated using synthetic blow-by to degrade oil and only has ZDDP as additives, has the largest amount of sulfate. However, carbon black extracted from formulation K where oxidation was accelerated using synthetic blow-by to degrade fully formulated commercial oil has higher sulfide to sulfate ratio When compared to formulation G the fully formulated oil has antioxidants present that mitigate the oxidation of sulfide to sulfate.

Carbon black extracted from milled formulation H that has ZDDP and detergent as additives have sulfide to sulfate ration of 0.319 which is higher than ratio of engine soot. On the other hand, extracted carbon black from milled formulation of fully formulated oil L has a sulfide to sulfate ratio of 1.09 which is significantly higher than formulation H. Lastly, when carbon black extracted from formulation I, which was oxidized without synthetic blow-by and followed by milling, has a sulfide to sulfate ratio of 0.872. While carbon black extracted from similar condition but from fully formulated oil solution M have sulfide to sulfate ratio 0.98.

Table 5.6 The height ratio of Sulfide / Sulfate for extracted carbon black

	Formulation from which Carbon Black was extracted	Sulfide/ Sulfate
	Diesel Soot	0.167
G	Mineral Oil + 0.1 wt.%P ZDDP + 5% Dispersant + 0.1 wt.% Iron Nepthanate +3% Carbon Black Oxidized	0.116
H	Mineral Oil + 0.1 wt.%P ZDDP + 5% Dispersant + 3% Carbon Black Milled	0.319
I	Mineral Oil + 0.1 wt.%P ZDDP + 5% Dispersant + 3% Carbon Black Milled & Oxidized	0.872
K	Fully Formulated Oil + 3% Carbon Black Oxidized	0.944
L	Fully Formulated Oil + 3% Carbon Black Milled	1.09
M	Fully Formulated Oil + 3% Carbon Black Milled & Oxidized	0.98

It is evident from the height ratio of sulfide to sulfate that carbon black extracted from formulation that contains only ZDDP as anti wear additives has smaller peak height ratio as compared to carbon black extracted from fully formulated commercial oil. However, the ratio of sulfide to sulfate in all laboratory treated carbon blacks are higher than the ratio observed in diesel soot suggesting that the treatment conditions in the laboratory test while severe were not as severe as the conditions experienced by the extracted diesel soot.

5.3.4.3 Calcium K absorption edge

Calcium K absorption edge was recorded in TEY and FLY mode for extracted carbon black and model compounds, as shown in Figure 5.18. Calcium sulfate, calcium oxide and tri-calcium phosphate were used for comparison. The white line for calcium sulfate, calcium oxide and tri-calcium phosphate lies at 4050 eV, 4049.8 eV and 4049. 4 eV. Calcium oxide has distinguishing pre edge at 4043 eV, which is absent in the other Ca compounds. Calcium sulfate has a more defined fine structure compared to tri-calcium phosphate. Comparison of the soot spectra and model compounds spectra clearly indicates that the spectra appear to be close to both calcium sulfate and tri-calcium phosphate with the absence of CaO. The P K-edge spectra indicates that the phosphates were most likely Zn based and not Ca based, and the S K-edge spectra also indicated that the presence of $CaSO_4$ and lesser extent the presence of $ZnSO_4$. It is safe to come to the conclusion that Ca largely exists as $CaSO_4$ and possibly to a smaller extent as the $Ca_3(PO_4)_2$.

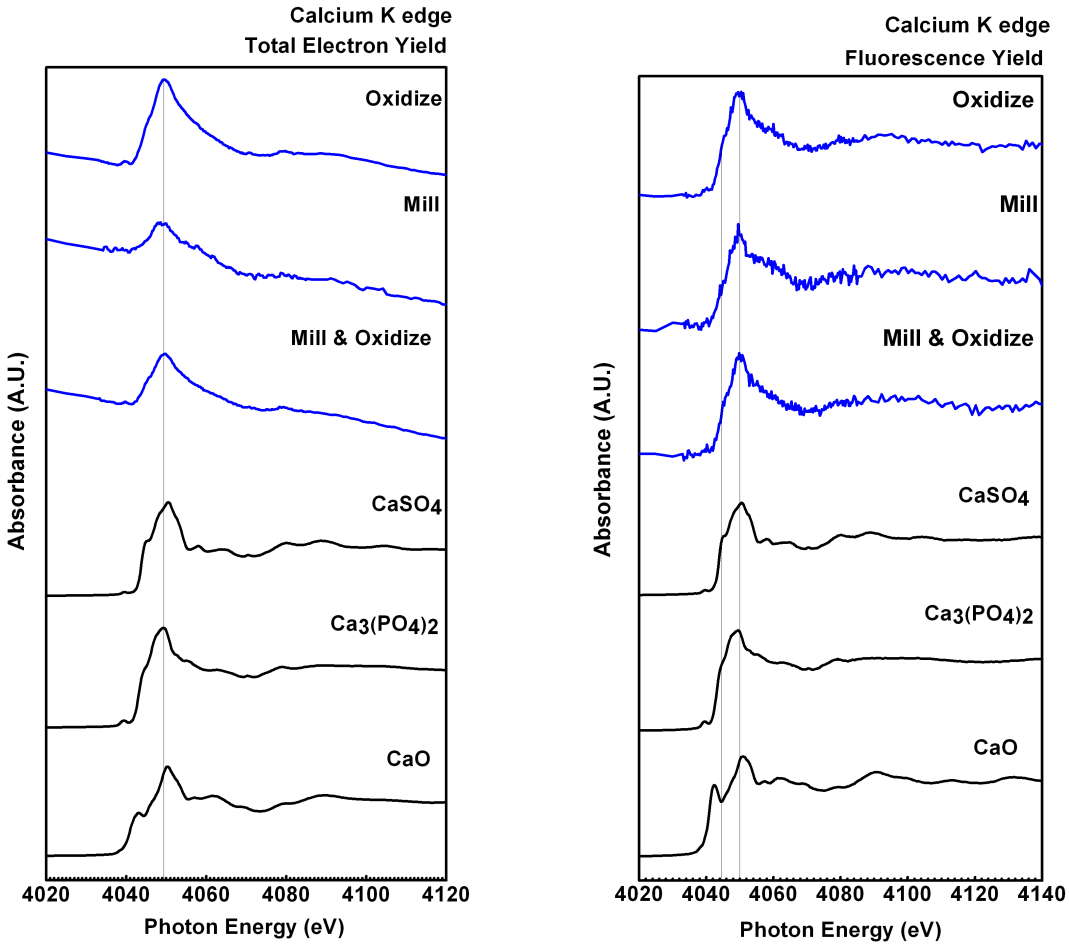

Figure 5.18 Normalized Total Electron Yield (TEY) and Fluorescent Yield (FLY) calcium K edge spectra of diesel soot and model compounds

5.4 Discussion

Use of carbon black as soot surrogate to understand the soot induced wear mechanism has always been the subject of debate. Carbon black is analogous to diesel soot in terms of the turbostratic structure, but significant differences have been observed between carbon black and diesel soot in terms of their morphology, agglomeration, elemental compositions, particle sizes etc. [70] Moreover, our previous studies have established that the interaction of soot with decomposition additives chemistries and tribofilm has changed the chemical make up of the diesel soot. These facts can certainly have significant implication on the tribological evaluation of lubrication oil using carbon black to understand soot induced wear mechanism. [71] Four ball

wear results have substantiated this fact where blend of carbon black without any treatment have produced smaller wear scar compare to wear scar that has produced by the formulation with the diesel soot. However, four ball results of treated carbon black have produced wear scar similar to the diesel soot. Moreover, wear tracks generated by treated carbon black formulations is similar to the formulation with the diesel soot F. In addition, XANES results also indicated the presence of decomposition chemistries of lubricants on the extracted carbon black sample that are similar to the diesel soot. XANES results of the extracted carbon black and diesel soot in collaboration with wear results indicate the influence of the various chemistries on the tribological evaluation. It also indicates that when carbon black is used without any treatment it does not simulate conditions similar to that seen with diesel soot.

The present study has also attempted to bring some light to the mechanism through which the decomposition chemistries of lubricants additives might get incorporated on to the soot structure. XANES results acquired from the treated carbon black samples and diesel soot indicate the efficacy of the treatment on carbon black to simulate the chemical makeup of diesel soot. Theory proposed by Round suggested the preferential absorption of ZDDP to the diesel soot structure. [72]. However, this mechanism has been disputed by many other studies. [124] In the present study, we forced the interaction between carbon black and lubrication additives chemistries by oxidizing the formulation blend with carbon black and also subjected them to milling and oxidizing treatment. XANES results confirm these interactions between additives chemistry and carbon black. Round suggested the physical absorption of the ZDDP on the soot structure. However, multiple washing and dilution using hexanes eliminates such possibilities of physical absorption and no evidence of undecomposed additives is found on the carbon black. The concentration of additive elements incorporated into the carbon black structure is relatively small and generally difficult to detect by energy dispersive spectroscopy. However, intense the very high photon flux in XANES acquisition makes it possible to detect small amounts of incorporated elements and their local coordination.

Formulation blended with carbon black were also milled to simulate the higher local hertzian point contact pressure, thereby to help us to understand the effect of three body wear on the structure of diesel soot during engine operation. Wear results of the formulations that were milled have produced severe abrasive conditions on the wear track. In addition, XANES results have also indicated the presence of zinc phosphates, zinc sulfate, zinc sulfide and calcium sulfate on the milled carbon black. TEM images of milled carbon black indicate the breaking of agglomerates. Kawamura et al used freeze fractal replica (FFR) method using TEM to investigate the state of soot in used diesel engine oil. He suggested that small soot particle in range of 0.02 μm do not affect the anti wear properties due to effectiveness of dispersant on smaller particles. While particle greater than 0.03 μm might play dominant role in increase wear. [18] Presence of smaller agglomerates along with decomposition chemistries might also promote wear in four ball wear test.

In a companion study on diesel soot have indicated the presence of abrasive nano particles that are mechanically embedded on the structure of the soot. [73,96] However, further studies is needed to understand this phenomena.

Milling of an carbon black were conducted on formulation H and L with an aim to replicate the three body wear condition by applying higher Hertzian contact pressure using impact of inert zirconia balls during planetary ball milling. Results indicate that the crystalline domains of the turbostratic structure of carbon black are unaffected. Raman spectroscopy was used to probe the short-range disorder structure. Although Raman spectra proved to be useful to distinguish between the contribution from crystalline and amorphous domains no additional spectral features were observed to indicate interaction between lubrication additives chemistries and diesel soot. Similar results were also recorded on the extracted carbon blacks from the various treatments. It can be speculated that decomposition chemistries of lubricants that are present on carbon black from H and L formulation might be reacted with these preferential locations indicated by the G/D1 ratio but further scientific evidence is required to validate it. If this speculation hold some validity, then higher WSD of formulation H compare to formulation L could be explained by higher

proportion of preferential site and presence of more abrasive chemistries on carbon black from formulation H than formulation L.

Lastly, cumulative effect of milling and oxidizing is conducted on formulation I and M. Four ball results indicates the most abrasive conditions. Although, Raman spectroscopy suggests that larger quantities of grapheme are present for carbon black extracted from formulation I than carbon black extracted from formulation M.

5.5 Conclusions

Treatment were carried out to force the interaction between carbon black (soot surrogate) and lubrication additives chemistries by oxidation and milling the formulations there by to simulate the composition and structure of the diesel soot. Tribological assessments of the treated formulations with and without carbon black were conducted using four-ball wear tester.

(i) Milling and oxidation condition have demonstrated the sever deterioration in the anti wear properties of test formulations. Abrasive wear track in the direction of rotation indicated the abrasive wear mechanism is most dominant wear mechanism in the given test configuration.

To verify the efficacy of treatments to mimic the composition and structure of diesel soot, carbon black were extracted after the treatment and characterized using TEM, XANES and Raman Spectroscopy.

(ii) TEM and raman spectroscopy results indicated no significant differences in the structure of the treated and untreated carbon black as compare to diesel soot.

(iii) XANES results indicate the efficacy of the treatment to incorporate various decomposition chemistries of the lubricants additives on the carbon black structure. However, sulfate to sulfide ration indicated the incorporation of more sulfides on the treated carbon black as compare to diesel soot.

(iv) Raman spectroscopy has successfully characterized the short-range crystalline domain of treated carbon black.

CHAPTER 6

A LABORATORY SIMULATION OF COMPOSTION AND STRUCTURE OF DIESEL SOOT BY TREATMENT OF CARBON BLACK AND ITS TRIBOLOGICAL ASSESSMENT PART I: FRICTION ASSESSMENT

6.1 Introduction

In the companion study, four ball wear tests were used to evaluate the anti wear properties of the formulations that were blended with and without carbon black and subjected to various treatments. These treatments were conducted on the formulations blended with carbon black to simulate the structure and composition of the diesel soot. Formulations were oxidized to force the interaction between decomposition products of lubrication additives and carbon black particles. Formulations were also milled using inert zirconia ball to study the changes in structure of carbon black by imparting higher impact energy to carbon black and there by provide information on the effect of change in turbostratic structure of carbon black on anti wear properties of formulations.

In the present study SRV friction tester have been used to study the frictional behavior of the formulations blended with carbon blacks and subjected to the various treatments carried out in previous chapter. In addition to that, tribofilm generated by the formulations with treated carbon black have analyzed using XANES. Wear track generated on the SRV samples were also analyzed to understand the wear pattern and thereby to comprehend the mode of wear mechanism.

6.2 Experimental set up

6.2.1 Bench test conditions and procedure

To understand the tribological behavior of treated carbon black SRV (Schwingun / Reibung / Verschleiss) was used. The SRV is used to evaluate the lubricating oil's coefficient of friction when subjected to high frequency linear oscillation motion.

6.2.1.1 SRV friction test conditions and procedure

A TE 77 Plint test rig was used to conduct the SRV test with an using oscillating cylinder at constant frequency of 50 Hz and stroke amplitude of 11 mm under the constant load of 220 N against the test disk that is submerged in the test formulation. The testing disk is attached to a platform, which is held at constant temperature of 75° C. Both reciprocating cylinder and clamped disk were made from 52100 steel. The test configuration yield Hertzian line contact geometry. The test was run for 60 minutes, and during the test the friction force is measured and the friction co-efficient calculated and recorded as function of time.

Table 6.1 Test formulations used for SRV friction test

No.	Test Formulations	Treatment
A	Mineral Oil + 0.1 wt.%P ZDDP + 5 wt.% Dispersant	--
C	Mineral Oil + 0.1 wt.%P ZDDP + 5 wt. % Dispersant + 3 wt.% Carbon Black	No Treatment
F	Mineral Oil + 0.1 wt.%P ZDDP + 5 wt.% Dispersant + 3 wt.% Diesel Soot	--
H	Mineral Oil + 0.1 wt.%P ZDDP + 5 wt.% Dispersant + 3 wt.% Carbon Black	Milled
I	Mineral Oil + 0.1 wt.%P ZDDP + 5 wt.% Dispersant + 3 wt.% Carbon Black	Milling + Oxidizing
L	Fully Formulated Oil + 3 wt.% Carbon Black	Milled
M	Fully Formulated Oil + 3 wt.% Carbon Black	Milling + Oxidizing

6.3 Results

6.3.1 SRV friction results of Treated Carbon Black

Figure 6.1 shows the SRV friction results for the formulations A, C, F, H, I, L and M. Formulation A has [Mineral Oil with 0.1 wt. % P from ZDDP with 5 wt. % Dispersant], hereafter referred as formulation A (same as previous chapter). Formulation C is blended by adding 3 wt. % carbon to formulation A. Formulation F was prepared by blending 3 wt. % diesel soot to formulation A. Formulation H was prepared by milling the formulation C using inter zirconia ball for 24 hours. Formulation C was also milled for 24 hours using inter zirconia ball followed by oxidized in air for 120°C for 100 hours followed by 24 hours and hereafter referred as formulation I. Formulation L was prepared by blending 3 wt. % carbon black to fully formulated oil and then subjected to milling for 24 hours using inter zirconia balls. Formulation M is prepared by blending 3 wt. & carbon black with fully formulated oil and subjected to milling for 24 hours using inert zirconia ball and followed by oxidation in air for 120°C for 100 hours followed by 24 hours.

Figure 6.1 are the SRV results that are plots of friction coefficient as a function of time for formulations as mentioned above. In each case at least 2 tests were conducted, shown are the representative test for each formulations. The formulation A that was blended without carbon black shows higher coefficient of friction. The coefficient of friction reduced for formulation C that is blend of formulation A and 3 wt.% carbon black. Further reduction in frictional coefficient was noted for formulation F that blended by mixing extracted diesel soot to formulation A.

Further drop of frictional coefficient was reported for formulation M and L respectively. As mentioned above, formulation M and L are prepared by blending 3 wt. % carbon black with fully formulated oil and subjected to milling and [milling & oxidation] respectively. While formulation H and I also subjected to similar treatment as formulation M and L but were prepared in the formulation that has only ZDDP as anti wear additives.

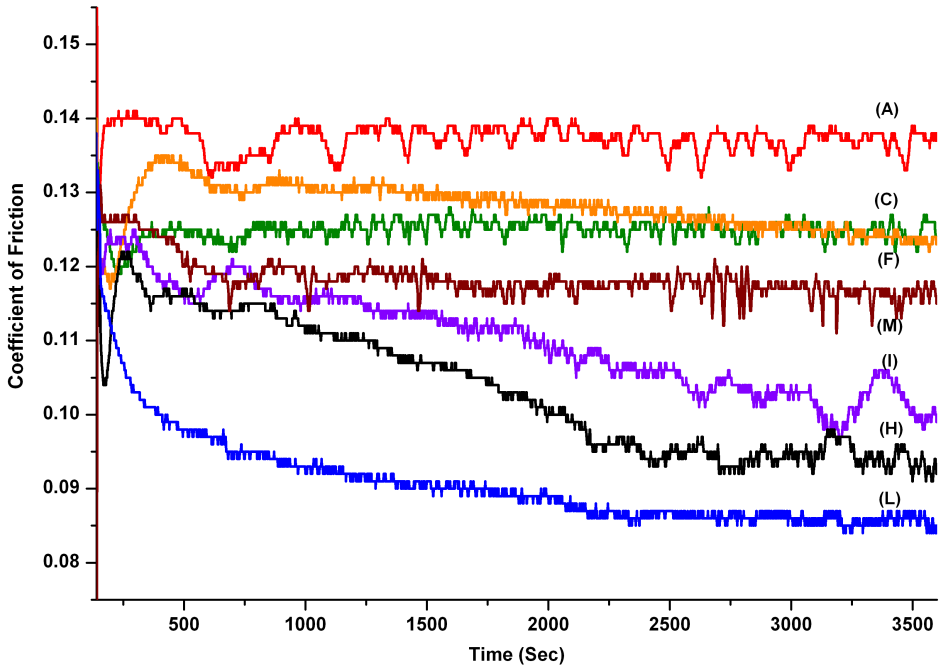

Figure 6.1 Friction coefficient of formulations A, C, F, M, I, H and L collected using SRV bench test

It is important to notice that four ball wear test, wear scar was increased ascending order for the above mentioned formulations A, C, F, M, L, H and I. However, SRV test results suggest completely opposite frictional behavior. Coefficient of friction was reduced in descending order for the formulations A, C, F, M, L, H and I.

6.3.2 SEM analysis of wear track of SRV test specimen

Figure 6.2 shows the SEM micrograph of wear track generated by formulation A, C, F, M, L, H and I. The wear scars produced by the above formulations have relatively similar morphology. The flat samples have irregular appearance of the liner striations randomly distributed on the specimen. High magnification of these features indicates that they are scratches in the metal. They most likely were formed during the preparation of the samples before experiments. Apart from random distribution of the striations, specimens have wide parallel groves in the sliding direction. These grooves are deeper and indicate some plowing might have occurred during the test. Along with parallel grooves, all the SRV samples that are tested with formulation, as mentioned above, have identical patchy appearance of the tribofilm.

The darker regions are most likely to be thicker tribofilm while regions that have light contrast are likely to be thinner film.

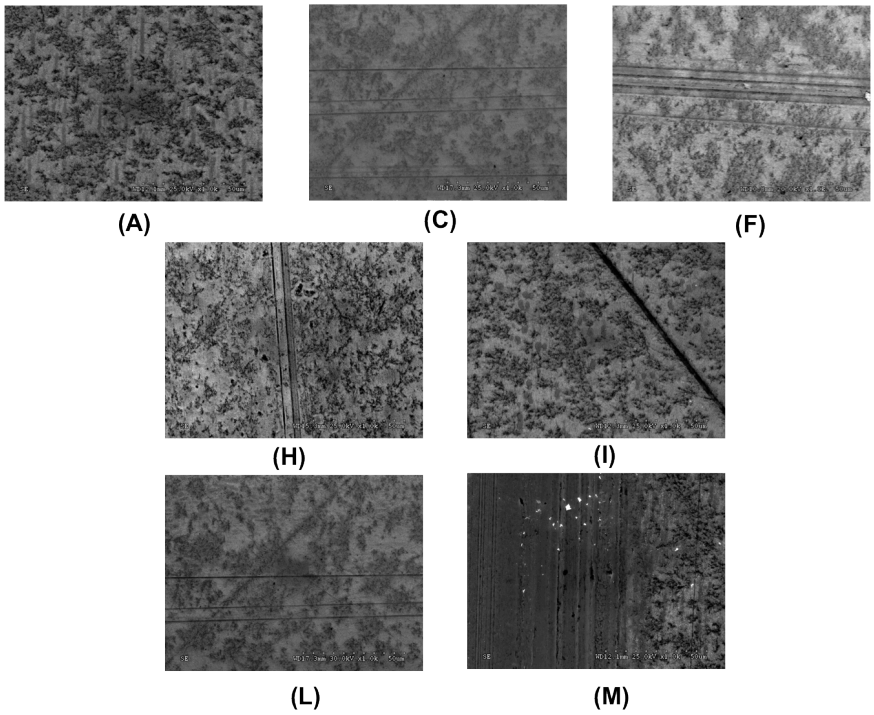

Figure 6.2 SEM micrographs of wear tracks of flat specimen of “cylinder on flat ” configuration tested for formulations A, C, F, M, I, H and L

6.3.3 Tribofilm analysis of SRV test specimen using XANES

XANES have been used to study the composition of tribofilm derived from the various formulations as mentioned in Table 6.1 along with model compounds. Spectra (1) is tribofilm derived from formulation A. Spectra (2) is tribofilm derived from formulation F that was prepared by blending 3 wt. % soot with formulation A. Spectra (3) is tribofilm generated by formulation C that was prepared by blending 3 wt. % carbon black with formulation A. Spectra (4) and (5) are tribofilm derived from formulation C that was subjected to milling and [milling + oxidation] treatment respectively. Spectra (6) and (7) are derived from tribofilm derived from formulation L that was prepared by blending 3 wt. % carbon black to fully formulated oil and subjected to milling treatment and [milling + oxidation] treatment respectively.

6.3.3.1 Phosphorous L edge

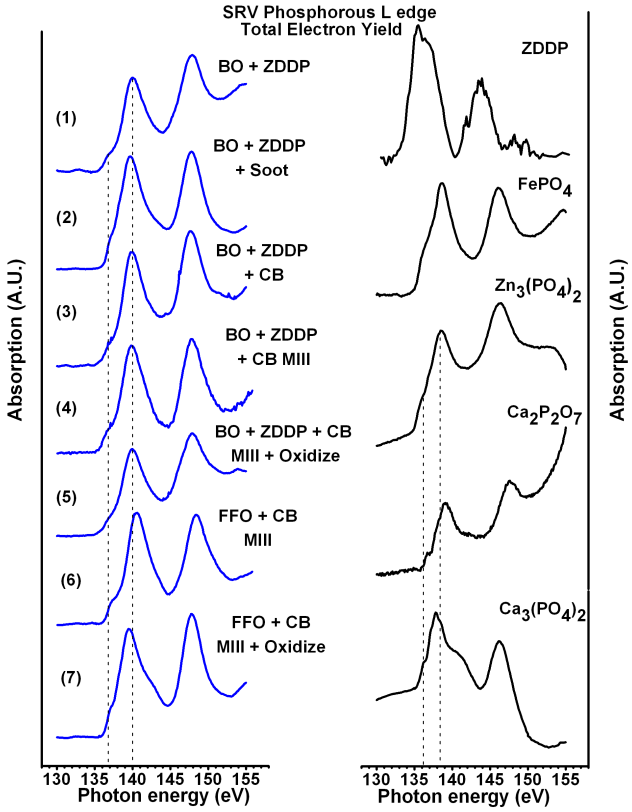

Figure 6.3 shows the phosphorous L edge XANES spectra for the tribofilm (1)-(7) in TEY mode along with the model compounds

Spectral features of model compound and usefulness of phosphorous L edge to study the tribofilm structure have been described in previous chapters. A white line of P-L edge of spectra (1)-(7) indicate closely aligns with zinc phosphate ($Zn_3(PO_4)_2$), calcium phosphate ($Ca_3(PO_4)_2$). However, It is not possible to have calcium phosphate ($Ca_3(PO_4)_2$) in the tribofilm (1)-(5), simply due to the fact that the formulation that was used to derived the tribofilm do not have any calcium compounds. However, tribofilm spectra (6) and (7) are derived from the fully formulation oil are likely to have zinc phosphate ($Zn_3(PO_4)_2$) as well as calcium phosphate ($Ca_3(PO_4)_2$). Careful observation of spectra (6) and (7) have post edge peak at 142 eV. This peak distinguish the zinc phosphate ($Zn_3(PO_4)_2$) from calcium phosphate ($Ca_3(PO_4)_2$). Present of this peak at 142 eV indicate that calcium phosphate ($Ca_3(PO_4)_2$) is more likely to constitute the tribofilm derived from fully formulated oil while zinc phosphate ($Zn_3(PO_4)_2$) is present as minor constituents.

6.3.3.2 Sulfur L edge

Figure 6.4 shows the sulfur L edge XANES spectra of tribofilm (1)-(7) in TEY mode derived from formulation mentioned in table 6.1 along with the model compounds. Spectral features of model compound and usefulness of sulfur L-edge to study the tribofilm structure have been described in previous chapters. S L-edge spectra are weak in intensity, which indicate that sulfur is present in smaller amount in all tribofilm samples. However, baseline subtraction of the spectra can produced distinguishable spectra features for further analysis.

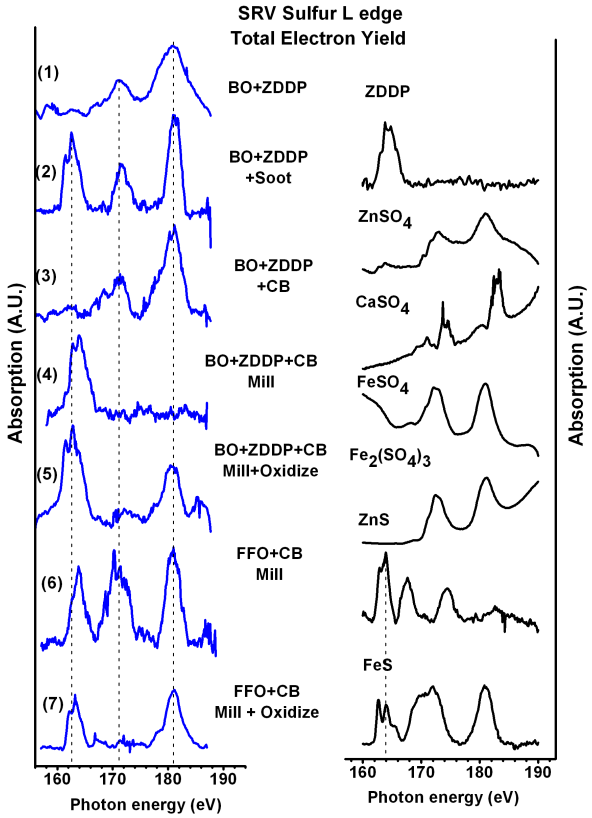

Figure 6.4 Normalized Total Electron Yield (TEY) sulfur L edge spectra of tribofilms and model compounds

Spectra (1) were recorded from the tribofilm derived from formulation A that had [mineral oil with ZDDP as anti wear additives]. White line of spectra (1) closely matched with zinc sulfate ($ZnSO_4$). Similar results have been recorded for tribofilm derived from formulation C and have shown as spectra (3). XANES spectra of tribofilm derived from formulation F that was blend of 3

wt. % diesel soot and formulation A, referred as spectra 2. Absorption edge of spectra (2) closely matches with zinc sulfate ($ZnSO_4$). In addition another peak located to left of main white line, closely aligns with zinc sulfide (ZnS) indicative of ZnS as another constituents of the tribofilm. Spectra (4) and (5) are recorded from the tribofilm derived from formulation H and I, indicate that the zinc sulfide is major constituent of tribofilm. While spectra (6) and (7) derived from the tribofilm generated using formulation L and M has zinc sulfide (ZnS) and zinc sulfate ($ZnSO_4$) are like to constitute tribofilm. However, careful observation of spectra (6) indicates that the zinc sulfide is present in tribofilm as major compound compare to zinc sulfate ($ZnSO_4$).

6.3.3.3 Iron L edge

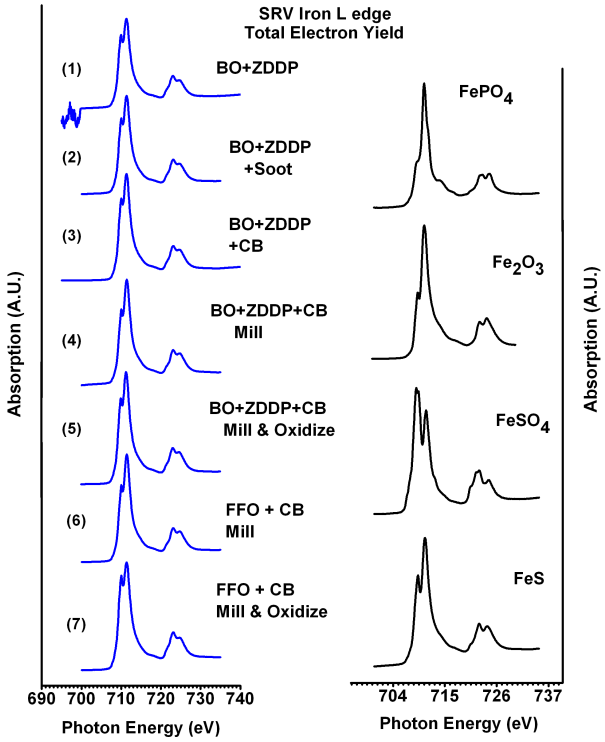

Figure 6.5 Normalized Total Electron Yield (TEY) iron L edge spectra of tribofilms and model compounds

Figure 6.4 shows the iron L edge spectra of tribofilm derived from formulation mentioned in table 6.1 in TEY mode. The TEY iron L-edge spectra of the model compounds Fe2O3, FeS, FePO4, FeSO4 have used for comparison. The Fe L-edge has the white line at approximately 710.75 eV and a pre-edge at approximately 709eV. The relative intensity of the pre-edge strongly

depends on chemistry. FePO4 has the smallest pre-edge while FeSO4 has a pre-edge that has a higher intensity than the white line. The TEY spectra of the all the tribofilms do not show distinctive differences. All tribofilms spectra have pre-edge peaks that are less intense than the white line indicating that the primary form of Fe is in the form of Fe2O3 and/or FeS, however, since the relative intensity of this pre-edge peak is stronger than what is observed in the FePO4 spectrum making this compound a less likely component of both tribofilms. In both cases it is not likely that the tribofilms contain measurable amounts of FeSO4 since this compound exhibits a pre- edge peak that is higher in intensity than the white line.

6.3.3.4 Phosphorous K edge

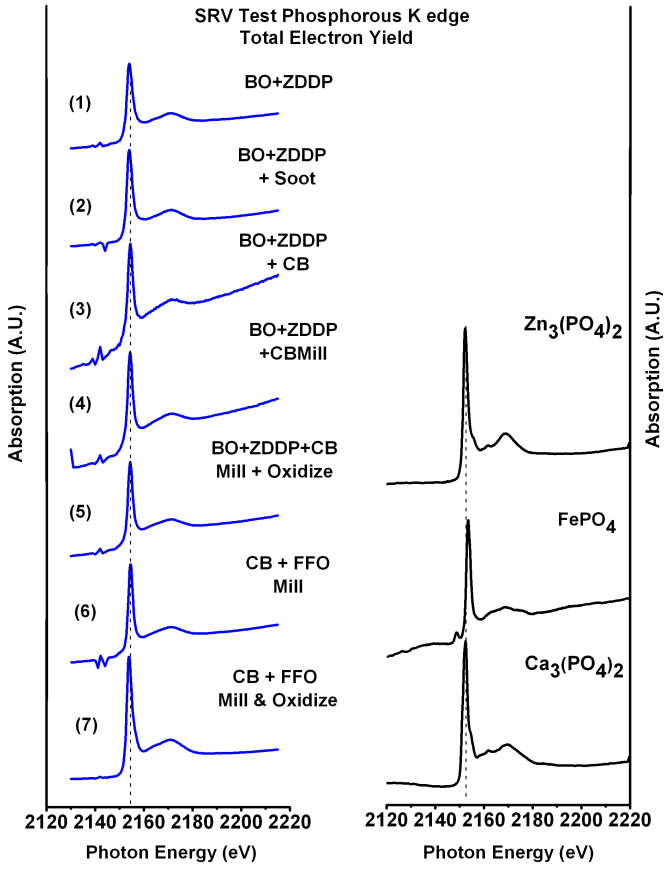

Figure 6.6 Normalized Total Electron Yield (TEY) phosphorous K edge spectra of tribofilms and model compounds

Figure shows the XANES phosphorus K edge spectra of tribofilm derived from the formulation as mentioned in table 6.1 along with their model compounds, recorded in TEY mode. Spectral features of the model compounds as well as tribofilms have been described in the previous chapters. All the tribofilm spectra have identical peak shape and single intense peak closely aligns with zinc phosphate and calcium phosphate. It is unlikely to have presence of iron (III) phosphate in the tribofilm due to the absence of distinguishing pre edge of iron (III) phosphate in tribofilm. However, It is not possible to have calcium phosphate ($Ca_3(PO_4)_2$) in the tribofilm (1)-(5), simply due to the fact that the formulation that was used to derived the tribofilm do not have any calcium compounds. However, tribofilm spectra (6) and (7) are derived from the fully formulation oil are likely to have zinc phosphate ($Zn_3(PO_4)_2$) as well as calcium phosphate ($Ca_3(PO_4)_2$). These results validate the results of P L-edge.

6.3.3.5 Sulfur K edge

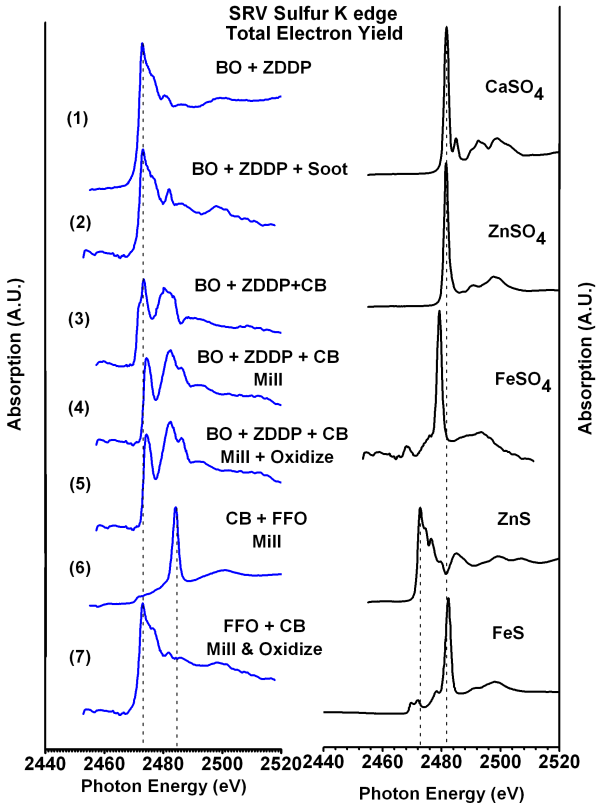

Figure 6.7 Normalized Total Electron Yield (TEY) sulfur K edge spectra of tribofilms and model compounds

Sulfur K edge XANES spectra collected in TEY mode for tribofilm (1)- (7) derived from formulation as mentioned in table 6.1 along with the model compounds. Spectral features of model compounds have described in the previous chapters. The sulfur K-edge spectra in TEY mode (Fig. 15) provide information from the surface region of the tribofilms (30–50 nm depth) and indicates that most of the sulfur in this region is in the form of sulfide but also contains noticeable amounts of zinc (II) sulfate which is evident by the presence of a peak in the energy range 2480–2490 eV.

6.4 Discussion

XANES has been extensively used to study the nature of antiwear film formation by many researches, especially AW tribofilm formation derived from ZDDP. [27-30]. Depending on the test conditions, researchers have reported that zinc sulfate as one of the major constituents of the tribofilm derived from the ZDDP. [10,15] Berbeizer et al have reported that the presence of soot (carbon black) modifies the film formation mechanism. [74] However, tribofilm derived from the formulation that was blended with carbon black have suggested the presence of zinc sulfate as one of the constituents of it. This infers that the tribofilm composition has not changed by the blending carbon black to baseline formulation.

However, the treatment of carbon black was aimed to mimic the chemical make up of the surface of diesel soot by forcing the interaction of lubrication additives chemistries and carbon black. Earlier studies have reported the efficacy of these treatments to mimic the chemical make up. These chemistries on the surface of carbon black have influenced the friction behavior as well the composition of the tribofilm. Friction coefficients of the formulations with treated carbon blacks have shows reduction in it. While XANES sulfur L edge indicate the formation of more zinc sulfide on the tribofilm derived from the formulations with treatments. These results postulate the modification in the film formation mechanism due to presence of diesel soot and treated carbon blacks.

Ryason have reported the polishing wear mechanism by diesel soot. [73] [47,76,77,98,104,116,127-135]Researches have reported the reduction in friction coefficient due

to presence of zinc sulfide and / or iron sulfide in the tribofilm.[65,136-139] Formation of zinc sulfide and iron sulfide on the tribofilm derived from the diesel soot and treated carbon black formulation and reduction in friction coefficient provides insight of the polishing wear mechanism. SEM analysis of flat specimen of SRV bench test indicated the randomly distributed irregular striations along with deeper grooves on the wear tracks. In addition, all the tribofilm samples have patchy appearance where dark regions are most likely to be thicker tribofilm. Along with patchy tribofilm, considerable are on the wear track have smooth appearances in high magnification micrograph. Tribological assessment of the test formulation in collaboration with XANES analysis of tribofilm and morphology of wear surfaces indicate the polishing wear might be the dominant wear mechanism in the given test configuration and in reciprocating motion of two sliding surfaces.

6.5 Conclusion

SRV friction bench test have used to evaluate the friction behavior of the formulation blended with and without carbon black and had subjected to treatments. XANES have been used to study the effect of carbon black treatment on tribofilm formation.

(i) Baseline formulation that was blended without carbon black have shown highest friction coefficient. While blending carbon black to the baseline formulation have demonstrated the reduction in friction coefficient. Blending extracted diesel soot to baseline formulation have reduced friction coefficient more than the formulation blended with and without carbon black.

(ii) Formulations were also prepared by blending carbon black to fully formulated oil and were subjected to milling and [milling + oxidation] treatments. These formulations have shown lower friction coefficient than the formulations that were prepared without treatment.

(iii) Formulations were also prepared by blending carbon black to [mineral oil + 0.1 wt.%P ZDDP + 5 wt.% Dispersant] and were subjected to milling and [milling + oxidation] treatments. These formulations have shown lowest friction coefficient.

(iv) SEM analysis of flat samples indicated the randomly distributed irregular striations along with deeper grooves on the wear tracks. In addition, all the tribofilm samples have patchy appearance where dark regions are most likely to be thicker tribofilm.

(v) XANES analysis of tribofilm using P L and K edge indicate that the tribofilm derived from the formulation that had ZDDP as only AW additives has zinc phosphate as major constituent while calcium phosphate ($Ca_3(PO_4)_2$) is more likely to constitute the tribofilm derived from fully formulated oil while zinc phosphate ($Zn_3(PO_4)_2$) is present as minor constituents.

(vi) Sulfur L and K edge XANES spectra indicate the formations those were prepared with and without blending carbon black formed tribofilm that has zinc sulfate while formulation those were prepared by treatment of carbon black has tribofilm with zinc sulfide as major compound.

(vii) Iron L edge indicates that the all tribofilms have iron in form of Fe_2O_3 or FeS.

CHAPTER 7

MORPHOLOGY, STRUCTURE AND CHEMISTRY OF EXTRACTED DIESEL SOOT FROM MACK T-12 DYNAMOMETER ENGINE TEST AND ITS CORRELATION WITH TRIBOFILM FORMATION OF PISTON RING

7.1 Introduction

Over the last three decades, heavy-duty diesel engines have evolved to comply with tighter pollution mandates and customer requirement. [24] Modifications in engine design have changed the combustion chamber and crankcase environment and hence have impacted heavy-duty engine oil technology. [37] Engine lubricants quality is very important to help ensure engine durability, engine performance and reduce maintenance downtime. [133] In last same period, various engine lubricants qualification tests have been developed and introduced to evaluate the heavy duty engine lubricants performance. Beginning in the late 1980's, a new Mack genuine oil specification and new American Petroleum Institute (API) heavy-duty engine lubricants category have been introduced with each new U.S. heavy duty, on highway emission specification such as Mack T-7, T-8, T-8A, T-8E, T-9, T-10, T-11 and T-12.[98,140] These tests simulate various field operations of the diesel engine and hence have been used by the engine oil formulator to evaluate and optimize their products.

In 2004, U.S. NOx emission standards caused most U.S heavy duty engine manufacturer to adopt cooler EGR to lower NOx emission to 2 gram/bhp-hr. [4] Heavy duty engine manufacturer could not use retarded timing injection to achieve stringent NOx restriction mandates hence use of cooled EGR was inevitable.[5]. In addition, a delay the ignition produces more soot in the combustion chamber along with contaminants inclusion through exhaust recirculation that degrades the lubricants of crankcase. [86] To evaluate the effectiveness of

engine oil to protect the engine in various harsh environments, engine oil formulators have been using diesel engine dynamometer engine tests. For example, Mack T-7, T-8 and T-11 have designed to evaluate the soot laden viscosity increase, while Mack T-9, T-10, T-12 have developed to evaluate the wear of piston liner, bearing wear and oil oxidation due to wear and higher EGR ratio. [5,9,10] Accumulation of soot and hence increased wear of engine components due to EGR is one of the harsh environment that needs effective engine oil formulation to mitigate the detrimental effect on engine components and prolonged the drain interval. [4,141]

In the previous studies, an interaction between crankcase soot and decomposition products of lubricating oil was reported. The crankcase soot used for characterization was extracted from the used crankcase oil acquired during drain interval from the commercially operated diesel trucks and hence represented realistic field operation of diesel engine. [5] Characterization of drain interval crankcase soot using XANES, HRTEM, Synchrotron radiation x-ray diffraction and Raman spectroscopy have provided information on the structure and composition of soot. These results, in collaboration, have suggested the mechanically embedded hard nano-crystalline particle of carbonate hydroxylapatite, hydoxyapetite, ferric oxide along with amorphous zinc polyphosphate, crystalline calcium sulfates were present on the turbostratic structure of soot. This insight provided a framework for speculating on the mechanism of soot induced wear mechanism.

Motivated by our previous research, the present studies have extended to understand the soot induced wear mechanism in controlled dynamometer engine tests. Mack T 12 dynamometer tests have been used for the study. This test method was developed to evaluate the wear performance of engine oils in turbocharged and inter-cooled four-cycle diesel engines equipped with EGR and running on ultra-low sulfur diesel fuel. [2,3,5,7,142]. The Mack T12 test uses a Mack E-TECH V-MAC III diesel engine with Exhaust Gas Recirculation (EGR). The Mack T-12 is a procedure that evaluates oil's ability to minimize wear of the cylinder liner, piston rings and bearing wear in engines with exhaust gas recirculation (EGR). The Mack T-12 is part of the API CJ-4 performance category of engine oil procedures, and it simulates heavy-duty, on-highway

truck operations after 2007.A warm-up and a 1-h break-in are followed by a two phase test consisting of 100 h at 1800 r/min and 200 h at 1200 r/min, both at constant speed and load conditions. The operational parameters of the Mack T 12 test are summarized in the table 7.1.

Table 7.1 Operating parameters for Mack T - 12

Parameter	Phase 1	Phase 2
Time, hours	100	200
Speed, rpm	1800	1200
Fuel Rate, kg/hr	59.2	63.5
Torque[1], N-m	1349	2576
Oil Gallery Temperature, °C	88	116
Oil Sump Temperature, °C	93	129
Coolant Outlet Temperature, °C	66	108
Intake Manifold Temperature, °C	90	80
EGR Rate, %	35	15
Air / Fuel Ratio	23.6	21.1
Soot, weight %	4.3 ± 0.3 at 100 hours	6.0 at 300 hours

Mack T 12 uses higher EGR ratio compare to other Mack lubricant tests. It is well established that higher EGR ratio increases wear of engine components. [5] Moreover, soot enters the lubricant with exhaust gas in the form of blow-by, or it is deposited on cylinder walls and subsequently scraped off by the rings and deposited into the oil. Thus, soot scrapped of from the cylinder wall and extracted from the crankcase oil can provide better insight of the soot mechanism. In addition, characterization of piston ring can also provide significant understanding of the interaction between piston rings and soot. Thereby, provide insight of the three body wear mechanism of piston cylinder.

Table 7.2 Elemental composition of used diesel engine oil of Mack T -12

Element	P	Zn	Ca	Fe	B	Mg
ppm	1374	1611	4176	331	2	10

To characterize the cylinder soot, crankcase soot and piston rings, XANES, HRTEM and SR-XRD were employed. Besides, ICP analysis of used engine oil was useful to correlate the chemistry of engine oil with composition of cylinder soot, crankcase soot and tribofilm of piston ring.

7.2 Experimental Results

7.2.1 XANES Analysis of Soot Extracted from Mack T-12

7.2.1.1 Phosphorous L edge

Phosphorous L edge XANES spectra recorded in total electron yield and fluorescence yield on crankcase soot, cylinder soot and tribofilm of piston ring is shown in Figure 7.1. The L-edge for phosphorus probes electronic transitions from the 2p orbitals to unoccupied higher level s and d orbitals [1,10-13,15,23-25,37,39,41,53,88,141]. The L-edge spectra provide a result that is appreciably more surface sensitive, better resolved and better detailed [73,96] than the P K-edge. To help elucidate the chemistry of the soot samples and tribofilm sample, we compare the spectra of the soot samples with those of model compounds of known structure and geometry as shown in Figure 7.1 in black color. These model compounds are characteristic of typical phosphate spectra of antiwar film as well as decomposition compounds of lubrication chemistries. Information about the peak position and typical spectral features has mentioned in previous chapters.

In TEY mode, A careful comparison of the soot spectra with model compounds suggest that the absorption edges of crankcase soot and cylinder soot closely align with tri-calcium phosphate. A characteristic post edge at 141 eV for try-calcium phosphate differential other phosphate compounds. In addition, characteristics absorption pre-edge of both soot spectra at 136 eV also match with pre-edge of try-calcium phosphate. In fluorescence yield mode, spectra of

crankcase soot and cylinder soot show differences in the spectral features. Crankcase soot has broad peak while cylinder soot have intense white line along with post edge at 141 eV. The broad spectral features of the crankcase soot indicate the possibility of zinc phosphate as well as calcium phosphate. While cylinder soot spectra is closely aligned with spectra of tri-calcium phosphate.

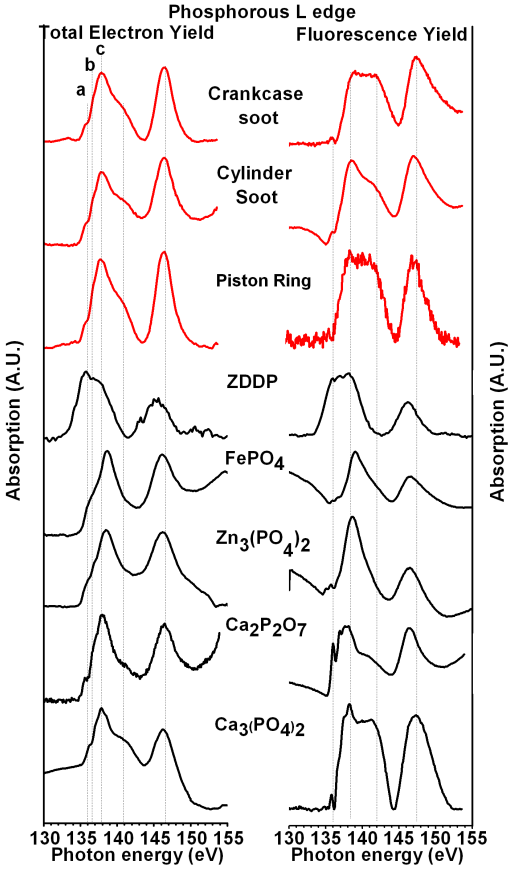

Figure 7.1 Normalized Total Electron Yield (TEY) and Fluorescent Yield (FY) phosphorous L edge spectra of crankcase soot, cylinder soot and piston ring of Mack T 12 engine test and model compounds

On the other hand, piston ring spectra recorded in TEY mode demonstrates identical absorption edges as crankcase and cylinder soot where characteristic pre-edge, post edge and white line closely aligns with try-calcium phosphate. In FY mode, noisier spectra were recorded but have similar absorption edge as recorded with crankcase soot. It is well known fact that TEY spectra much more surface sensitive than FY mode spectra. Spectra were recorded in both TEY

and FY modes, thus allowing for surface (~ 50 Å) and bulk (~ 500 Å) analyses of the film. [5]

This fact suggests that protective tribofilm on the piston ring is largly made up of try-calcium phosphate. In general, tribofilm spectra are made up of Iron and/or zinc phosphate with different chain length. Addition of detergent chemistry induces formation of calcium phosphate film on the surface. [5]

Earlier studies using the phosphorous L-edge have focused on evaluating polyphosphate glasses where the fine structure of polyphosphate glasses resulted from the spin orbit splitting of the 2p level electrons and the local symmetry of the phosphorus[143] which is generally characterized by three peaks (a), (b) and (c) as show in Figure 7.1. The peaks (a) and (b) at the low energy side are generally separated by about 1eV and are assigned to the transition of spin orbit split 2p electrons between 2p3/2 (L_3 edge) and 2p1/2 (L_2 edge). The change in intensity of the doublet (a and b peak) is due to the distortion of the phosphate tetrahedral. [48]The main peak (c) has been attributed to transitions to 3p orbitals, which are sensitive to the presence of other elements such as oxygen and other cation like Fe or Zn. In comparison the white line (c) peaks of model compounds, zinc phosphate has a slightly lower energy state at 138.7 eV than two iron phosphates at 139.0 eV of $FePO_4$ and at 135 eV of unreacted ZDDP. Also, zinc phosphate has a slightly lower pre-edge (a) peak. In addition two more calcium phosphate compounds were used for comparison. Between two calcium phosphates, β-TCP has an additional post edge compare to calcium pyrophosphate.

Earlier studies have shown that the intensity of peaks (a) and (b) relative to peak (c) depend on the polyphosphate chain length. [48,100,135,144] [Yin et al. in their paper [128] have shown the relative intensities of peak (a) and (b) with respect to peak (c) are sensitive to the number of phosphorus in the linear polyphosphate glasses using various chain lengths of sodium phosphate glasses. [62,83,106,145,146] In order to obtain accurate peak positions, widths, and intensities, their all spectra were fitted using a Gaussian function using a least-squares program. These peaks have been subtracted by arctangent base lines to consider the excitonic states, which are observed in certain solids. Kim et al have used linear background subtraction instead of

act tangent and have shown reported the similar results with linear background subtraction method. [102,143,147] Similar background subtraction methods have been in this study to deconvolute the spectra. Moreover, deconvolution using linear background subtraction can distinguish between orthophosphate, pyrophosphate, and short chain polyphosphate, while arctangent background subtraction cannot.

Zhang et al. [102,143,147,148] and Nicholls et al. [148,149] have used the rule for the phosphate chain length: an a/c ratio of about 0.3 is short chain length polyphosphate, and the a/c ratio of about 0.6 indicates a long chain polyphosphate. Since, linear background subtraction was used in this study instead of arctangent function, the results of a/c ratios was changed. In this study, the new standard of chain length of polyphosphate to be suitable for this deconvolution method is used. The a/c ratio below 0.2 means common orthophosphate or pyrophosphate. The value between 0.2 and 0.35 indicates the short chain polyphosphate and the value from 0.35 to 0.55 is the medium chain length of polyphosphate. The polyphosphate with above 0.55 a/c ratio is called as the long chain polyphosphate.

Table 7.3 Phosphorous L edge a/c ratio and chain length of crankcase soot, cylinder soot and piston ring of Mack T 12 dynamometer engine test

Dynamometer Engine Test	Phosphorous L edge a/c ratio	Chain Length
Mack T 12 Crankcase soot	0.223	Short Chain
Mack T 12 Cylinder soot	0.23	Short Chain
Piston Ring	0.27	Short Chain

As shown in Figure 7.1, phosphorous the L - edge spectra of all soot samples are characteristics of polyphosphate glasses. Mack T 12 crankcase soot, cylinder soot have a/c ratio 0.224 and 0.23 respectively which is suggestive of short chain polyphosphate. Analogous results were calculated for tribofilm of piston ring where a/c ratio is 0.27, which, is indicative of presence of short chain polyphosphate. These results were validated by the a/c ratio of try-calcium phosphate where a/c ratio was calculated as 0.33, which is indicative of short chain

polyphosphate. These results are contrary to the previous studies which suggested that interaction of ZDDP with detergent inhibit formation of long chain poly phosphates.[21 from Kasrai paper on combination of ZDDP and over based].

7.2.1.2 Phosphorous K edge

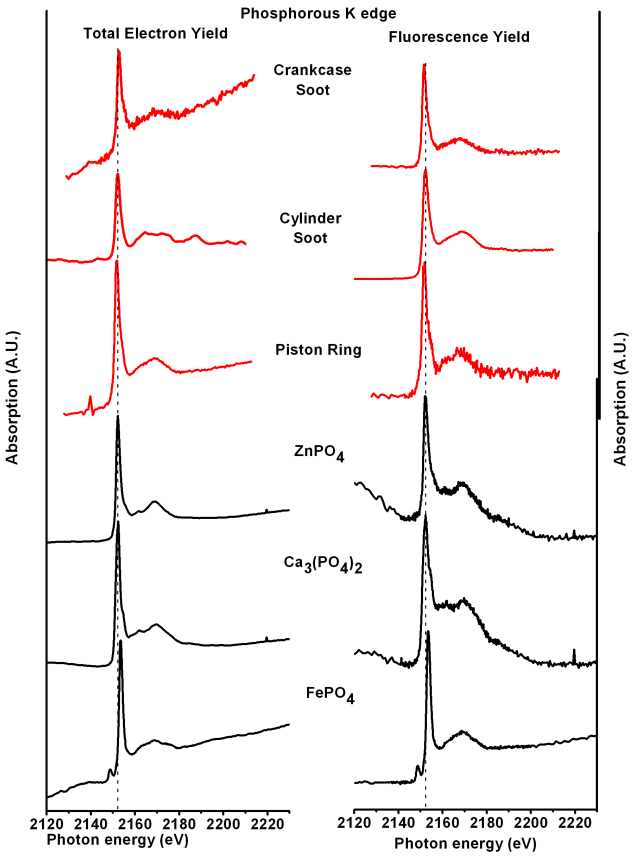

Figure 7.2 Normalized Total Electron Yield (TEY) and Fluorescent Yield (FY) phosphorous K edge spectra of crankcase soot, cylinder soot and piston ring of Mack T 12 engine test and model compounds

Figure 7.2 is phosphorous K edge spectra recorded in TEY and FY mode for the experimental samples. These spectra were compared with phosphates of zinc, calcium and iron. The white line for the phosphorous K - edge spectrum arises from transitions of 1s electrons to unoccupied 2p orbitals. $FePO_4$ has distinctive pre edge at 2150eV, which is absent in $Zn_3(PO_4)_2$ and $Ca_3(PO_4)_2$. Also the main peak of $FePO_4$ lies at 2154.5eV, which is higher energy state than $Zn_3(PO_4)_2$ and $Ca_3(PO_4)_2$. In addition a careful examination of the post edge structure indicates the presence of distinctive shoulder in the case of $Ca_3(PO_4)_2$ which is absent in the case of either

the $Zn_3(PO_4)_2$ or $FePO_4$.

The characteristics K absorption edge of all the soot samples and tribofilm samples closely aligns with $Zn_3(PO_4)_2$ and $(Ca_3(PO_4)_2)$ try-calcium phosphate in both the TEY and FLY mode. Possibility of $FePO_4$ is not likely due to absence of pre edge in soot spectrum. Phosphorous L absorption edge spectra suggest the presence of $(Ca_3(PO_4)_2)$, while the K-edge clearly confirms the presence of $Zn_3(PO_4)_2$ and $(Ca_3(PO_4)_2)$ and absence of any $FePO_4$.

7.2.1.3 Sulfur L edge

The sulfur L absorption edge spectra of different diesel soot were recorded in TEY and FY mode. These spectra were compared using model compounds of sulfates and sulfides of zinc, calcium and iron as well as unreacted ZDDP as shown in figure 3. All sulfates and sulfides have unique distinctive characteristic absorption spectra except $FeSO_4$ and $Fe_2(SO_4)_3$ which are quite similar. Model compounds of the sulfides have distinctive peaks at lower energy, which distinguishes sulfides form sulfates.

Both crankcase and cylinder soot spectra indicate the characteristics $ZnSO_4$ and $CaSO_4$. Analysis of tribofilm of piston ring spectra indicates presence of $ZnSO_4$ and $CaSO_4$, which is analogous to soot spectra. However, soot spectra of sulfur L edge are rather noisier indicative of low concentrate of sulfur species on the soot structure and on the tribofilm. An additional peak also recorded for tribofilm that is closely aligns with characteristics zinc sulfide peak at lower energy. This peak is interestingly absent in the FY mode. Presence of zinc sulfide peak in TEY mode indicate the tribofilm have protective zinc sulfide near the surface of tribofilm while absence of sulfide species in bulk of tribofilm.

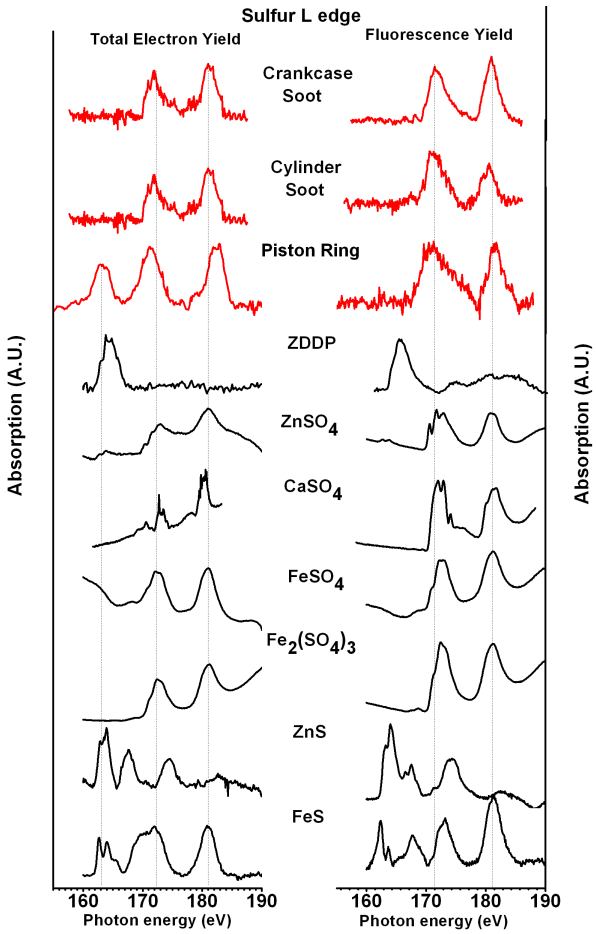

Figure 7.3 Normalized Total Electron Yield (TEY) and Fluorescent Yield (FY) sulfur L edge spectra of crankcase soot, cylinder soot and piston ring of Mack T 12 engine test and model compounds

7.2.1.4 Sulfur K edge

The spectrum of sulfur K absorption edge was compared with sulfates of zinc, calcium and iron and with sulfides of zinc and iron as shown in Figure 7.4. Higher energy states of iron sulfate at 2482.3 eV differentiate it from zinc and calcium sulfate. Zinc sulfate and calcium sulfate can be differentiated by the presence of a post edge at 2484.8 eV in the case of $CaSO_4$, which is absent in the case of ZnSO4. The sulfides have their white lines at lower energies than the sulfates with the zinc sulfide having an absorption edge at 2473 eV and a fairly rich post edge structure. Iron sulfide two strong peaks at 2471 eV and 2482 eV.

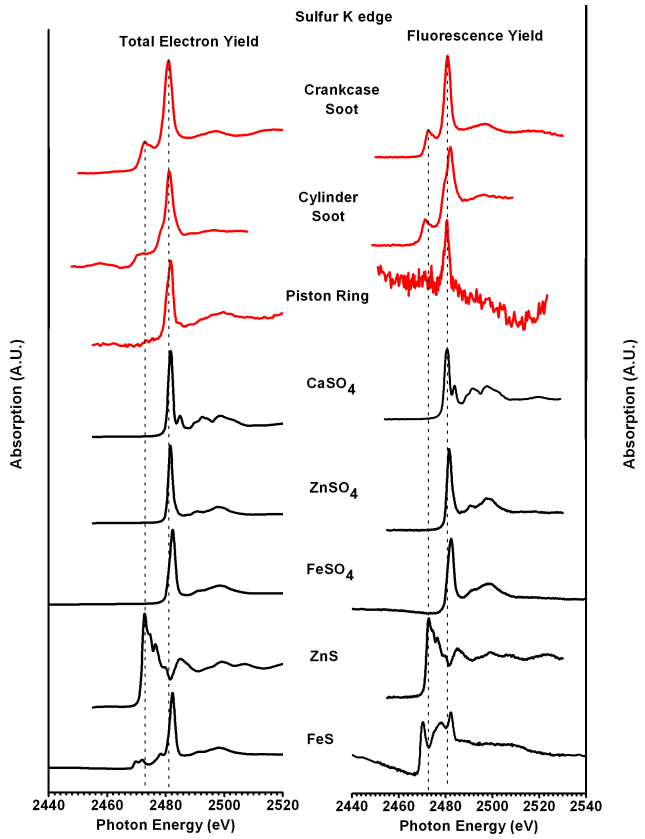

Figure 7.4 Normalized Total Electron Yield (TEY) and Fluorescent Yield (FY) sulfur K edge spectra of crankcase soot, cylinder soot and piston ring of Mack T 12 engine test and model compounds

In TEY mode, significant differences have been observed in sulfur K edge spectra of soot. White line of crankcase soot closely aligns with zinc sulfate. Moreover, another absorption edge 2473 eV matches with characteristic zinc sulfide peak. Also, it is unlikely to have calcium sulfate on soot structure due to absence of characteristic post edge peak of calcium sulfate at 2484. 8 eV. While, white line of cylinder soot is well aligned with white line of iron sulfate and iron sulfide. In addition, cylinder soot spectra has shoulder peak appears at 2479 eV closely aligns with pre edge of iron sulfide. In addition, iron sulfide has characteristics absorption edge at lower energy 2470 eV and 2471 eV, which is well aligned with absorption edge of cylinder soot. These observations indicate the presence of zinc sulfate in crankcase soot while iron sulfide is present in cylinder soot. In FY mode, white line of crankcase soot is well aligned with zinc sulfate peak

and not likely to have calcium sulfate. Crankcase soot white line aligns with iron sulfate peak. It is interesting to notice that in FY mode, iron sulfide has very distinctive spectral features, which does not match with any of the cylinder soot. These contrary results of FY mode from TEY mode suggest the presence of iron sulfide as well as iron sulfate on the cylinder soot. While crankcase soot spectra indicate the presence of zinc sulfate, which collaborates with the sulfur L edge spectra.

On the hand, analysis of the spectra of tribofilm formed on the piston ring indicate the presence of zinc sulfate in TEY as well as in FY mode. These results substantiate the results of sulfur L edge results. It is also interesting to notice the absence of zinc sulfide peak in S K edge, which is otherwise present in sulfur L edge spectra. Moreover, sulfur L edge spectra provide more surface sensitive information as compare to sulfur K edge. The higher flux of photons in the K-edge spectra helps in identifying the presence of ZnS in soot as well as evident in case of crankcase soot. Hence, we can infers that tribofilm has more protective sulfide film on the surface while the bulk of tribofilm has sulfate of zinc.

It also important to notice that in the analysis of sulfur K edge spectra we are able to distinguish between the cation species most likely to be present on the soot as well as on the tribofilm which was otherwise difficult with noisy sulfur L edge spectra. Hence, information infer from sulfur L edge and sulfur K edge together have provided distinguishable results to isolate the difference in the chemistries present on the two soot samples.

Quantification of the sulfur compound present was done by deconvolution the sulfur K edge spectra. The relative amount of sulfide and sulfate compound was analyzed by calculation height ratio of sulfide to sulfate peak. As shown in the figure, relative amount of sulfide is varying among the different soot samples. Soot sample from the Mack T 12 engine crankcase soot have relative sulfide amount 0.39 with respect to sulfate while very small amount of sulfide was present Mack T 12 piston cylinder soot.

Table 7.4 Sulfide/sulfate ratio of crankcase soot, cylinder soot and piston ring of Mack T 12 dynamometer engine test

Dynamometer Engine Test	Sulfide / sulfate ratio
Mack T 12	0.39
Mack T 12 Cylinder soot	0.066
Piston Ring	0.05

7.2.1.5 Zinc L edge

The zinc L absorption edge spectrum was recorded in TEY and FLY mode and examines the state of Zn in different soot samples as shown in Figure 7.5. For the comparison oxide, sulfate, sulfide and phosphates of zinc were used as model compounds as shown in figure 3. $ZnSO_4$ and $Zn_3(PO_4)_2$ has distinctive white line energy peak at 1024±1 eV which is absent in ZnS and ZnO. ZnS and ZnO have a broader peak compared to $ZnSO_4$ and $Zn_3(PO_4)_2$. Although the white line peaks of $ZnSO_4$ and $Zn_3(PO_4)_2$ lie close to each other the post edge fine structure of $ZnSO_4$ and $Zn_3(PO_4)_2$ differentiate them.

The spectra of crankcase soot and cylinder soot closely aligns with $Zn_3(PO_4)_2$. Analogous results have also been demonstrated in TEY and FY mode. However, the spectra from crankcase soot is rather noisy due to the low concentration of Zn and hence it is difficult to differentiate between $ZnSO_4$ and $Zn_3(PO_4)_2$ based on the Zn L-edge. It can be speculated that both compounds are presence on the soot. Similar results have also been recorded for the tribofilm on the piston ring and indicates the presence of $Zn_3(PO_4)_2$. However, no spectral features have recorded for tribofilm in FY mode and hence, it has not been reported in the figure. Analysis of zinc L edge substantiates the results analyzed in the P K edge.

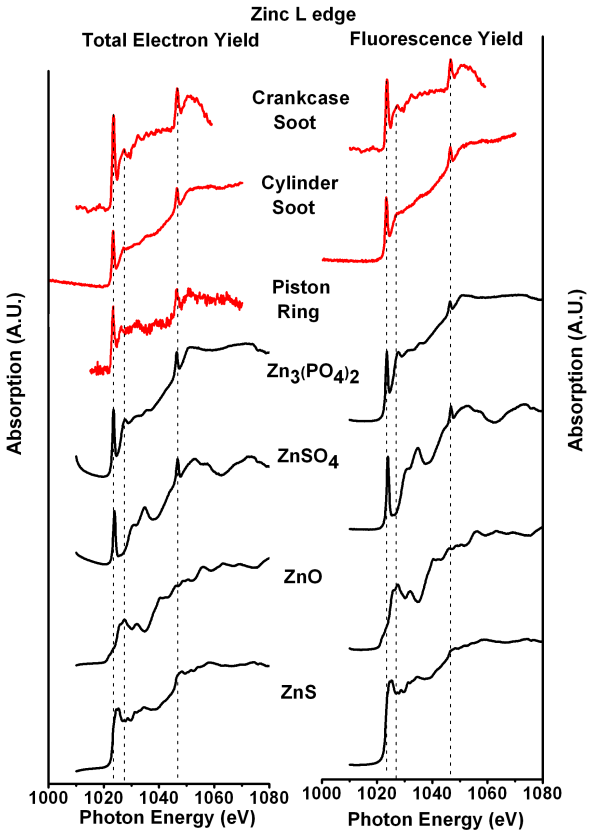

Figure 7.5 Normalized Total Electron Yield (TEY) and Fluorescent Yield (FY) zinc L edge spectra of crankcase soot, cylinder soot and piston ring of Mack T 12 engine test and model compounds

7.2.1.6 Calcium L edge

Ca has an electronic configuration of $2p^6$ $3d^0$ with a high probability of transition of electrons from the 2p to the 3d shells. Earlier studies on calcium $L_{2,3}$ edge using density of states and other approaches have taken into account the 2p-3d spin-orbit interactions as well as 3d-3d coulomb and exchange interactions. [150] Fine structure of the Ca 2p X-ray-absorption edge for bulk compounds, surfaces, and interfaces. [98,151] Model compounds of calcium sulfate ($CaSO_4$), calcium hydroxide ($Ca(OH)_2$), calcium phosphate $Ca_3(PO_4)_2$, calcium carbonate ($CaCO_3$) and hydroxy apatite ($Ca_{10}(PO_4)_6(OH)_2$) were examined.

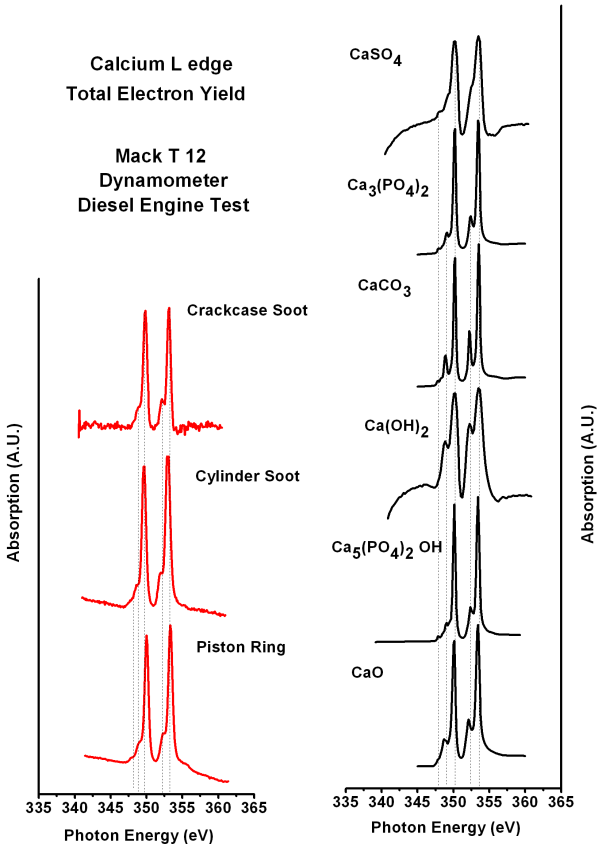

Figure 7.6 Normalized Total Electron Yield (TEY) calcium L edge spectra of crankcase soot, cylinder soot and piston ring of Mack T 12 engine test and model compounds

Shown in Figure 7.6 is the calcium absorption edge recorded in TEY mode to elucidate the state of calcium on the soot and tribofilm samples. The two primary peaks in the spectra located at 350 eV and 353 eV correspond to the L_3 and L_2 absorption edges [152], The other minor peaks before the L_3 and L_2edges correspond to various different 2p transitions. Absorption edges of $Ca(OH)_2$ and $Ca_{10}(PO_4)_6(OH)_2$ are slightly lower energy state than $CaSO_4$ and $Ca_3(PO_4)_2$. $Ca_3(PO_4)_2$ has a much more pronounced pre- edges compare to calcium sulfate. The crankcase soot spectrum closely resembles the spectra from calcium sulfate and to a lesser extent that of $Ca_3(PO_4)_2$ and $Ca_{10}(PO_4)_6(OH)_2$. However, spectra from the dynamometer soot samples are noisy hence difficult to differentiate the pre edge peaks of L_3 and L_2 absorption edge. On the contrary, cylinder soot spectrum closely resemble with $Ca_3(PO_4)_2$. It is also important to notice that

$Ca_3(PO_4)_2$ spectra another minor peak appears before the L_3 peak corresponds to various 2p transition. This characteristic peak is present in cylinder soot and as well as in tribofilm of piston ring. Further analysis is needed to characterize the calcium compound on soot samples.

7.2.1.7 Calcium K edge

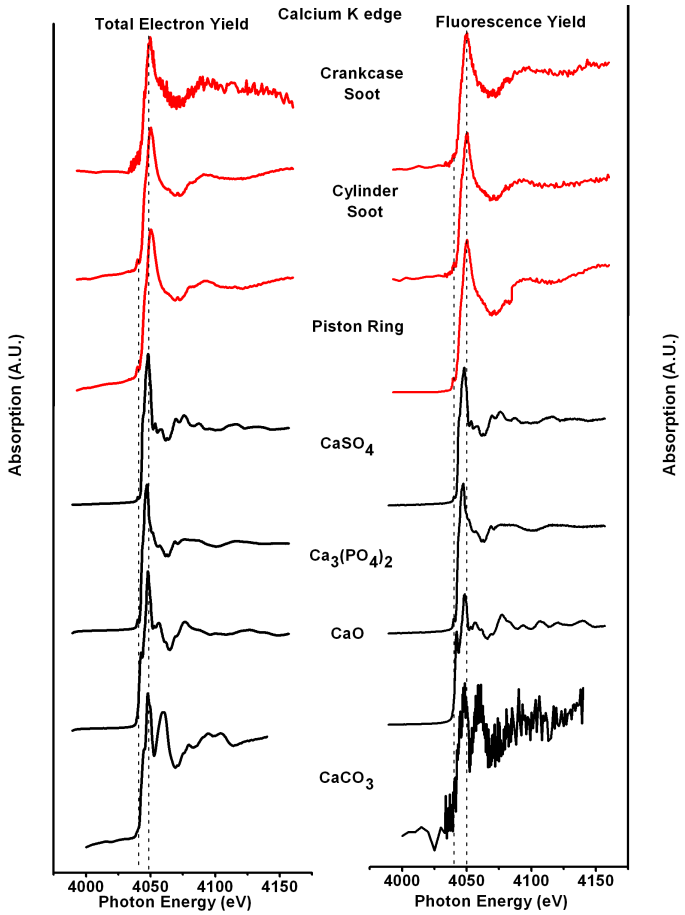

Figure 7.7 Normalized Total Electron Yield (TEY) and Fluorescent Yield (FLY) calcium K edge spectra of crankcase soot, cylinder soot and piston ring of Mack T 12 engine test and model compounds

Figure 7.7 shows the calcium K absorption edge was recorded in TEY and FLY mode for the soot samples and piston ring. Calcium sulfate, calcium oxide and tri-calcium phosphate were used for comparison. The white line for calcium sulfate, calcium oxide and tri-calcium phosphate lies at 4050 eV, 4049.8 eV and 4049. 4 eV. Calcium oxide has distinguishing pre edge at 4043 eV which is absent in the other Ca compounds. Calcium sulfate has more defined fine structure

compared to tri-calcium phosphate. Comparison of the soot spectra and model compounds spectra clearly indicates that the spectra appears to be close to both calcium sulfate and tri-calcium phosphate and the absence of CaO. The P K-edge spectra indicates that the phosphates were most likely Zn based and not Ca based, and the S K-edge spectra also indicated that the presence of $ZnSO_4$ and lesser extent the presence of $CaSO_4$. It is safe to come to the conclusion that Ca largely exists as $Ca_3(PO_4)_2$ and possibly to a smaller extent as the $CaSO_4$.

Tribofilm on the piston ring also exhibits similar characteristic absorption edge matches with calcium sulfate or calcium phosphate.

7.2.2 High Resolution Transmission Electron Microscopy

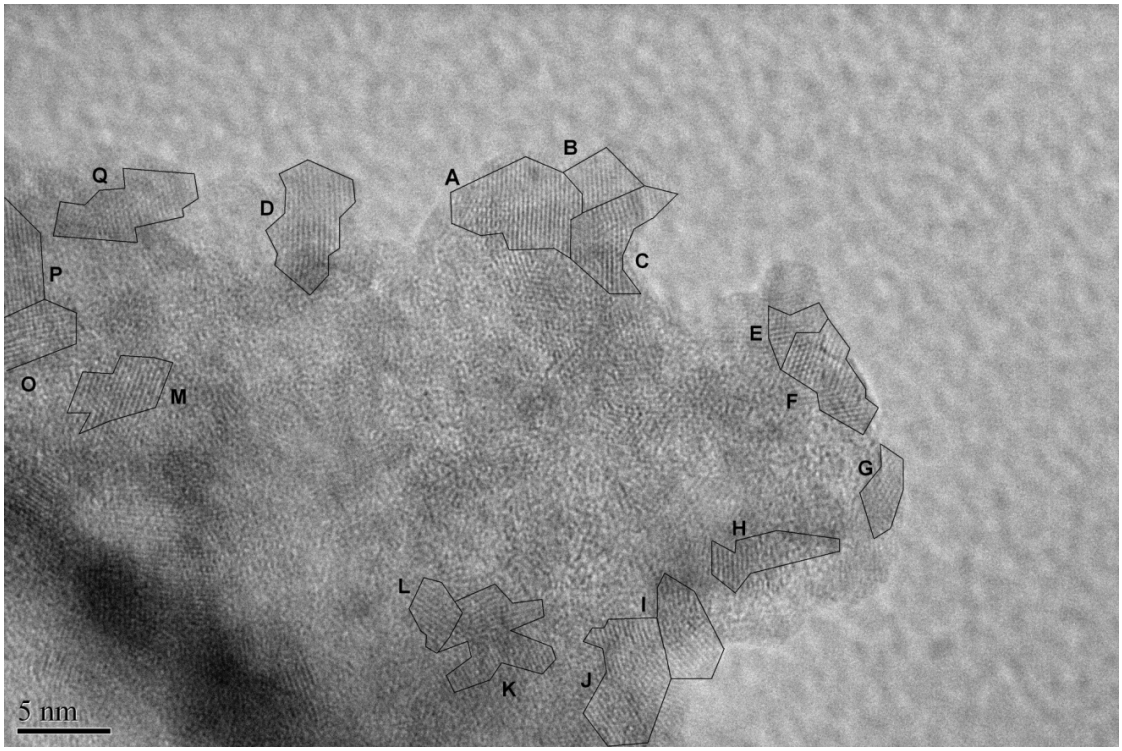

Figure 7.8 High-resolution bright field transmission electron micrograph of cylinder soot showing nano crystalline particle, turbostratic and amorphous regions

In previous study, high-resolution transmission electron microscopy was used to examine the nature of the turbostratic structure of the diesel soot extracted from the drain interval. High-resolution bright field transmission electron microscopic image of diesel soot that demonstrated regions encompassing turbostratic carbon structure, which is the main constituent of diesel soot

[reference]. In addition, there were several nano crystalline regions identified that were embedded within the soot. These nano crystalline particles were identified as Fe_2O_3, hydroxyapatite ($Ca_5(PO_4)_3OH$) and carbonate hydroxyl apatite ($Ca_5(PO_4,CO_3)_3OH$. [47]

Similar approach was adopted to examine the state of cylinder soot and crankcase soot acquired from the Mack T 12 dynamometer diesel engine test. Figure 7.8 is high-resolution bright field transmission electron microscopic image of cylinder soot that shows typical turbostratic structure of diesel soot. In addition, several nano crystalline regions identified that are embedded with turbostratic structure of soot.

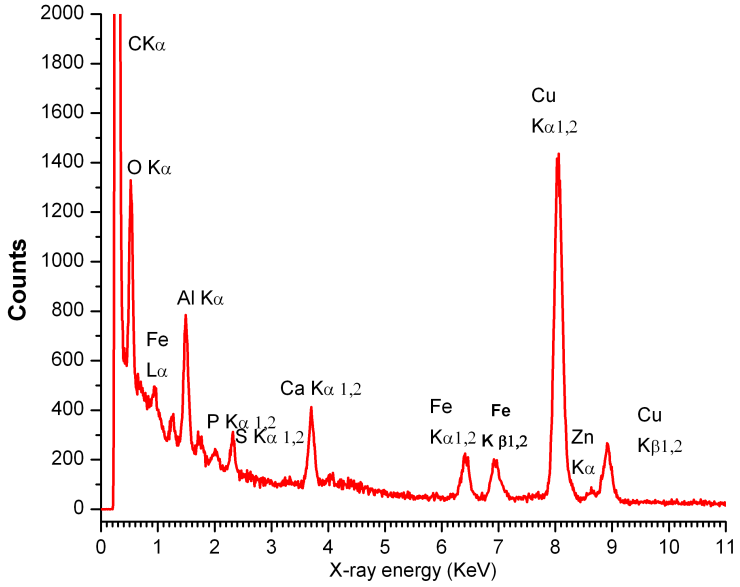

Figure 7.9 EDS spectra of cylinder soot

Table 7.5 Inter-planar crystal spacing and indices of crystallographic plane of nano-crystalline particles present on cylinder soot of Mack T-12 dynamometer engine test

Nano crystalline Particles	Inter-planar crystal spacing d (Å)		The indices of crystallographic plane (hkl)
	Standard	Measured	
A	2.47	2.480	ZnO
B	2.47	2.48	ZnO
C	2.47	2.479	ZnO
D	2.69 / 2.72	2.685	Fe_2O_3 (104)/$Ca_5(PO_4)_3$ OH (300)
E	2.778 / 2.811	2.781	$Ca_5(PO_4)_3OH$ (112)/$Ca_5(PO_4,CO_3)_3OH$ (211)
F	2.778 / 2.811	2.77	$Ca_5(PO_4)_3OH$ (112)/$Ca_5(PO_4,CO_3)_3OH$ (211)
G	2.778 / 2.811	2.79	$Ca_5(PO_4)_3OH$ (112)/$Ca_5(PO_4,CO_3)_3OH$ (211)
H	2.51	2.53	Fe_2O_3 (110)
I	2.09	2.256	FeS
J	2.51	2.522	Fe_2O_3 (110)
K	2.47	2.472	ZnO
L	2.72	2.738	$Ca_5(PO_4)_3OH$ (112)
M	2.814	2.80	$Ca_5(PO_4)_3)OH$ (211)
N	2.47	2.451	ZnO
O	2.47	2.449	ZnO
P	2.51	2.54	Fe_2O_3 (110)
Q	2.778 / 2.811	2.78	$Ca_5(PO_4)_3OH$ (112)/$Ca_5(PO_4,CO_3)_3OH$ (211)
R	2.66	2.65	FeS
S	2.66	2.64	FeS
T	2.778 / 2.811	2.78	$Ca_5(PO_4)_3OH$ (112)/$Ca_5(PO_4,CO_3)_3OH$ (211)
U	2.47	2.420	ZnO
V	2.47	2.421	ZnO
W	2.66	2.62	FeS
X	2.66	2.6	FeS
Y	2.66	2.65	FeS
Z	2.47	2.42	ZnO

A corresponding energy dispersive spectrum was recorded on the region that suggest the presence of P, S, Ca, Fe, Zn and O as shown in Figure 7.9. Peak for the Cu corresponds to the sample holder. An associated XANES spectra on the cylinder soot revealed the presence of tri-calcium phosphate, zinc phosphate and iron sulfide on the soot structure. To collaborate the spectroscopy results of XANES with microscopy results of HRTEM, inter planar spacing of the nano crystalline region was measured and reported in the table 7.3. The measured values were compared with various compounds that are speculated based on the XANES results. It is evident from the matched data that the likely candidates for the crystalline particles include Fe_2O_3, ZnO, hydroxyapatite ($Ca_5(PO_4)_3OH$) and carbonate hydroxyl apatite ($Ca_5(PO_4,CO_3)_3OH$.

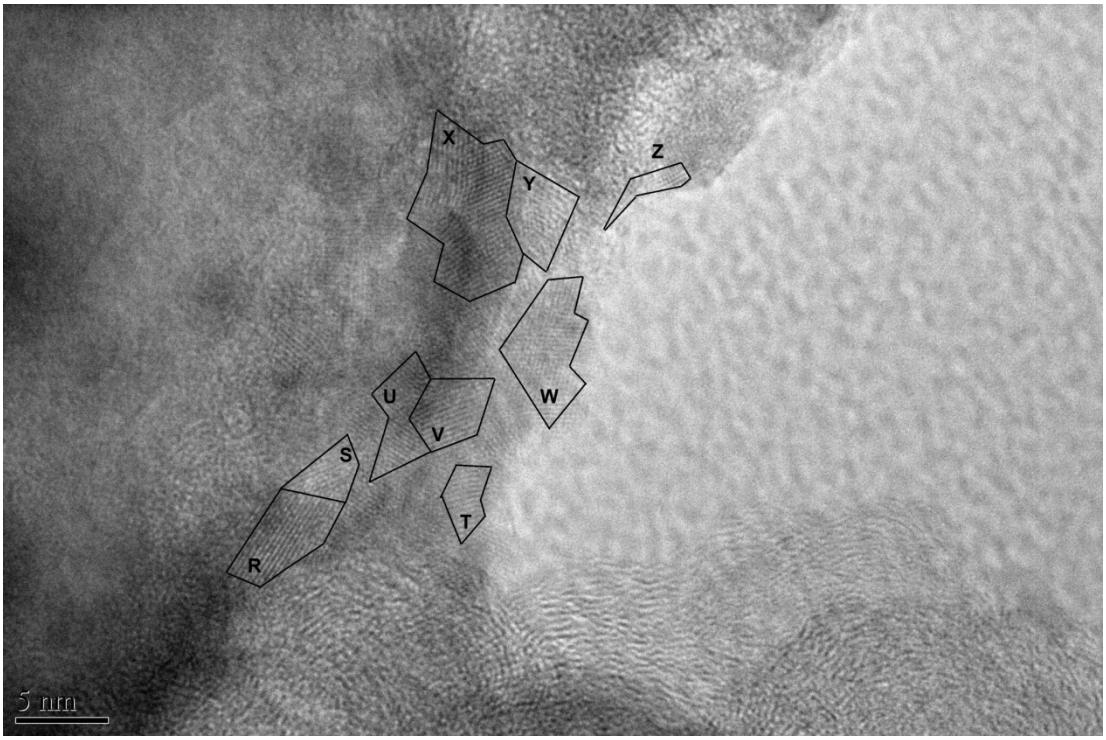

Figure 7.10 High-resolution bright field transmission electron micrograph of cylinder soot showing nano crystalline particle, turbostratic and amorphous regions

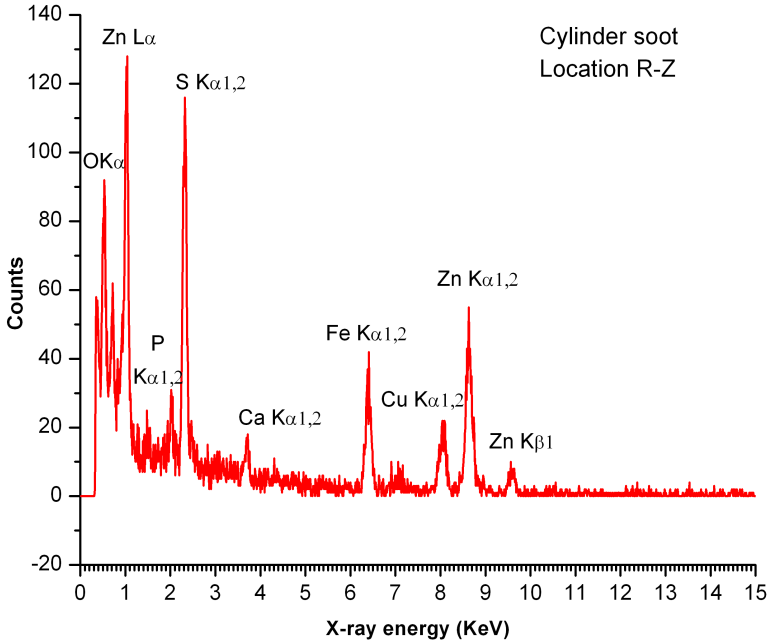

Figure 7.11 EDS spectra of cylinder soot

Figure 7.10 is another representation of HRTEM on cylinder soot from different area. Analogous results have been observed on another location. Measurement of interplant spacing of nano crystalline particle is reported in the table 7.3. The corresponding EDS spectra, as shown in Figure 7.11, suggests that presence of O, P, S, Ca, Fe and Zn. Comparison with standards values of inter planar spacing from speculated compound closely match with zinc oxide, iron sulfide, hydroxyapatite ($Ca_5(PO_4)_3OH$) and carbonate hydroxyl apatite ($Ca_5(PO_4,CO_3)_3OH$.

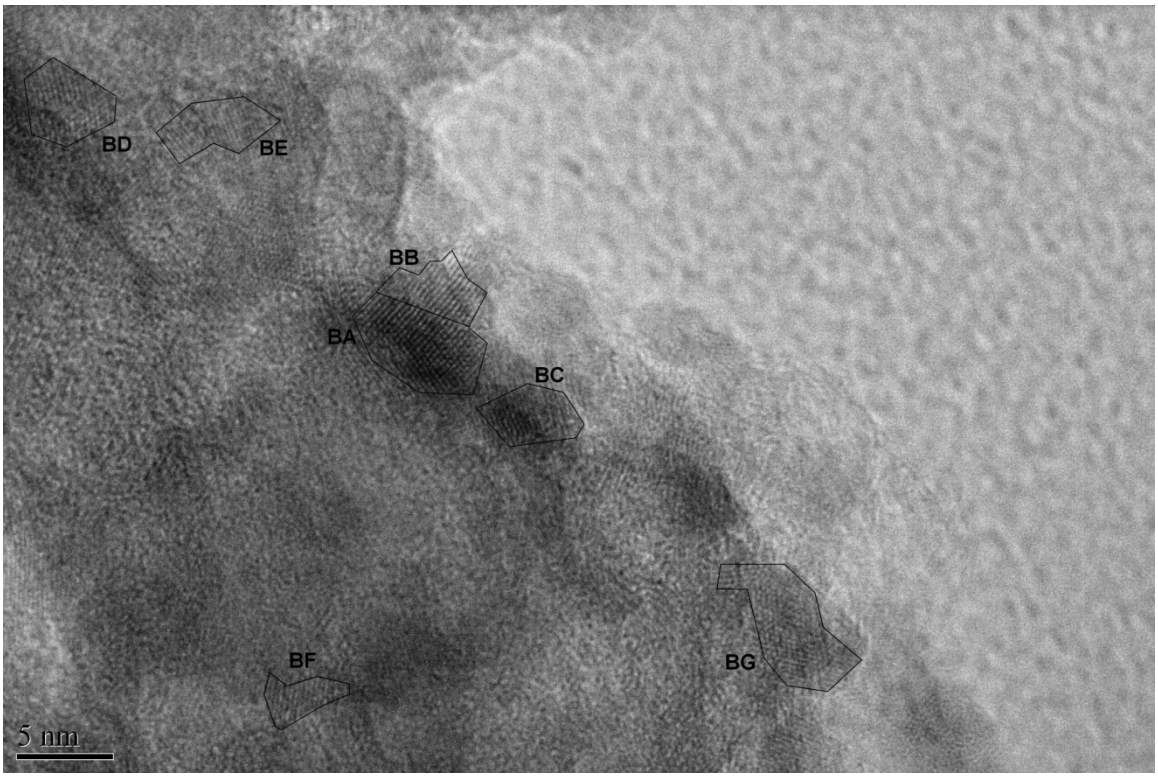

Figure 7.12 High-resolution bright field transmission electron micrograph of cylinder soot showing nano crystalline particle, turbostratic and amorphous regions

In addition, HRTEM images were acquired from crankcase soot. Figure 7.12 is bright field HRTEM images that indicate carbonaceous turbostratic structure along with embedded nano crystalline particles. Measurement of inter planar spacing between these nano particle have been reported in Table 7.4. These inter planar spacing between to diffracting planes of nano crystalline particle is at equidistance to the inter planar spacing of Fe_2O_3, hydroxyapatite ($Ca_5(PO_4)_3OH$) and carbonate hydroxyl apatite ($Ca_5(PO_4,CO_3)_3OH$.These results corroborates to the previous results obtained from the drain interval soot as well as from cylinder soot of mack T 12 engine.

Table 7.6 Inter-planar crystal spacing and indices of crystallographic plane of nano-crystalline particles present on crankcase soot of Mack T-12 dynamometer engine test

Nano crystalline Particles	Inter-planar crystal spacing d (Å)		The indices of crystallographic plane (hkl)
	Standard value	Measured value	
BA	2.814	2.892	$Ca_5(PO_4)_3OH$ (112)/
BB	2.778 / 2.811	2.789	$Ca_5(PO_4)_3OH$ (112)/ $Ca_5(PO_4,CO_3)_3OH$ (211)
BC	2.814	2.852	$Ca_5(PO_4)_3OH$ (112)
BD	2.814	2.823	$Ca_5(PO_4)_3OH$ (112)
BE	2.778 / 2.811	2.77	$Ca_5(PO_4)_3OH$ (112)/ $Ca_5(PO_4,CO_3)_3OH$ (211)
BG	2.77	2.74	$Ca_5(PO_4)_3OH$ (112)

In an earlier studies of wear in the presence of diesel soot it was suggested that polishing wear is a possible mechanism to account for enhanced wear [108,153,154], in addition in a study with ashless antiwear agents it was shown that the presence of small (<20 nm) particles of Fe_2O_3 promotes polishing wear [154]. The hardness of Fe_2O_3, ZnO and phosphates of calcium is in the range of 4.5-6 in the Moh's scale, which is much larger than the 2-3 for gypsum and bassanite [108]. Interestingly, XANES indicates that Zn is present as short chain Zn-phosphates that likely originated from the tribofilm and is generally present as an amorphous tribofilm at contacting surfaces. In addition, HRTEM results indicate presence of zinc in nano crystalline zinc oxide form. These high-resolution microscopy and spectroscopy in tandem have provided discernible results between cylinder soot and crankcase soot.

Careful observation of the both HRTEM images of cylinder soot and crankcase soot imply that the crystalline region is present on the edge of the primary particle of soot Moreover, they

appear as embedded on the outer periphery of the primary particle rather than loosely incorporated between the soot primary particles as wear debris. The crystalline phase of nano crystalline particles is continuous with crystalline domain of turbostratic soot structure. This continuity of crystalline phase on the surface of diesel soot primary particle suggests that possibility of mechanical embedding or chemical bonding of nano crystalline particle on surface of diesel soot primary particles and hence cannot be removed by washing, ultra sonication and centrifuging the soot.

7.2.3 SEM Analysis of Tribofilm

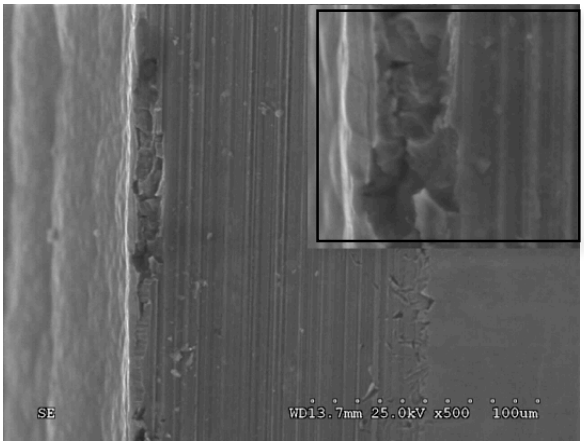

Figure 7.13 Secondary electron SEM micrograph of wear track of piston ring

Figure 7.13 is secondary electron SEM micrograph of the piston ring surface. The inset image is high-resolution micrograph images; 25KeV, 500 x magnification images of wear track and 25 KeV, 2500 x magnification images of center of wear track. SEM image suggest displays the wear track in the direction of reciprocating motion. The scratches running the direction of sliding indicate that abrasive wear is the predominant wear mode.

7.3 Discussion

Mach T 12 lubricants qualification tests run in two steps format where a dedicated lubrication degradation phase is followed by high load phase. As shown in table 7.1, the operating condition was targeted to maximize EGR rate. EGR increases ignition delay and thereby increases soot formation. The soot formation occurs later in the combustion cycle when more of

the lubricants film on the cylinder wall is exposed. Hence, soot is trapped in the larger oil film surface and carried into the crankcase lubricants. During this operation, trapped soot between piston and cylinder wall represent typical three-body wear condition. During second phase of T-12 test, the ring and liner wear rate is maximized using combination of low speed and high load that create boundary lubrication condition. [73,96] .

The interaction between soot and piston due to higher Hertzian point contact pressure can be substantiated by the identical XANES results of piston ring and soot samples. All experimental samples studied using calcium L edge, calcium K edge, phosphorus L edge and phosphorus K edge indicate the presence of phosphates of calcium. It has been reported that the impact of Mack T 12 test promote changes in the lubricant formulation such as optimized detergency, increased anti oxidants and sulfates ash. [10,37] . Effect of calcium detergent chemistry on the tribofilm formation was studied by Kasrai et al and has reported the formation of calcium phosphate film. Presence of calcium as cation forms a film that composed of small chain polyphosphate of calcium phosphate. [65,98,151] Moreover, interplanar spacing between nano particles matches with interplanar spacing of phosphate of calcium in form of harder apatite and carbonate hydroxylapatite.

It is well documented Fe_2O_3 originated from the tribofilm delaminating during two surface in relative motion under boundary lubrication conditions. [117]. In the previous study using drain interval soot, it was speculated that the mechanical embedding or chemical bonding of these nano crystalline particles on soot surface might take place due to three body wear during operation. During engine operation, trapped diesel soot particles / agglomerates between two rubbing surfaces experiences repeated extreme local temperature and Hertzian contact pressure which might responsible for mechanical embedding or chemical bonding of identified nano crystalline particles.

As mentioned previously that these nano crystalline particles composed of Fe_2O_3, hydroxyapatite ($Ca_5(PO_4)_3OH$) and carbonate hydroxyl apatite ($Ca_5(PO_4,CO_3)_3OH$. are harder on moh's scale [5,49]. Hence, it is speculated that mechanically embedded or chemically bonded

harder nano crystalline particle might promote higher wear, abrasive in some cases, and catastrophic failure in extreme conditions. [5]

The tribological interaction between piston cylinder assembly in presence of soot have studied by Mitsuru et al where they reported the effect of soot on the friction force of piston ring when EGR is activates. They reported the increase in the friction force of piston in the latter half of the compression stroke where the EGR system is activated, while the friction force is decreased at the each stroke center. Although the reduction of piston force at the stroke center reduces the piston friction force loss, the increase of friction force in the later half of the compression stroke is caused by the friction coefficient, which becomes higher at this point. Hence it can be anticipated that wear on the piston rings and cylinders would increase accordingly.[83,106,134,145,146] In addition, study done by Tokura et. al on wear of piston ring in diesel engine with EGR have reported that the wear of piston ring was 4.5 mg with EGR rate 0% and increased to 20mg when EGR rate was 30%. [75,78,98]. Increase wear of piston ring with EGR can be explained due to presence of mechanically embedded harder particle on the soot particle. SEM analysis of piston ring surface indicate abrasive wear tracks in direction of sliding motion validate the study of Mitsure et al and Tokura et al.

Moreover, Mack T – 12 uses cooled EGR that increases the amount of heat that has to be dissipated by the cooling system. But newly designed truck with aerodynamics would not allow larger radiators and modeling performed by the Mack indicated the heat rejection to the crankcase lubricants increase by 30-40%. This would drive up oil temperature in crankcase and increases potential lubricants degradation.[73,96] This increases the potential interaction between decomposition additives chemistries and soot. XANES results reveals the presence of various decomposition products such as zinc phosphates, zinc sulfide etc. In addition, EDS, XANES and HR-TEM results on the cylinder soot has relatively higher amount of phosphates of calcium, phosphates of zinc compare to crankcase soot. In addition, cylinder soot also contains nano crystalline particle of zinc oxides and iron sulfide. It can be speculated that cylinders soot that scrapped off from the piston might have experienced more severe environment as compare to

crankcase soot that had accumulated in the sump. It can be speculated that instead of recirculation of crankcase soot, cylinder soot might increase wear of piston cylinder.

7.4 Conclusion

X-ray absorption near edge structure (XANES) was used to examine the chemistry of diesel soot that was harvested from an exhaust gas recirculated dynamometer Mack T-12 diesel engine. XANES spectra were acquired at the P L and K edge, S L and K edge, Ca L and K edge and Zn L-edge.

(i) The L-edge spectra of P indicates the presence of P in crankcase soot and cylinder soot from decomposition products of ZDDP as well as from the detergent chemistry and not fresh ZDDP and a/c ratio of the phosphates present are likely short chain phosphates. Presence of post edge indicated the significant contribution from the calcium phosphate compounds.

(ii)The sulfur L-edge spectra suggests that most of the sulfur is present in the form of sulfates and the likely candidates are $CaSO_4$ and those of $ZnSO_4$ are also possible. $FeSO_4$ is likely to be present in the cylinder soot Fe is present from EDS analysis. Analysis of tribofilm of piston ring spectra indicates presence of $ZnSO_4$ and $CaSO_4$, which is analogous to soot spectra.

(iii) The Zn L-edge spectra clearly indicates that ZnO is not present, the phosphates and sulfates of Zn can be differentiated based on their fine structure post edge, however, the low concentration of Zn in the crankcase soot results in a noisy spectra and it is difficult to resolve between the phosphates and sulfates of Zn. While cylinder soot spectra indicate the presence of zinc phosphate and indicate the significant amount of zinc present in it, which can be validated by the EDS results of the cylinder soot. Tribofilm derived on the piston ring has noise zinc spectra and it is difficult to resolve between the phosphates and sulfates of Zn.

(iv) The Ca L-edge absorption edges of the crankcase soot, cylinder soot and piston ring indicate the presence of calcium phosphate and calcium sulfate.

(viii) The P K-absorption edge provides information from a larger volume of material due to the larger interaction volume at higher energies. The phosphates of Fe and Zn are clearly distinguished by the pre-edge peak which is present in $FePO_4$ but absent in Zn and Ca

phosphates. In addition, a post edge shoulder present in $Ca_3(PO_4)_2$ is absent in $Zn_3(PO_4)_2$. The K-edge spectra of soot closely match that of $Zn_3(PO_4)_2$.

(ix) The S K-edge spectra are very useful in distinguishing between sulfides and sulfates as well as between different sulfides. In addition, one can distinguish between the different sulfates. The S K-edge spectra indicate that sulfur in crankcase soot and cylinder soot is largely present as $ZnS/ZnSO_4$ and to a smaller extent as with almost the complete absence of $FeSO_4$.

(x) Ca K-edge spectra can clearly distinguish between CaO and CaSO4 and $Ca_3(PO_4)_2$ and the spectra indicates an absence of CaO, P K-edge spectra and S K-edge spectra indicates that P is coordinated with Zn and S with Ca and from the Ca K-edge spectra the Ca largely exists as $CaSO_4$ and to a lesser extent as $Ca_3(PO_4)_2$.

(xi) High resolution transmission electron microscopy couple with energy dispersive spectroscopy reveals the presence of crystalline nano-particles embedded on the periphery of the turbostratic structure of soot. A closer examination of the interplanar spacing with lattice imaging coupled with elemental analysis of these nano-particles indicates that the particles are constituted of phosphates of Ca as well as Fe_2O_3. These compounds have a hardness of around 5-6 on the Moh' scale and can contribute to polishing wear under 3 body boundary lubrication conditions.

CHAPTER 8

EFFECT OF OPERATIONAL PARAMETERS OF DIESEL ENGINE DYNAMOMETER TESTS ON DIESEL SOOT CHEMISTRY AND TRIBOFILM FORMATION

8.1 Introduction

Over the past 25 years, heavy-duty diesel engine design and engine oil formulations have changed considerably. [51,155] Stringent emission standards and customer requirements are the primary driving force for these changes. These changes have caused significant modification in the engine oil formulations to combat the crankcase environment, in particular higher level of soot. Soot related problems began to appear in early 1980's in heavy duty engines operating in stop-and-go or mixed service. Turbocharger lag and inertia of air cause insufficient air, which momentarily results in over fueling during engine acceleration. When this phenomenon is repeated over and over, high soot levels may appear in the crankcase lubricants especially in high load application with rapid acceleration. [155] These engines often had high oil viscosity increase, oil gelling and sludge build up, and all resulting from insufficient soot dispersancy. [156][5]

To evaluate the performance of lubricants in severe conditions various lubricants qualification tests evolved with tighter emission norms. From 1985 to 2007 various lubrication tests have been developed and standardized. In the heavy duty engine oil, there are number of industry standard engine test that measure the wear performance as well as viscosity increase due to soot. [4,86]These tests were designed to meet both industry and engine manufacturer requirement such as API CJ 4 and various specifications from Caterpillar, Cummins, Mack, Detroit Diesel and Volvo. The key wear tests assess the ability of an oil to control valve train or ring and liner wear under severe operating conditions which includes high load duty cycle, use of exhaust gas recirculation and high level of soot contamination. [5]

The API CJ-4 category requires various tests that include valve train and ring liner wear as a pass / fail parameters. For example, GM Roller Follower Wear Test (RFWT) (ASTM D 5966), The Cummins ISB test (ASTM 7484), Cummins ISM test (ASTM D 7468), Mack T-12 (ASTM D 7422). Also, Mack T-8 test (ASTM D – 5867), Mack T-11 (ASTM D- 7156) etc. to evaluate the viscosity increase of lubricants oil due to soot. [5,11,12]

In previous studies, the approach used was to correlate composition, structure and wear behavior of soot extracted from drain interval oil from field trucks and laboratory Mack T-12 engine test. Microscopy on field and laboratory soot has revealed significant compositional and structural similarity between soot samples acquired from field and laboratory crankcase oil. Moreover, both soots also revealed presence of mechanically embedded harder nano crystalline particles of Fe_2O_3, hydroxyapatite ($Ca_5(PO_4)_3OH$) and carbonate hydroxyl apatite ($Ca_5(PO_4,CO_3)_3OH$ with turbostratic structure of soot. [11,12]

This study is further extended to other lubricant qualification test that includes Mack T 8-A, Mack T-11, Mack T-12, Cummins ISM, Cummins ISB and GM RFWT. The operating conditions of these tests vary with emission requirement and different parameters that qualify the testing lubricant such as load, speed, duration, temperature, fuel flow, crankcase temperature, EGR rate, air to fuel ratio etc. These operational parameters might influence the interaction between diesel soot and lubricants additives chemistries.

In the present study, attempts have been made to establish the effect of engine parameters on the soot chemistries & structure. It is not feasible to distinguish the effect of each parameter separately on the structure and composition of soot for each standard engine tests. However, characterization of extracted soot from these standard dynamometer tests might provide better comprehension of the effect of engine parameters, if any. To study the correlation between tests conditions and soot chemistries, x-ray absorption near edge structures (XANES) spectroscopy and Raman spectroscopy have been employed. In addition, piston ring and header from Cummins ISM engine test, roller follower pin from GM RFWT engine test have been characterized to understand the tribofilm formation and generation of wear track.

8.2 Experimental Procedure

8.2.1 Diesel Engine Dynamometer Tests

8.2.1.1 Mack T 8 A

The Mack T 8A is an abbreviated version of Mack T-8 test to provide the lubricant performance equivalency between previously developed Mack T-7 test and Mack T-8 with limits of the 150 hours version of Mack T-8 test. The Mack T-8A procedure, which simulates field-service, heavy-duty operation, stop-and-go operation, and high-soot loading, evaluates the soot-handling capability of engine crankcase oil with regard to viscosity. The tests utilize a Mack E7-350 mechanically governed diesel engine with turbocharger, four cycle EGR equipped diesel engine. Tests are conducted on a flush-and-run format - with a warm-up, a 2-h flush for each test, and then a constant speed and fuel rate input for the duration of the test. Typically, the engine is rebuilt before a reference (calibration) test. The T- 8A test is 150 hours in duration, specified in the CF-4 category. [5] Operational parameters of the Mack T-8A engine test are summarized in table 8.1.

Table 8.1 Operating parameters for Mack T 8A

Parameter	Phase 1
Time, hours	150
Speed, rpm	1800
Fuel Rate, kg/hr	63.3
Torque[1], N-m	1375
Oil Gallery Temperature, °C	103
Oil Sump Temperature, °C	109
Coolant Outlet Temperature, °C	85
Intake Manifold Temperature, °C	43
EGR Rate, %	N/A
Air / Fuel Ratio	N/A
Soot, weight %, target (range)	2.9 (2.4 to 3.4) at 150 hours

8.2.1.2 Mack T 11

The Mack T-11 procedure evaluates the soot handling performance, as measured by viscosity increase, of lubricating oils operating in diesel engines equipped with cooled exhaust gas recirculation. The Mack T-11 test involves the use of a Mack E-TECH V-MAC III diesel engine with Exhaust Gas Recirculation (EGR). Two 30-min oil flushes are followed by a 252-h test at constant speed and load conditions. The V-MAC III consists of an electronically controlled fuel injection with six electronic unit pumps, using 2002 model year cylinder heads. It is an open chamber, in-line, six-cylinder, four-stroke, turbocharged, charge air-cooled, and compression ignition engine. The bore and stroke are 124 by 165 mm (4 7/8 X 6 1/2 in.), and the displacement is 12 L (728 in^3). This test was developed to evaluate the viscosity increase and soot concentration (loading) performance of engine oils in turbocharged and intercooled four-cycle diesel engines equipped with EGR. [86] Operational parameters of the Mack T- 11A engine test are summarized in table 8.2.

Table 8.2 Operating parameters for Mack T 11

Parameter	Phase 1
Time, hours	252
Speed, rpm	1800
Fuel Rate, kg/hr	53.3
Torque[1], N-m	1349
Oil Gallery Temperature, °C	88
Oil Sump Temperature, °C	93
Coolant Outlet Temperature, °C	66
Intake Manifold Temperature, °C	70
EGR Rate, %	17.7
Air / Fuel Ratio	24
Soot, weight %	4.8 to 5.8

8.2.1.3 Mack T 12

The Mack T-12 is a procedure that evaluates an oil's ability to minimize wear of the cylinder liner, piston rings and bearing wear following in engines with exhaust gas recirculation (EGR). The Mack T-12 is part of the API CJ-4 performance category of engine oil procedures, and it simulates heavy-duty, on-highway truck operations after 2007.The Mack T12 test uses a Mack E-TECH V-MAC III diesel engine with Exhaust Gas Recirculation (EGR). A warm-up and a 1-h break-in are followed by a two-phase test consisting of 100 h at 1800 r/min and 200 h at 1200 r/min, both at constant speed and load conditions. This test method was developed to evaluate the wear performance of engine oils in turbocharged and inter-cooled four-cycle diesel engines equipped with EGR and running on ultra-low sulfur diesel fuel. [5]

8.2.1.4 Cummins ISB

The Cummins ISB procedure is used to evaluate a crankcase lubricant's ability to reduce camshaft lobe and valve train wear. This procedure simulates repetitive cyclic operation found in the field with engines configured to meet 2007 emissions regulations. The Cummins ISB test method is a 350-hour test developed to evaluate the durability and reliability of the camshaft and tappet interface when run with different lubricating oils. The test method utilizes a modern medium-duty diesel engine equipped with exhaust gas recirculation. The test method uses a 2004 EPA emission compliant Cummins 5.9L ISB diesel engine. Test duration is 350 hours in two stages. During the 100 hours stage A, the engine is operated with retarded fuel injection timing to generate excess soot. During the 250 hours stage B, the engine is operated at cyclic conditions to induce valve train wear. Operational parameters of the Cummins ISB engine test are summarized in table 8.3.

Prior to each test, the engine is cleaned and assembled with new overhead valve train components. All aspects of the assembly are specified. A forced oil drain, an oil sample, and an oil addition are performed at the end of each 25-hour period for the first 100 hours of the test. Oil samples are taken every 50 hours. Oil additions are not made during the last 250 hours of the

test cycle. Oil performance is determined by assessing crosshead wear, tappet weight loss, and cam profile wear at 3.35% soot.

Table 8.3 Operating Parameters for Cummins ISB

Parameter	Phase 1	Phase 2
Time, hours	100	200
Speed, rpm	1600	Varies
Fuel Rate, kg/hr	20	Varies
Torque[1], N-m	--	--
Oil Gallery Temperature, °C	--	--
Oil Sump Temperature, °C	110	110
Coolant Outlet Temperature, °C	--	--
Intake Manifold Temperature, °C	68	68
EGR Rate, %	--	--
Air / Fuel Ratio	--	--
Soot, weight %	--	--

8.2.1.5 Cummins ISM Test Method

The Cummins ISM procedure is used to evaluate a lubricant's effectiveness at reducing soot-related wear of overhead components, sludge, and oil filter plugging. High-load, heavy-duty field conditions with high soot and exhaust gas recirculation (EGR) flow rates using a 2007 emission-compliant engine are simulated.

The Cummins ISM test method assesses the performance of engine oils, to control engine wear and deposits under heavy-duty operating conditions selected to accelerate soot generation, valve train wear, and deposit formation in a turbocharged, after cooled four-stroke-cycle diesel engine equipped with exhaust gas recirculation hardware. This test method uses a 2002 Cummins ISM diesel engine. Test duration is 200 hours in four 50-h stages. During stages 1 and 3, the engine is operated with retarded fuel injection timing and is over fueled to generate

excess soot. During stages 2 and 4, the engine is operated at conditions to induce valve train wear. [73,96] Operational parameters of the Cummins ISM engine test are summarized in table 8.4.

Table 8.4 Operating Parameters for Cummins ISM

Parameters	Phase 1	Phase 2	Phase 3	Phase 4
Time, hours	50 hours	50 hours	50 hours	50 hours
Speed, rpm	1800	1600	1800	1600
Fuel Rate, kg/hr	58	64.4	58	64.4
Torque[1], N-m	1220	1830	1220	1830
Oil Gallery Temperature, °C	110	115	110	115
Oil Sump Temperature, °C	80	65.5	80	65.5
Coolant Outlet Temperature, °C	--	--	--	--
Intake Manifold Temperature, °C	80	65.5	80	65.5
EGR Rate, %	--	--	--	--
Air / Fuel Ratio	--	--	--	--
Soot, weight %	--	--	--	--

8.2.1.6 Roller Follower Wear Test (RFWT)

Table 8.5 Operating Parameters for GM Roller Follower Wear Test

Parameter	Phase 1
Time, hours	50
Speed, rpm	100
Fuel Rate, kg/hr	9
Torque[1], N-m	Record
Oil Gallery Temperature, °C	--
Oil Sump Temperature, °C	97
Coolant Outlet Temperature, °C	--
Intake Manifold Temperature, °C	--
EGR Rate, %	--
Air / Fuel Ratio	--
Soot, weight %	--

The roller follower wear procedure simulates commercial and military applications. It determines the effect of lubricating oils on camshaft roller follower axle wears. The test engine is a General Motors 6.5-liter, indirect-injected diesel. The engine is rated at 160 horsepower at 3,400 rpm and is run at 1,000 rpm with near maximum load for 50 hours without an oil change.

Make-up oil is added at 25 hours. Oil gallery and coolant-out temperatures are controlled to 120°C. New roller followers are installed at the beginning of each test. At test end, the roller follower axles are removed and their wear is measured using a linear profilometer. Samples are taken at 25 and 50 hours. The used lubricant is analyzed for Viscosity at 40°C, Viscosity at 100°C, Total base number (TBN), wear and additive metals as specified. [49] Operational parameters of the GM RFWT engine test are summarized in table 8.5.

8.3 Results

8.3.1 Chemical characterization of diesel soot

8.3.1.1 Phosphorous L edge

Phosphorous L edge XANES spectra recorded on different diesel soot samples is shown in Figure 8.1. Phosphorous L edge spectra in red color is acquired soot sample extracted from the crankcase oil during drain interval from commercially operated diesel engine, which represent realistic field conditions of diesel engine. On the other hand, spectra in blue, green and orange are acquired from soot samples extracted from different dynamometer diesel engine tests as mentioned in Figure 8.1, which represent standard controlled diesel engine test configurations. The L-edge for phosphorus probes electronic transitions from the 2p orbitals to unoccupied higher level s and d orbitals [49]. To help elucidate the chemistry of the soot samples, we compare the spectra of the soot samples with those of model compounds of known structure and geometry as shown on right hand side of Figure 8.1 in black color. The L-edge spectra provide results that is appreciably more surface sensitive, better resolved and better detailed [49] than the P K-edge.

Earlier studies on polyphosphate glasses using XANES using phosphorus L-edge have focused on examining the fine structure of polyphosphate glasses resulted from the spin orbit splitting of the 2p level electrons and the local symmetry of the phosphorus. [49] which generally characterized by there peaks (a),(b) and (c) as show in Figure 8.1. The peaks (a) and (b) at the low energy side are generally separated by about 1eV and are assigned to the transition of spin orbit split 2p electrons between $2p^{3/2}$ (L_3 edge) and $2p^{1/2}$ (L_2 edge). The change in intensity of the doublet (a and b peak) is due to the distortion of the phosphate tetrahedral. [49] The main peak (c) has been attributed to transitions to 3p orbitals, which are sensitive to the presence of other elements such as oxygen and other cations like Fe or Zn. In comparison to the white line (c) peaks of model compounds, zinc phosphate has a slightly lower energy state at 138.7 eV than iron phosphates at 139.0 eV of $FePO_4$ and at 135 eV of unreacted ZDDP. In addition, zinc phosphate has a slightly lower energy pre-edge (a) peak. Two calcium phosphate compounds

were also used for comparison. Comparing the two calcium phosphates, β-TCP has an additional post edge compare to calcium pyrophosphate.

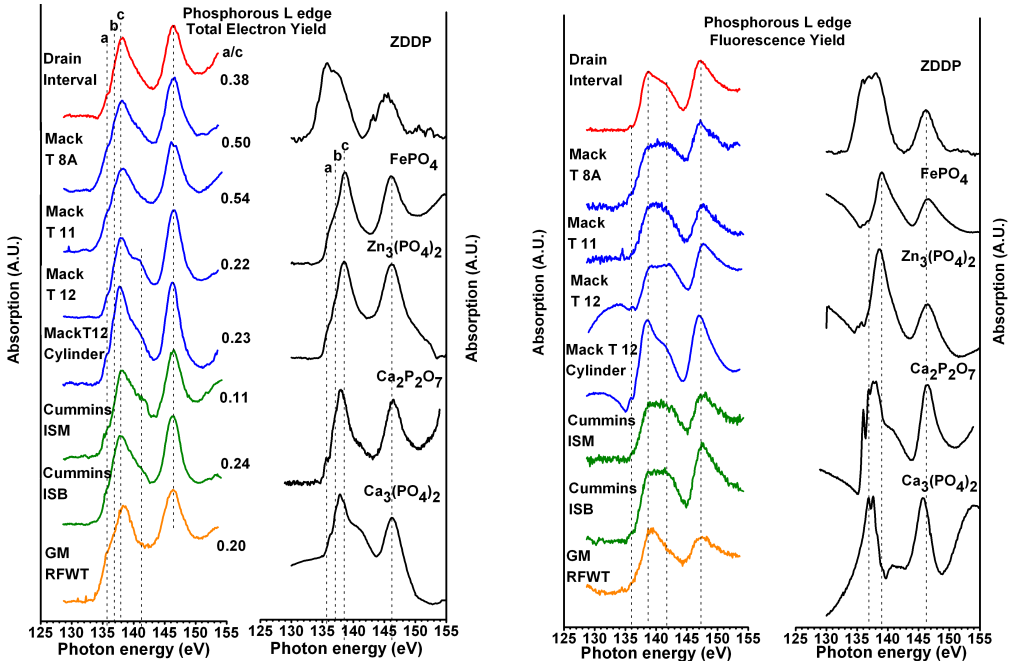

Figure 8.1 Normalized Total Electron Yield (TEY) and Fluorescent Yield (FY) phosphorous L edge spectra of dynamometer crankcase soot and model compounds

Earlier studies have shown that the intensity of peaks (a) and (b) relative to peak (c) has been found to depend on the polyphosphate chain length. [47,103] Yin et al. in their paper [47,48,76-78,104,137-139,152,157] have shown the relative intensities of peak (a) and (b) with respect to peak (c) are sensitive to the number of phosphorus in the linear polyphosphate glasses using various chain lengths of sodium phosphate glasses. In order to obtain accurate peak positions, widths, and intensities, the spectra were fitted to Gaussian function using a least-squares program. These peaks have been subtracted by arctangent base lines to consider the excitonic states that are observed in certain solids. Kim et al have used linear background subtraction instead of act tangent and have shown reported the similar results with linear background subtraction method. [102,143,147] Similar background subtraction methods have been used in this study to deconvolute the spectra. Moreover, deconvolution using linear

background subtraction can distinguish between orthophosphate, pyrophosphate, and short chain polyphosphate, while arctangent background subtraction cannot.

Zhang et al. [102,143,147,148] and Nicholls et al. [148,149]have used the rule for the phosphate chain length: an a/c ratio of about 0.3 is short chain length polyphosphate, and the a/c ratio of about 0.6 indicates a long chain polyphosphate. Since, linear background subtraction was used in this study instead of arctangent function, the results of a/c ratios was changed. In this study, the new standard of chain length of polyphosphate to be suitable for this deconvolution method is used. The a/c ratio below 0.2 means common orthophosphate or pyrophosphate. The value between 0.2 and 0.35 indicates the short chain polyphosphate and the value from 0.35 to 0.55 is the medium chain length of polyphosphate. The polyphosphate with above 0.55 a/c ratios is called as the long chain polyphosphate. [150]

As shown in Figure 8.1, phosphorous L - edge spectra of all soot samples are characteristics of polyphosphate glasses except the soot acquired from Mack T 12 cylinder and crankcase. Drain interval oil was acquired from freightliner diesel engine after 15,000 miles. Assuming the average speed of 40 miles per hours, the engine might have run for approximately 375 hours of field operation. An a/c ratio is 0.38, which is suggestive of presence of medium chain polyphosphate. The white line of drain interval soot closely aligns with zinc phosphate. This suggests that medium chain zinc polyphosphate is present on drain interval soot. Analogous results have been found on the soot from dynamometer tests of T 8A and T 11 with a/c ratio is 0.50 and 0.54 respectively. While Mack T 12 and Cummins ISB soot have a/c ratio 0.23 and 0.24 respectively which is suggestive of short chain polyphosphate. While a/c ratio of soot extracted from Cummins ISM, RFWT and Mack T 12 cylinder are 0.11, 0.199, 0.17 respectively which are suggestive of presence of orthophosphate or pyrophosphate.

It is interesting to note that, Mack T 8A test configuration engine operates in single phase for duration of 150 hours at 1800 rpm and constant load. While Mack T 11 test operates the engine in single phase for 252 hours at 1800 rpm and constant load.

While Mack T - 12 and Cummins ISB operate engine in two phase where first phase is used for excess soot generation and second phase simulate cyclic operation of engine. Drained oil of Mack T 12 experience 200 hours during second phase while drained oil of Cummins ISB experience 250 hours of second phase. It is also worth to note that P L edge spectra of Mach T 12 soot and Cummins ISB soot has post edge at 141 eV which closely aligns to peak of tri-calcium phosphate.

8.3.1.2 Sulfur L edge XANES Spectra Analysis

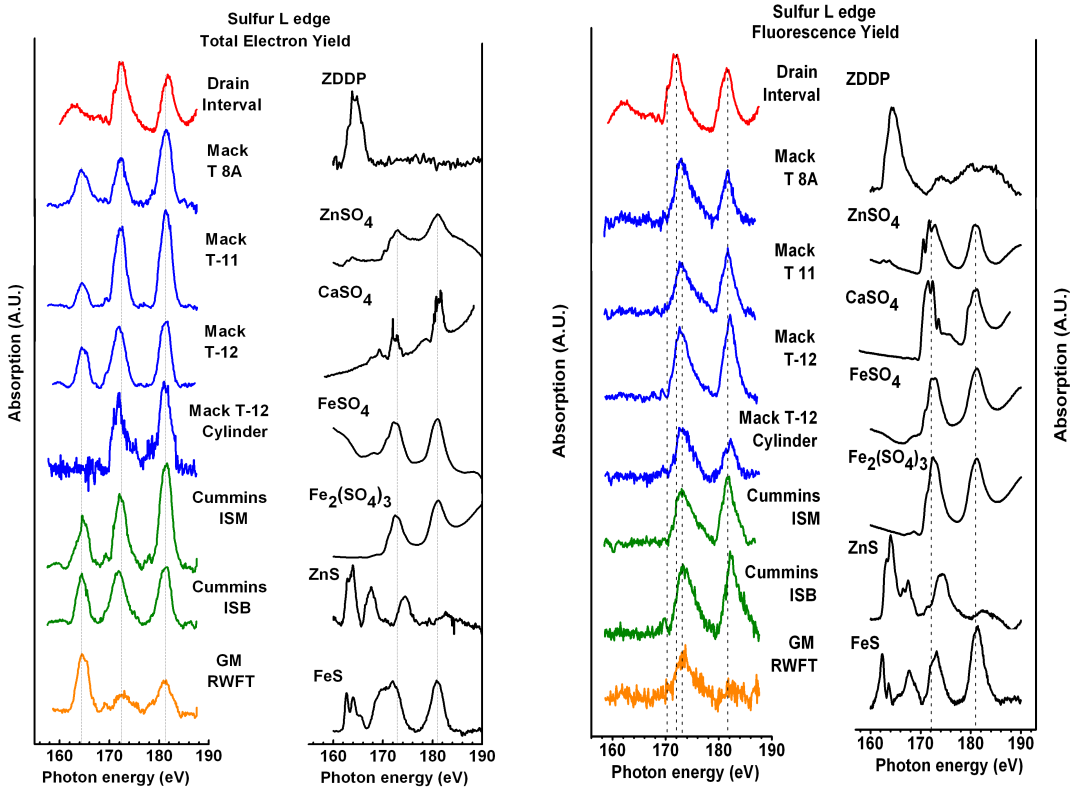

Figure 8.2 Normalized Total Electron Yield (TEY) and Fluorescent Yield (FY) sulfur edge spectra of dynamometer crankcase soot and model compounds

The sulfur L absorption edge spectra of different diesel soot were recorded in TEY and FY mode. These spectra were compared using model compounds of sulfates and sulfides of zinc, calcium and iron as well as unreacted ZDDP as shown in Figure 8.2. All sulfates and sulfides have unique distinctive characteristic absorption spectra except $FeSO_4$ and $Fe_2(SO_4)_3$ which are quite similar. Model compounds of the sulfides have distinctive peaks at lower energy, which

distinguishes sulfides form sulfates. All the diesel soot spectra closely align with the characteristics $ZnSO_4$ and $CaSO_4$ spectra. Moreover, all dynamometer soot samples have an additional absorption edge that closely aligns with the absorption edge of ZnS, which is completely absent in drain interval soot and cylinder soot from Mack T 12 test. Interestingly, in FY mode all soot spectra suggest absence of zinc sulfide.

8.3.1.3 Zinc L edge

The zinc L absorption edge spectrum was recorded in TEY and FLY mode to examine the state of Zn in different soot samples. An earlier study using synchrotron radiation indicates no crystalline phases are present but suggests presence of Zn possibly as amorphous phases due to the different levels of energy absorption on either side of the Zn K-absorption edge [reference]. For the comparison, oxide, sulfate, sulfide and phosphates of zinc were used as model compounds as shown in Figure 8.3.

$ZnSO_4$ and $Zn_3(PO_4)_2$ have distinctive white line energy peak at 1024±1 eV which is absent in ZnS and ZnO. ZnS and ZnO have a broader peak compared to $ZnSO_4$ and $Zn_3(PO_4)_2$. Although the white line peaks of $ZnSO_4$ and $Zn_3(PO_4)_2$ lie close to each other the post edge fine structure of $ZnSO_4$ and $Zn_3(PO_4)_2$ differentiate them. The spectra of drain interval soot closely aligns with $Zn_3(PO_4)_2$. Similar results have also been seen in the dynamometer tests. However, the spectra from Mack T 11 soot is rather noisy due to the low concentration of Zn and hence it is difficult to differentiate between $ZnSO_4$ and $Zn_3(PO_4)_2$ based on the Zn L-edge. And it can be speculated that both compounds are present in the soot. However, further analysis is needed to distinguish these compounds.

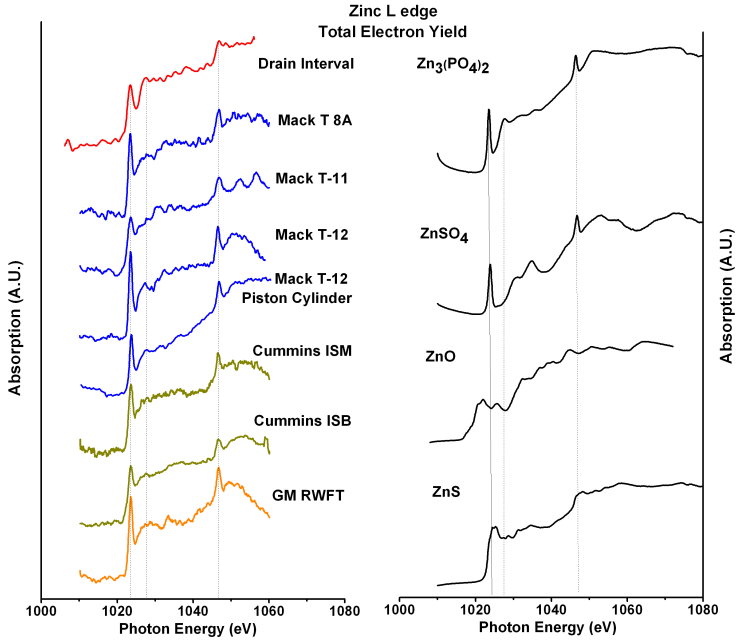

(a)

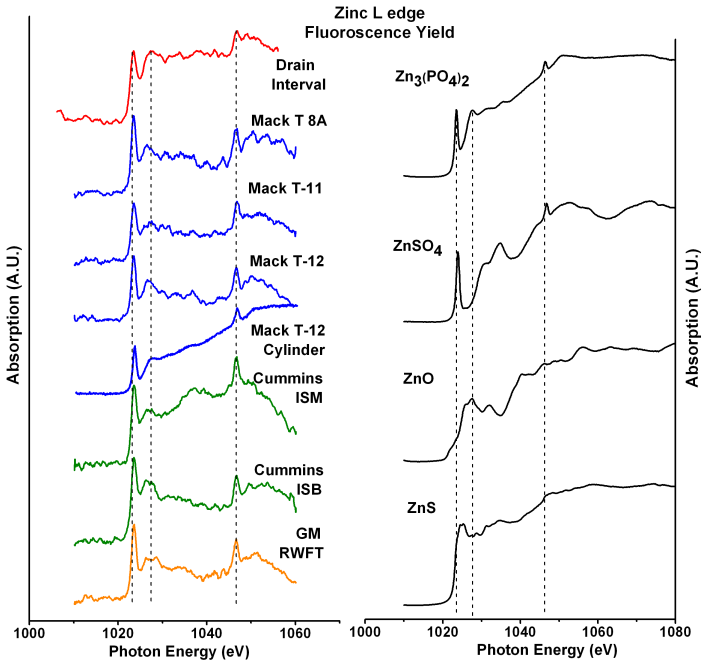

(b)

Figure 8.3 Normalized (a) Total Electron Yield (TEY) and (b) Fluorescent Yield (FY) zinc L edge spectra of dynamometer crankcase soot and model compounds

8.3.1.4 Calcium L edge

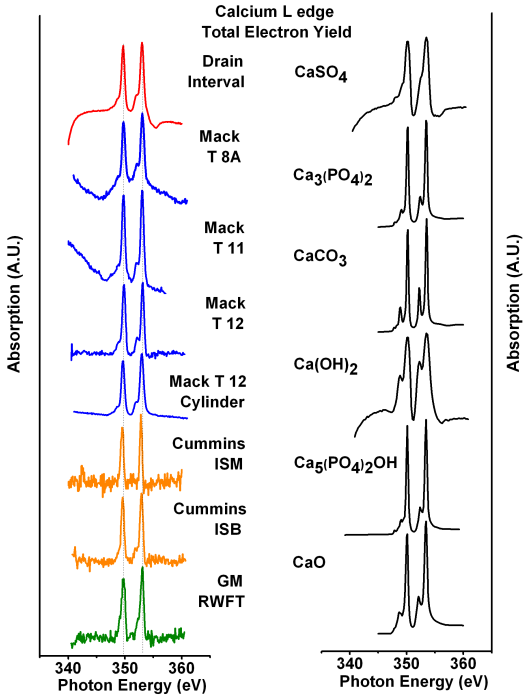

Figure 8.4 Normalized Total Electron Yield (TEY) calcium L edge spectra of dynamometer crankcase soot and model compounds

Ca has an electronic configuration of $2p^6$ $3d^0$ with a high probability of transition of electrons from the 2p to the 3d shells. Earlier studies on calcium L 2,3 edge using density of states and other approaches have taken into account the 2p-3d spin-orbit interactions as well as 3d-3d coulomb and exchange interactions. [98,151] Fine structure of the Ca 2p X-ray-absorption edge for bulk compounds, surfaces, and interfaces. [152] Model compounds of calcium sulfate ($CaSO_4$), calcium hydroxide ($Ca(OH)_2$), calcium phosphate ($Ca_3(PO_4)_2$), calcium carbonate ($CaCO_3$) and hydroxy apatite ($Ca_{10}(PO_4)_6(OH)_2$) were examined. Shown in Figure 8.4 is the calcium absorption edge recorded in TEY mode to elucidate the results acquired from high-resolution x-ray diffraction, synchrotron x-ray diffraction and energy dispersive spectroscopy illustrated in the companion study. [47] The two primary peaks in the spectra located at 350 eV and 353 eV correspond to the L_3 and L_2 absorption edges, [151] The other minor peaks before the L_3 and L_2 edges correspond to various different 2p transitions. Absorption edges of Ca(OH)2

and $Ca_{10}(PO_4)_6(OH)_2$ are slightly lower energy state than $CaSO_4$ and $Ca_3(PO_4)_2$. $Ca_3(PO_4)_2$ has a much more pronounced pre- edges compared to calcium sulfate. The diesel soot spectrum closely resembles the spectra from calcium sulfate and to a lesser extent that of $Ca_3(PO_4)_2$ and $Ca_{10}(PO_4)_6(OH)_2$. Similar results were obtained on the dynamometer soot samples. However, spectra from the dynamometer soot samples are noisy hence difficult to differentiate the pre edge peaks of L_2 and L_3 absorption edge. Further analysis is needed to characterize the calcium compound on soot samples.

8.3.1.5 Phosphorus K edge

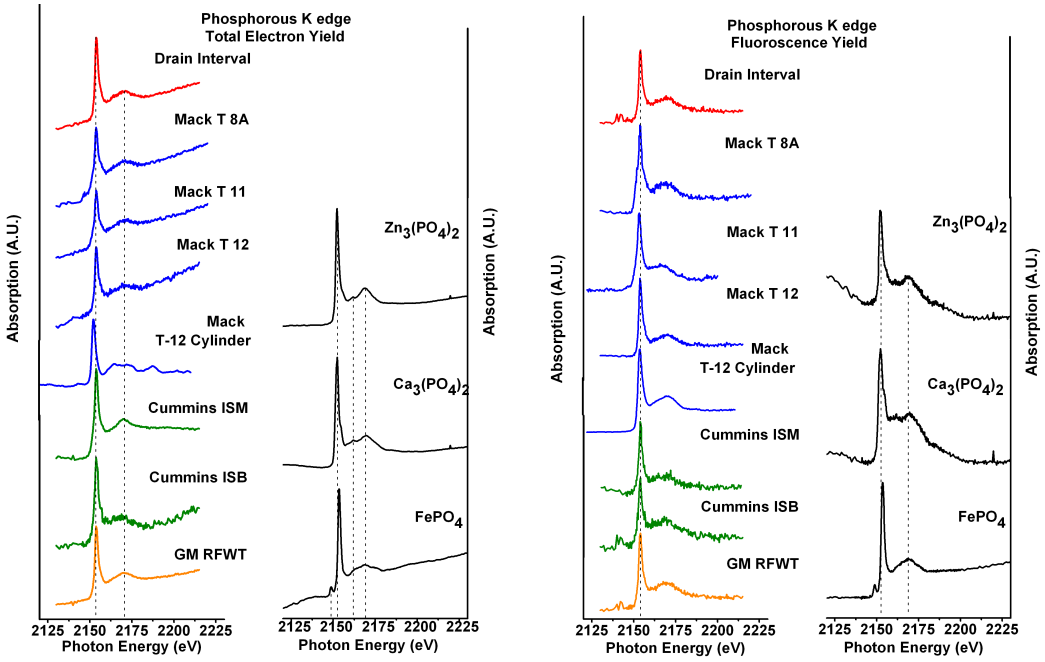

Figure 8.5 Normalized Total Electron Yield (TEY) and Fluorescent Yield (FY) phosphorous K edge spectra of dynamometer crankcase soot and model compounds

The white line for the phosphorous K-edge spectrum arises from transitions of 1s electrons to unoccupied 2p orbitals. Phosphorus K absorption edge of diesel soot was recorded in TEY and FLY mode as shown in Figure 8.5. This spectrum was compared with phosphates of zinc, calcium and iron. $FePO_4$ has distinctive pre edge at 2150eV, which is absent in $Zn_3(PO_4)_2$ and $Ca_3(PO_4)_2$. Also the main peak of $FePO_4$ lies at 2154.5eV, which is higher energy state than $Zn_3(PO_4)_2$ and $Ca_3(PO_4)_2$. In addition a careful examination of the post edge structure indicates

the presence of distinctive shoulder in the case of $Ca_3(PO_4)_2$ which is absent in the case of either the $Zn_3(PO_4)_2$ or $FePO_4$.

ZDDP main peak is observed at 2149.4 eV, while the main peak of zinc phosphate is observed at 2152.0 eV. In ZDDP the phosphorous atom is coordinated with two oxygen atoms while in polyphosphate the phosphorous atom is coordinated with four oxygen atoms. Moreover, higher electro-negativity of oxygen as compared sulfur induces as energy shifts of phosphorous peak in polyphosphate towards higher energy as compared to ZDDP. Hence, The difference in the atom coordination of P in ZDDP and polyphosphate contributes to peak shift due to different photon excitation energy of P K edge of ZDDP and polyphosphate. [108,153,154].

The characteristics K absorption edge of all the soot samples closely aligns with $Zn_3(PO_4)$ in both the TEY and FLY mode. Possibility of $FePO_4$ is not likely due to absence of pre edge in soot spectrum. Phosphorous L absorption edge spectra suggest the presence of zinc phosphate and calcium phosphate, while the K-edge clearly confirms the presence of phosphates of zinc and calcium and absence of any $FePO_4$.

8.3.1.6 Sulfur K edge

The spectrum of sulfur K absorption edge was compared with sulfates of zinc, calcium and iron and with sulfides of zinc and iron as shown in Figure 8.6. Higher energy states of iron sulfate at 2482.3 eV differentiate it from zinc and calcium sulfate. Zinc sulfate and calcium sulfate can be differentiated by the presence of a post edge at 2484.8 eV in the case of $CaSO_4$, which is absent in the case of $ZnSO_4$. The sulfides have their white lines at lower energies than the sulfates with the zinc sulfide having an absorption edge at 2473 eV and a fairly rich post edge structure. FeS has two strong peaks at 2471 eV and 2482 eV.

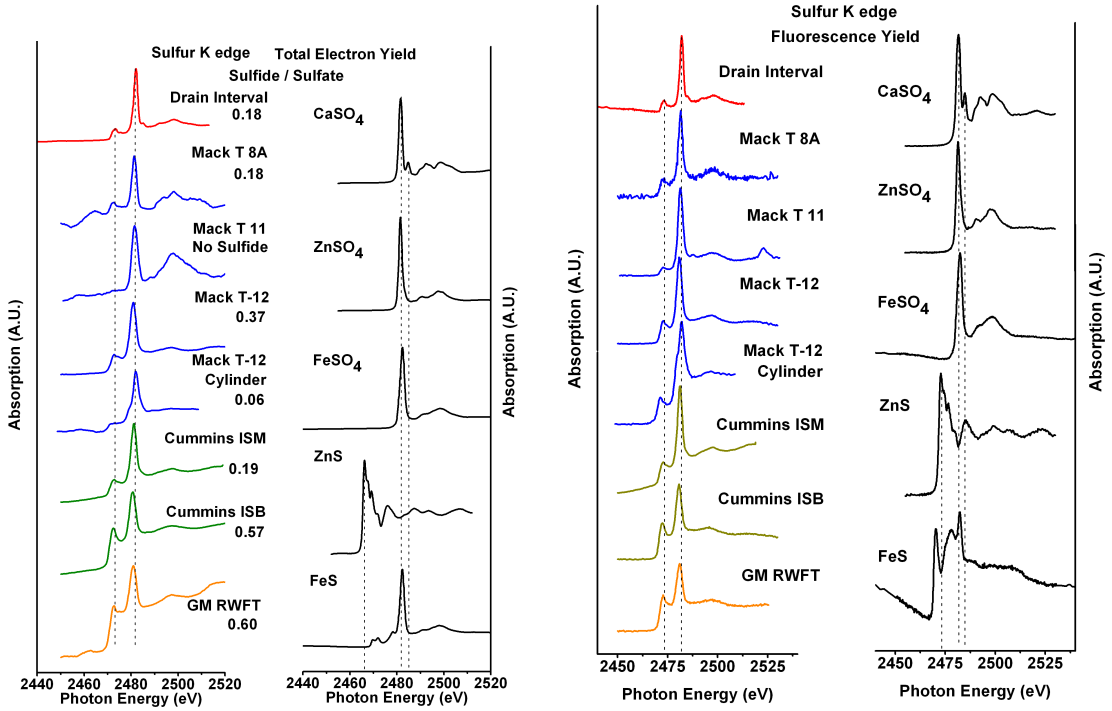

Figure 8.6 Normalized Total Electron Yield (TEY) and Fluorescent Yield (FY) sulfur K edge spectra of dynamometer crankcase soot and model compounds

A careful examination of the spectra of drain interval diesel soot (both TEY and FY) indicates that in addition to the sharp absorption edge at 2481.2 eV that is common to both $ZnSO_4$ and $CaSO_4$ there is a post edge at 2484.8 eV that is only present in $CaSO_4$. This post absorption edge is only present in the drain interval diesel soot while It is completely absent in the other dynamometer engine test soot. Spectra of drain interval diesel soot indicate the presence of an additional peak at 2472 eV that likely arises from ZnS as a minor constituent of soot. Similar results have been recorded for the other dynamometer engine test soot. The L-edge spectra of sulfur clearly suggest the presence of sulfates in the drain interval diesel soot, the K-edge spectra is able to distinguish between the cationic species most likely present in the soot. In addition, the higher flux of photons in the K-edge spectra helps in identifying the presence of ZnS in soot as well. In addition, it is important to note the absence of $FeSO_4$ in soot which collaborates the evidence seen in Fe L-edge spectra and the EDS spectra as well. Similarly, L edge spectra of

dynamometer engine test soot indicate presence of sulfide peak, which is validated from the K edge spectra.

Quantification of the sulfur compound was done by deconvoltuing the sulfur K edge spectra. The relative amount of sulfide and sulfate compound was analyzed by calculation height ratio of sulfide to sulfate peak. As shown in the figure, relative amount of sulfide is varying among the different soot samples. Soot samples of Cummins ISM, Mack T 8 A have relative amount of sulfide with respect to sulfate are 0.18 and 0.19 which is close to realistic field conditions of drain interval soot. While, soot extracted from Cummins ISB and GM RFWT have significantly more sulfide present with respect to sulfate. Moreover, Mack T 12 engine crankcase soot have relative sulfide amount 0.39 with respect to sulfate while very small amount of sulfide was present Mack T 12 piston cylinder soot. Interestingly, Mack T 11 engine crankcase soot has no sulfide formation.

8.3.1.7 Calcium K edge

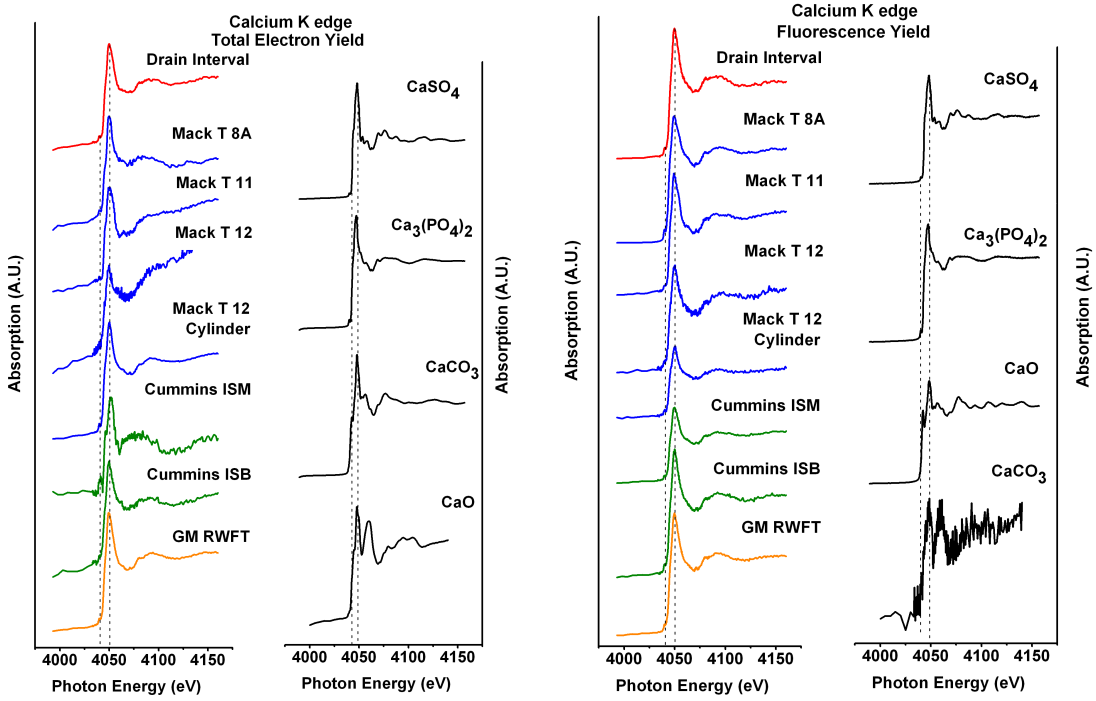

Figure 8.7 Normalized Total Electron Yield (TEY) and Fluorescent Yield (FY) calcium K edge spectra of dynamometer crankcase soot and model compounds

Calcium K absorption edge was recorded in TEY and FLY mode for all soot samples and model compounds, as shown in Figure 8.7. Calcium sulfate, CaO and $Ca_3(PO_4)_2$ were used for comparison. The white line for calcium sulfate, CaO and $Ca_3(PO_4)_2$ lies at 4050 eV, 4049.8 eV and 4049. 4 eV. CaO has a distinguishing pre edge at 4043 eV, which is absent in the other Ca compounds. Calcium sulfate has more defined fine structure compared to $Ca_3(PO_4)_2$. Comparison of the soot spectra and model compounds spectra clearly indicates that the spectra appears to be close to both calcium sulfate and $Ca_3(PO_4)_2$ and the absence of CaO. The P K-edge spectra indicates that the phosphates were most likely Zn based and not Ca based, and the S K-edge spectra also indicated that the presence of $CaSO_4$ and lesser extent the presence of $ZnSO_4$. It is safe to come to the conclusion that Ca largely exists as $CaSO_4$ and possibly to a smaller extent as the $Ca_3(PO_4)_2$.

Dynamometer test crankcase soot also exhibit similar characteristic absorption edge matches with calcium sulfate or $Ca_3(PO_4)_2$. Mack T - 12, Cummins ISB and Cummins ISM soot spectra are noisy which might indicate the lesser amount of calcium compound on the soot structure.

8.3.2 Synchrotron X-Ray Diffraction

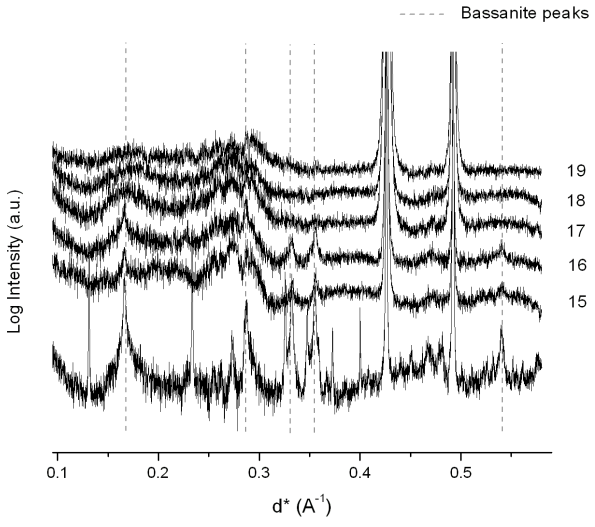

Figure 8.8 Synchrotron X-ray Diffraction of dynamometer crankcase soot

Synchrotron x-ray diffraction was conducted to characterize the compositional information of the different diesel soot samples. Figure 8.7 shows SR XRD patterns of Diesel-soot samples acquired at 9.4 keV. The measurement conditions have already described in the chapter 3. Similar approach has been used to analyze the soot samples.

The dotted line in the figure corresponds to Bassanite peaks. These peaks are present in the drain interval crank case soot. Similar peak was also present in the soot sample extracted from T 8A and T 11 engine crankcase oil. Peak intensity of the bassanite peak of drain interval soot is higher than T 8 A and T 11 soot. On the contrary, bassanite peak was completely absent in Cummins ISB, Cummins ISM and Mack T 12 soot. Presence of very broad peak at the first position of the bassanite peak indicate the possibilities of nano-crystalline phase of bassanite present on the Cummins ISB, Cummins ISM and Mack T 12 soot samples. A GM RFWT spectrum is not available for the analysis.

8.3.3 Tribofilm analysis of Engine Parts

8.3.3.1 Phosphorous L edge

Corresponding phosphorus L edge spectra of tribofilm of engine components from Cummins ISM and GM RFWT are shown in figure in TEY and FY mode along with their model compounds. P-L edge spectra can provide surface sensitive information than P K edge. P L edge spectra in TEY and FY modes, this allowing for surface (~ 5 nm) and bulk (~ 50 nm) analyses of the tribofilm. The white line of tribofilms from Cummins ISM components (spectra A and B) closely aligns with zinc phosphates. P- L edge spectra Zinc sulfate ($Zn_3(PO_4)_2$) and calcium phosphate ($Ca_3(PO_4)_2$) can be easily distinguished by post edge of calcium phosphate ($Ca_3(PO_4)_2$) at 141.5 eV. Absence of distinguish peak of calcium phosphate ($Ca_3(PO_4)_2$) at 141.5 eV in tribofilm spectra (A,B and C) indicate the zinc phosphate ($Zn_3(PO_4)_2$) is most likely to constitute the tribofilm of engine components, iron (III) phosphates ($FePO_4$) is unlikely.

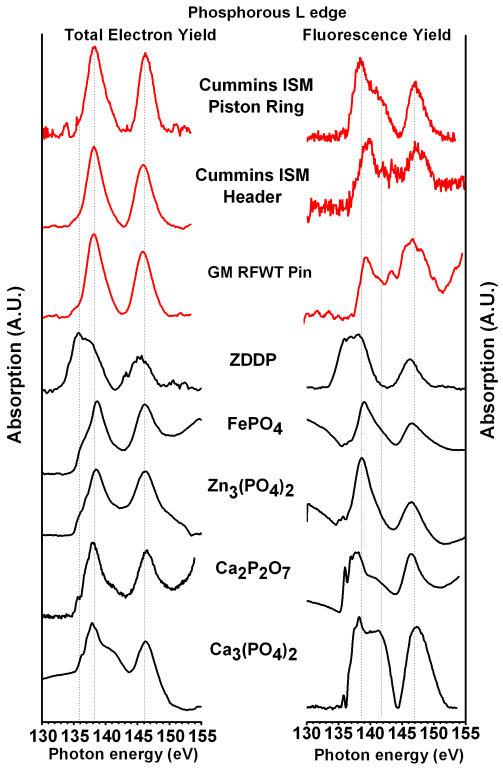

Figure 8.9 Normalized Total Electron Yield (TEY) and Fluorescent Yield (FY) phosphorous L edge spectra of engine components of Cummins ISM and GM RFWT and model compounds

8.3.3.2 Sulfur L edge spectra

The corresponding S L-edge XANES spectra of tribofilm A, B and C were also examined and are shown in figure along with model compounds model compounds; unreacted ZDDP, $ZnSO_4$, $CaSO_4$, $Fe_2(SO_4)_3$, $FeSO_4$, FeS and ZnS. The collected S L-edge signal for all tribofilms are weak in intensity, thus the peaks observed in all cases are very small and only visible after baseline subtraction. For all tribofilms, the location of the peak at around 173 eV in the TEY spectra (Fig. 8.10) is indicative of the presence of zinc sulfate ($Zn_3(SO_4)_2$) in the surface region of the tribofilms. However, peak intensity of Cummins ISM piston ring and header are higher than the intensity of GM RFWT pin spectra, which indicate the higher amount of sulfate present in tribofilm of Cummins ISM engine components.

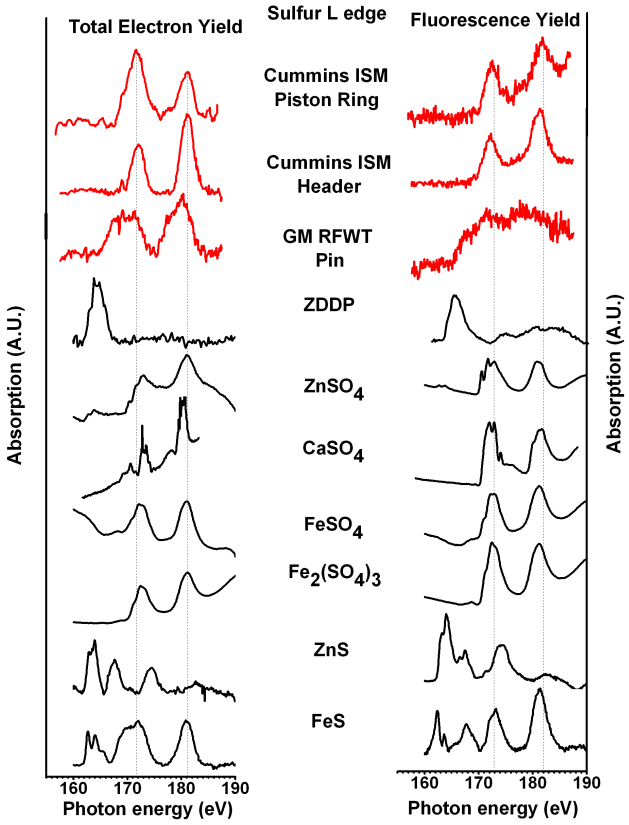

Figure 8.10 Normalized Total Electron Yield (TEY) and Fluorescent Yield (FY) sulfur L edge spectra of engine components of Cummins ISM and GM RFWT and model compounds

8.3.3.3 Calcium L edge

A corresponding calcium L edge spectrum of tribofilm of engine components are shown in figure along with model compounds. The two primary peaks in the spectra located at 350 eV and 353 eV correspond to the L_3 and L_2 absorption edges [Fleet et. Al. American Mineralogist], The other minor peaks before the L_3 and L_2 edges correspond to various different 2p transitions. Absorption edges of $Ca(OH)_2$ and $Ca_{10}(PO_4)_6(OH)_2$ are slightly lower energy state than $CaSO_4$ and $Ca_3(PO_4)_2$. $Ca_3(PO_4)_2$ has a much more pronounced pre-edges compare to calcium sulfate. The tribofilm of piston ring of Cummins ISM spectrum closely resemble the spectra to calcium phosphate ($Ca_3(PO_4)_2$) and apatite ($Ca_{10}(PO_4)_6(OH)_2$). While, the Cummins header spectra is noisy hence making it difficult to identify the spectra. It closely resembles the spectra from calcium sulfate and to a lesser extent that of $Ca_3(PO_4)_2$ and $Ca_{10}(PO_4)_6(OH)_2$. On the other hand,

spectrum Ca of GM RFWT tribofilm matches with calcium phosphate ($Ca_3(PO_4)_2$) and apatite ($Ca_{10}(PO_4)_6(OH)_2$) and to lesser extent calcium sulfate ($CaSO_4$). These results substantiate the results obtained in the calcium K edge XANES spectra to be discussed later.

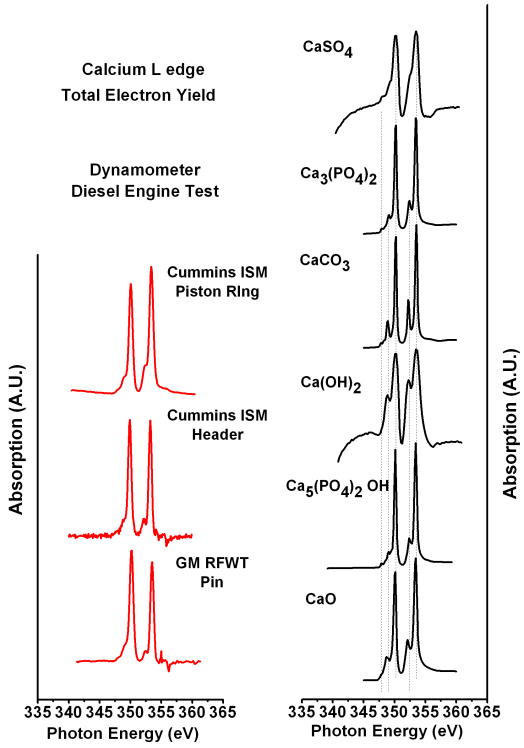

Figure 8.11 Normalized Total Electron Yield (TEY) calcium L edge spectra of engine components of Cummins ISM and GM RFWT and model compounds

8.3.3.4 Zinc L edge

Fig. 8.12 shows the TEY and FY zinc L-edge spectra of the model compounds $Zn_3(PO_4)_2$, ZnO, ZnS and $ZnSO_4$ together with spectra from tribofilms of engine components of Cummins ISM and GM RFWT engine test. The model compounds show some distinctive differences making it possible to distinguish between the different chemistries. Both $Zn_3(PO_4)_2$ and $ZnSO_4$ exhibit sharp edges at 1023 eV while the edges associated with ZnO and ZnS, are made up of multiple peaks and the location of the white line is shifted to 1025 eV. The spectra from Zn in TEY tribofilms are weak as evident by the low signal to noise ratio of the spectra. From the TEY spectra (Fig.8. 12) it is clearly evident that both $Zn_3(PO_4)_2$ and $ZnSO_4$ are likely to be present in

the Cummins ISM engine test piston ring and header tribofilm since the spectra of tribofilms exhibits a peak at around 1028 eV. The location of the white line for engine components tribofilms matches that of $Zn_3(PO_4)_2$ and $ZnSO_4$ indicating the presence of both in the ZDDP tribofilm.

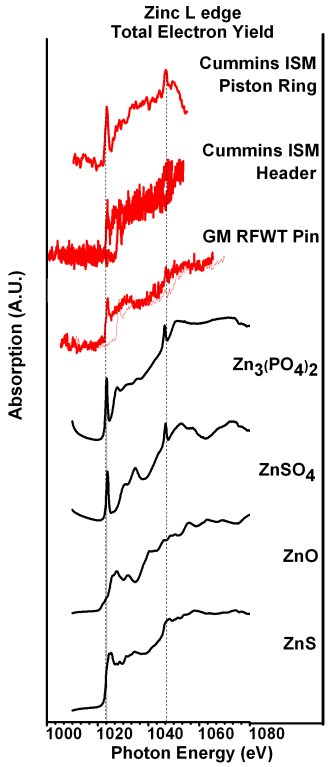

Figure 8.12 Normalized Total Electron Yield (TEY) and Fluorescent Yield (FY) zinc L edge spectra of engine components of Cummins ISM and GM RFWT and model compounds

8.3.3.5 Iron L edge

The TEY iron L-edge spectra of the model compounds Fe_2O_3, FeS, $FePO_4$, $FeSO_4$ as well as of the tribofilms formed on Cummins ISM piston ring, Cummins ISM header and GM RFWT pin are shown in Fig. 20. The Fe L-edge has the white line at approximately 710.75 eV and a pre-edge at approximately 709eV. The relative intensity of the pre-edge strongly depends on chemistry. $FePO_4$ has the smallest pre-edge while $FeSO_4$ has a pre-edge that has a higher intensity than the white line. The TEY spectra of the tribofilms from all Cummins ISM piston ring and header do not show distinctive differences. Both tribofilms have pre-edge peaks that are less intense than the white line indicating that the primary form of Fe is in the form of Fe_2O_3, $Fe_2(SO_4)_2$

and/or FeS, The FY spectra of the tribofilms turned out to be more diffuse with two broad peaks that cover the entire range for phosphates, sulfates and sulfides and did not yield distinguishable information and are not shown here.

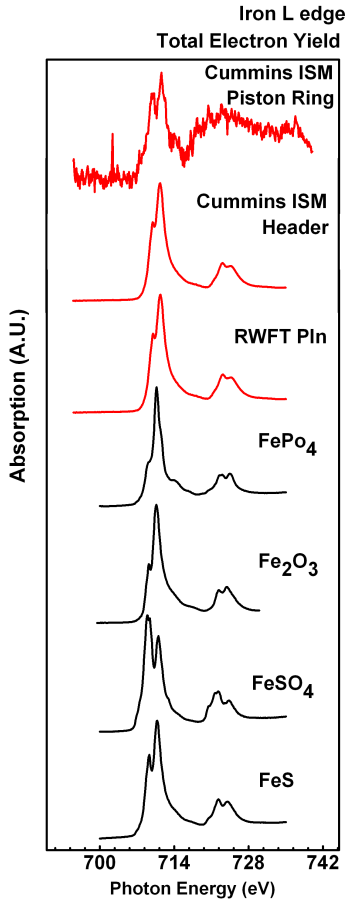

Figure 8.13 Normalized Total Electron Yield (TEY) and Fluorescent Yield (FY) iron L edge spectra of engine components of Cummins ISM and GM RFWT and model compounds

8.3.3.6 Phosphorous K edge

Phosphorus K-edge XANES spectra collected in TEY and FY mode for both tribofilms generated on engine components as well as the selected model compounds are plotted in Fig. 11. Spectrum A and B refers to tribofilm generated on piston ring and header of Cummins ISM engine test respectively. Spectrum C refers to tribofilm generated on the roller follower pin of GM RFWT engine test. The single intense peak in each spectrum is characteristic of phosphorus K-edge that is attributed to the transition of a phosphorus 1s electron to an empty p-like anti-

bonding state. [154] The dotted lines in both figures show the location of the main P K-edge peak for the tribofilms. It is observed that in both TEY and FY modes, the location of the main peak of tribofilm of all engine components is closely aligns with zinc phosphate and calcium phosphate. However, spectra A, B and C have absence of pre edge at ~ 2149eV that is present in iron (III) phosphate. However, The relative location of the dotted lines in comparison to the main peak for each of the model compounds indicates that while zinc phosphate ($Zn_3(PO_4)_2$ and calcium phosphate ($Ca_3(PO_4)_2$) are most likely to constitute the tribofilm of engine components, iron (III) phosphates ($FePO_4$) is unlikely.

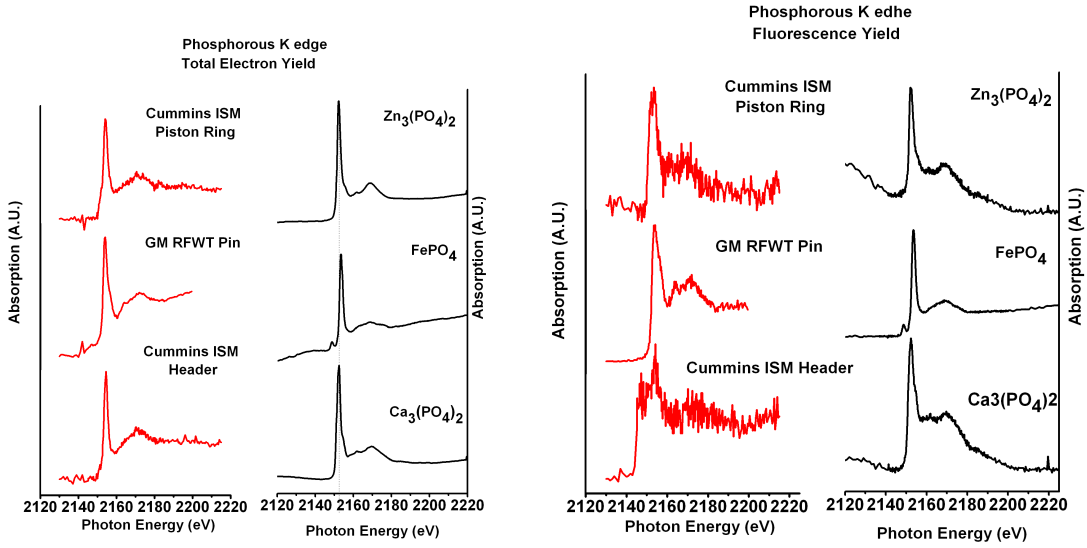

Figure 8.14 Normalized Total Electron Yield (TEY) and Fluorescent Yield (FY) phosphorous K edge spectra of engine components of Cummins ISM and GM RFWT and model compounds

However, the spectrum (A and B) of piston ring and header of Cummins ISM and spectrum (c) of GM RFWT are quite similar to spectrum of $Zn_3(PO_4)_2$ and $Ca_3(PO_4)_2$ making it likely that calcium is incorporated into the tribofilm. Earlier studies have [73,96]indicated that when detergent is blended with either DTP additive, calcium phosphate has formed and has become incorporated into the film. Kasrai and coworker have reported the exchange of Fe for Ca in the AW film on the surface. They reported that the ΔH^0 formation for these substances. The ΔH^0 values for $FePO_4$ and $Ca_3(PO_4)_2$ are -1297 kJ and -4120 kJ $molK^{-1}$, respectively. Thus, it is obvious that under similar conditions, formation of $Ca_3(PO_4)_2$ is preferred to $FePO_4$. However, the

ΔH^0 value for $Ca_3(PO_4)_2$ is -3884 kJ $molK^{-1}$, a change of 236 kJ $molK^{-1}$ from the ΔH^0 value. A number of studies [reference] have showed that when ZDDP has been combined with calcium detergents, replacement of Zn for Ca in the AW film occurs where the - ΔH^0 for zinc phosphate is much lower than that of calcium phosphate [108].

8.3.3.7 Sulfur K edge spectra

S K edge TEY spectra of tribofilm of piston ring from Cummins ISM (spectrum A), header from Cummins ISM (spectrum B) and pin from GM RFWT (Spectrum C) are shown in figure along with the model compounds. Intense white line of all tribofilm spectra (A, B and C) closely align with zinc sulfate ($ZnSO_4$), indicate that the tribofilm is most like to be constitutes of zinc sulfate. In addition, Cummins ISM engine components spectra (A and B) as well as GM RFWT pin (spectrum C) have additional pre edge closely aligns with zinc sulfide (ZnS) in small amount. Sulfur signal in FY mode is weak and hence not reported.

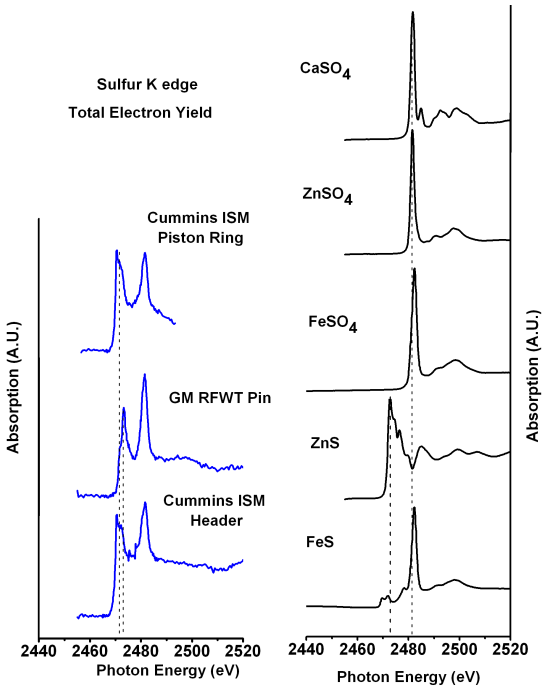

Figure 8.15 Normalized Total Electron Yield (TEY) and Fluorescent Yield (FY) sulfur K edge spectra of engine components of Cummins ISM and GM RFWT and model compounds

8.3.3.8 Calcium K edge

Calcium K edge TEY spectra of tribofilm of engine components of Cummins ISM and GM RFWT are show in figure along with model compounds. Sulfate, phosphate, oxide and carbonate of calcium have used as model compounds. Calcium oxide (CaO) and calcium carbonate ($CaCO_3$) have distinguishable spectral features as compare to calcium sulfate ($CaSO_4$) and calcium phosphate ($Ca_3(PO_4)_2$). However, post edge perturbation of calcium sulfate ($CaSO_4$) and calcium phosphate ($Ca_3(PO_4)_2$) distinguish them. Comparison of model compounds with tribofilm of dynamometer engine test indicate the close match of main white line of tribofilm with calcium sulfate ($CaSO_4$) and calcium phosphate ($Ca_3(PO_4)_2$). However, post edge spectral feature of tribofilm spectra (A, B and C) is broad, making is difficult to analyze if tribofilm is formed by calcium sulfate ($CaSO_4$) or calcium phosphate ($Ca_3(PO_4)_2$).

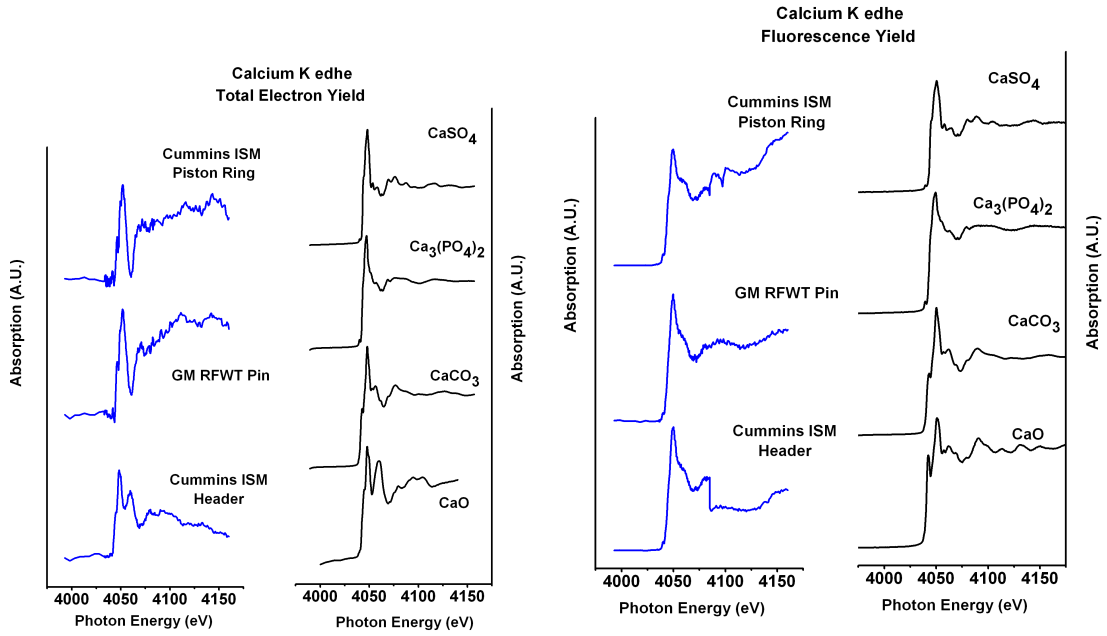

Figure 8.16 Normalized Total Electron Yield (TEY) and Fluorescent Yield (FY) calcium K edge spectra of engine components of Cummins ISM and GM RFWT and model compounds

8.3.4 SEM analysis of tribofilm

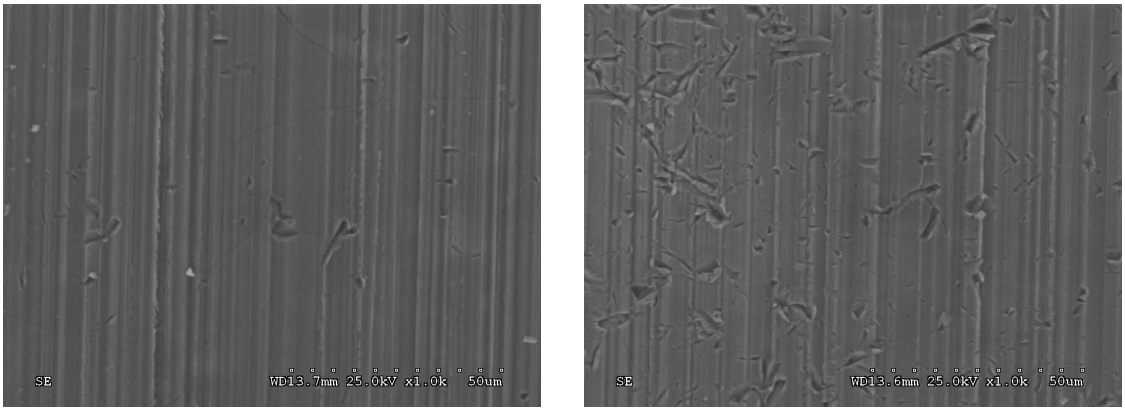

Figure 8.17 SEM micrographs of tribofilm of piston ring and header of Cummins ISM and GM RFWT pin

Scanning electron micrograph of the wear tracks are shown in figure for the Cummins ISM piston ring and header. The wear track in the case of piston ring exhibits scratches and patches of tribofilm in the direction of sliding motion and several locations where there is pullout and breakdown of the film which indicate the abrasive wear is predominant mechanism. SEM micrograph of tribofilm of Cummins header exhibit patchy region and does not cover entire region of contact. This indicates that the actual engine conditions are generally more severe than the laboratory tests which generally show well defined tribofilm which cover large areas of the wear track [reference include Kasrai work and our work as well]

8.4 Discussion

Mack T-8 and Mack T-11 engine test were developed to evaluate the viscosity increase due to soot for the API CG-4 and API CI-4 plus category respectively with different allowable limits of emission of NOx. Target value of soot weight % in T 8A at 150 hours is 2.4-3.4 weight% while T-11 target range is 4.8 to 5.8 weight%. [137-139,158] Higher soot target level of T-11 test indicates the severity of test to evaluate the lubricants performance to handle higher soot level. Higher soot level is associated with higher wear and viscosity increase of oil which can be controlled by selection of proper dispersant in the engine oil formulation. [102,143,147] Studies done by Bardasz et al. [67,83,106,134,145,146,159] have reported that oil thickening was not

caused by oxidation but was caused by the amount of soot present and/or soot particle agglomeration. However, oil gallery temperature of Mack T-8 and T-11 is 103°C and 88°C respectively. [67,83,106,134,145,146,159] Our previous studies, have reported the effect of oxidation treatment on the chemistry of carbon black. Mineral oil with antiwear formulation blended with 3 weight % carbon black was oxidized in air for 120°C for 100 hours. The oxidation forced the interaction between lubrication additives chemistries and carbon black resulted in the chemisorption of lubrication decomposition chemistries such as zinc sulfate, zinc sulfide onto carbon black. In the present studies, XANES spectra of extracted soot from Mack T 8A and T 11 indicate the presence of zinc sulfate, zinc sulfide and calcium sulfate on the soot structure. This indicates the role of oxidative environment in modifying the chemical make up of soot. Presence of the lubricants additives decomposition chemistries may play an important role to promote wear of engine components. It may be important to note here that from our other paper we have shown that treatment of carbon black by milling and baking makes it more abrasive and it that case we are incorporating decomposition products into the soot. Hence it is not a stretch to extent the argument to say that in this case if the soot is chemically modified it may be responsible for increased wear.

Mack T-11 uses low swirl combustion and cooled EGR that changes the soot quality. [5] In addition to the different engine design, Mack T-8A and T-11 run with different operational parameters. Mack T-8A is an abbreviated version of T-8 test, developed to establish to provide lubricant performance equivalency to the Mack T-7 and T-8 tests with limits of 150 hours duration while T-11 is more extended duration test that run for 252 hours. Shank et al have summarized the effect of Mack engine lubricants test on changes on engine design, on crankcase lubricants and changes in lubrication formulation. [11,12,38,160] Mack T-8 A use higher injection pressure which increase soot loading crankcase lubricants and hence required increased dispersancy. Mack T-11uses low swirl combustion that changes soot quality. [12,161] Moreover, M-11 also uses cooled EGR hence requires better dispersancy and effective anti oxidants. Moreover, with stringent pollution norms, T-11 test represent severe condition for lubricants to qualify. The

lubricants that were used for the test also have different amount of phosphorus lever as indicates in table 8.6. However, similar results have been recorded by analysis of different L and K absorption edges P, S, Ca and Zn of soot extracted from Mack T 8A and Mack T-11 regardless of engine configuration and operational parameters. XANES results indicate the presence of phosphates of zinc and calcium. Height ratio of peak a / peak c indicates the presence of medium chain polyphosphates.

For the API CH-4 heavy-duty diesel lubricant specification in 1998, soot-related engine wear was assessed using the Cummins M11 HST (high soot test). [5] Kuo et al have studied the wear mechanism of Cummins M-11 diesel engine test. They reported the abrasive wear by primary soot particles is the key wear mechanism in the Cummins M-11 high soot diesel engine. [5]Such abrasive wear can be prevented by the oil, which forms a sufficient film thickness. In the soot abrasive process, carbide particles, graphite nodules and other wear debris will be abraded off of the crosshead and rocker arm surfaces. These particles will further accelerate the abrasive wear process. In addition, to abrasive wear, fatigue wear was evident as cracking and micro spalling on the engine parts. Oil film thickness was determined to be critical factors in preventing M-11 wear. Li et al have used Cummins M-11 engine to evaluate the lubricants for PC-9 category and reported the abrasive wear on the crossheads and rocker arms. He also reported that the soot provides the major contribution to abrasive wear, since scar closely match the primary soot particle sizes. In addition to that, soot produced by the M-11 EGR was found to be harder than the engine parts.[5,49]

As EGR effects were introduced into the API CI-4 category in 2002, the Cummins M11 HST engine test was upgraded to the M11 EGR engine test. For API CJ-4 in 2007, the Cummins ISM test has replaced the M11 EGR, and the Cummins ISB test has been added to measure soot-related wear in a cam follower contact. [5]

In the present studies, XANES analysis of crankcase soot extracted from the Cummins ISM and ISB indicate the presence of zinc sulfate, zinc sulfide, calcium sulfate and calcium phosphate. In addition, the phosphate that is present on the Cummins ISM and ISB is small chain

polyphosphate. These chemistries indicate the interaction of decomposition products of lubricants additives chemistries and crankcase soot during engine operation. In addition to that, Li et al have employed electron energy loss spectroscopy (EELS) to study the relative hardness of soot and have reported that soot produced by the M-11 EGR was found to be harder than the engine parts. [49,162] In addition, usage cooled EGR in 2007 engine tests increases the temperature of crankcase soot which forces the oxidation of oil and increases the possibility of interaction between decomposition products of additives and crankcase soot. Usages of XANES in the present study have provided high spatial surface sensitive information. Presence of decomposition products of lubricants additives chemistries alters the surface of primary soot particles.

Study of piston ring as counter parts of Cummins ISM indicate the abrasive wear track in the direction of sliding. In addition, zinc sulfate, zinc phosphate and calcium phosphate are main constituents of tribofilm formed on the piston ring and header while zinc sulfide and calcium sulfate are minor contributors. Similar XANES results of piston ring, header and crankcase soot indicate the interaction of tribofilm with soot primary particles during three body wear action. Harder particles of soot as suggested by the Li et al and presence of various sulfate and phosphate chemistries of decomposition products of additives on the soot surface might induce abrasive wear tracks on the piston ring and header. [9]

In addition, similar results have been observed with GM RFWT test where various decomposition products of lubricants additives chemistries are present on the surface of extracted crankcase soot. Similar results have been observed on the counter parts of RFWT.

In the present study, the extracted crankcase soot from various dynamometer tests have experienced different environments during their operation. These dynamometer tests were designed with different operational parameters in mind where load, rpm, oil gallery temperature, fuel, lubricants additives chemistry, etc. were suitably changed. These parameters might influences the structure and chemical make up of diesel soot. However, high spatial surface sensitive results using XANES have provided detailed insight of the surface chemical make up

and indicated the interaction of additives chemistries and diesel soot particles regardless of operational parameters of diesel engine.

Analysis of counter parts of Cummins ISM also indicates that the tribofilm formed on the piston ring and header have abrasive wear track in the direction of motion. In addition, zinc sulfate, zinc phosphate and calcium phosphate are main constituents of tribofilm formed on the piston ring and header while zinc sulfide and calcium sulfate are minor contributors.

8.5 Conclusions

Soot extracted from the crankcase oil of the different dynamometer engine tests that include Mack T 8A, Mack T 11, Mack T 12, Cummins ISM, Cummins ISB, GM RFWT. It was infeasible to separate out the effect of the individual engines' operational parameters on the composition of crankcase soot. However, XANES have been used to probe the chemical make up of the extracted soot from the different dynamometer tests subjected to different operational conditions. In addition, piston ring from Cummins ISM, header from Cummins ISM and pin from GM RFWT were used to understand influence of crankcase soot on the film formation.

(i) Phosphorous analysis using L and K edge indicated the presence of phosphate of zinc and calcium with different chain length depending on the test conditions and chemistries of lubricants.

(ii) Sulfur analysis using XANES indicate the presence of sulfides on the soot samples in varying amount.

(iii) It was difficult to differentiate the presence of zinc sulfate and zinc phosphate on the soot samples using zinc L edge due to noisy spectra.

(iv) SEM micrograph of the piston ring and header revealed the abrasive wear track in the sliding direction indicative of three body wear action between piston ring cylinder with trapped soot particles.

CHAPTER 9

COMPARATIVE NEXAFS STUDY OF DIESEL SOOT OBTAINED FROM CRANKCASE OIL OF FIELD AND DYANOMETER DIESEL ENGINE

9.1 Introduction

Formation of soot is inherent in the operation of compression ignition engines. The models that describe the formation of soot involve nine generic steps, i.e., fuel pyrolysis, precursor species (including acetylene) formation and oxidation, soot particle inception, particle coagulation, surface growth and oxidation. [53] Soot formation has been found to be strongly dependent on air entrainment in the lifted portion of the jet as well as by oxygen in the fuel and to a lesser extent the composition and structure of hydrocarbons in the fuel. [86] Characterization of the carbonaceous structure of the exhaust soot that obtained from various diesel engines is well documented. [53] However, study on the crankcase diesel soot is yet to understand thoroughly.

Diesel soot present in crankcase oil is considered as one the main cause of lubrication oil deterioration and to promote higher wear of engine components.[53] [reference]. In our previous studies, the structure and chemistry of crack case diesel soot has been characterized using x-ray absorption near edge structure (XANES), high-resolution transmission electron microscope (HRTEM), synchrotron x-ray diffraction and raman spectroscopy. Significant similarities have been observed in the chemical make of crank case diesel soot extracted from the used diesel engine oil acquired during drain interval as well as from diesel engine dynamometer tests. Usage of the high-resolution spectroscopy and microscopy has revealed the presence of various chemistries present on the soot structure. These chemistries have originated from tribofilm as well as from lubrication additives decomposition products. Our previous studies using high resolution TEM have revealed that nano crystalline particles of apatite, carbonate hydroxylapatite and iron oxides are mechanically embedded on soot surface.

The present work is focused on apprehending the surface chemical structure of crankcase soot. Carbon Near Edge X-ray Absorption Fine Structure (NEXAFS) spectroscopy is presented as an analytical technique for the carbon specific characterization of various soot samples extracted from different crankcase used diesel engine oil from different diesel engine dynamometer tests.[44] Various diesel soot, carbon black NEXAFS spectra are studies in relation to graphite as reference materials. NEXAFS characteristic resonance spectra furnish useful information on the molecular speciation of the graphite like solid core in soot, various surface functional groups as well as various aromatic and aliphatic components present in the soot depending on the origin of soot from different diesel engines.[42] NEXAFS offer higher surface sensitivity along with no radiation damage to characterize the surface of various soot samples and there by provide valuable information on surface reactivity of crankcase soot.[17,71,163] In addition, raman spectroscopy have employed to acquired extremely useful information about the small range crystalline structure of different crankcase soot. More information about the raman spectroscopy can be found elsewhere. [2,10,13,15,23,28,32,37,41,53,58,59,87,88,141]

9.2 Experimental Technique

Crankcase soot samples have been extracted from crankcase oils. Diesel soot extracted from commercially operated diesel engine oil during the drain interval represents realistic conditions in which diesel engine operates on highways. While other soot have been acquired from laboratory dynamometer diesel engine tests. These tests include Mack T - 8A, Mack T-11, Mack T-12, Cummins ISM, Cummins ISB and GM RWFT.

The aforementioned samples were subject to carbon K-edge NEXAFS at HERMON beamline at Synchrotron Radiation Center, Madison Wisconsin. The soot samples were pressed on the indium foil to avoid contamination from other sources of carbon such as carbon tape etc. These samples are then mounted on a stainless steel sample holder. Using a load lock, we transferred samples to an ultrahigh vacuum recipient. The synchrotron storage ring was operated at 800 MeV. An energy resolution was of approximately 0.01 eV for the relevant carbon K-shell absorption edge energy (285 eV). The incident beam intensity was recorded with a gold mesh

reference monitor (Io), and the NEXAFS signal of the sample was detected in both total electron yield (TEY) modus. For every sample, scans ranging from 260 to 330 eV were made with energy steps of 0.1 eV. The NEXAFS spectra were obtained by normalize TEY by Io for the electron yield mode. For quantitative analysis, the crankcase soot spectra were deconvoluted using OriginPro program.

9.3 Results and Discussion

9.3.1 NEXAFS Analysis of Diesel Soot

The background subtracted and normalized NEXAFS spectra of graphite, different crankcase soot and carbon black are displayed in Figure 1. The differing graphitic nature of these soot samples is dependent upon the conditions of the combustion process in which they were formed. The general process is believed to result from polycyclic aromatic hydrocarbons (PAHs) undergoing nucleation to produce soot nuclei [164], which then grow in mass due to addition of gas-phase species and small PAHs. Another potential mechanism involves reactive coagulation via particle–particle collisions. Amorphous polyaromatic carbon is then believed to undergo dehydrogenation, resulting in ring condensation and fusion leading to partial micro structural ordering and progressively higher degrees of graphitization.

Spectral assessment of the normalized NEXAFS results provides useful information to distinguish the various carbonaceous products. C K edge spectra collected from the crankcase soot samples and carbon black exhibit typical graphite like spectra where major spectral contour includes π transition at around 285 eV arising from unsaturated carbon carbon multiple bonds and the corresponding σ-peak at 292 eV. Carbon black and diesel soot from dynamometer engine test also exhibit similar graphitic peak at 285 eV and 292 eV. Moreover, graphite structure also exhibits additional pronounced resonance at 291 eV; an exciton due to long-range crystalline domain. Intensity shoulder at 291 eV in diesel soot is not as pronounced as graphite but little resonance at 291 eV can be interpreted as tendency of diesel soot for long-range crystalline order. However, such intensity shoulder at 291 eV is absence in carbon black. Additional resonance in the spectrum for energies above 300 eV exhibits short-range order in graphite.

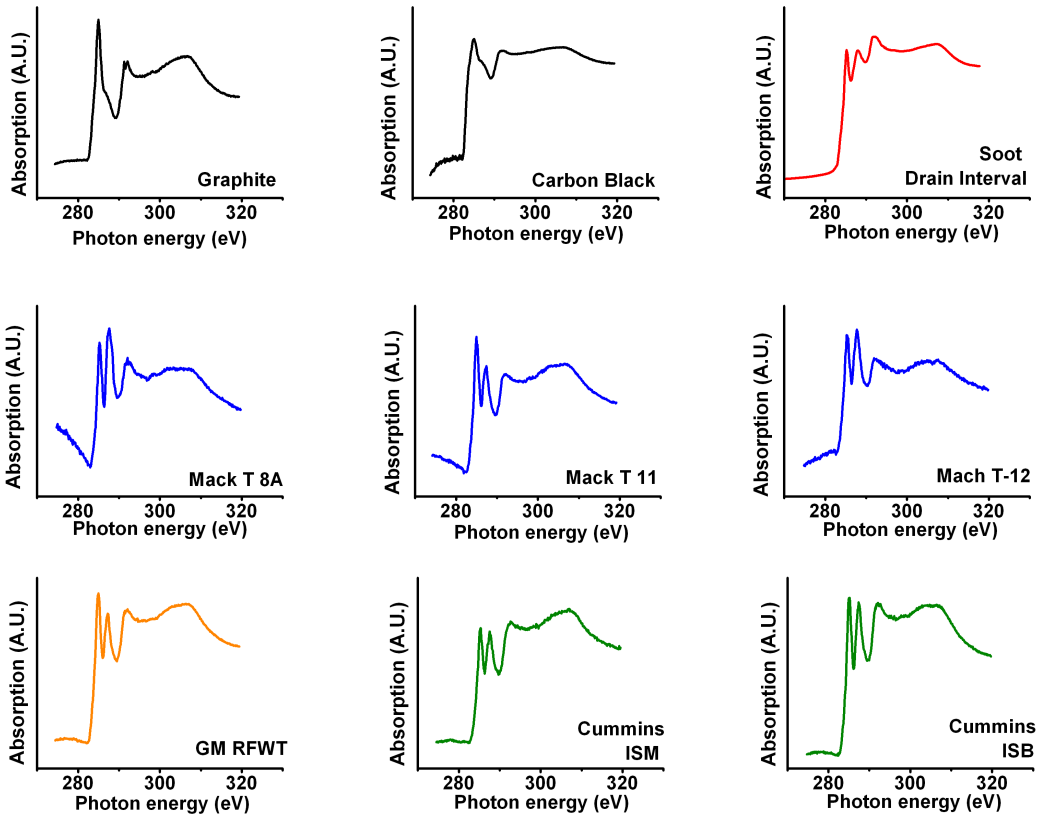

Figure 9.1 Normalized Total Electron Yield (TEY) carbon K edge spectra of diesel soot

However, crankcase soot from dynamometer engine test and carbon black has more diffuse rather noisy peak in the energies above 300 eV. All soot samples demonstrated first peak maximum at the around 285.3 eV below the π^* features. Chen et al. have demonstrated using MWNT that the shift of 0.3 eV is due to weakening of the C-C bong due the curvature of the grapheme sheets and larger interlayer distance spacing of nano tubes samples.[17,165,166]. It is well documented that turbostratic structure of diesel soot also has curvature in grapheme sheets. [16,112] The peak shift of 0.3 eV can be explained in terms of curved grapheme layer present in the all diesel soot obtained form different diesel engine dynamometer tests.

Moreover, a pronounce peak between 285 eV to 290 eV distinguish the C K edge of graphite and crankcase soot. The most striking difference between diesel soot as opposed to graphite is an accumulation of peaks at 286.5-288.5 eV, which is due to phenol groups (286.5

eV), aliphatic side chains (287.3 eV), and carboxyl groups (288.4 eV). In all our studies thus far, we have not found a single diesel soot sample that did not show enhanced intensity at these energies. However, assignment of the spectral features between this energy range is quite controversial in the literature. [69-71,167,168] Cody et. al have assigned various peak position for the energy range from 284- 290 for different molecular species such as aromatic, quinone, phenolic, Ketones, aliphatic, aromatic carbonyl, C=O, COOH, C-OH etc. [169] Manfred et al have reported these contrasting explanations for the spectral features between 286-290 eV. [170] For example, Urguhart et al. have described functionalized aromatic group give resonance peak between 286-290 eV with C1s (C-R) - 1 π* transitions. [171] Similarly, strong resonance had been reported between 286 to 290 eV of C 1s - $\boldsymbol{\pi}$ transition of C60. Moreover, it was reported that presence of contamination of C-H on the surface could give σ transition. On the other hand Researches have reported the structural features between 284-285 eV originated from zig-zag edge of graphite.[170] These contrasting explanations infer the difficulty to interpret the structural features of C K edge NEXAFS spectrum for highly heterogeneous materials like soot.

However, structural information of crankcase soot can be important to understand the reactivity of surface in different diesel engine environment. Braum et al have reported the presence of different volatiles originated from residual fuel, lubrication oil and volatiles reaction products on the idle and load soot obtained from exhaust. [172] They have also reported that idle soot contain significantly more volatiles than load soot. Moreover, Dale et al have described the effect of fuel injection parameters, composition of fuel, temperature, and pressure in the formation of soot.[170] Dynamometer engine tests have designed with different operational parameters such as load, speed, crankcase temperature, EGR rate, fuel composition, amount of soot, crankcase pressure, fuel injection system etc. Our earlier studies have well established that interactions between reactive decomposition products of lubricant additives chemistries and soot modify the chemical make up of soot. Above mention factor might alter that soot surface and various volatile species might get attached to the surface of soot.

Soot extracted from the Mack T-8A, Mack T-11 and Mack T-12 tests have main peak at ~ 287.7 eV originating from C=O. Peak at 287.1, and 287. 4 eV carbon atoms are present in aliphatic chain for 1s- π * transition. Soot also has shoulder at 288. 4 eV, which might be contributed by COOH for 1s- π * transition.

Soot extracted from the Cummins ISB and ISM have peak at 287.6 and 287.7 eV, which might originate from C=O. However, soot extracted from Cummins ISM have peak at 287 originating from aliphatic carbon, but similar peak at 287 eV was absence with Cummins ISB soot. Similarly, soot extracted from GM RFWT test have peak position like Cummins ISB and have presence of only C=O. Soot extracted from engine oil during drain interval which represent more realistic conditions of diesel engine also show similar peak like controlled dynamiter tests. It has peak at 287.8 eV represent C=O. Residual fuel and oil are most likely responsible for this signature in the diesel soot spectrum. Lubricant oil and diesel fuel have pronounced intensity in exactly this energy region.

The graphitic nature of the samples is assessed by calculating their sp^2 hybridization. This quantity is determined by normalizing the area of the 1s - π^* C=C peak at 285.3 eV ($A_{C=C}$ Sample) with the area of the spectrum over the energy range of 280–310 eV ($A_{C=C}$ Sample) for the sample of interest. This ratio is compared with the ratio obtained by normalizing the 280 - 310 area of the 1s - π^* C=C peak at 285.3 eV ($A_{Graphite}$) with the area of the spectrum in the energy range of 280–320 eV ($A_{C=C}$ Graphite, which is a sp^2 is unity reference sample.[173] This calculation is performed using the following expression

$$\text{Relative } sp^2 = \left[\frac{A_{C=C}^{Sample}}{A_{280-310}^{Sample}} \Big/ \frac{A_{C=C}^{Graphite}}{A_{280-310}^{Graphite}} \right]$$

The calculated sp^2 hybridization of different diesel soot with respect to unity sp2 hybridization of graphite is shown in table 9.1.

Table 9.1 sp^2 hybridization of different diesel soot with respect to unity sp2 hybridization of graphite

	Area under Peak $A_{C=C}$	Area Under Peak $A_{280-310}$	Unity sp^2 hybridization with respect to graphite
Graphite	1257.512	10213.59	1
Soot (Commercially Operated Diesel Engine	1.42	16.20	0.71
Soot Mack T 8A	427.44	5295.19	0.65
Soot Mack T 11	1.56	16.18	0.78
Soot Mack T 12	804.22	8720.57	0.74
Soot Mack T 12 Cylinder	0.726	14.15	0.41
Soot Cummins ISM	763.48	10860.89	0.56
Soot Cummins ISB	953.71	13072.98	059
Soot GM RFWT	1020.52	12036.71	068

9.3.2 Raman Spectroscopy

Raman spectroscopy is a promising characterization tool to investigate the short-range highly disordered graphitic structure. Interpretation of the spectral features of the graphite, carbon black and diesel soot has been described in the previous chapters in detail. To analyze the raman spectra, similar approach have used as described in previous chapters.

For the analysis and determination of spectral parameters by curve fittings various line shapes were evaluated. Raman spectra of extracted carbon blacks and diesel soot exhibit a broad band at about ~1500 cm-1. The band at 1500 cm-1 is associated with amorphous sp2 bonded carbon. It is also worth taking into consideration that sp3 bonded carbon have vibrational features frequency below 1500 cm-1.

9.3.2.1 Spectra analysis by curve fitting

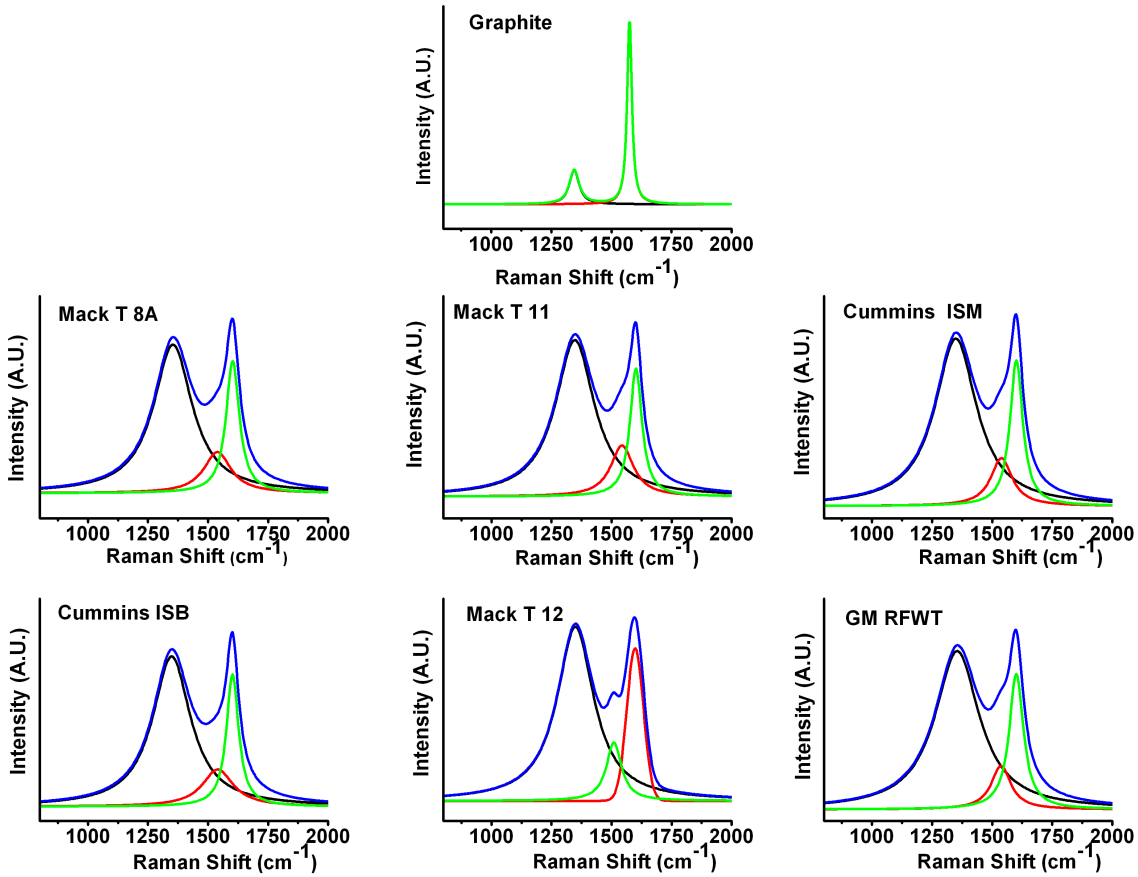

Figure 9.2 Deconvoluted Raman spectra of dynamometer diesel engine soot using Lorentzian curve fit for the D1, D3, D4 and G peaks

This observation suggests the higher probability of sp^2 bonded amorphous carbons. The best fit was invariably achieved by either one or two combination of line shape for G, D1 and D3 peaks. One can use the Lorentz line shape for all three G, D1 and D3 peaks or one can use the Lorentzian line shape for G and D1 peak and Gaussian like shape for D3 peak. In this study we have used the Lorentzian peak fit for all three peaks of soot as it offers the best fit. This fitting of the spectrum is in good agreement with recent studies by Sadezky et. Al. The polycrystalline graphite exhibits two sharp peaks at ~ 1345 cm-1 and 1575cm-1 that correspond to the D1 and G peak respectively. The peak at ~ 1500 cm-1 is not observed in graphite. The graphite with just the D1 and G peak was fitted with two Lorentzian curve fits. The curve fitted spectra of different soot,

carbon black and graphite are show in Figure (a),(b), (c). For the carbon black a fourth peak was introduced in the fitting (D4), which takes into account for the disordered graphitic lattice due to polyenes and/or ionic impurities. Figure (a) - (f) are curve fitted spectra of dynamometer diesel soot from Mack T8A, Mack T-11, Mach T-12, Cummins ISM, Cummins ISB, GM RFWT.

Further analysis of the spectra can be obtained by analyzing full width half maximum (FWHM) of the peaks, peak intensity and peak position. Table 9.2 details the curve fitted data and ratio of G/D peak intensity. The curve fitted spectral data reveals that for all samples FWHM of G peak is narrower than that of other two bands. This validates the fact that G peak corresponds to crystalline phase of carbon. Comparing the FWHM of graphite with diesel soot extracted from dynamometer engine tests, it evident that graphite has greater portion of crystalline phase.

In addition, Table 9.2 breaks down the contribution from the different disordered forms of soot samples including D1 the disordered graphitic lattice with contributions from graphene layer edges that are wrapped around, D3(A) the amorphous carbon and D4(I) arising from disordered graphitic layers from ionic impurities and polyenes. Overall the ratio of G/(D1+D3+D4) for all T-8A and Cummins ISB diesel soots are very similar for suggesting a similar ratio of idealized graphite lattice and disordered carbon. The ratio of G/(D1+D3+D4)s is similar for other soot samples. However, a careful examination of the ratio's G/D1, G/D3 and G/D4 indicate some significant differences. The smaller G/D1 ratio for diesel soot indicates a larger proportion of graphene layer edges have reacted in soot resulting in a higher level of disorder. The G/D1 ratio is smaller for Mack T-11, Mach T-12, Cummins ISB, GM RFWT compare to Mack T8A and Cummins ISM suggest higher disorder due to greater proportion of grapheme layer edge that have reacted during treatments. Other studies in functionalizing of graphene have shown that edges of the graphene layer may be functionalized more easily resulting in smaller G/D1 ratios {{3235 Sharma,Richa 2010 2010}}. This might be preferential location for reactive decomposition species for absorption. But more scientific investigation is required to validate the speculation.

Table 9.2 Raman spectroscopic data for dynamometer diesel soot

		Peak Position	Intensity	G/D1	G/D3	G/D4	G/(D1+D3+D4)
T 8A	G	1601.53	623.50				
	D1	1356.13	1174.76	0.53			
	D3(A)	1528.29	389.38		1.60		0.40
T 11	G	1599.57	1045.97				
	D1	1347.47	2385.22	0.44			
	D3(A)	1532.60	626.58		1.67		0.35
Cummins ISM	G	1599.27	830.45				
	D1	1349.48	1236.21	0.67			
	D3(A)	1511.94	530.55		1.57		
	D4 (I)	1219.08	388.80			2.14	0.39
Cummins ISB	G	1601.45	661.96				
	D1	1349.44	1608.13	0.41			
	D3(A)	1535.51	387.00		1.71		0.33
T 12	G	1600.30	889.88				
	D1	1349.03	2118.37	0.42			
	D3(A)	1535.37	517.10		1.72		0.34
RFWT	G	1600.79	816.59				
	D1	1354.59	1974.31	0.41			
	D3(A)	1537.09	495.11		1.65		0.33

On the other hand G/D3 ratio for all diesel soots are similar. Lastly, the D4(I) peak is present in Cummins ISM while absence of D4(I) peak in other diesel soot indicates the absence of polyenes and/or other ionic impurities.

These results confirm the usefulness of Raman Spectroscopy to probe short-range disorder structure. Although raman spectra distinguish the contribution from crystalline and amorphous domains but no additional spectral features were observed to confirm contribution from interaction between lubrication additives chemistries and diesel soot. Analogues results were also recorded on the extracted carbon blacks from various treatments.

9.4 Conclusion

Carbon K edge NEXAFS was utilized to study the structure of the diesel soot extracted from the field and dynamometer diesel engines, carbon black and graphite. Spectral signature of the all the soot samples differs from graphite and carbon black due to presence of resonance peak between 286 to 290 eV, attributed to various volatile chemistries present on the surface of the soot. Contrasting explanations for the peak between 286 to 290 eV make it difficult to interpret the origin of the various edges in that region. However, each soot samples have revealed different peak height in the region between 286-290 eV. This infers the influence of various operational parameters such as crankcase pressure, crankcase temperature, fuel compositions, injection method, lubrication composition etc. Raman spectra of all the soot samples do not reflect significant differences to probe the interaction between lubricant additives chemistries and soot.

CHAPTER 10

CONCLUSION

10.1 Summary of Work

Global efforts to reduce the emission of NOx and PMs from diesel engine have resulted in modification in the engine design especially in post combustion protocols such as Exhaust Gas Recirculation (EGR). Effectiveness of EGR to restrict the emission of NOx have realized at the cost deterioration of lubrication oil by inclusion of various contaminants, especially soot, and there by promote higher wear of critical engine components and reduced drain interval. At University of Texas at Arlington, research had led to comprehend fundamental understanding of soot induced wear mechanism of diesel engine. The fundamental understanding of the soot induced wear mechanism can help the lubricant additives formulators and OEMs to optimize their products to mitigate the wear of components and also to comply with emission norms. This research has examined the structure, composition and morphology of diesel soot in collaboration with its tribological assessment. The diesel soot samples were extracted from the drain interval oil from commercially operated diesel engine as well as from laboratory operated dynamometer engine test. The former sample represents field operated engine condition while later samples represents controlled laboratory operated engine conditions. Research was also conducted to simulate the structure and composition of diesel soot by treating carbon black in various laboratory set-up. A brief summery of studies conducted and results obtained is provided herein.

Diesel soot extracted from the drain interval oil of field-operated engine was characterized to study the interaction between lubricants additives chemistries and soot. The interactions were studies using XANES, HR-TEM, TEM, and Raman spectroscopy, Synchrotron radiation X-ray Diffraction. Their impact on the wear performance was examined using four ball wear tester and SRV friction tester.

- Raman spectroscopy and synchrotron x-ray diffraction. Results indicate that the primary structure of diesel soot is similar to carbon black with a turbostratic structure.
- TEM results revealed that the differences between diesel soot and carbon black are primarily in the incorporation of tribological by products and decomposition products of the engine oil additive package in diesel soot.
- XANES analysis revealed the tribological by products and decomposition products were present in form of zinc phosphate ($Zn_3(PO_4)_2$), calcium phosphate ($Ca_3(PO_4)_2$), calcium sulfate ($CaSO_4$), zinc sulfate ($ZnSO_4$) on the soot structure.
- Synchrotron radiation x-ray diffraction indicated that the zinc phosphate ($Zn_3(PO_4)_2$) were present in the amorphous phase while calcium sulfate was present in crystalline phase in the hydrated form which include gypsum and bassanite.
- High-resolution transmission electron microscopy couple with energy dispersive spectroscopy reveals the presence of crystalline nano-particles embedded on the periphery of the turbostratic structure of soot. A closer examination of the inter-planar spacing with lattice imaging coupled with elemental analysis of these nano-particles indicates that the particles are constituted of phosphates of Ca as well as Fe_2O_3. These compounds have a hardness of around 5-6 on the Moh scale and can contribute to polishing wear under 3 body boundary lubrication conditions.
- Tribological assessment using four ball wear tester indicated the abrasive wear on the test samples while SRV friction indicate the reduction in friction coefficient in presence of diesel soot.

Experiments were conducted to force the interaction between lubricants additives and carbon black (soot surrogate) by oxidation and milling to mimic the composition and structure of diesel soot. The interactions were studies using XANES, TEM, and Raman spectroscopy. Their impact on the wear performance was examined using four ball wear tester and SRV friction tester.

- Comparison of treated carbon black and diesel soot using XANES indicate the presence of similar chemistries on the carbon black. However, treated carbon black indicated more zinc sulfide present on the carbon black.
- TEM and raman spectroscopy results indicated the primary structure of treated carbon black and diesel soot was similar.
- Four ball wear test results and morphology of wear track indicated that abrasive wear is the dominants mode of wear for the lubricants with the oxidized and milled carbon black.
- SRV friction results indicated that the presence of treated carbon black in the lubricants lowered the friction coefficient.
- XANES analysis of tribofilm coupled with SRV test results indicated the polishing wear is the dominant wear mechanism for the reciprocating test configuration.

Diesel soots extracted from the laboratory dynamometer engine test were examined to validate the results obtained from the soot extracted from the field engine. The dynamometer crankcase soots were studies using XANES, HR-TEM and Raman spectroscopy, Synchrotron radiation X-ray Diffraction. Engine components from the dynamometer tests were examined for tribological assessments. Tribofilm on the engine components were analyzed using XANES. Crankcase soot were extracted from the Mack T-8A, Mack T-11, Mack T-12, Cummins ISM, Cummins ISB and GM RFWT dynamometer engine test. Piston ring from Mack T-12 and Cummins ISM, header from Cummins ISM and pin of GM RFWT tests were used for the wear track analysis.

- Raman spectroscopy and synchrotron x-ray diffraction results indicate that the primary structure of diesel soot is similar to carbon black with a turbostratic structure. No significant differences were noticed.
- XANES analysis revealed similar results as field engine crankcase soot where the tribological by products and decomposition products were present in form of zinc phosphate ($Zn_3(PO_4)_2$), calcium phosphate ($Ca_3(PO_4)_2$), calcium sulfate ($CaSO_4$), zinc sulfate ($ZnSO_4$) on the soot structure.

- Phosphates observed on the soot structure are orthophosphate, small chain and medium chain phosphate. Sulfate to sulfide ration also vary case to case. It was difficult to correlate phosphate chain length or sulfate to sulfide ration of decomposition products due to considerable variability on the operation parameters of engine tests.
- Synchrotron radiation x-ray diffraction revealed the presence of calcium sulfate in crystalline form in varying amount.
- High-resolution transmission electron microscopy couple with energy dispersive spectroscopy reveals the presence of crystalline nano-particles embedded on the periphery of the turbostratic structure of soot. A closer examination of the interplanar spacing with lattice imaging coupled with elemental analysis of these nano-particles indicates that the particles are constituted of phosphates of Ca as well as Fe_2O_3. These compounds have a hardness of around 5-6 on the Moh' scale and can contribute to polishing wear under 3 body boundary lubrication conditions. In addition, cylinder soot extracted from the Mack T-12 reveals the presence larger crystalline particles along with smaller nano crystalline particles embedded on the soot structure. Extreme combustion chamber environment with repetitive fluctuation in the temperature and pressure might induce higher order of crystallinity in it.
- Tribofilm of piston ring from the Mack T-12 and Cummins ISM engine test contained phosphate and sulfate of Zn and Ca, Fe_2O_3 in different proportions throughout the thickness of tribofilm. Header of Cummins ISM and GM RFWT demonstrated similar composition for the tribofilm.
- SEM analysis of wear track on the engine components demonstrated abrasive wear track in the sliding direction. The straight abrasive grooves indicated the three body interaction of two sliding engine components and trapped soot particles.

10.2 Direction for Further Study

The research presented herein has so far examined the composition and structure of the diesel soot extracted from the field engine, dynamometer engines and laboratory simulation set-up and their correlation to the tribological assessment. However, presence of mechanically embedded harder nano crystalline particles along with by products of tribological by products and decomposition products of additives chemistries have provided comprehensive understanding of the wear mechanism to solve many unexplained phenomena.

One of the many directions that could be pursued would involve expanding the scope of controlled dynamometer test where study the effect of each chemistry individually on the composition of soot and corresponding wear effect on the engine components. Specifically, the detergent chemistries and anti wear chemistries could be studied individually. A more comprehensive understanding could be achieved by studying the effect of operational parameters on the soot composition for the specific lubricant composition.

Higher EGR rate, cooled EGR and low SAPS oil are unavoidable protocols to comply with stringent emission norms. Higher EGR rate and thus unavoidable and higher amount of soot inclusion to crankcase oil could be controlled by novel dispersant technology. However, comprehensive understanding of soot formation mechanism and improved combustion chamber dynamics could be important for the modern diesel engine.

REFERENCES

[1] Aldajah S, Ajayi OO, Fenske GR, Goldblatt IL. Effect of exhaust gas recirculation (EGR) contamination of diesel engine oil on wear. Wear 2007;263:93-8.

[2] Cadman W, Johnson JH. Study of the effect of exhaust gas recirculation on engine wear in a heavy duty diesel engine using analytical ferrography. International Congress and Exposition - Society of Automotive Engineers. 1986:SAE, Warrendae, PA, USA.

[3] D.T. H, Mavropolos GC, Binder KB. Effect of exhaust gas recirculation (EGR) temperature for various EGR rates on heavy duty DI diesel engine performance and emissions.

[4] Lawrence L. Heavy-duty Diesel Engine Oil Developments and Trends. Machinery Lubrication 2007.

[5] Shank G, Goshorn K, Cooper M, Dam W, Richards S. A History of mack engine lubricants tests from 1985-2005: Mack T-7 through Mack T-12. SAE Technical Paper 2005;2005-01-3713.

[6] Green DA, Lewis R. The effects of soot-contaminated engine oil on wear and friction: A review. Proc Inst Mech Eng Pt D: J Automobile Eng 2008;222:1669-89.

[7] Aldajah S, Ajayi OO, Fenske GR, Goldblatt IL. Effect of exhaust gas recirculation (EGR) contamination of diesel engine oil on wear. Wear 2007;263:93-8.

[8] Singh SK, Agarwal AK, Sharma M. Experimental investigations of heavy metal addition in lubricating oil and soot deposition in an EGR operated engine. Appl Therm Eng 2006;26:259-66.

[9] Kuo CC, Passut CA, Jao T, Csontos AA, Hzowe JM. Wear mechanism in Cummins M-11 high soot diesel test engines. Proceedings of the 1998 SAE International Spring Fuels & Lubricants Meeting & Exposition, May 4, 1998 - May 6 1998;1368:21-32.

[10] Yamaguchi ES, Utermann M, Roby SH, Ryason SH, Yeh SW. Soot wear in diesel engines. Proc Inst Mech Eng Part J 2006;220:463-9.

[11] Bardasz EA, Carrick VA, Ebeling VL, George HF, Graf MM, Kornbrekke RE et al. Understanding soot mediated oil thickening through designed experimentation - Part 2: GM 6.5 L. Proceedings of the 1996 International Fall Fuels & Lubricants Meeting & Exposition, October 14, 1996 - October 17 1996;1210:57-68.

[12] Bardasz EA, Carrick VA, George HF, Graf MM, Kornbrekke RE, Pocinki SB. Understanding soot mediated oil thickening through designed experimentation - Part 5: Knowledge exhancement in the GM 6.5 L. Proceedings of the 1997 International Fall Fuels & Lubricants Meeting & Exposition, October 13, 1997 - October 16 1997;1304:126-40.

[13] Dennis AJ, Garner CP, Taylor DHT. The Effect of EGR on Diesel Engine Wear. SAE Technical Paper 1999:Paper Number 1999-01-0839.

[14] Gautam M, Durbha M, Chitoor K, Jaraiedi M, Mariwalla N, Ripple D. Contribution of soot contaminated oils to wear. Proceedings of the 1998 SAE International Spring Fuels & Lubricants Meeting & Exposition, May 4, 1998 - May 6 1998;1372:55-67.

[15] Nagai I, Endo H, Nakamura H, Yano H. Soot and valve train wear in passenger car diesel engines. Lubricant and Additive Effects on Engine Wear. 1983:87-101.

[16] Braun A, Huggins FE, Shah N, Chen Y, Wirick S, Mun SB et al. Advantages of soft X-ray absorption over TEM-EELS for solid carbon studies - A comparative study on diesel soot with EELS and NEXAFS. Carbon 2005;43:117-24.

[17] Braun A, Shah N, Huggins FE, Kelly KE, Sarofim A, Jacobsen C et al. X-ray scattering and spectroscopy studies on diesel soot from oxygenated fuel under various engine load conditions. Carbon 2005;43:2588-99.

[18] Clague ADH, Donnet JB, Wang TK, Peng JCM. Comparison of diesel engine soot with carbon black. Carbon 1999;37:1553-65.

[19] Cuesta A, Dhamelincourt P, Laureyns J, Martinez-Alonso A, Tascon JMD. Raman microprobe studies on carbon materials. Carbon 1994;32:1523-32.

[20] Donnet JB. Carbon Black : Science and Technology. 1993.: New York Marcel Dekker, Inc, 1993.

[21] Dippel B, Heintzenberg J. Soot characterization in atmospheric particles from different sources by NIR FT Raman spectroscopy. J Aerosol Sci 1999;30:S907-8.

[22] Mikhailov EF, Vlasenko SS, Ryshkevitch TI, Kiselev AA. Soot structure investigation: Adsorptional properties. J Aerosol Sci 1996;27:S709-10.

[23] Mainwaring R. Soot and wear in heavy duty diesel engines. Proceedings of the 1997 International Spring Fuels & Lubricants Meeting, May 5, 1997 - May 8 1997;1273:47-63.

[24] Berbezier I, Martin JM, Kapsa P. Role of carbon in lubricated mild wear. Tribol Int 1986;19:115-22.

[25] Colacicco P, Mazuyer D. Role of soot aggregation on the lubrication of diesel engines. Tribol Trans 1995;38:959-65.

[26] Yoshida K. Effects of sliding speed and temperature on tribological behavior with oils containing a polymer additive or soot. Tribol Trans 1990;33:221-8.

[27] Rounds FG. Effect of lubricant additives on the prowear characteristics of synthetic diesel soots. Lubrication Engineering 1987;43:273-82.

[28] Rounds FG. Generation of synthetic diesel engine oil soots for wear studies. Lubrication Engineering 1984;40:394-401.

[29] Rounds FG. Soots from used diesel engine oils - Their effects on wear as measured in 4-ball wear tests. SAE Technical Paper 1981:Paper Number 810499.

[30] Rounds FG. Carbon: Cause of diesel engine wear? SAE Technical Paper 1977:Paper Number 770829.

[31] Corso S, Adamo R. Effect of diesel soot on reactivity of oil additives and valve train materials. Heavy Duty Diesel Lubrication. Fuels and Lubricants Meeting & Exposition. 1984:41-55.

[32] Akiyama K, Masunaga K, Kado K, Yoshioka T. Cylinder wear mechanism in an EGR-equipped diesel engine and wear protection by the engine oil. SAE Technical Paper 1987:Paper Number 872158.

[33] Hosonuma K, Yoshida K, Matsunaga A. Decomposition products of zinc dialkydithiophosphate in an engine and their interaction with diesel soot. Wear 1985;103:297-309.

[34] Morey CJ, Mark J. Diesel Passenger Vehicles-Can They Meet Air Quality Needs and Climate Goals. SAE Technical Paper 2000:1599-2000.

[35] Morey CJ, Mark J. Diesel Passenger Vehicles-Can They Meet Air Quality Needs and Climate Goals. SAE Technical Paper 2000:1599-2000.

[36] Yu RC, Shahed SM. Effects of injection timing and exhaust gas recirculation on emission from a D.I diesel engine. SAE Preprints 1981.

[37] Ryason PR, Chan IY, Gilmore JT. Polishing wear by soot. Symposium on Selective Catalytic Oxidation of Hydrocarbons - Presented before the Division of Petroleum Chemistry, ACS, Boston Meeting, April 22, 1990 - April 272 1990;35:250.

[38] Ratoi M, Castle RC, Bovington CH, Spikes HA. The influence of soot and dispersant on ZDDP film thickness and friction. Lubr Sci 2004;17:25-43.

[39] Castilloa C, Spikes HA. The behavior of diluted sooted oils in lubricated contacts. Tribology Letters May, 2004;16:317.

[40] Gautam M, Chitoor K, Durbha M, Summers JC. Effect of diesel soot contaminated oil on engine wear - investigation of novel oil formulations. Tribol Int 1999;32:687-99.

[41] Corso S, Adamo R. Incipient scuffing detection by ferrography in a diesel valve train system. Engine Lubrication. International Fuels and Lubricants Meeting and Exposition. 1985:33-49.

[42] Tree DR, Svensson KI. Soot processes in compression ignition engines. Progress in Energy and Combustion Science 2007;33:272-309.

[43] Lahaye J. Mechanisms of soot formation. Polym Degrad Stab 1990;30:111-21.

[44] Tao F, Reitz RD, Foster DE, Liu Y. Nine-step phenomenological diesel soot model validated over a wide range of engine conditions. International Journal of Thermal Sciences 2009;48:1223-34.

[45] Xi J, Zhong B. Soot in diesel combustion systems. Chemical Engineering and Technology 2006;29:665-73.

[46] Mathis U, Mohr M, Kaegi R, Bertola A, Boulouchos K. Influence of diesel engine combustion parameters on primary soot particle diameter. Environ Sci Technol 2005;39:1887-92.

[47] Nicholls M, Najman MN, Zhang Z, Kasrai M, Norton PR, Gilbert PUPA. The contribution of XANES spectroscopy to tribology. Canadian Journal of Chemistry 2007;85:816-30.

[48] Kasrai M, Lennard WN, Brunner RW, Bancroft GM, Bardwell JA, Tan KH. Sampling depth of total electron and fluorescence measurements in Si L- and K-edge absorption spectroscopy. Appl Surf Sci 1996;99:303-12.

[49] ASM International. Annual Book of ASTM Standards : Petroleum Products and Lubricants (III). 2010;05.03:1563.

[50] Sasaki M, Kishi Y, Hyuga T, Okazaki K, Tanaka M, Kurihara I. Effect of EGR on diesel engine oil, and its countermeasures. Proceedings of the 1997 International Spring Fuels & Lubricants Meeting, May 5, 1997 - May 8 1997;1271:39-44.

[51] Devlin MT, Li S, Burgess T, Jao TC. Film formation properties of polymers in the presence of abrasive contaminants. SAE Technical Paper 2002;21.

[52] George S, Balla S, Gautam M. Effect of diesel soot contaminated oil on engine wear. Wear 2007;262:1113-22.

[53] Jap T-, Li S, Yatsunami K, Chen SJ, Csontos AA, Howe JM. Soot Characterisation and Diesel Engine Wear. Lubr Sci 2004;16:111-26.

[54] Kagaya M. Study on Diesel Soot (Part 1) Effect of Diesel Soot on Valve Train Wear in Passenger Car Diesel Engines. Journal of the Japan Petroleum Institute 1997;40:482-.

[55] Kagaya M. Study on Diesel Soot (Part 2) Discussion Concerning the Mechanism of Valve Train Wear by Diesel Soot. Journal of the Japan Petroleum Institute 1997;40:488-.

[56] Kagaya M, Kagawa T, Takahashi Y. Study on Diesel Soot (Part 3) A New Proposal on the Mechanism of Wear Promoted by Soot. Journal of the Japan Petroleum Institute 1997;40:494-.

[57] Kaneta M, Irie T, Nishikawa H, Matsuda K. Effects of soot on wear in elastohydrodynamic lubrication contacts. Proc Inst Mech Eng Part J 2006;220:307-17.

[58] Kano M, Tanimoto I, Nakamura K, Fujiki A. Effect of the EGR system on valve train wear in diesel engine. Journal of JSLE.International edition 1988:133-8.

[59] Kuo CC, Passut CA, Jao T, Csontos AA, Howe JM. Wear mechanism in Cummins M-11 high soot diesel test engines. Proceedings of the 1998 SAE International Spring Fuels & Lubricants Meeting & Exposition, May 4, 1998 - May 6 1998;1368:21-32.

[60] McGeehan JA, Rynbrandt JD, Hansel TJ. Effect of oil formulations in minimizing viscosity increase and sludge due to diesel engine soot. Fuels and Lubricants Meeting & Exposition. 1984:SAE, Warrendae, PA, USA.

[61] Narita K. Effects of diesel soot on engine oil performance. Journal of Japanese Society of Tribologists 1997;42:425-.

[62] Selby K, Urbanak M, Leonhardt H, Colbourne D, Burnett P, Machatschek F et al. Meeting the lubrication challenges of heavy duty low emission diesel engines. 2005 World Tribology Congress III, September 12, 2005 - September 16 2005:547-8.

[63] Lahaye J. Mechanisms of soot formation. Polym Degrad Stab 1990;30:111-21.

[64] Tumolva L, Park J, Kim J, Miller AL, Chow JC, Watson JG et al. Morphological and elemental classification of freshly emitted soot particles and atmospheric ultrafine particles using the TEM/EDS. Aerosol Science and Technology 2010;44:202-15.

[65] Nehme G, Mourhatch R, Aswath PB. Effect of contact load and lubricant volume on the properties of tribofilms formed under boundary lubrication in a fully formulated oil under extreme load conditions. Wear 2010:1-19.

[66] Costello MT, Kasrai M. Study of surface films of overbased sulfonates and sulfurized olefins by X-Ray Absorption Near Edge Structure (XANES) spectroscopy. Tribology Letters 2006;24:163-9.

[67] Costello MT, Urrego RA. Study of surface films of the ZDDP and the MoDTC with crystalline and amorphous overbased calcium sulfonates by XPS. Tribol Trans 2007;50:217-26.

[68] Escribano R, Sloan JJ, Siddique N, Sze N, Dudev T. Raman spectroscopy of carbon-containing particles. Vibrational Spectroscopy 2001;26:179-86.

[69] Gruber T, Zerda TW, Gerspacher M. Raman studies of heat-treated carbon blacks. Carbon 1994;32:1377-82.

[70] Jawhari T, Roid A, Casado J. Raman spectroscopic characterization of some commercially available carbon black materials. Carbon 1995;33:1561-5.

[71] Sadezky A, Muckenhuber H, Grothe H, Niessner R, Poschl U. Raman microspectroscopy of soot and related carbonaceous materials: Spectral analysis and structural information. Carbon 2005;43:1731-42.

[72] Sharma R, Baik JH, Perera CJ, Strano MS. Anomalously Large Reactivity of Single Graphene Layers and Edges toward Electron Transfer Chemistries. Nano Letters 2010;10:398-405.

[73] Patel M, Aswath PB. Morphology, Structure and Chemistry of Extracted Diesel Soot: Part II: High Resolution Transmission Electron Microscopy, X-ray Absorption Near Edge Structure Spectroscopy. Tribology International In Review.

[74] Kawamura M, Ishiguro T, Fujita K, Hidetake M. Deterioration of antiwear properties of diesel engine oils during use. Wear 1988;123:269-80.

[75] Huq MZ, Aswath PB, Elsenbaumer RL. TEM studies of anti-wear films/wear particles generated under boundary conditions lubrication. Tribol Int 2007;39:111-6.

[76] Mourhatch R, Aswath PB. Tribological behavior and nature of tribofilms generated from fluorinated ZDDP in comparison to ZDDP under extreme pressure conditions---Part 1: Structure and chemistry of tribofilms. Tribol Int 2011;44:187-200.

[77] Mourhatch R, Aswath PB. Tribological behavior and nature of tribofilms generated from fluorinated ZDDP in comparison to ZDDP under extreme pressure conditions-Part II: Morphology and nanoscale properties of tribofilms. Tribol Int 2011;44:201-10.

[78] Mourhatch R, Aswath PB. Nanoscale Properties of Tribofilms formed with Zinc Dialkyl Dithiophosphate (ZDDP) under Extreme Pressure Condition. Journal of Nanoscience and Nanotechnology 2008;9:2682-91.

[79] Ji H, Nicholls MA, Norton PR, Kasrai M, Capehart TW, Perry TA et al. Zinc-dialkyl-dithiophosphate antiwear films: Dependence on contact pressure and sliding speed. Wear 2005;258:789-99.

[80] Fujita H, Spikes HA. The formation of zinc dithiophosphate antiwear films. Proc Inst Mech Eng Part J 2004;218:265-77.

[81] Mosey NJ, Woo TK. Formation of zinc phosphate polymers and networks through the insertion of metathiophosphates into zinc dialkyldithiophosphates. Inorganic Chemistry 2005;44(21):7274-6.

[82] Mosey NJ, Woo TK, Kasrai M, Norton PR, Bancroft GM, Müser MH. Interpretation of experiments on ZDDP anti-wear films through pressure-induced cross-linking. Tribology Letters 2006;24:105,105-114.

[83] Yu LG, Yamaguchi ES, Kasrai M, Bancroft GM. The chemical characterization of tribofilms using XANES - Interaction of nanosize calciumcontaining detergents with zinc dialkyldithiophosphate. Canadian Journal of Chemistry 2007;85:675-84.

[84] Selby K, Urbanak M, Leonhardt H, Colbourne D, Burnett P, Machatschek F et al. Meeting the lubrication challenges of heavy duty low emission diesel engines. 2005 World Tribology Congress III, September 12, 2005 - September 16 2005:547-8.

[85] Mosey NJ, Woo TK, Müser MH. Mechanism of wear inhibition by ZDDP lubricant additives - Insights from molecular scale simulations. American Chemical Society, Division of Petroleum Chemistry, Preprints 2005;50:332-5.

[86] Leslie R. Rudnick. Lubricants Additives: Chemistry and Applications. January 29, 2003;1:758.

[87] Kawamura M, Ishiguro T, Fujita K, Hidetake M. Deterioration of antiwear properties of diesel engine oils during use. Wear 1988;123:269-80.

[88] Hirose Y, Kunoki T. Recent studies on diesel soot and valve train wear. Journal of Japan Society of Lubrication Engineers 1987;32:159-64.

[89] Olomolehin Y, Kapadia R, Spikes H. Antagonistic interaction of antiwear additives and carbon black. Tribology Letters 2010;37:49-58.

[90] Coy RC, Jones RB. The Thermal Degradation and EP Performance of Zinc Dialkyldithiophosphate Additives in White Oil. Tribol Trans 1981;24:77-90.

[91] Jones RB, Coy RC. Chemistry of the Thermal Degradation of Zinc Dialkyldithiophosphate Additives. ASLE Trans 1981;24:91-97.

[92] Parekh K, Mourhatch R, Aswath PB. ZDDP-additive-catalyst interactions in engine oil. Proceedings of the World Tribology Conference III 2005:661-2.

[93] Parekh K. Interactions between antiwear agent and novel additive in engine oils. 2006M. S. ThesisUniversity of Texas at ArlingtonArlington, TX.

[94] Willermet PA, Dailey DP, Carter RO,III, Schmitz PJ, Zhu W. Mechanism of formation of antiwear films from zinc dialkyldithiophosphates. Tribology International 1995;28:177-87.

[95] Willermet PA, Kandah SK. Lubricant degradation and wear v. Reaction products of Zinc dialkyldithiophosphate and peroxy radicals. ASLE Trans 1984;27:67,67-72.

[96] Patel M, Ricardo CLA, Scardi P, Aswath PB.
Morphology, Structure and Chemistry of Extracted Diesel Soot: Part I: Transmission Electron Microscopy, Raman Spectroscopy, X-ray Photoelectron Spectroscopy and Synchrotron X-Ray Diffraction Study. Tribology International In Review.

[97] Bare SR. XANES Measurements and Interpretation. 2005;EXAFS Data Collection and Analysis Course, APS, July 26-29,2005.

[98] Kim B, Mourhatch R, Aswath PB. Properties of tribofilms formed with ashless dithiophosphate and zinc dialkyl dithiophosphate under extreme pressure conditions. Wear 2010;268:579-91.

[99] Mourhatch R, Parekh K, Aswath PB. A multi technique study of the tribological behavior and the tribofilms generated from fluorinated thiophosphate compounds in comparison to normal ZDDP. STLE/ASME International Joint Tribology Conference, IJTC 2006 2006; 2006;2006:12.

[100] Kasrai M, Yin Z, Fuller M, Bancroft GM, Fyfe K, Tan KH. Application of XAFS in tribology: P and S L-edge XANES spectroscopy of antiwear films. Journal De Physique IV : JP 1997;7:2-847.

[101] Somayaji A, Aswath PB. Role of Antioxidants on Oxidation Stability of Oils with ZDDP and F-ZDDP and Chemical Structure of Tribofilms with XANES. Trib Trans 2009;52:511-25.

[102] Nicholls MA, Norton PR, Bancroft GM, Kasrai M, Do T, Frazer BH et al. Nanometer Scale Chemomechanical Characterization of Antiwear Films. Tribol Lett 2004;17:205-16.

[103] Nicholls MA, Norton PR, Bancroft GM, Kasrai M. X-ray absorption spectroscopy of tribofilms produced from zinc dialkyl dithiophosphates on Al-Si alloys. Wear 2004;257:311-28.

[104] M.A. Nicholls, P.R. Norton, G.M. Bancroft, M. Kasrai, T. Do, B.H. Frazer,G.De Stasio. Nanometer Scale Chemomechanical Characterization of Antiwear Films. Tribol Lett 2004;17:205,205-216.

[105] Bakunin VN, Kasrai M, Kuzmina GN, Bancroft GM, Parenago OP. Influence of temperature and ZDDP concentration on tribochemistry of surface-capped molybdenum sulfide nanoparticles studied by XANES spectroscopy. Tribology Letters 2007;26:33-43.

[106] Najman M, Kasrai M, Michael Bancroft G, Davidson R. Combination of ashless antiwear additives with metallic detergents: Interactions with neutral and overbased calcium sulfonates. Tribology International 2006;39:342-55.

[107] Spikes HA. The history and mechanisms of ZDDP. Trib Lett 2004;17:469-489.

[108] Fleet ME, Liu X. Calcium L2,3-edge XANES of carbonates, carbonate apatite, and oldhamite (CaS). American Mineralogist 2009;94:1235-41.

[109] Zhang Z, Yamaguchi ES, Kasrai M, Bancroft GM. Interaction of ZDDP with borated dispersant using XANES and XPS. Tribol Trans 2004;47:527-36.

[110] Huang W, Tan Y, Dong J, Chen B. Tribological properties of the film formed by borated dioctyl dithiocarbamate as an additive in liquid paraffin. Tribol Int 2002;35:787-91.

[111] Hosonuma K, Yoshida K, Matsunaga A. Decomposition products of zinc dialkydithiophosphate in an engine and their interaction with diesel soot. Wear 1985;103:297-309.

[112] Braun A, Kubatova A, Wirick S, Mun SB. Radiation damage from EELS and NEXAFS in diesel soot and diesel soot extracts. Journal of Electron Spectroscopy 2009;170:42-8.

[113] Rightor EG, Hitchcock AP, Ade H, Leapman RD, Urquhart SG, Smith AP et al. Spectromicroscopy of Poly(ethylene terephthalate): Comparison of Spectra and Radiation Damage Rates in X-ray Absorption and Electron Energy Loss. J Phys Chem B 1997;101:1950-60.

[114] K. Patel PB Aswath. Development of Low Phosphorous Engine Oils. 2005:557-558.

[115] Martin JM, Mansot JL, Berbezier I, Dexpert H. The nature and origin of wear particles from boundary lubrication with a zinc dialkyl dithiophosphate. Wear 1984; 16;93:117-26.

[116] Yamaguchi ES, Wilson DM, Kasrai M, Bancroft GM. XANES analysis of used engine oils and relationship to wear. Tribol Trans 2002;45:437-43.

[117] Antony JW, Bideaux RA, Bladh KW, Nichols MC. Handbook of Minerology. 2002-2004;I-VI.

[118] Giasson S, Espinat D, Palermo T. Study of microstructural transformation of overbased calcium sulphonates during friction. Lubr Sci 1993;5:91-111.

[119] Yu LG, Yamaguchi ES, Kasrai M, Bancroft GM. The chemical characterization of tribofilms using XANES - Interaction of nanosize calciumcontaining detergents with zinc dialkyldithiophosphate. Canadian Journal of Chemistry 2007;85:675-84.

[120] Kimijima T, Haneishi T, Okabe H. Effect of soot on anti-wear properties of marine diesel engine oils. Journal of Japanese Society of Tribologists 1994;39:337-.

[121] Singh SK, Agarwal AK, Sharma M. Experimental investigations of heavy metal addition in lubricating oil and soot deposition in an EGR operated engine. Appl Therm Eng 2006;26:259-66.

[122] Yahagi Y. CORROSIVE WEAR OF DIESEL ENGINE CYLINDER BORE. Tribol Int 1987;20:365-73.

[123] Prado G, Lahaye J, Haynes BS. Soot Particle Nucleation and Agglomeration. Soot in Combustion Systems and Its Toxic Properties - Proceedings of a NATO Workshop on Soot in Combustion Systems. 1983;7:145-61.

[124] Li ZQ, Zhou Y. Structural evolution of a graphite-diamond mixture during ball milling. Physica B: Condensed Matter 2010;405:1004-10.

[125] Parekh K, Chen X, Aswath PB. Synthesis of Fluorinated ZDDP Compounds. Tribol Lett 2009;34:141-53.

[126] Parekh K, Mourhatch R, Aswath PB. ZDDP-additive-catalyst interactions in engine oil. Proceedings of the World Tribology Congress III - 2005 2005:661-2.

[127] Ferrari ES, Roberts KJ, Sansone M, Adams D. A multi-edge X-ray absorption spectroscopy study of the reactivity of zinc di-alkyl-di-thiophosphates anti-wear additives: 2. In situ studies of steel/oil interfaces. Wear 1999;236:259-75.

[128] Martin JM, Grossiord C, Le Mogne T, Bec S, Tonck A. The two-layer structure of Zndtp tribofilms: Part I: AES, XPS and XANES analyses. Tribology International 2001;34:523-30.

[129] Martin JM, Minfray C. Antiwear chemistry in presence of ZDDP. 2005 World Tribology Congress III, Sep 12-16 2005 2005:599-600.

[130] Li Y, Pereira G, Kasrai M, Norton PR. Studies on ZDDP anti-wear films formed under different conditions by XANES spectroscopy, atomic force microscopy and 31P NMR. Tribology Letters 2007;28:319-28.

[131] Somayaji A, Mourhatch R, Aswath PB. Nanoscale Properties of Tribofilms from ZDDP and Fluorinated ZDDP in the Presence and Absence of Antioxidants. Journal of Nanoscience and Nanotechnology 2007;7:4378-4390.

[132] Mourhatch R, Aswath PB. Mechanism of Boundary Lubrication with Zinc Dialkyl Dithiophosphate. 2006; 2006;Under Review; San Antonio, TX, USA:IJTC-12054.

[133] Kasrai M, Fuller MS, Bancroft GM, Yamaguchi ES, Ryason PR. X-ray absorption study of the effect of calcium sulfonate on antiwear film formation generated from neutral and basic ZDDPs: Part 2 - Sulfur species. Tribology Transactions 2003;46:543-9.

[134] Wan Y, Suominen Fuller ML, Kasrai M, Bancroft GM, Fyfe K, Torkelson JR et al. Effects of detergent on the chemistry of tribofilms from ZDDP: studied by X-ray absorption spectroscopy and XPS. In: D. Dowson, M. Priest,G.Dalmaz and A.A.Lubrecht, editor. Tribology Series: Elsevier; 2002, p. 155-166.

[135] Kasrai M, Vasiga M, Fuller MS, Bancroft GM, Fyfe K. Study of the effects of Ca sulfonate on antiwear film formation by X-ray absorption spectroscopy using synchrotron radiation. Journal of Synchrotron Radiation 1999;6:719-21.

[136] Li Y, Pereira G, Kasrai M, Norton PR. The Effect of Steel Hardness on the Performance of ZDDP Antiwear Films: A Multi-Technique Approach. Tribol Lett 2008;29:201-11.

[137] Pereira G, Lachenwitzer A, Kasrai M, Bancroft GM, Norton PR, Abrecht M et al. Chemical and mechanical analysis of tribofilms from fully formulated oils Part 1 – Films on 52100 steel. Tribology 2007;1:48-61.

[138] Pereira G, Lachenwitzer A, Kasrai M, Norton PR, Capehart TW, Perry TA et al. A multi-technique characterization of ZDDP antiwear films formed on Al (Si) alloy (A383) under various conditions. Tribology Letters 2007;26:103-17.

[139] Pereira G, Munoz-Paniagua D, Lachenwitzer A, Kasrai M, Norton PR, Capehart TW et al. A variable temperature mechanical analysis of ZDDP-derived antiwear films formed on 52100 steel. Wear 2007;262:461-70.

[140] De Barros MI, Bouchet J, Raoult I, Le Mogne T, Martin JM, Kasrai M et al. Friction reduction by metal sulfides in boundary lubrication studied by XPS and XANES analyses. Wear 2003;254:863-70.

[141] Green DA, Lewis R. The effects of soot-contaminated engine oil on wear and friction: A review. Proc Inst Mech Eng Pt D: J Automobile Eng 2008;222:1669-89.

[142] Yu RC, Shahed SM. Effects of injection timing and exhaust gas recirculation on emission from a D.I diesel engine. SAE Preprints 1981.

[143] Suominen Fuller ML, Rodriguez Fernandez L, Massoumi GR, Lennard WN, Kasrai M, Bancroft GM. The use of Xâ€ray absorption spectroscopy for monitoring the thickness of antiwear films from ZDDP. Trib Lett 2000;8:187,187-192.

[144] Kasrai M, Puller M, Scaini M, Yin Z, Brunner RW, Bancroft GM et al. Study of tribochemical film formation using x-ray absorption and photoelectron spectroscopies. In: D. Dowson, C.M. Taylor,T.H.C.Childs and G.Dalmaz, editor. Tribology Series: Elsevier; 1995, p. 659-669.

[145] Yin Z, Kasrai M, Bancroft GM, Fyfe K, Colaianni ML, Tan KH. Application of soft x-ray absorption spectroscopy in chemical characterization of antiwear films generated by ZDDP Part II: the effect of detergents and dispersants. Wear 1997;202:192-201.

[146] Kapsa P, Martin JM, Blanc C, Georges JM. Antiwear Mechanism of Zddp in the Presence of Calcium Sulfonate Detergent. Journal of Lubrication Technology, Transactions ASME 1981;103:486-96.

[147] Nicholls MA, Do T, Bancroft GM, Norton PR, Kasrai M, Capehart TW et al. Chemical and mechanical properties of ZDDP antiwear films on steel and thermal spray coatings studied by XANES spectroscopy and nanoindentation techniques. Tribology Letters 2003;15(3):241-8.

[148] Fuller MLS, Kasrai M, Bancroft GM, Fyfe K, Tan KH. Solution decomposition of zinc dialkyl dithiophosphate and its effect on antiwear and thermal film formation studied by X-ray absorption spectroscopy. Tribol Int 1998;31:627-44.

[149] Fuller M, Yin Z, Kasrai M, Bancroft GM, Yamaguchi ES, Ryason PR et al. Chemical characterization of tribochemical and thermal films generated from neutral and basic ZDDPs using X-ray absorption spectroscopy. Tribology International 1997;30:305-15.

[150] Yin Z, Kasrai M, Fuller M, Bancroft GM, Fyfe K, Tan KH. Application of soft x-ray absorption spectroscopy in chemical characterization of antiwear films generated by ZDDP Part I: the effects of physical parameters. Wear 1997;202:172-91.

[151] Kim B. Tribological Performance of Ashless Antiwear Additives Under Extreme Pressure Conditions. 2009Ph.DUniversity of Texas at ArlingtonArlington, Texas.

[152] Zhang Z, Yamaguchi ES, Kasrai M, Bancroft GM. Tribofilms generated from ZDDP and DDP on steel surfaces: Part 1. Growth, wear and morphology. 2005 World Tribology Congress III 2005; 2005:617-8.

[153] DeGroot FMF, Fuggle JC, Thole BT, Sawatzy GA. L2,3 X-ray-Absorption Edges of D0 Compounds - K+, Ca-2+, Sc-3+ and Ti-4+ in OH (Octahedgral) Symmetry. Physical Review B 1990;41:928-37.

[154] Himpsel FJ, Karlsson UO, McLean AB, Terminello LJ, DeGroot FMF, Abbate M et al. Fine-Structure of the Ca 2P X-ray absorption edge for bulk compounds, surfaces and interfaces. Physical Review B 1991;43:6899-907.

[155] Urabe M, Tomomatsu T, Sato K, Takiguchi M. Piston friction force with EGR activated. JSAE Rev 1998;19:52-3.

[156] Sato T, Saito H, Korematsu K, Tanaka J. Study on wear of piston rings in diesel engines with exhaust gas recirculation. Proceedings of the 2001 Spring Technical Conference of the ASME Internal Combustion Engine Division, April 29, 2001 - May 23 2001;36:39-45.

[157] Mourhatch R. Tribological and Antiwear Mechanisms of Fluorinated Zinc Dialkyl Dithiophosphate in Comparison to Zinc Dialkyl Dithiophosphate in Engine Oils. 2008:161.

[158] Pereira G, Lachenwitzer A, Munoz-Paniagua D, Kasrai M, Norton PR, Abrecht M et al. The role of the cation in antiwear films formed from ZDDP on 52100 steel. Tribology Letters 2006;23:109-19.

[159] Huq MZ, Chen X, Aswath PB, Elsenbaumer RL. Thermal degradation behavior of zinc dialkyldithiophosphate in presence of catalyst and detergents in neutral oil. Tribology Letters 2005;19:127-34.

[160] Ramakumar SSV, Aggarwal N, Madhusudhana Rao A, Sarpal AS, Srivastava SP, Bhatnagar AK. Studies on additive-additive interactions: Effects of dispersant and antioxidant additives on the synergistic combination of overbased sulphonate and ZDDP. Lubr Sci 1994;7:25-38.

[161] Bardasz EA, Carrick VA, George HF, Graf MM, Kornbrekke RE, Pocinki SB. Understanding soot mediated oil thickening through designed experimentation - Part 5: Knowledge exhancement in the GM 6.5 L. Proceedings of the 1997 International Fall Fuels & Lubricants Meeting & Exposition, October 13, 1997 - October 16 1997;1304:126-40.

[162] ASM International. Annual Book of ASTM Standards : Petroleum Products and Lubricants (II). 2010;05.02:1433-1453.

[163] Tumolva L, Park J, Kim J, Miller AL, Chow JC, Watson JG et al. Morphological and elemental classification of freshly emitted soot particles and atmospheric ultrafine particles using the TEM/EDS. Aerosol Science and Technology 2010;44:202-15.

[164] di Stasio S, Braun A. Comparative NEXAFS study on soot obtained from an ethylene/air flame, a diesel engine, and graphite. Energy and Fuels 2006;20:187-94.

[165] Hopkins RJ, Tivanski AV, Marten BD, Gilles MK. Chemical bonding and structure of black carbon reference materials and individual carbonaceous atmospheric aerosols. J Aerosol Sci 2007;38:573-91.

[166] Braun A, Huggins FE, Kelly KE, Mun BS, Ehrlich SN, Huffman GP. Impact of ferrocene on the structure of diesel exhaust soot as probed with wide-angle X-ray scattering and C(1s) NEXAFS spectroscopy. Carbon 2006;44:2904-11.

[167] Nikiel L, Jagodzinski PW. Raman spectroscopic characterization of graphites: A re-evaluation of spectra/ structure correlation. Carbon 1993;31:1313-7.

[168] Mernagh TP, Cooney RP, Johnson RA. Raman spectra of Graphon carbon black. Carbon 1984;22:39-42.

[169] Richter H, Howard JB. Formation of polycyclic aromatic hydrocarbons and their growth to soot-a review of chemical reaction pathways. Progress in Energy and Combustion Science 2000;26:565-608.

[170] Schuster ME, Havecker M, Arrigo R, Blume R, Knauer M, Ivleva NP et al. Surface sensitive study to determine the reactivity of soot with the focus on the European emission standards IV and VI. Journal of Physical Chemistry A 2011;115:2568-80.

[171] Donnet JB. Carbon Black : Science and Technology. 1993.: New York Marcel Dekker, Inc, 1993.

[172] Cody GD, Botto RE, Ade H, Behal S, Disko M, Wirick S. C-NEXAFS microanalysis and scanning x-ray microscopy of microheterogeneities in a high-volatile a bituminous coal. Energy and Fuels 1995;9:75-83.

[173] Urquhart SG, Gillies R. Matrix effects in the carbon 1s near edge x-ray absorption fine structure spectra of condensed alkanes. J Chem Phys 2006;124.

BIOGRAPHICAL INFORMATION

MIhir Patel received his Bachelor of Engineering in Mechanical Engineering from University of Pune (India) in 2002. He has received his Master of Business Administration Degree from Sardar Patel University (India) in 2005. During his doctoral program at the University of Texas at Arlington, he served as President of American Society of Materials UTA Student Chapter and lead various departmental programs to outreach community and educate high school students with material science and engineering. He is also a recipient of Carl D. Wiseman Service Award for outstanding service to his department at UT Arlington. He is also a recipient of University Scholar Award for his exceptional academic achievement. He also served Society of Tribology and Lubrication Engineers as Program Chair of Lubrication Fundamental Session.